

Faculty of Science, Charles University
Institute of Geochemistry, Mineralogy and Mineral Resources

GEOCHEMISTRY OF UPPER MANTLE ROCKS FROM KOZÁKOV AND HORNÍ BORY, BOHEMIAN MASSIF

Lukáš Ackerman

Dissertation



Supervisors: Doc. RNDr. Emil Jelínek, CSc. (Faculty of Science, Charles University)
Doc. RNDr. Jaromír Ulrych, DrSc. (Institute of Geology, v.v.i. AS CR)

Consultants: Prof. Gordon L. Medaris (University of Wisconsin-Madison)
Prof. Richard J. Walker (University of Maryland)

Prague 2008

Statement of originality

The research presented in this dissertation is the result of my original scientific work, in collaboration with my supervisors, consultants and other colleagues. This dissertation represents work during my PhD. study at the Faculty of Science, Charles University.

To the best of my knowledge and belief, I declare that the results presented in my dissertation have not been published or presented by someone else. This dissertation has not been submitted for any other academic degrees at other university or educational institution.

Prague, June 2008

Lukáš Ackerman, MSc.

Statement of co-authors

On behalf of the co-authors, I declare that Lukáš Ackerman was the principal investigator of the scientific study presented in this dissertation and performed majority of the work. The contribution of the co-authors was mainly supplying of the analytical data and critical comments on the final versions of the manuscripts.

Prague, June 2008

Doc. RNDr. Emil Jelínek, CSc.

Acknowledgments

I would like to thank both of my supervisors, Emil Jelínek and Jaromír Ulrych. They provided me not only with scientific support during the whole course of my PhD. study, but also created amazing familiar and friendly environment for my research.

I am greatly indebted to my consultants, Gordon Medaris and Rich Walker. Many thanks to Gordon for his unbelievable kind approach, never ending discussions and patience. I am grateful to Rich for his invitation to University of Maryland, where I spent marvellous months learning the essentials of lab work and isotope geochemistry.

Of course, there are many others, I would like to thank especially Ladislav Strnad and Wolfgang Siebel for providing analytical data and helpful discussions. Lynnette Pitcher and Igor Puchtel for their help in the lab during my stay in Maryland and for analytical data. I also thank Martin Svojtka for discussions during which we became rather friends than a colleagues in Academy of Sciences.

Thanks to my girlfriend Markéta for her astonishing support during my work. She was standing behind me in every moment and I would not finish my PhD. study without her. Last, but not least of all, there are my parents and my sister, providing me with support during all my life.

This work was supported by project No. IAA3013403 (Grant Agency of the Academy of Sciences), project No. KJB300130612 (Grant Agency of the Academy of Sciences), project No. 248/2006/B-GEO (Grant Agency of the Charles University), project No. EAR-0330528 (US National Science Foundation), Student Mobility Fund of Charles University and Scientific Programs CEZ: Z3-013-912 of the Institute of Geology v.v.i., Academy of Sciences of the Czech Republic and MSM 0021620855 of the Charles University.

Table of contents

Introduction	4
Chapter 1. Geochemistry of upper mantle rocks in the Bohemian Massif	
a review	7
1.1. Introduction	7
1.2. Upper mantle rocks in the Bohemian Massif	7
1.2.1. Spinel peridotite xenoliths	7
1.2.2. Spinel/garnet peridotites in gneisses and granulites	8
1.2.3. Ophiolite complexes	9
1.3. Summary of the studies, results and open questions	9
Chapter 2. Geochemistry and Evolution of Subcontinental Lithospheric Mantle in Central Europe: Evidence from Peridotite Xenoliths of the Kozákov Volcano, Czech Republic	11
2.1. Introduction	12
2.2. Locality and Geological Setting	12
2.3. Kozákov xenoliths	14
2.3.1. Lithology	15
2.3.2. Texture	15
2.4. Analytical methods	17
2.5. Geothermometry, thermal history, and depth estimates	22
2.6. Rock compositions	26
2.6.1. Modes	26
2.6.2. Major elements	26
2.6.3. Trace elements	30
2.6.4. Compositional variation with depth	31
2.7. Mineral compositions	34
2.7.1. Major elements	34
2.7.2. Trace elements	36
2.7.3. Compositional variation with depth	36
2.8. Sr and Nd isotopes in clinopyroxene	39
2.9. Discussion	40
2.9.1. Partial melting and depletion of the mantle sources of the xenoliths	40
2.9.2. Metasomatism of the xenoliths	43
2.9.3. Timing of depletion and metasomatism	46
2.10. Conclusions	46

Chapter 3. Effects of melt percolation on highly siderophile elements and Os isotopes in subcontinental lithospheric mantle: a study of the upper mantle profile beneath Central Europe	48
3.1. Introduction	48
3.2. Mantle xenoliths	49
3.3. Analytical methods	52
3.4. Results	54
3.4.1. Sulfur and copper	54
3.4.2. HSE concentrations	54
3.4.3. Osmium isotopes	58
3.5. Discussion	59
3.5.1. HSE mobility during eruption and emplacement of the xenoliths	61
3.5.2. Effects of partial melting on HSE	62
3.5.3. Melt percolation	63
3.5.3.1. Evidence for metasomatism in the Kozákov xenoliths	63
3.5.3.2. HSE fractionation during melt percolation	64
3.5.3.3. Evolution of HSE and $^{187}\text{Os}/^{188}\text{Os}$ of the upper mantle profile beneath the Kozákov volcano	65
3.5.4. Consideration of model melt depletion ages	67
3.6. Conclusions	69
Chapter 4. Geochemistry of Fe-rich peridotites and associated pyroxenites from Horní Bory, Bohemian Massif: insights into subduction-related melt-rock reactions	70
4.1. Introduction	71
4.2. Geological settings	71
4.3. Analytical methods	73
4.4. Petrography	75
4.4.1. Mg-peridotite	75
4.4.2. Fe-peridotite	76
4.4.3. Pyroxenites	77
4.5. Whole-rock chemistry	78
4.5.1. Major and minor elements	78
4.5.2. Rare earth and other trace elements	80
4.6. Mineral compositions and T-P estimates	84
4.6.1. Major and minor elements	84
4.6.2. Trace elements	86

4.6.3. Temperature-Pressure estimates	89
4.7. Sr-Nd geochemistry	89
4.7.1. Sm-Nd geochronology	89
4.7.2. Sr and Nd isotopes	91
4.8. Discussion	92
4.8.1. Petrogenetic model	92
4.8.2. Constraints on the origin and evolution of Mg-pd and Fe-pd-px	94
4.8.3. Mg-Fe modelling	94
4.8.4. Sr-Nd isotopic constraints	96
4.8.5. Composition and source of infiltrating melt	96
4.9. Conclusions	98
Chapter 5. General conclusions	108
References	111
Curriculum Vitae of Lukáš Ackerman	125

Introduction

Geochemical studies of upper mantle rocks (peridotites) provide insights into the Earth's upper mantle evolution from the Archean to the present. This is because mantle processes play a key role in the formation of continents and largely assign geochemical properties of the Earth's crust.

Peridotites (lherzolite, harzburgite, dunite, wehrlite) occur in orogenic massifs, ophiolite complexes and xenoliths enclosed in volcanic rocks. In spite of their limited amounts compared to crustal rocks found on the surface, they have been widely studied since 1970s. An overall general evolution pattern is usually found in mantle peridotites – ancient **depletion** by partial melting processes and later **metasomatism** by various agents. However, the degree of mantle depletion and the nature of metasomatism largely reflect the age of the peridotites and their position within upper mantle during Earth's evolution.

Mantle depletion is ascribed to partial melting processes resulting in the formation of mantle-derived magmas of predominant basaltic composition. During such process, mantle becomes depleted in incompatible elements (e.g. alkalis, light rare earth elements – LREE and large ion lithophile elements – LILE). The extent of depletion depends on the degree of partial melting. If higher, clinopyroxene or even orthopyroxene are melted leading to the origin of mantle harzburgites and dunites, respectively. This process plays a key role especially in the depleted mantle (DMM) reservoir (abyssal peridotites) representing the source of MORB magmas.

In contrast, mantle metasomatism represents the process of mantle enrichment by fluids or melts of mantle-derived or crustal origin. With respect to the composition and nature of metasomatic agent, three most common metasomatic patterns can be usually recognized: (1) metasomatism by silicate, mostly basaltic melts (e.g. Norman, 1998; Neumann et al., 2004), (2) metasomatism by carbonatitic melts (Yaxley et al., 1991) and (3) metasomatism by hydrous subduction-related fluids/melts (e.g. Zanetti et al., 1999; McInnes et al., 2001). Each type of metasomatism has its own pattern (see Downes, 2001 and references therein), however, several studies recognized that complex studies of mantle-derived rocks are necessary to get a complete picture of mantle evolution (e.g. Ionov et al., 2002).

Understanding of the mantle evolution has undergone a boom during the last decade. This is due to broad developments in geophysical methods and an increasing amount of experimental data, and, most importantly, due to an enormous development in analytical techniques. Recent improvements in especially mass spectrometry techniques provide a stepping stone for this boom and bring on unconventional isotopic techniques (e.g. Lu-Hf, Re-Os systems) to mantle geochemistry. These methods allow us to determine ages of mantle peridotites, mantle depletion and in some cases also the age of metasomatic processes (e.g. Pearson et al., 2004; Carlson, 2005). However, with new high-resolution techniques, many new questions about mantle evolution occur. For example, it was widely accepted for many years that dunites and harzburgites represent mantle residues after high degrees of partial melting (> 25 %). On the contrary, experimental studies and results of numerical models (e.g. Kelemen, 1990; Kelemen et al., 1990, 1992, 1998; Ionov et al. 2005) showed that this type of rocks could be formed

during intensive melt-rock reactions between peridotite and migrating upper mantle melts. One of the biggest issues in mantle geochemistry is the process and extent of mantle refertilization (enrichment) by mantle-derived and subduction-related melts/fluids. Ophiolite complexes and orogenic massifs commonly contain lenses and/or layers of pyroxenites, whose origin is still a matter of debate (see Downes, 2007 and references therein), but it is clear that they play a very important role in mantle refertilization.

The purpose of this dissertation is geochemical study of upper mantle rocks at two sites from different geological settings of the Bohemian Massif (Czech Republic) – Kozákov and Horní Bory. In spite of the title of this dissertation, this work does not represent just a case study of these two localities. In contrast, Kozákov and Horní Bory were chosen as unique mantle suites, which could provide insights into the upper mantle processes (mantle depletion, metasomatism, melt-rock reactions) and behaviour of specific trace elements (e.g. highly siderophile elements) in the upper mantle. This is of a broad relevance to all people involved in the Earth's upper mantle and I hope that the reader will be attracted.

The dissertation is divided into four chapters. Chapter 1 represents a review of petrological and geochemical studies of upper mantle rocks found in the Bohemian Massif, which have been published or presented so far, and a presentation of open questions. Chapters 2 to 4 constitute three manuscripts of original research dealing with geochemistry of upper mantle rocks from Kozákov and Horní Bory. These manuscripts have been already published (*Journal of Petrology* - Chapter 2), are under review (*Geochimica et Cosmochimica Acta* - Chapter 3) or have been submitted (*Chemical Geology* - Chapter 4) to international scientific journals.

Chapter 2 presents a geochemical study of major elements, trace elements, and Sr-Nd isotopes combined with mineral chemistry of upper mantle xenoliths from the Kozákov volcano. This unique suite of xenoliths samples upper 2/3 of the upper mantle in this region and, therefore, provides a great possibility to study upper mantle composition variations with depth. The results show that upper mantle beneath Kozákov volcano underwent different degrees of partial melting which increase with decreasing depth. Subsequent metasomatism, most likely by basaltic melt, occurred as a result of mantle upwelling, and mantle interacted with percolating melt at variable melt/rock ratios. Progressive changes in trace element ratios through the mantle profile point to a significant fractionation of percolating melt with its ascent and suggest Cenozoic age of metasomatism.

Chapter 3 deals with the effects of melt percolation on highly siderophile element (HSE - Os, Ir, Ru, Rh, Pd, Pt, Re) geochemistry and osmium isotopes. The Kozákov suite of samples was chosen for this study to provide a complex picture of HSE behaviour with respect to major/trace elements and Sr-Nd isotopes. Whole-rock HSE analyses combined with high-precision osmium isotopic data revealed large-scale incompatible behaviour of HSE during melt percolation, suggesting a sulphur-undersaturated character of the melt. In contrast to other studies, our investigation did not document an import of rhenium and, as a consequence, demonstrated that osmium isotopes were not affected by melt percolation and should provide geochronologically meaningful data even in pervasively metasomatized

mantle. On the other hand, in case of some samples, I-PGE (Os, Ir, Ru) were imported from the percolating melt, suggesting precipitation of I-PGE bearing alloys from the melt.

Chapter 4 investigates geochemistry and origin of unusually Fe-rich peridotites and associated pyroxenite boudins in Moldanubian granulites from Horní Bory. Two different types of peridotites can be distinguished at Horní Bory based on Mg-numbers and modal composition: (1) Mg-Cr lherzolites similar in composition to other mantle-derived rocks elsewhere and (2) Fe-rich dunite-wehrlite rocks accompanied with pyroxenites. A major/trace element study combined with Sr-Nd isotopic constrains and numerical models have shown that Fe-rich peridotites originated during melt-rock reactions between peridotite and basaltic melt with a subduction-related signature at different melt/rock ratios.

The last Chapter 5 provides overall conclusions, emphasizes the differences between the Kozákov and Horní Bory mantle suites and presents general notes to the composition and evolution of the upper mantle beneath the Bohemian Massif. Concluding remarks of broad relevance to Earth's upper mantle evolution and possibilities for future studies are presented at the end of this chapter.

CHAPTER 1. Geochemistry of upper mantle rocks in the Bohemian Massif - a review

1.1. INTRODUCTION

The Bohemian Massif represents the easternmost part of the Variscan orogenic chain assembled during Devonian-Permian times. The Central European subcontinental lithospheric mantle (SCLM) represents a tectonic collage due to the Devonian convergence and Carboniferous collision of Laurasia, Gondwana, and intervening continental and oceanic microplates, which resulted in a juxtaposition of disparate lithospheric fragments of various ages and provenances (Franke, 2000; Matte, 2001). These processes are also recorded by lithospheric mantle, which yields divergently dipping anisotropic structures in the Moldanubian and Saxothuringian zones (Babuška and Plomerová, 2001; Plomerová et al., 2005). Additionally, Babuška and Plomerová (2006) revealed the presence of lithospheric domains with different orientation of anisotropy throughout the European lithosphere that closely coincides with major crustal tectonic boundaries. This suggests that the Variscan orogeny had a large impact on mantle structure preserved in the European SCLM. However, the composition and evolution of the upper mantle beneath the Bohemian Massif is poorly understood.

1.2. UPPER MANTLE ROCKS IN THE BOHEMIAN MASSIF

Mantle-derived rocks occurring in the Bohemian Massif (BM) can be subdivided into several categories with respect to their position and composition: spinel peridotites occurring as xenoliths in volcanic rocks, spinel-garnet peridotite bodies enclosed in gneisses or granulites and metamorphosed dismembered ophiolite complexes.

1.2.1. Spinel peridotite xenoliths

These rocks occur as xenoliths in volcanic rocks of mostly Neogene age. A summary of their occurrences together with the estimated modal composition is given in Ulrych and Adamovič (2004). Peridotites are predominantly of harzburgitic composition accompanied with lherzolites, dunites and rare clinopyroxenites/wehrlites (Ulrych and Adamovič, 2004). They are usually fresh with size smaller than 15 cm, but locally - as in the case of the Kozákov volcano - reach 70 cm in diameter, concentrated in Neogene volcanic rocks of basanitic composition in the northern part of the BM along the Ohře/Eger rift and regional fault systems (e.g. Kozákov, Dobkovičky, Brtníky, Okrouhlé Hradiště) or rarely in northern Silesia (e.g. Zálesí, Bruntál). In spite of their abundance, only upper mantle xenoliths of the Kozákov volcano have been previously studied in detail (Medaris et al., 1997; Christensen et al., 2001; Konečný et al., 2006). These studies described the layered structure of the mantle beneath the Kozákov volcano and documented metasomatism by silicate melts. In addition, Frýda and Vokurka (1995) reported evidence for carbonatite metasomatism in a single harzburgite xenolith from Dobkovičky in the České

Středohoří Mts. and several studies dealt with mineral chemistry of the xenoliths (e.g. Fediuk, 1971; Vokurka and Povondra, 1983).

Ulrych et al. (2000) studied upper mantle xenoliths from the Osečná melilitite complex of Cretaceous-Paleogene age. Dunite-harzburgite xenoliths were interpreted as samples of depleted mantle whereas glimmerites and phlogopite-bearing clinopyroxenites represent metasomatized mantle.

Quaternary xenoliths are very rare, but Geissler et al. (2007) described phlogopite/amphibole-bearing wehrlites from Quaternary tephra deposit in the Mýtina maar (Western Bohemia) and interpreted them as mantle fragments metasomatized by alkaline melts.

1.2.2. Spinel/garnet peridotites in gneisses and granulites

The peridotites form large bodies (e.g. Mohelno, Biskoupky) or boudins (e.g. Horní Bory, Sklenné, Klet', Libín) in the HT-HP Gföhl Unit (uppermost stratigraphic unit of the Moldanubian Zone) granulites or gneisses (e.g. Nové Dvory). They are commonly accompanied with garnet pyroxenites or eclogites of variable composition. Medaris et al. (2005) divided peridotites into three groups according to their composition, mineralogy and P-T regime: (1) Type I low P-T regime spinel and garnet peridotites (Mohelno, Biskoupky, Lom pod Libínem), (2) Type II variable P-T regime spinel and garnet peridotites associated with common pyroxenite (Horní Bory) and (3) Type III medium P-T regime garnet peridotites (Nové Dvory). Type I peridotites from Mohelno and Biskoupky have characteristics of depleted oceanic mantle (e.g. LREE depletion; highly radiogenic $^{143}\text{Nd}/^{144}\text{Nd}$) and their very high temperatures (~ 1300 °C) point to derivation from asthenospheric mantle (Medaris et al., 2005). On the contrary, type II and type III show major/trace element compositions consistent with derivation from subcontinental lithospheric mantle.

Garnet pyroxenites and eclogites were interpreted as a high-pressure cumulates from melts which migrated through the lithospheric mantle and their isotopic composition points to a significant contribution of crustal (subduction-related?) material (Medaris et al., 1995a; Becker, 1996b; Medaris et al., 2006).

Garnet peridotites and pyroxenites yielded Sm-Nd ages of 324 to 354 Ma, with the exception of 371 Ma for Mohelno (Beard et al., 1992; Becker, 1997) and 370-377 Ma for Níhov and Bečváry pyroxenites and Lower Austria pyroxenites from Mitterbachgraben (Carswell and Jamtveit, 1990; Brueckner et al., 1991; Beard et al., 1992; Becker, 1997). Medaris et al. (2005) presented a model of peridotite provenance in the context of Franke (2000) tectonic scenario of the Bohemian Massif consolidation. In this model, Type I peridotite represents a relict of oceanic mantle during the closure of the oceanic basin and the collision of Moldanubia and Bohemia. Types II and III may represent peridotites from the overlying lithospheric wedge which interacted with infiltrated melts (pyroxenites, eclogites).

1.2.3. Ophiolite complexes

Dismembered metamorphosed ophiolites form two complexes – the Mariánské Lázně complex and the Letovice complex.

The *Mariánské Lázně* high-grade ophiolite complex consists of a discontinuous profile of oceanic mantle-crust located at the border between the Teplá-Barrandian Unit and the Saxothuringian Unit (Cháb, 1973; Kastl and Tonika, 1984). Upper mantle rocks are represented by a layer of strongly serpentinized peridotites several metres thick, accompanied by metagabbros, amphibolites and eclogites. The equilibrium temperatures of peridotites were estimated at 850-900 °C (Jelínek et al., 1997) whereas eclogites yielded 570-740 °C and pressures up to 1.6 GPa (Jelínek et al., 1997). Sm-Nd ages of eclogites range from 367 Ma (Mnichov eclogite) to 377 Ma (Louka eclogite) (Beard et al., 1995) and their Sr-Nd isotopic composition corresponds either with their origin from a MORB-like source or with an island-arc/oceanic-island origin.

The *Letovice complex* is located in the eastern part of the Bohemian Cretaceous Basin, forming a part of the Letovice crystalline unit. It probably belongs to a N-S elongated metabasite zone. About 70 % of the complex consists of serpentinized spinel/plagioclase peridotites (mostly dunite-harzburgite) and orthopyroxenites, websterites accompanied by layered or massive metagabbros, amphibolites and minor dolerite dykes (Jelínek et al., 1984). Major and trace element data point to the origin of lower parts of the ophiolite by different partial melting degrees whereas fractional processes play the dominant role in the upper parts of the complex. In general, the complex has similar geochemical characteristics as the ophiolites from New Caledonia or Papua New Guinea and is likely to be related to marginal sea environment (Jelínek et al., 1984).

1.3. SUMMARY OF THE STUDIES, RESULTS AND OPEN QUESTIONS

The studies of the upper mantle rocks in the Bohemian Massif summarized in Chapter 1.2. have shown the existence of plentiful data on geochemistry of the BM upper mantle rocks. However, most data, except the Kozákov xenolith suite and Gföhl Unit peridotites/pyroxenites, are of older date. Therefore, there is a lack of precise trace element data and complex isotopic data (e.g. Sr, Nd, Pb, Os). This means that most published data do not contribute significantly to the composition and evolution of the upper mantle beneath the BM. Consequently, a lot of principal questions remain open and can be summarized as follows:

- compositional chemical variation of the upper mantle remains unknown. While the geophysical studies revealed at least three mantle domains beneath the BM with different seismic anisotropy (Plomerová et al., 2005), it is not clear if there are also some chemical compositional variations
- age of the BM subcontinental lithospheric mantle and the connection between the mantle and the Variscan/Cadomian orogeny are poorly understood. For example, does upper mantle

beneath the BM can represent an orogenic root of overlying Variscan crust? Or, were the crustal terranes rather thrust on?

- there is only a limited idea on the degrees and extent of partial melting of upper mantle beneath the BM. Harzburgites, usually assumed to represent residues after high partial melting degrees, are common rock types within the BM upper mantle rocks. However, several studies have shown (e.g. Kelemen et al., 1998) that they can be formed also by melt-rock reactions in the upper mantle
- in spite of evidence for metasomatism by different agents found in some xenoliths and peridotite bodies, only a little attention was paid to this issue. One of the important questions is the kind of tectonic or magmatic processes connected with the different types of metasomatism connected
- the entire lack of geochronological information on the age of peridotite protoliths, mantle depletion and metasomatism. Even though there is a lot of generally consistent Sm-Nd data on the age of HT-HP metamorphism of peridotites, pyroxenites and eclogites, other geochronological information remain unknown

CHAPTER 2. Geochemistry and Evolution of Subcontinental Lithospheric Mantle in Central Europe: Evidence from Peridotite Xenoliths of the Kozákov Volcano, Czech Republic

Lukáš Ackerman^{1,2}, Nancy Mahlen³, Emil Jelínek¹, Gordon Medaris, Jr.³, Jaromír Ulrych², Ladislav Strnad⁴, Martin Mihaljevič¹

¹*Institute of Geochemistry, Mineralogy and Mineral Resources, Faculty of Science, Charles University, Albertov 6, 128 43, Praha 2, Czech Republic*

²*Institute of Geology v.v.i., Academy of Sciences of the Czech Republic, Rozvojová 269, 165 00, Praha 6, Czech Republic*

³*Department of Geology and Geophysics, University of Wisconsin-Madison, WI 53706, USA*

⁴*Laboratories of the Geological Institutes, Faculty of Science, Charles University, Albertov 6, 128 43, Praha 2, Czech Republic*

Status: Published in *Journal of Petrology* 48, 2007, 2235-2260

Abstract

Neogene basanite lavas of Kozákov volcano, located along the Lusatian fault in the northeastern Czech Republic, contain abundant anhydrous spinel lherzolite xenoliths that provide an exceptionally continuous sampling of the upper two-thirds of central European lithospheric mantle. The xenoliths yield a range of two-pyroxene equilibration temperatures from 680° C to 1070° C, and are estimated to originate from depths of 32-70 km, based on a tectonothermal model for basaltic underplating associated with Neogene rifting. The sub-Kozákov mantle is layered, consisting of an equigranular upper layer (32-43 km), a protogranular intermediate layer that contains spinel-pyroxene symplectites after garnet (43-67 km), and an equigranular lower layer (67-70 km). Negative correlations of wt % TiO₂, Al₂O₃, and CaO with MgO and clinopyroxene mode with Cr-number in the lherzolites record the effects of partial fusion and melt extraction; Y and Yb contents of clinopyroxene and the Cr-number in spinel indicate ~5 to ~15% partial melting. Subsequent metasomatism of a depleted lherzolite protolith, probably by a silicate melt, produced enrichments in the large ion lithophile elements, light rare earth elements and high field strength elements, and positive anomalies in primitive mantle normalized trace element patterns for P, Zr, and Hf. Although there are slight geochemical discontinuities at the boundaries between the three textural layers of mantle, there tends to be an overall decrease in the degree of depletion with depth, accompanied by a decrease in the magnitude of metasomatism. Clinopyroxene separates from the intermediate protogranular layer and the lower equigranular layer yield ¹⁴³Nd/¹⁴⁴Nd values of 0.51287-0.51307 ($\epsilon_{\text{Nd}} = +4.6$ to $+8.4$) and ⁸⁷Sr/⁸⁶Sr values of 0.70328-0.70339. Such values are intermediate with respect to the Nd-Sr isotopic array defined by anhydrous spinel peridotite xenoliths from central Europe and are similar to those associated with the present-day low-velocity anomaly in the upper mantle beneath Europe. The geochemical characteristics of the central European lithospheric mantle reflect a complex evolution related to Devonian to Early Carboniferous plate convergence, accretion, and crustal thickening, Late Carboniferous to Permian extension and gravitational collapse, and Neogene rifting, lithospheric thinning, and magmatism.

Keywords: xenoliths; lithospheric mantle; REE-LILE-HFSE; Sr-Nd isotopes; Bohemian Massif

2.1. INTRODUCTION

Studies of ultramafic xenoliths exhumed within the volcanic centers of the Cenozoic European Rift System (CERS) have provided substantial information regarding the physical and chemical characteristics of the subcontinental lithospheric mantle (SCLM) (Menzies and Bodinier, 1993; Downes, 2001). Such studies have established a general pattern of incompatible element depletion in the peridotites through removal of basaltic melts, followed locally by cryptic or modal metasomatism via interaction with transient melts or fluids, the details of which vary between xenolith localities (Downes, 2001, and references therein).

The Pliocene Kozákov volcano in the Czech Republic is one of a number of eruptive centres located along the Ohře (Eger) Graben in the central European part of the CERS (Fig. 1). Spinel lherzolite xenoliths from Kozákov volcano yield a continuous range of equilibration temperatures from 680° C to 1065° C and have been estimated to originate from depths of 32-70 km, corresponding to the upper two-thirds of the SCLM in this region (Christensen et al., 2001). This suite of spinel lherzolite xenoliths from a single eruptive site provides a rare opportunity to evaluate the depth variation in physical and chemical characteristics of the SCLM in central Europe, similar to that provided for Western Europe by the xenolith suite from the Ray Pic volcano in the French Massif Central (Zangana et al., 1997, 1999).

The Kozákov xenoliths were first described by Farský (1876), several bulk-rock and mineral analyses were reported by Fediuk (1971) and Vokurka and Povondra (1983), detailed geothermometry calculations were performed on several samples by Medaris et al. (1999), seismic properties were calculated from olivine petrofabrics by Christensen et al. (2001), and major element and rare earth element (REE) compositions for several bulk-rocks and clinopyroxene separates were determined by Konečný et al. (2006). In this investigation we examine the depth variation in chemical composition of the Kozákov sample suite, including major and trace elements for whole-rocks, major elements for the constituent minerals, and trace elements and Nd and Sr isotopes for clinopyroxene separates. As for many spinel lherzolite xenolith suites elsewhere, the data indicate the decoupling of major and trace elements caused by melt extraction during partial fusion (e.g. a decrease in CaO and Al₂O₃) and subsequent metasomatism [e.g. an increase in light REE (LREE), large ion lithophile elements (LILE) and high field strength elements (HFSE)]. In the Kozákov xenolith suite, the degree of depletion tends to decrease with depth, which is a general phenomenon in the SCLM (Gaul et al., 2003), whereas in contrast the pattern of metasomatism is distinctive for the different textural types of xenoliths.

2.2. LOCALITY AND GEOLOGICAL SETTING

The central European lithosphere is a tectonic collage, resulting from the Devonian convergence and Carboniferous collision of Laurussia, Gondwana, and intervening continental and oceanic microplates, which juxtaposed disparate lithospheric fragments of various ages and provenance (Franke, 2000; Matte, 2001). This collage assembly is reflected in Kossmat's (1927) prescient division of central Europe into the Moldanubian, Saxothuringian, and Rhenohercynian zones (Fig. 1), each of which itself is a

composite of terranes. A collage assembly is also recorded by the lithospheric mantle, which exhibits divergently dipping anisotropic structures in the Moldanubian and Saxothuringian zones (Babuška and Plomerová, 2001; Plomerová et al., 2005).

Superimposed on this lithospheric collage is the CERS, which evolved in the Alpine foreland during late Eocene to Recent times (Fig. 1; Wilson and Downes, 1991; Ziegler, 1992). The distribution of grabens in the rift system is controlled by Cenozoic tensional reactivation of basement fracture systems, most of which originated during the late stages of the Middle to Late Paleozoic Variscan orogeny.

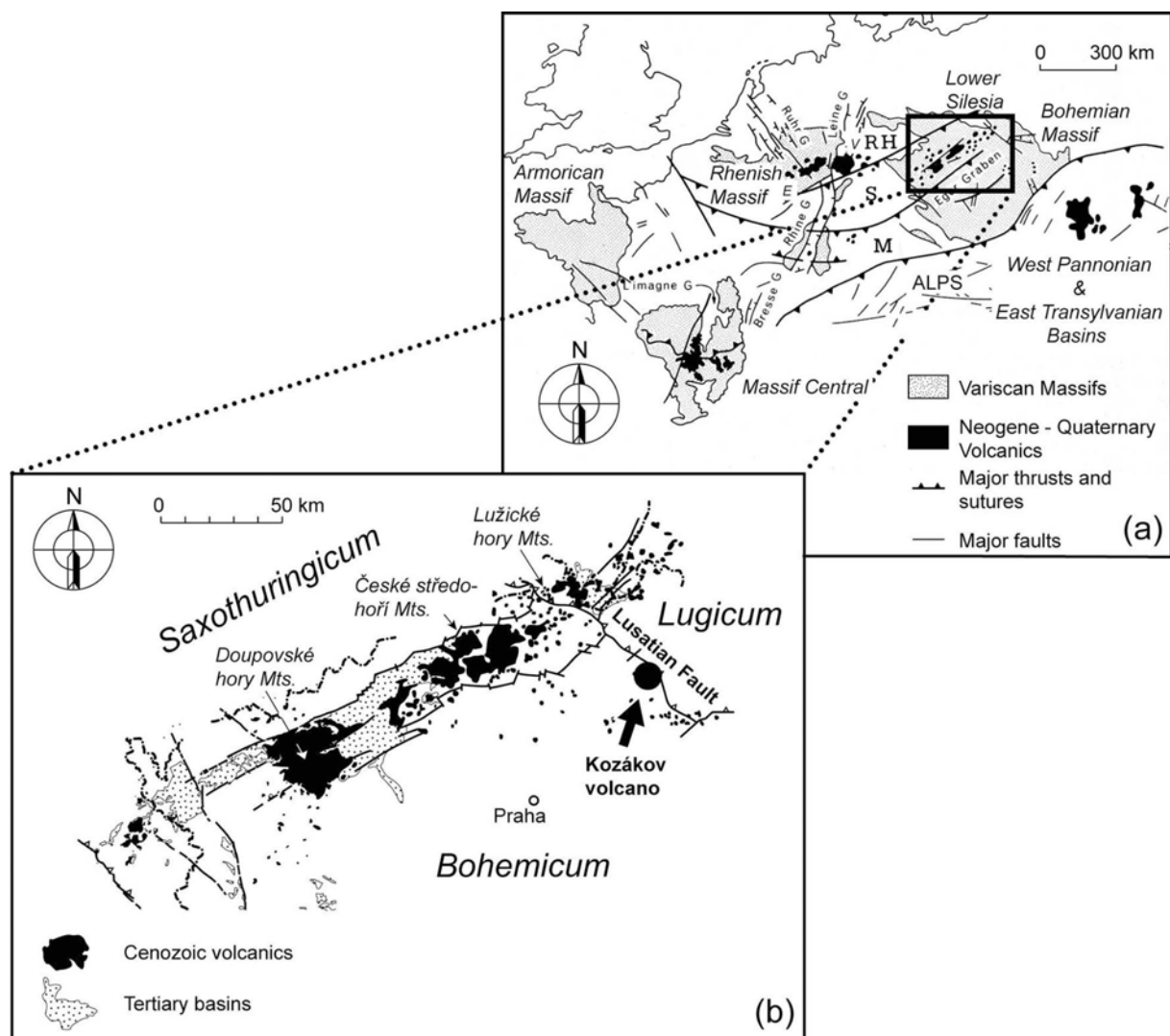


Fig. 1 (a) The distribution of Variscan massifs, Variscan tectonostratigraphic terranes, and Tertiary to Quaternary volcanic rocks in central Europe (RH, Rhenohercynian; S, Saxothuringian; M, Moldanubian; modified from Franke, 1989, and Wilson and Downes, 1991). (b) Simplified geologic map of the Ohre Graben and location of Kozákov volcano (modified from Christensen et al., 2001).

Late Cretaceous to Pleistocene intraplate volcanism in the Bohemian Massif is concentrated along the Ohře (Eger) Graben, which developed in late Eocene to sub-Recent time (Kopecký, 1986), and along the Labe Tectono-Volcanic Zone, which coincides approximately with the Lusatian (Lužice) fault (Fig. 1). Four episodes of alkaline magmatism are recognized in this region, one prior to development of the Ohře rift, and three related to rifting (Ulrych et al., 1999). The pre-rift volcanic rocks were erupted from late Cretaceous to middle Eocene times (79-49 Ma), whereas the syn-rift volcanic rocks were erupted during the late Eocene to early Miocene (43-16 Ma), middle Miocene to late Miocene (13-9 Ma), and Plio-Pleistocene (6-0.26 Ma).

Three major lithospheric blocks are juxtaposed along the Ohře Graben and Lusatian fault: the Saxothuringicum on the north, Bohemicum on the south and Lugicum on the east (Fig. 1). The Saxothuringicum in the vicinity of the rift consists of a polymetamorphic complex, locally containing eclogite and garnet peridotite, and late Variscan granitoids; the Bohemicum is composed of an anchimetamorphic Proterozoic basement and Lower Cambrian to Middle Devonian sedimentary cover; and the Lugicum is a complex mosaic, predominantly of metamorphic rocks, locally including eclogite and garnet peridotite, subordinate Cambrian to Carboniferous sedimentary rocks, and extensive Variscan granitoids. In addition to crustal distinctions between the three lithospheric blocks, the orientations of anisotropic structures in lithospheric mantle are different in each (Plomerová et al., 2005).

Kozákov volcano is situated along the Lusatian fault system (Fig. 1) about 45 km from the Litoměřice deep fault, which bounds the Ohře Graben on the south, and presumably taps mantle along the Lugicum-Bohemicum boundary. The crust diminishes in thickness from 40 km beneath the central Bohemian Massif to 31 km beneath the Ohře Graben and 32 km beneath Kozákov (Čermák et al., 1991). Seismic velocity-depth profiles for crust in the Bohemicum and Lugicum blocks on either side of Kozákov reveal a relatively high-velocity layer (6.9 km/s) at the base of the crust (Čermák, 1989) that may represent the crystallized products of underplated magma. The lithosphere also decreases in thickness from 140 km in the central Bohemian Massif to 90 km beneath the Ohře rift (Čermák et al., 1991; Babuška and Plomerová, 1992).

2.3. KOZÁKOV XENOLITHS

Mantle xenoliths were collected at Kozákov volcano from three quarries: Chuchelna, Slap, and Smrčí. Exposed in each of the quarries are two Early Pliocene nepheline basanite lava flows, whose ages are 3.95 Ma (upper flow) and 4.14 Ma (lower flow) (Šibrava and Havlíček, 1980). The sample suite was collected from the lower flow, which is notable for containing the highest concentration and largest size of mantle xenoliths among the many xenolith-bearing alkali basalts of the Bohemian Massif.

2.3.1. Lithology

The nepheline basanite lava flow at Kozákov contains abundant mantle xenoliths and rare, lower crustal xenoliths of olivine gabbonorite (Fediuk, 1971). Mantle xenoliths make up 2-3% of the lava

flow, and olivine xenocrysts account for another 7-8%. Peridotite xenoliths are commonly 6-10 cm in diameter and rarely up to 70 cm; larger xenoliths are spheroidal to ellipsoidal in shape, and smaller ones tend to be subangular. The Kozákov mantle suite is anhydrous and consists of variable proportions of olivine, orthopyroxene, clinopyroxene and spinel. Spinel lherzolite is the predominant rock type in the mantle suite and is the focus of this investigation. Also found in the mantle suite are subordinate amounts of harzburgite and dunite, and, rarely, websterite, olivine clinopyroxenite, clinopyroxenite and orthopyroxenite (Fediuk, 1994).

2.3.2. Texture

Two principal textural varieties of lherzolite occur at Kozákov [following the classification scheme of Mercier and Nicolas (1975)]: medium-grained equigranular lherzolite, which contains discrete, intergranular spinel (Fig. 2a-c, g and h), and coarse- to very coarse-grained protogranular lherzolite, in which spinel occurs only in symplectic intergrowth with orthopyroxene and clinopyroxene (Fig. 2d-f). In both textural types small amounts of very fine-grained plagioclase, clinopyroxene and Al-rich spinel occur locally at spinel-pyroxene boundaries, as a result of incipient partial melting and subsequent quenching during eruption. No samples with porphyroclastic texture have been found so far at Kozákov.

In equigranular lherzolite, mineral grains are 1-4mm in diameter, mosaic and triple-junction grain boundaries are common, and spinel occurs as discrete, dispersed grains (Fig. 2a, c, g and h). Most samples have a weak foliation and are devoid of phase layering, except for sample 95KZS4 (36 km), which displays prominent spinel layering and is a dunite, rather than a lherzolite (Fig. 2b).

Protogranular lherzolite is characterized by large grains (in some cases up to 2 cm in diameter), curvilinear grain boundaries, and prominent domains of spinel-pyroxene symplectite (Fig. 2d-f). Based on the reconstructed bulk chemical composition of the symplectites, Medaris et al. (1997) demonstrated that the symplectite represents the product of reaction between pre-existing garnet and matrix olivine.

A previous investigation by Christensen et al. (2001) indicated that the sub-Kozákov lithosphere is layered, consisting of a lower temperature equigranular layer at a depth of 32-43 km, an intermediate protogranular layer at 43-67 km, and a higher temperature equigranular layer below 67 km. This layered structure is thought to be inherited from Variscan orogenesis, during which garnet peridotite was tectonically injected into spinel peridotite. Subsequently, Neogene underplating and heating of the upper lithospheric mantle promoted recrystallization of the metastable garnet peridotite to spinel peridotite, in which the former presence of garnet is indicated by prominent spinel-pyroxene symplectites (Medaris et al., 1997).

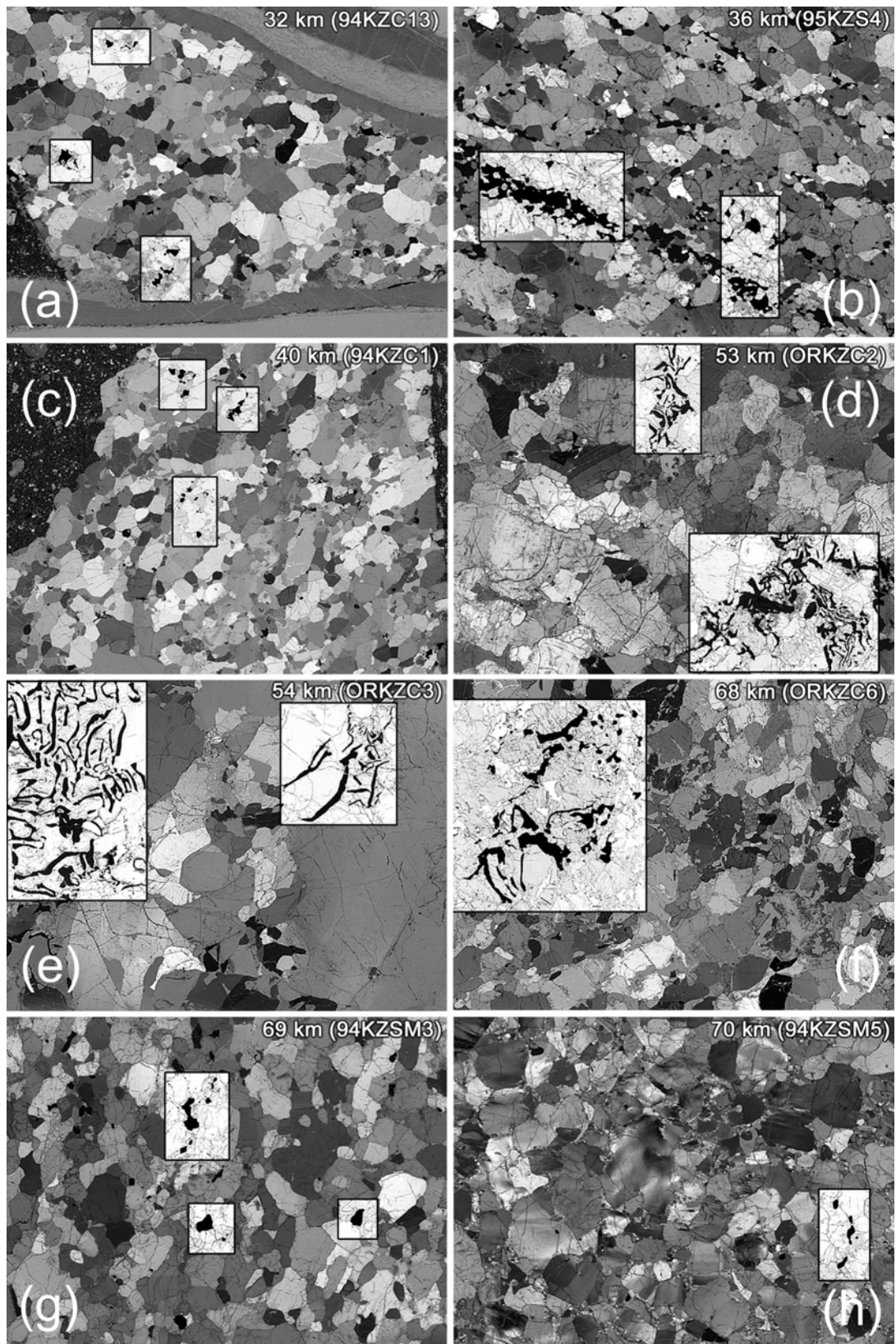


Fig. 2 Photomicrographs of representative Kozákov mantle xenoliths, arranged in order of increasing depth (partly crossed polarizers; insets with plane polarized light; width of field is 2 cm in each photomicrograph). The textural types are: (a) and (c), equigranular with discrete spinel, upper layer; (b), equigranular dunite with layered, discrete spinel, upper layer; (d)-(f), protogranular with symplectite spinel, middle layer; (g)-(h), equigranular with discrete spinel, lower layer.

2.4. ANALYTICAL METHODS

Rock samples were crushed manually and then powdered using an agate mortar. Whole-rock major element analyses (wet chemistry technique) and trace-element analyses (by inductively coupled plasma mass spectrometry; ICP-MS) were performed at the Faculty of Science, Charles University, Prague. Replicate analyses of international reference whole-rock material (PCC-1; USGS) by the wet chemistry technique yield an average error (1σ) for whole-rock analyses of $\pm 5\%$ (Table 1). Trace element ICP-MS analysis followed the methods of Strnad et al. (2005), and analysis of international peridotite reference material UB-N (CNRS) yields an average precision better than 11% for all corresponding elements (Table 1) with respect to recommended values (Govindaraju, 1989).

Clinopyroxene separates were obtained by hand-picking under a binocular microscope and subsequently acid-leached in hot HCl. The REE were extracted using ion exchange columns and then analyzed by ICP-MS.

Analyses of major elements in minerals from 21 xenoliths, which were utilized, but not tabulated, by Christensen et al. (2001), were obtained by Medaris by electron microprobe analysis (EMPA) using a CAMECA SX 50 system at the University of Wisconsin-Madison. Analytical conditions were an accelerating voltage of 15 kV, a beam current of 20 nA, and a beam diameter of 2 mm. Synthetic and natural minerals were used as internal standards for corresponding elements, and data reduction was performed using the Phi-rho-z program of Armstrong (1988). Minerals in two additional samples were analyzed by Ackerman by EMPA using a CAMECA SX 100 system equipped with a wavelength-dispersive spectrometry (WDS) analyzer at the Institute of Geology, Academy of Sciences of the Czech Republic, Prague. Analytical conditions were 15 kV accelerating voltage, 10 nA beam current and 2 mm beam diameter. Synthetic and natural minerals were used as standards, and data reduction was performed using the Merlet data reduction program (Merlet, 1994).

Clinopyroxene separates for Nd and Sr isotope analysis were prepared as described by Beard et al. (1992). Sample sizes ranged from 20 to 100 mg, and samples were spiked with Rb-Sr and Sm-Nd tracers for concentration and isotopic analyses prior to dissolution. Sample dissolution, chemical, and mass analysis procedures follow those of Johnson and Thompson (1991); all chemical separations and mass analyses were performed in the Radiogenic Isotope Laboratory at the University of Wisconsin-Madison. Strontium isotope compositions were measured by thermal ionization mass spectrometry (TIMS) with a Micromass Sector 54 instrument using a three-jump dynamic multi-collector analysis; $^{87}\text{Sr}/^{86}\text{Sr}$ isotope ratios were exponentially normalized to $^{86}\text{Sr}/^{88}\text{Sr} = 0.1194$. Using this analysis method, the measured $^{87}\text{Sr}/^{86}\text{Sr}$ of NBS-987 was 0.710268 ± 14 (2 SD, $n=9$) during the course of this study. Laboratory blanks were typically ~ 350 pg for Sr and < 150 pg for Rb, which are negligible. Neodymium was analyzed as NdO^+ using single Re filaments and silica gel and phosphoric acid as the oxygen source, and $^{18}\text{O}/^{16}\text{O}$ and $^{17}\text{O}/^{16}\text{O}$ ratios of 0.002110 and 0.000387, respectively, were used to correct the data. Mass analysis was performed by TIMS using a Sector 54 instrument via a three-jump multicollector dynamic analysis and a power-law normalization to $^{146}\text{Nd}/^{144}\text{Nd} = 0.7219$. During the course of this study, the measured

$^{143}\text{Nd}/^{144}\text{Nd}$ of the BCR-1 USGS rock standard was 0.512643 ± 9 (2 SD, $n=2$), and this is taken to be equal to present-day CHUR (e.g. Jacobsen and Wasserburg, 1980). Laboratory blanks were ~ 150 pg for Nd and < 40 pg for Sm, which are negligible.

Table 1. Results for whole-rock (wet method) and trace element (ICP-MS) analyses of reference materials

	PCC-1 peridotite	SD (1σ)	Reference value
SiO ₂	41.24	1.02	41.71
TiO ₂	<0.01		0.01
Al ₂ O ₃	0.61	0.02	0.68
Fe ₂ O ₃ ^a	8.31	0.24	8.25
MnO	0.11	0.00	0.12
MgO	43.34	0.72	43.43
CaO	0.50	0.02	0.52
Na ₂ O	0.02	0.00	0.03
K ₂ O	0.01	0.00	0.01
P ₂ O ₅	<0.01		0.00
H ₂ O+	4.90	0.25	4.71
H ₂ O-	0.31	0.01	0.44
CO ₂	0.17	0.01	0.15
Total	99.04	0.82	100.06
	UB-N peridotite	SD (1σ)	Reference value
Sc	13.8	1.72	13
V	75.2	7.61	75
Co	100.3	1.33	100
Ni	1970	69.51	2000
Cu	28.2	1.26	28
Zn	80.9	1.83	85
Rb	3.31	0.05	4
Sr	8.24	0.54	9
Y	2.42	0.04	2.5
Zr	5.23	0.69	4
Nb	0.07	0.04	0.05
Cs	10.66	0.12	10
Ba	25.1	0.83	27
La	0.33	0.002	0.35
Ce	0.8	0.012	0.8
Pr	0.11	0.006	0.12
Nd	0.59	0.038	0.6
Sm	0.22	0.016	0.2
Eu	0.08	0.006	0.08
Gd	0.29	0.084	0.3
Tb	0.06	0.004	0.06
Dy	0.42	0.011	0.38
Ho	0.09	0.004	0.09
Er	0.28	0.008	0.28
Tm	0.044	0.002	0.045
Yb	0.29	0.032	0.28
Lu	0.042	0.005	0.045
Hf	0.15	0.05	0.1
Pb	12.6	2.00	13
Th	0.08	0.03	0.07
U	0.07	0.02	0.07

^a Fe₂O₃ calculated from FeO and Fe₂O₃ concentrations

Table 2. Results of electron microprobe analysis (wt % oxides) of olivine, orthopyroxene, clinopyroxene and spinel from Kozákov mantle xenoliths

Olivine												
Sample	94KZC13	94KZS4	95KZS4	94KZC4	94KZC1	94KZC8	ORKZC7	KS2	94KZSM1	ORKZS5	95KZS3	ORKZC2
Texture	E	E	LE	E	E	E	P	P	P	P	P	P
SiO ₂	40.81	41.05	40.61	40.82	40.95	40.94	41.01	41.15	40.72	40.73	40.72	40.79
FeO	8.56	8.62	11.27	8.30	8.06	8.16	8.36	8.26	9.35	8.93	8.81	9.11
MnO	0.12	0.15	0.17	0.12	0.11	0.12	0.14	0.12	0.12	0.14	0.14	0.14
MgO	49.53	49.74	47.46	50.02	49.94	49.75	50.01	49.87	49.20	49.50	49.58	49.79
NiO	0.38	0.41	0.37	0.40	0.40	0.40	0.38	0.37	0.38	0.37	0.44	0.43
CaO	0.06	0.08	0.05	0.05	0.05	0.05	0.05	0.03	0.05	0.05	0.05	0.05
Total	99.47	100.05	99.93	99.71	99.51	99.41	99.95	99.80	99.82	99.72	99.74	100.31
Mg#	91.2	91.1	88.2	91.5	91.7	91.6	91.4	91.5	90.4	90.8	90.9	90.7

Olivine											
Sample	ORKZC3	94KZS1	KS4	ORKZS6	94KZSM6	94KZC16	94KZSM4	ORKZC6	94KZSM3	94KZSM5	94KZSM7
Texture	P	P	P	P	P	P	E	P	E	E	E
SiO ₂	40.65	40.76	41.25	40.68	40.78	40.95	40.83	40.57	40.64	40.70	41.07
FeO	8.71	8.97	9.15	9.02	8.85	9.03	8.61	9.55	9.29	8.96	9.40
MnO	0.14	0.15	0.15	0.12	0.10	0.15	0.14	0.15	0.15	0.13	0.13
MgO	49.59	49.42	49.42	49.31	49.37	49.75	49.32	49.10	48.90	49.22	49.96
NiO	0.46	0.38	0.21	0.39	0.42	0.39	0.39	0.41	0.42	0.39	0.42
CaO	0.05	0.05	0.07	0.05	0.05	0.05	0.05	0.05	0.05	0.05	0.05
Total	99.60	99.73	100.25	99.57	99.58	100.32	99.34	99.83	99.44	99.45	101.03
Mg#	91.0	90.8	90.6	90.7	90.9	90.8	91.1	90.2	90.4	90.7	90.5

Orthopyroxene												
Sample	94KZC13	94KZS4	95KZS4	94KZC4	94KZC1	94KZC8	ORKZC7	KS2	94KZSM1	ORKZS5	95KZS3	ORKZC2
Texture	E	E	LE	E	E	E	P	P	P	P	P	P
SiO ₂	56.65	56.46	55.51	56.55	56.83	56.64	56.39	56.79	55.74	55.31	55.70	55.44
TiO ₂	0.03	0.04	0.11	0.08	0.01	0.02	0.03	0.03	0.04	0.04	0.04	0.02
Al ₂ O ₃	2.32	2.28	3.16	2.75	2.15	2.13	2.89	2.49	3.53	3.87	3.68	4.05
Cr ₂ O ₃	0.47	0.46	0.41	0.47	0.43	0.45	0.48	0.32	0.52	0.54	0.56	0.50
FeO	5.70	5.70	7.62	5.50	5.41	5.37	5.51	5.31	6.17	5.92	5.69	5.99
MnO	0.14	0.19	0.18	0.15	0.13	0.14	0.14	0.13	0.14	0.12	0.13	0.14
MgO	34.52	33.80	32.51	34.58	34.60	34.53	34.30	34.51	33.74	33.62	33.27	33.56
CaO	0.36	0.85	0.48	0.43	0.51	0.53	0.62	0.43	0.67	0.68	0.75	0.78
Na ₂ O	0.00	0.03	0.01	0.01	0.03	0.00	0.03	0.03	0.02	0.05	0.07	0.06
Total	100.18	99.79	99.99	100.50	100.10	99.81	100.39	100.04	100.55	100.17	99.88	100.54
Mg #	91.5	91.4	88.4	91.8	91.9	92.0	91.7	92.1	90.7	91.0	91.3	90.9
Cr #	12.0	12.0	8.0	10.3	11.8	12.5	10.1	7.9	8.9	8.6	9.3	7.6

(continued)

Table 2. Continued

Orthopyroxene											
Sample	ORKZC3	94KZS1	KS4	ORKZS6	94KZSM6	94KZC16	94KZSM4	ORKZC6	94KZSM3	94KZSM5	94KZSM7
Texture	P	P	P	P	P	P	E	P	E	E	E
SiO ₂	55.61	55.29	55.78	54.92	55.33	55.04	55.19	54.92	54.72	55.51	54.21
TiO ₂	0.04	0.05	0.07	0.03	0.10	0.06	0.09	0.07	0.07	0.10	0.08
Al ₂ O ₃	3.78	4.39	3.94	4.74	4.23	4.54	4.26	4.95	4.88	3.55	5.44
Cr ₂ O ₃	0.52	0.44	0.57	0.44	0.59	0.54	0.64	0.49	0.60	0.80	0.50
FeO	5.74	5.88	5.83	5.91	5.73	5.85	5.41	5.95	5.91	5.63	6.15
MnO	0.12	0.14	0.14	0.15	0.11	0.15	0.15	0.11	0.12	0.15	0.14
MgO	33.91	33.42	33.21	32.63	32.73	33.09	32.99	32.60	32.47	33.27	32.67
CaO	0.80	0.81	0.76	0.90	0.93	0.94	0.94	1.03	1.01	1.12	1.02
Na ₂ O	0.04	0.06	0.06	0.09	0.10	0.13	0.09	0.11	0.13	0.08	0.12
Total	100.56	100.47	100.36	99.81	99.85	100.33	99.76	100.23	99.92	100.21	100.34
Mg #	91.3	91.0	91.0	90.8	91.1	91.0	91.6	90.7	90.7	91.3	90.4
Cr #	8.4	6.3	8.8	5.9	8.6	7.4	9.2	6.2	7.7	13.1	5.8

Clinopyroxene												
Sample	94KZC13	94KZS4	95KZS4	94KZC4	94KZC1	94KZC8	ORKZC7	KS2	94KZSM1	ORKZS5	95KZS3	ORKZC2
Texture	E	E	LE	E	E	E	P	P	P	P	P	P
SiO ₂	54.67	53.91	52.02	53.32	53.45	53.71	53.54	53.45	52.85	52.36	52.69	52.52
TiO ₂	0.04	0.08	0.38	0.21	0.03	0.01	0.06	0.04	0.08	0.21	0.11	0.05
Al ₂ O ₃	0.84	2.05	4.43	2.77	2.45	2.57	3.20	3.21	3.79	4.50	4.49	4.54
Cr ₂ O ₃	0.16	0.84	0.90	0.96	0.96	0.98	0.92	0.68	0.84	1.00	0.98	0.78
FeO	1.56	1.76	2.85	1.70	1.88	1.75	2.27	2.26	2.67	2.77	2.65	2.93
MnO	0.05	0.06	0.09	0.07	0.07	0.08	0.07	0.06	0.10	0.08	0.08	0.08
MgO	17.75	16.77	15.36	16.82	16.84	16.81	16.62	16.67	16.63	16.18	16.13	16.53
CaO	24.70	23.87	22.96	23.80	23.38	23.27	22.56	22.23	22.42	21.78	21.37	21.73
Na ₂ O	0.11	0.51	0.76	0.43	0.46	0.57	0.80	0.91	0.66	0.89	1.02	0.79
Total	99.86	99.85	99.75	100.08	99.51	99.75	100.04	99.51	100.03	99.77	99.52	99.95
Mg #	95.3	94.5	90.6	94.6	94.1	94.5	92.9	92.9	91.7	91.2	91.6	91.0
Cr #	11.2	21.5	12.0	18.8	20.8	20.4	16.2	12.4	13.0	13.0	12.7	10.3

Clinopyroxene											
Sample	ORKZC3	94KZS1	KS4	ORKZS6	94KZSM6	94KZC16	94KZSM4	ORKZC6	94KZSM3	94KZSM5	94KZSM7
Texture	P	P	P	P	P	P	E	P	E	E	E
SiO ₂	52.48	52.46	52.54	52.08	52.39	52.48	52.51	52.23	52.07	52.46	51.68
TiO ₂	0.09	0.08	0.25	0.15	0.28	0.20	0.25	0.20	0.19	0.27	0.26
Al ₂ O ₃	4.41	4.98	4.83	5.66	5.34	5.50	5.29	5.98	5.99	4.30	6.54
Cr ₂ O ₃	0.83	0.74	1.02	0.77	1.80	0.95	1.11	0.85	1.01	1.38	0.79
FeO	2.68	2.88	2.94	2.98	2.93	2.85	2.76	3.00	3.14	2.95	3.39
MnO	0.05	0.10	0.07	0.07	0.09	0.10	0.07	0.08	0.12	0.10	0.09
MgO	16.71	16.38	16.14	16.11	15.99	16.33	16.24	16.36	16.10	17.02	16.11

(continued)

Table 2. Continued

Clinopyroxene											
Sample	ORKZC3	94KZS1	KS4	ORKZS6	94KZSM6	94KZC16	94KZSM4	ORKZC6	94KZSM3	94KZSM5	94KZSM7
Texture	P	P	P	P	P	P	E	P	E	E	E
CaO	21.73	21.31	20.85	20.62	20.22	20.17	20.07	20.05	19.52	20.14	19.38
Na ₂ O	0.81	0.93	1.08	1.10	1.22	1.15	1.19	1.15	1.32	0.96	1.30
Total	99.79	99.86	99.72	99.53	100.27	99.72	99.49	99.90	99.45	99.58	99.54
Mg #	91.7	91.0	90.7	90.6	90.7	91.1	91.3	90.7	90.1	91.1	89.4
Cr #	11.2	9.0	12.4	8.3	18.4	10.3	12.3	8.7	10.2	17.7	7.5

Spinel												
Sample	94KZC13	94KZS4	95KZS4	94KZC4	94KZC1	94KZC8	ORKZC7	KS2	94KZSM1	ORKZS5	95KZS3	ORKZC2
Texture	E	E	LE	E	E	E	P	P	P	P	P	P
TiO ₂	0.04	0.06	0.18	0.05	0.02	0.02	0.06	0.02	0.06	0.17	0.08	0.03
Al ₂ O ₃	35.48	33.70	43.97	41.39	31.83	32.90	40.76	44.23	44.35	42.99	45.66	49.14
Cr ₂ O ₃	30.91	34.13	20.87	26.71	35.83	35.86	26.41	22.57	21.50	22.73	21.09	16.74
V ₂ O ₃	0.11	0.21	0.14	0.10	0.16	0.12	0.10	0.11	0.14	0.09	0.09	0.10
FeO	16.19	14.89	18.59	11.73	15.38	13.55	14.21	13.15	14.86	15.23	13.12	13.95
MnO	0.18	0.14	0.18	0.14	0.14	0.00	0.15	0.01	0.14	0.11	0.13	0.12
MgO	16.15	16.15	15.59	18.69	15.72	16.51	17.74	18.67	18.08	18.16	18.70	19.03
ZnO	0.24	0.22	0.14	0.19	0.27	0.27	0.15	0.13	0.18	0.09	0.11	0.12
NiO	0.19	0.15	0.25	0.18	0.18	0.16	0.29	0.26	0.29	0.30	0.45	0.37
Total	99.48	99.65	99.93	99.19	99.52	99.38	99.87	99.15	99.59	99.85	99.43	99.60
Mg #	70.0	70.3	65.3	78.1	69.3	72.0	74.4	77.1	74.9	75.0	77.0	77.1
Cr #	36.9	40.5	24.1	30.2	43.0	42.2	30.3	25.5	24.5	26.2	23.7	18.6

Spinel											
Sample	ORKZC3	94KZS1	KS4	ORKZS6	94KZSM6	94KZC16	94KZSM4	ORKZC6	94KZSM3	94KZSM5	94KZSM7
Texture	P	P	P	P	P	P	E	P	E	E	E
TiO ₂	0.04	0.03	0.11	0.06	0.22	0.12	0.20	0.10	0.14	0.44	0.12
Al ₂ O ₃	46.86	50.79	43.86	52.92	44.54	48.99	44.34	53.96	49.23	33.12	53.36
Cr ₂ O ₃	19.46	15.26	22.52	13.77	21.57	17.82	22.34	13.36	17.08	32.65	12.57
V ₂ O ₃	0.08	0.06	0.11	0.06	0.09	0.09	0.11	0.08	0.09	0.20	0.08
FeO	13.43	12.92	13.91	11.54	13.56	11.58	13.03	11.56	12.71	15.42	12.28
MnO	0.12	0.07	0.00	0.09	0.13	0.14	0.00	0.10	0.13	0.11	0.13
MgO	19.13	19.88	18.54	20.39	18.84	19.90	18.84	20.24	19.51	17.21	20.52
ZnO	0.10	0.10	0.11	0.12	0.06	0.14	0.14	0.10	0.12	0.05	0.12
NiO	0.40	0.34	0.32	0.39	0.33	0.37	0.31	0.39	0.38	0.28	0.40
Total	99.62	99.45	99.48	99.32	99.34	99.15	99.31	99.89	99.38	99.50	99.57
Mg #	78.1	79.6	76.4	81.0	77.4	80.5	77.4	79.8	78.8	73.9	81.2
Cr #	21.8	16.8	25.6	14.9	24.5	19.6	25.3	14.2	18.9	39.8	13.6

2.5. GEOTHERMOMETRY, THERMAL HISTORY, AND DEPTH ESTIMATES

The mineral compositions originally determined by Medaris were discussed, but not tabulated, by Christensen et al. (2001); these compositions and our new mineral analyses are given in Table 2. Temperatures were calculated for several domains in each sample using three calibrations of the two-pyroxene geothermometer (Bertrand and Mercier, 1985; Brey and Köhler, 1990; Taylor, 1998), the Al-in-orthopyroxene geothermometer (Witt-Eickschen and Seck, 1991), and the olivine-spinel Mg-Fe²⁺ exchange geothermometer (Ballhaus et al., 1991). In general, there is good agreement between the different methods (Table 3), reflecting equilibrium distribution of most elements between coexisting olivine, orthopyroxene, clinopyroxene, and spinel at the time of exhumation in the host basalt [see Medaris et al. (1999) for a detailed comparison of results].

Table 3. Model temperatures and depths for Kozákov mantle xenoliths and comparison of results from various geothermometers at P = 15 kbar

Sample	Texture	model T, °C	model depth km	2Px	2Px	2Px	Al-in-Opx	OlSpl
				[BM85]	[BK 90]	[T98]	[WS91]	[BBG91]
94KZC13	E	679	32	683	657	686	905	838
94KZS4	E	692	33	695	686	690	904	863
95KZS4	LE	726	36	728	763	744	918	760
94KZC4	E	749	37	751	753	750	920	973
94KZC1	E	785	40	787	802	796	886	833
94KZC8	E	790	41	792	803	794	893	885
ORKZC7	P	837	45	837	875	853	934	866
KS2	P	847	46	847	886	852	859	892
94KZSM1	P	874	48	874	921	907	973	903
ORKZS5	P	896	50	895	951	922	1000	906
95KZS3	P	921	53	920	972	941	1003	914
ORKZC2	P	928	53	926	983	962	993	887
ORKZC3	P	933	54	931	981	954	986	937
94KZS1	P	952	56	950	1005	980	983	964
KS4	P	967	58	964	1022	983	1012	949
ORKZS6	P	989	60	985	1040	1009	1006	1001
94KZSM6	P	1023	64	1017	1070	1025	1037	959
94KZC16	P	1040	66	1033	1078	1044	1032	1033
94KZSM4	E	1041	66	1034	1082	1040	1056	939
ORKZC6	P	1053	68	1045	1091	1059	1030	966
94KZSM3	E	1063	69	1055	1105	1065	1072	981
94KZSM5	E	1068	70	1059	1103	1061	1081	1030
94KZSM7	E	1072	70	1064	1116	1078	1055	1037

P, protogranular; E, equigranular; LE, layered equigranular

In particular, results from the three versions of the two-pyroxene geothermometer are in good agreement (Fig. 3a). Bertrand and Mercier (1985) temperatures for the entire peridotite xenolith suite range continuously from 685 °C to 1065 °C (at $P = 15$ kbar), but the two different textural types of xenolith fall into three groups according to temperature (Fig. 3a): low-temperature equigranular (685–790 °C), medium-temperature protogranular (835–1045 °C), and high-temperature equigranular (1035–1065 °C). It is unlikely that this temperature grouping is due to the effect of grain size on blocking temperatures, because some medium-grained equigranular samples yield higher temperatures than coarse-grained protogranular samples. The 10 °C overlap in temperature estimates for the protogranular and high-temperature equigranular groups is within the estimated precision of the two-pyroxene geothermometers (~ 20 °C) and may not reflect a true overlap in temperatures for the two groups.

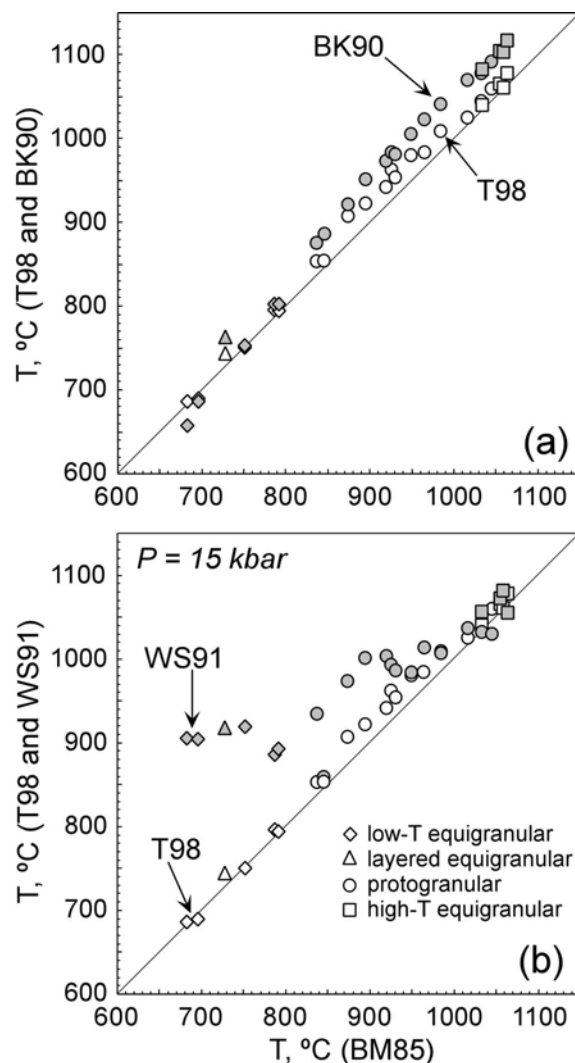


Fig. 3 (a) Comparison of temperature estimates ($P = 15$ kbar) from the Bertrand and Mercier (1985), Taylor (1998) and Brey and Köhler (1990) two-pyroxene geothermometers. (b) Comparison of temperature estimates ($P = 15$ kbar) from the Bertrand and Mercier (1985) and Taylor (1998) two-pyroxene geothermometers and the Witt-Eickschen and Seck (1991) Al-in-orthopyroxene geothermometer.

In the absence of a viable geobarometer for spinel peridotites, extraction depths for a suite of spinel peridotite xenoliths may be estimated from the intersection of temperature determined using an appropriate geothermometer with the estimated geotherm at the time of exhumation. Following this procedure, depths for the Kozákov mantle xenoliths have been estimated by combining temperatures from the Bertrand and Mercier (1985) two-pyroxene geothermometer (taking into account the pressure dependence of the geothermometer) with a model geotherm at 5 Ma, based on a magmatic underplating scenario, whose thermal evolution is summarized in Fig. 4 and the details of which have been given by Christensen et al. (2001). Apart from the choice of boundary conditions for the underplating model, a precision of $\pm 20^\circ\text{C}$ in the two-pyroxene geothermometer translates to an uncertainty of ± 4 km at a depth of 50 km. For the purposes of plotting, however, depth estimates for each sample are cited to the nearest kilometre (Table 3).

This approach suggests that the Kozákov xenoliths were derived from depths ranging from 32 km, near the crust-mantle boundary, to 70 km, representing $\sim 65\%$ of the lithospheric mantle. In addition, it appears that the sub-Kozákov lithosphere is layered, consisting of an upper equigranular layer from 32 to 43 km, an intermediate protogranular layer from 43 to ~ 67 km, and a lower equigranular layer below ~ 67 km (Fig. 4), as previously noted by Christensen et al. (2001).

The approximation of the boundary at 67 km arises from the overlap in estimated temperature for the highest temperature protogranular sample and the lowest temperature equigranular sample from the lower layer. The depth estimates for these samples are consistent with the presence of spinel as the principal aluminous phase in the xenoliths, rather than garnet, as predicted from the measured spinel compositions and experimental determination of the spinel-garnet phase transition (O'Neill, 1981).

Two petrological lines of evidence support the veracity of the underplating model for Kozákov and its use in estimating depths. The model predicts that shallow mantle will experience greater heating and faster cooling than the deeper mantle. These phenomena are reflected by the presence of thin exsolution lamellae in pyroxene in the low-temperature equigranular samples, but their absence in higher temperature protogranular and equigranular samples. Further support is provided by results from the Al-in-orthopyroxene (Witt-Eickschen and Seck, 1991) and two-pyroxene (Bertrand and Mercier, 1985) geothermometers, which are comparable above 950°C , but increasingly diverge at lower temperatures (Fig. 3b). Such divergence is probably due to the difference in blocking temperatures for Al (slower diffusion) and Ca-Mg (faster diffusion) in shallow, rapidly cooled pyroxene, compared with deeper, more slowly cooled pyroxene.

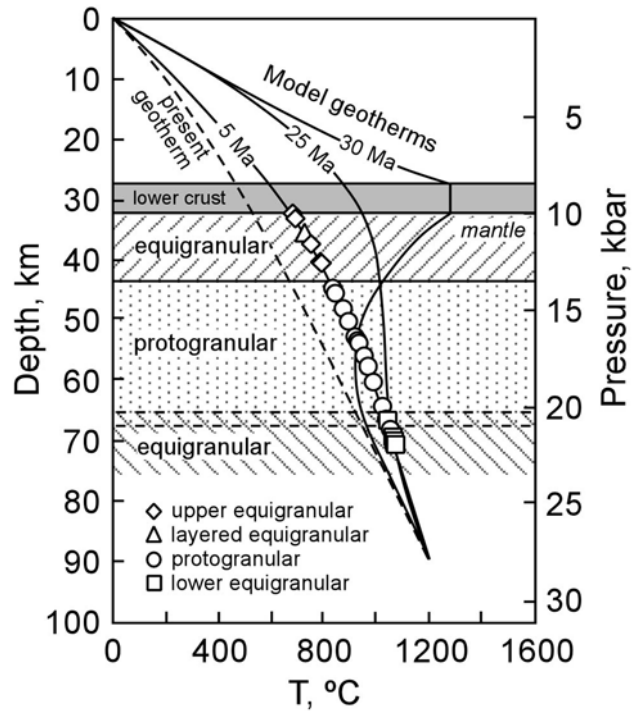


Fig. 4 Depth estimates for the Kozákov xenoliths and model geotherms, based on an underplating scenario (after Christensen et al., 2001); see text for discussion. Depth estimates for the xenoliths are obtained by combining the loci of two-pyroxene temperatures (Bertrand and Mercier, 1985) with the 5 Ma model geotherm (the time of eruption).

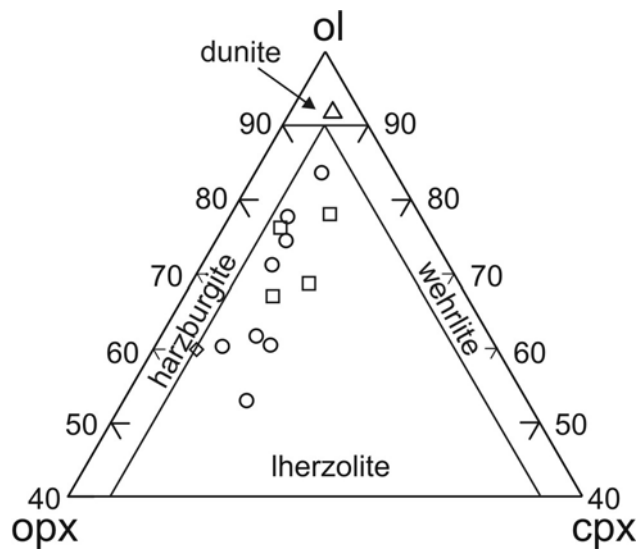


Fig. 5 Modal compositions of investigated Kozákov mantle xenoliths, calculated using the mass-balance method of Albarède (1995) (symbols as in Fig. 3). Plot was made using GCDkit software (Janoušek et al., 2003).

2.6. ROCK COMPOSITION

2.6.1. Modes

Modal compositions (Fig. 5, Table 4) of the Kozákov mantle xenoliths were determined by mass-balance calculations from the major element compositions of the whole-rocks (Table 4) and the constituent minerals (Table 2), using the least-squares inversion method of Albarède (1995). Of 14 analyzed rock samples, 12 are lherzolite, including eight protogranular samples from the intermediate layer and four equigranular samples from the lower layer (Fig. 5). The equigranular sample from the upper layer (33 km) plots on the boundary between harzburgite and lherzolite, and the layered equigranular sample (36 km) is dunite, which contains a larger proportion of clinopyroxene than orthopyroxene and has a high spinel content (~ 7%). Although these calculated modes are generally representative, they may not be very precise, because of the difficulty in obtaining fully representative whole-rock analyses of relatively coarse-grained, but small-sized samples.

2.6.2. Major elements

With the exception of the equigranular dunite (at 36 km), the analyzed Kozákov xenoliths (Table 4) are typical of depleted lithospheric mantle, with high Mg-numbers (88.8-91.0), relatively high Cr₂O₃ contents (0.38-1.37 wt %), and relatively low TiO₂ contents (0.03-0.17 wt %). In most samples the concentrations of SiO₂, TiO₂, Al₂O₃, and CaO exhibit negative correlations with MgO (Fig. 6), which are similar to those described from other localities in the CERS (Downes, 2001) and elsewhere (Yaxley et al., 1991; Griffin et al., 1998). Such negative correlations are commonly attributed to depletion of incompatible elements in the lithospheric mantle during partial fusion and melt extraction. The negative correlations of clinopyroxene mode with whole-rock Cr-number (Fig. 6) is also consistent with partial fusion and melt extraction.

The equigranular dunite (at 36 km) differs from the other samples in having a lower Mg-number (86.3), lower SiO₂, and higher FeO (Fig. 6), and by a higher spinel content (7.2%) and higher proportion of clinopyroxene relative to orthopyroxene (5.6% vs 3.2%). These features and the prominent layering of spinel suggest that the composition of this sample may largely reflect cumulate, rather than partial melting, processes.

One protogranular sample (ORKZS6; 60.1 km) is anomalous for containing less MgO and more Al₂O₃ than primitive mantle (Fig. 6). It is likely that the analyzed split of this coarse-grained and small-sized sample contained a high, and non-representative, content of spinel, which resulted in its discrepant MgO and Al₂O₃ contents and high calculated spinel mode (7%).

Table 4. Major and trace element compositions, and modes for Kozákov mantle xenoliths

Sample	94KZS4	95KZS4	ORKZC7A	KS2	94KZSM1	ORKZS5	ORKZC2
Quarry	Slap	Slap	Chuchelná	Smrčí	Smrčí	Slap	Chuchelná
Texture	E	LE	P	P	P	P	P
SiO ₂	45.56	38.24	42.92	43.42	44.82	44.34	44.56
TiO ₂	0.21	0.24	0.03	0.03	0.22	0.11	0.07
Al ₂ O ₃	1.81	3.11	1.75	1.12	2.41	2.96	2.45
Cr ₂ O ₃	1.37	1.57	0.90	0.50	0.91	1.09	0.65
Fe ₂ O ₃	2.24	3.59	1.24	1.84	2.79	1.42	1.85
FeO	5.89	8.64	6.52	6.70	6.30	6.72	6.55
MnO	0.13	0.16	0.12	0.12	0.13	0.13	0.13
MgO	41.40	42.01	43.29	44.32	40.53	40.54	39.89
CaO	1.46	1.26	1.67	1.51	1.79	2.54	2.69
Na ₂ O	0.10	0.04	0.18	0.13	0.06	0.26	0.18
K ₂ O	0.06	0.01	0.05	0.02	0.01	0.07	0.02
P ₂ O ₅	0.08	0.09	0.04	0.03	0.06	0.05	0.05
H ₂ O-	0.12	0.16	0.04	0.06	0.06	0.08	0.10
H ₂ O+	0.18	0.98	n.a.	n.a.	0.11	n.a.	n.a.
CO ₂	0.53	1.08	n.a.	n.a.	0.34	n.a.	n.a.
Total	101.09	101.02	98.75	99.80	100.36	100.31	99.19
<i>mg-number</i>	90.3	86.3	90.9	90.4	89.1	90.0	89.6
<i>cr-number</i>	33.7	25.3	25.6	23.0	20.2	19.8	15.1
Ni	1431	1780	2172	2101	2292	1957	1927
Cu	9.51	5.7	12.1	11.5	19.55	17.9	21.0
Rb	2.00	1.24	1.43	0.69	0.37	2.32	0.79
Sr	29.25	3.8	20.8	8.2	9.11	44.5	33.1
Zr	48.74	16.4	36.6	9.9	3.61	21.3	16.7
Nb	12.40	1.34	9.38	1.31	1.93	3.80	2.37
Cs	0.14	0.05	0.03	0.04	0.03	0.06	0.05
Ba	10.64	57	52	19	15.44	47	19
Hf	1.49	0.51	1.36	0.31	0.07	0.47	0.38
Th	6.16	0.23	0.80	0.28	0.07	0.47	0.48
U	1.27	0.09	0.09	0.12	0.12	0.11	0.11
Y	0.34	1.49	0.56	0.46	0.22	1.82	1.33
La	1.016	0.937	1.509	0.517	0.364	2.787	3.651
Ce	1.247	1.041	2.513	1.013	0.488	5.654	5.623
Pr	0.145	0.162	0.220	0.106	0.053	0.711	0.572
Nd	0.445	0.567	0.669	0.413	0.144	2.613	1.789
Sm	0.073	0.131	0.127	0.103	0.014	0.455	0.280
Eu	0.023	0.044	0.031	0.025	0.006	0.139	0.071
Gd	0.060	0.152	0.081	0.086	0.014	0.388	0.263
Tb	0.010	0.034	0.012	0.014	0.003	0.056	0.037
Dy	0.063	0.234	0.069	0.062	0.030	0.310	0.226
Ho	0.013	0.052	0.014	0.016	0.008	0.062	0.055
Er	0.040	0.163	0.063	0.067	0.030	0.174	0.154
Tm	0.007	0.024	0.014	0.012	0.005	0.033	0.026
Yb	0.052	0.180	0.086	0.079	0.045	0.183	0.224
Lu	0.010	0.029	0.020	0.017	0.008	0.036	0.033
Eu/Eu*	1.016	0.937	1.509	0.517	0.364	2.787	3.651
Ce _N /Yb _N	1.247	1.041	2.513	1.013	0.488	5.654	5.623
Ce _N /Sm _N	0.145	0.162	0.220	0.106	0.053	0.711	0.572
Eu* _N /Yb _N	0.445	0.567	0.669	0.413	0.144	2.613	1.789

(continued)

Table 4. Continued

Sample	94KZS4	95KZS4	ORKZC7A	KS2	94KZSM1	ORKZS5	ORKZC2
Quarry	Slap	Slap	Chuchelná	Smrčí	Smrčí	Slap	Chuchelná
Texture	E	LE	P	P	P	P	P
<i>Modal compositions</i>							
Ol	57.5	84.0	76.6	72.2	58.3	59.5	58.7
Opx	34.1	3.2	14.2	17.7	30.9	25.8	26.4
Cpx	5.0	5.6	7.4	7.2	7.7	11.1	12.4
Sp	3.4	7.2	1.8	2.8	3.2	3.7	2.5

Sample	ORKZC 3	KS4	ORKZS6	94KZSM4	94KZSM3	94KZSM5	94KZSM7
Quarry	Chuchelná	Smrčí	Slap	Smrčí	Smrčí	Smrčí	Smrčí
Texture	P	P	P	E	E	E	E
SiO ₂	41.72	43.98	43.42	42.48	43.74	43.47	43.41
TiO ₂	0.26	0.07	0.17	0.23	0.08	0.22	0.22
Al ₂ O ₃	0.95	1.94	5.65	2.09	2.85	0.95	2.46
Cr ₂ O ₃	0.38	0.68	1.21	0.77	0.71	0.64	0.47
Fe ₂ O ₃	2.39	1.76	2.44	2.40	2.56	9.08	2.45
FeO	6.98	6.77	6.19	6.19	6.65	n.a.	6.71
MnO	0.13	0.13	0.13	0.12	0.13	0.13	0.13
MgO	44.47	42.25	37.29	42.90	40.85	43.74	41.08
CaO	1.43	1.83	2.84	2.38	2.18	1.54	2.39
Na ₂ O	0.06	0.20	0.20	0.14	0.15	0.10	0.19
K ₂ O	0.02	0.05	0.13	0.01	0.03	0.02	0.04
P ₂ O ₅	0.06	0.06	0.05	0.06	0.04	0.04	0.07
H ₂ O-	0.14	0.08	0.24	0.08	0.10	0.15	0.12
H ₂ O+	0.16	n.a.	0.54	0.49	0.46	0.07	0.07
CO ₂	1.05	n.a.	0.13	0.02	0.03	n.a.	0.48
Total	99.99	99.80	100.63	100.20	100.56	100.30	100.17
<i>mg-number</i>	89.7	90.0	88.8	90.2	89.1	89.5	89.1
<i>cr-number</i>	21.2	19.0	12.6	19.8	14.3	31.1	11.4
Ni	2346	1901	1904	3394	1964	1979	2827
Cu	5.6	11.6	n.a.	26.14	n.a.	18.6	17.75
Rb	0.39	1.62	4.51	0.63	1.06	0.63	0.71
Sr	9.2	30.0	48.26	26.90	37.19	13.7	25.62
Zr	14.5	22.9	22.81	7.59	19.03	14.6	6.61
Nb	1.46	2.01	5.40	1.14	1.54	1.29	1.74
Cs	0.02	0.05	0.08	0.044	0.08	0.03	0.008
Ba	12	1000	14.01	8.37	42.80	40	11.48
Hf	0.36	0.52	0.51	0.15	0.43	0.49	0.18
Th	0.28	0.51	1.316	0.83	0.849	0.46	553
U	0.05	0.10	0.183	16.47	0.035	0.06	6.83
Y	0.25	1.17	1.404	0.61	1.88	1.29	2.04

(continued)

Table 4. Continued

Sample	ORKZC 3	KS4	ORKZS6	94KZSM4	94KZSM3	94KZSM5	94KZSM7
Quarry	Chuchelná	Smrčí	Slap	Smrčí	Smrčí	Smrčí	Smrčí
Texture	P	P	P	E	E	E	E
La	0.544	1.349	3.755	0.671	1.395	1.493	2.058
Ce	0.421	2.932	4.788	1.133	3.063	2.385	3.206
Pr	0.065	0.344	0.364	0.136	0.428	0.366	0.445
Nd	0.214	1.404	1.282	0.483	1.547	1.414	1.568
Sm	0.034	0.292	0.238	0.096	0.270	0.267	0.285
Eu	0.011	0.186	0.080	0.034	0.094	0.087	0.100
Gd	0.029	0.228	0.198	0.086	0.223	0.215	0.263
Tb	0.006	0.027	0.038	0.016	0.048	0.038	0.051
Dy	0.039	0.194	0.238	0.105	0.321	0.230	0.344
Ho	0.009	0.042	0.052	0.023	0.072	0.047	0.074
Er	0.032	0.126	0.166	0.074	0.217	0.139	0.227
Tm	0.005	0.021	0.025	0.011	0.033	0.021	0.033
Yb	0.042	0.167	0.181	0.092	0.220	0.166	0.236
Lu	0.008	0.022	0.030	0.015	0.036	0.025	0.037
Eu/Eu*	1.02	2.25	1.11	0.97	1.13	1.15	1.13
Ce _N /Yb _N	2.76	4.54	7.01	3.31	3.66	3.69	3.52
Ce _N /Sm _N	3.39	2.45	4.84	2.74	2.75	2.14	2.78
Eu* _N /Yb _N	0.70	1.43	1.14	0.99	1.04	1.31	1.05
Σ REE	1.45	7.33	11.44	2.96	7.97	6.89	8.92
<i>Modal compositions</i>							
Ol	82.2	69.8	49.0	76.0	65.1	75.5	67.1
Opx	9.7	18.9	30.8	10.1	21.8	16.3	17.4
Cpx	6.8	9.3	13.1	11.4	10.3	6.9	13.3
Sp	1.4	2.1	7.1	2.6	2.8	1.3	2.2

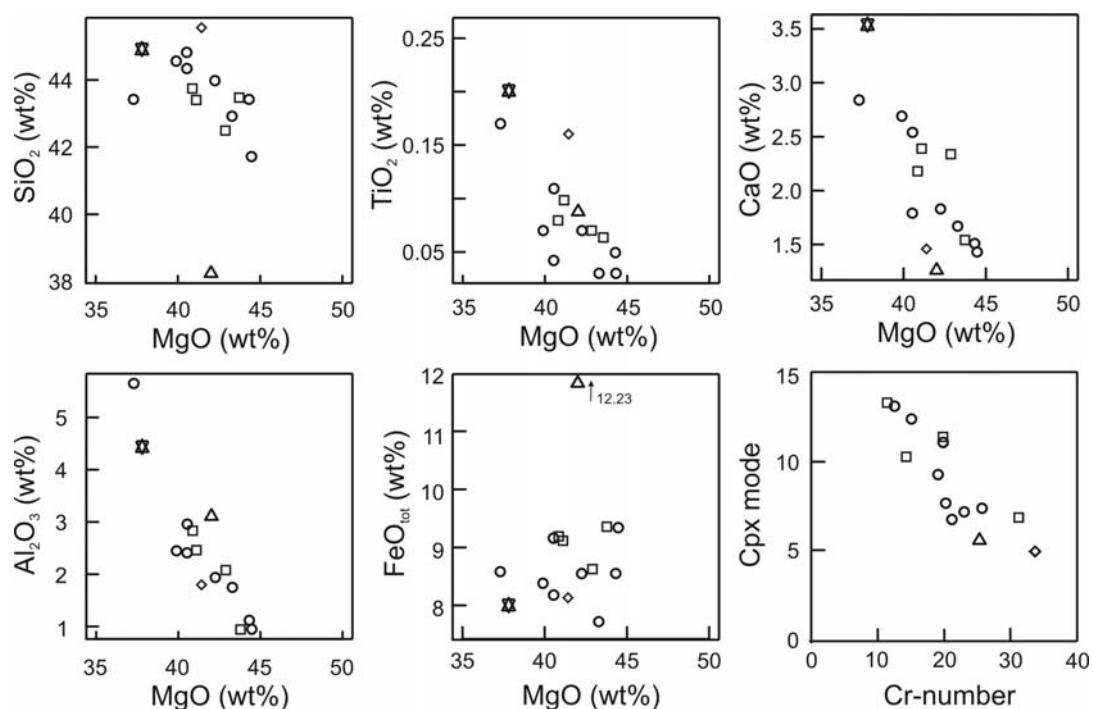


Fig. 6 Variations in whole-rock major oxides with MgO and clinopyroxene mode with Cr-number. The xenoliths display regular depletion trends, except for equigranular dunite (LE 35 km) and one protogranular sample (P 60 km). The composition of primitive mantle (McDonough and Sun, 1995) is represented by a star; other symbols as in Fig. 3.

2.6.3. Trace elements

All of the Kozákov mantle xenoliths are depleted in the heavy REE (HREE) relative to primitive mantle, but are enriched in LREE relative to HREE (Table 4; Fig. 7). Such patterns are characteristic for cryptic metasomatism subsequent to partial fusion and melt extraction. The protogranular xenoliths tend to have a concave-upward pattern, which is more pronounced in those samples with lower Yb and Lu contents. The equigranular xenolith from the upper layer (at 33 km), which is low in Lu and Yb, also has a pronounced concave-upward pattern. Equigranular xenoliths from the lower layer tend to have relatively flat patterns from Gd to Lu and marked LREE enrichment. The layered equigranular dunite from the upper layer (at 36 km) is distinct from the other samples in having a flat middle REE (MREE) and HREE pattern (Sm to Lu) and slight enrichment in LREE. Two protogranular xenoliths have marked positive Eu anomalies.

In addition to LREE enrichment, Kozákov peridotite xenoliths are enriched in the LILE and HFSE and have positive P, Zr, and Hf anomalies (Fig. 8), the magnitudes of which are negatively correlated with Yb contents. The upper equigranular sample also has a pronounced positive anomaly in Nb and Ti. Normalized U/Th ratios show a wide range in values (0.2-6.8), which are negatively correlated with normalized values of Th (16.5-0.9).

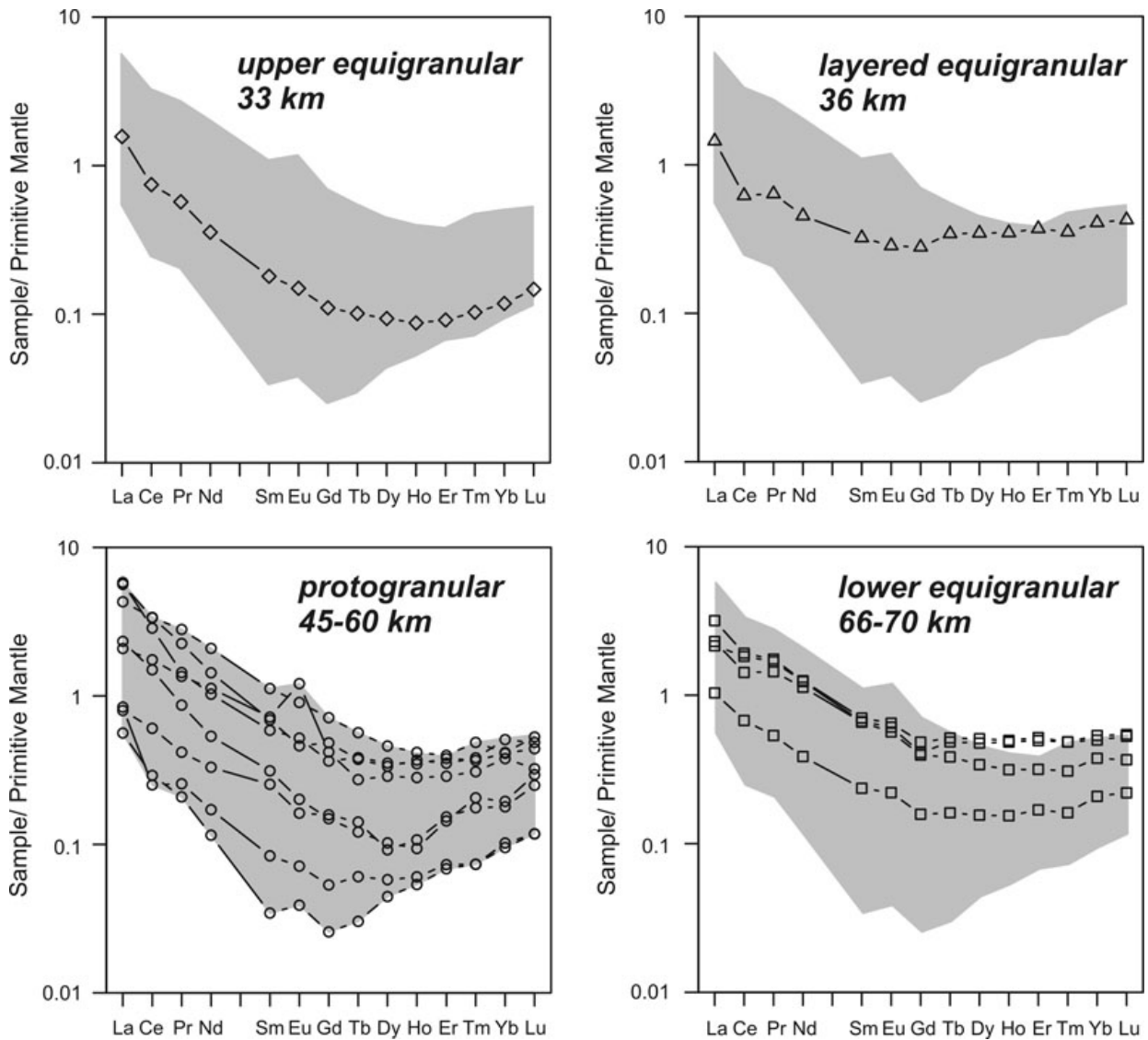


Fig. 7 REE abundance patterns for whole-rocks, normalized to primitive mantle (McDonough and Sun, 1995). The field for protogranular samples is shown in grey for comparison. Symbols as in Fig. 3.

2.6.4. Compositional variation with depth

Disregarding the chemically distinct equigranular dunite (95KSZ4), plots of various chemical parameters with depth reveal subtle variations in the xenolith suite, despite appreciable overlap in the compositions of samples from the upper equigranular, protogranular, and lower equigranular layers. Regarding major elements (Fig. 9), there is a general tendency across the entire xenolith suite for whole-rock Mg-number and Cr-number to decrease with increasing depth and CaO (wt %) and modal clinopyroxene to increase. The single sample from the upper equigranular layer has the most depleted composition. Protogranular samples show the clearest trends of compositional variation with depth, and samples from the lower equigranular layer (with one exception) tend to be the least depleted.

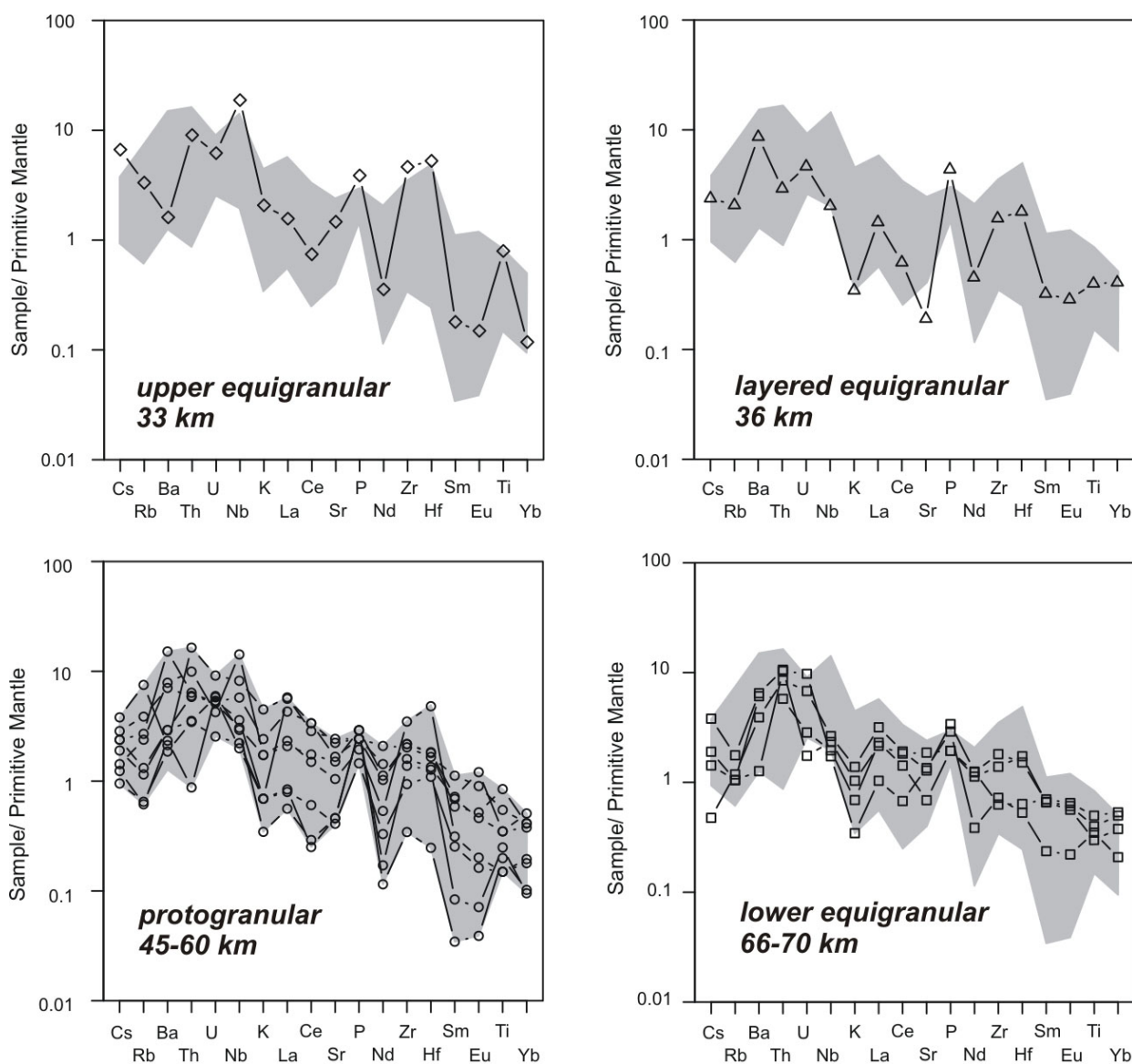


Fig. 8 Trace element abundance patterns for whole-rocks, normalized to primitive mantle (McDonough and Sun, 1995). The field for protogranular samples is shown in grey for comparison. Symbols as in Fig. 3.

These patterns of compositional variation suggest that the degree of depletion in Kozákov lithospheric mantle decreases with depth, a feature that is also found in mantle xenoliths in southeastern Australia (Gaul et al., 2003).

The patterns of trace element variations with depth (Fig. 10) are consistent with those for major elements. Yb contents are lowest in samples above 50 km and, with two exceptions, are highest in samples below 50 km. The degree of LREE enrichment, as measured by $(Ce/Tb)_N$, tends to decrease with increasing depth. The magnitudes of Nb and Hf anomalies, represented by $(Nb/La)_N$ and $(Hf/Sm)_N$, are appreciable in the shallow samples, but decrease with increasing depth in concert with the increase in Yb contents. The clearest trends in trace element variations with depth are seen within the protogranular layer, as is the case for major elements.

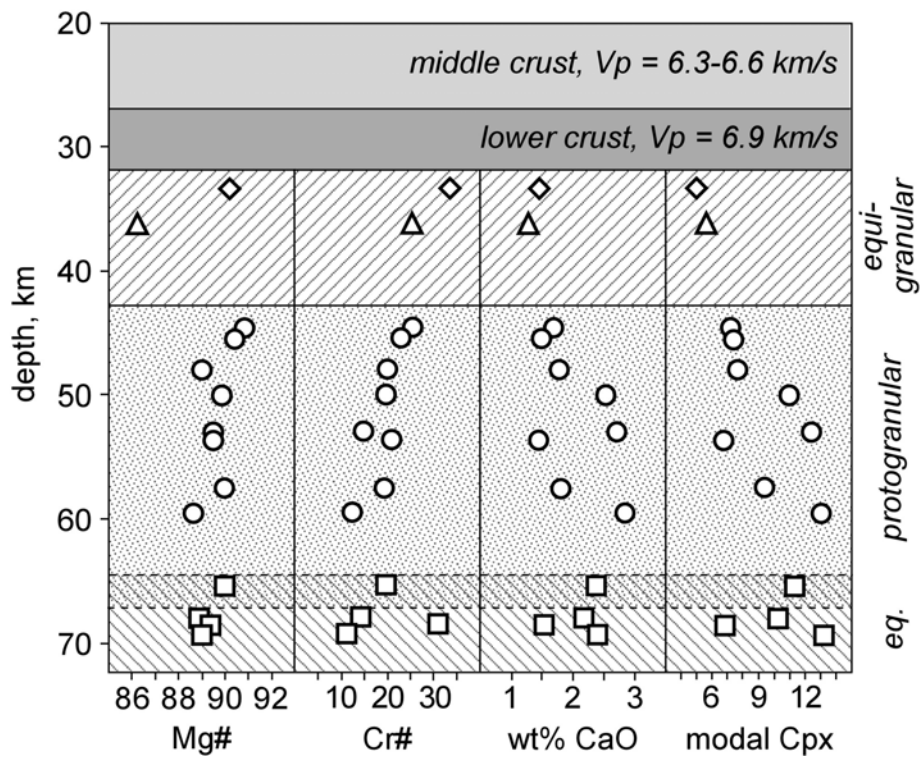


Fig. 9 Whole-rock variation in Mg-number, Cr-number, wt% CaO, and modal clinopyroxene with depth. Symbols as in Fig. 3.

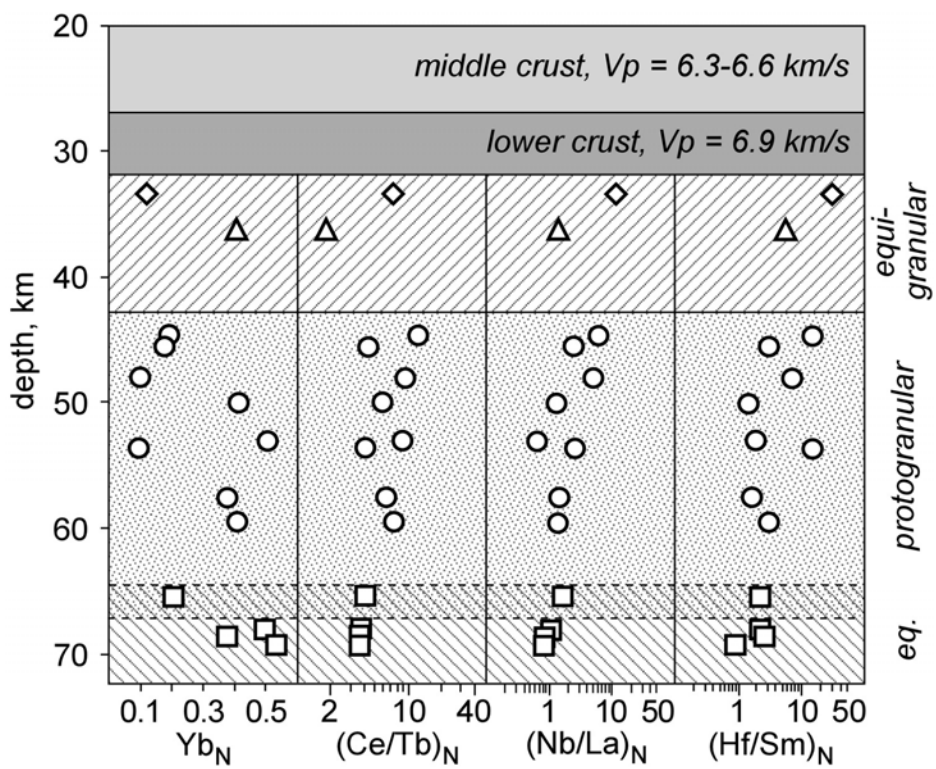


Fig. 10 Whole-rock trace element variation with depth. Symbols as in Fig. 3.

2.7. MINERAL COMPOSITION

2.7.1. Major elements

Mineralogically, the Kozákov mantle xenoliths consist of variable proportions of magnesian olivine and orthopyroxene, Cr-diopside, and aluminous spinel, the compositions of which are summarized in Table 2. Each mineral species is homogeneous within a given xenolith, except for orthopyroxene and clinopyroxene in the upper equigranular layer, which contain thin exsolution lamellae of the complementary pyroxene and spinel. No significant differences in composition were found between cores and rims of grains, except locally in the vicinity of domains where incipient partial melting has occurred.

The Mg-number for olivine in the entire xenolith suite ranges from 90.2 to 91.7, except for that in the layered equigranular dunite, whose Mg-number is 88.2. The Mg-number is highest in the upper equigranular samples (91.1-91.7), shows the widest variation in the protogranular samples (90.2-91.4), and is relatively low in the lower equigranular samples (90.4-91.1). The NiO contents of olivine largely overlap between samples from the different layers, and the variation within the protogranular samples (0.37-0.46 wt %) encompasses the values from the equigranular samples.

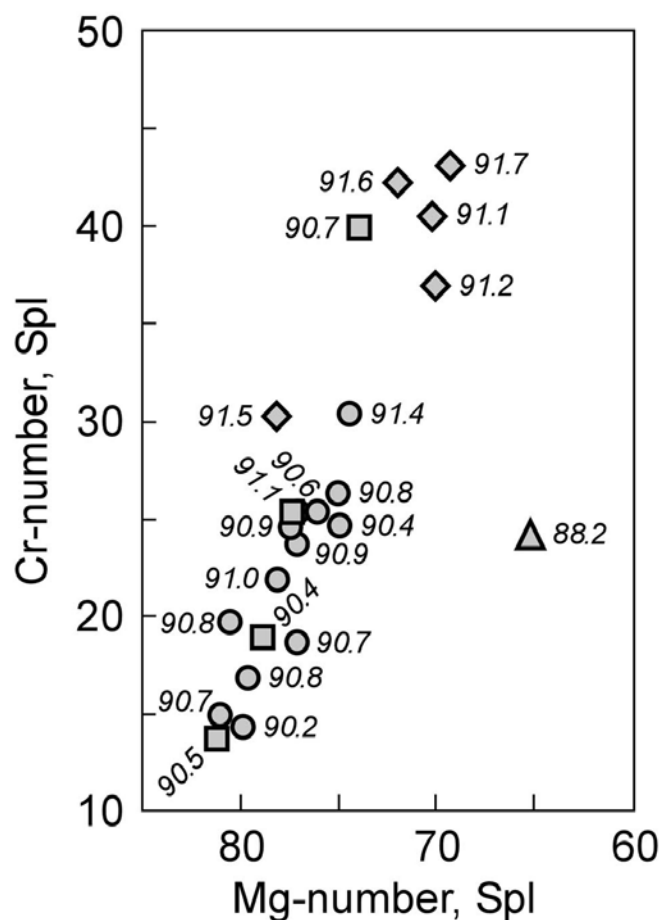


Fig. 11 Variation in spinel composition and Mg-numbers in coexisting olivine (italics). Symbols as in Fig. 3.

The compositional range for spinel is similar to that in basalt-hosted mantle xenoliths elsewhere (Barnes and Roeder, 2001), exhibiting a variation in Mg-number from 69.3 to 81.2 and in Cr-number from 13.6 to 43.0 (Fig. 11). The most Cr-rich spinel occurs in the upper equigranular xenoliths, whereas spinel compositions from protogranular and lower equigranular xenoliths are more aluminous and largely overlap. Spinel in the layered equigranular dunite (95KZS4) is compositionally distinct from that in the other samples, with an Mg-number of 65.3. The compositions of olivine and spinel are well correlated (Fig. 11), with higher Mg-numbers in olivine being associated with lower Mg-numbers and higher Cr-numbers in spinel, a general relation demonstrated previously by Irvine (1965). TiO₂ contents are generally low, ranging from 0.02 to 0.44 wt % with a mean value of 0.07±0.09 wt %. The Fe³⁺ number [$100 \times \text{Fe}^{3+}/(\text{Fe}^{3+} + \text{Cr} + \text{Al})$] of spinel is consistently low, having a calculated mean value of 3.9±0.8, which shows no correlation with TiO₂ or Cr₂O₃ contents. Values of oxygen fugacity, calculated from the compositions of spinel and coexisting silicates (Ballhaus et al., 1991), range from -0.04 to +0.65 log units relative to the fayalite-magnetite-quartz buffer (FMQ), which are similar to the values obtained by Konečný et al. (2006) for other Kozákov samples and by Ballhaus et al. (1991) for slightly metasomatized mantle xenoliths elsewhere.

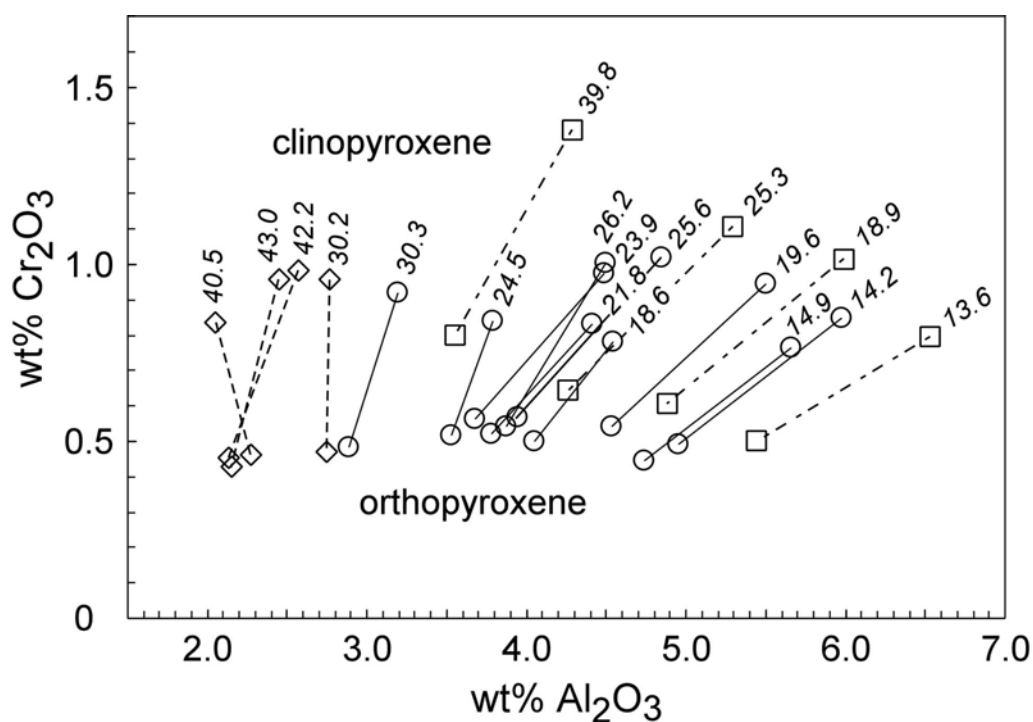


Fig. 12 Variation in Al₂O₃ and Cr₂O₃ contents of orthopyroxene and clinopyroxene and Cr-numbers of coexisting spinel (italics). Symbols as in Fig. 3.

EMPA of pyroxene shows no compositional difference between grains in symplectites and those in the matrix of protogranular samples. For pyroxene from the upper equigranular xenoliths, which contain exsolution lamellae, only the host compositions are reported, because such compositions record conditions when the xenoliths were extracted from the mantle. Orthopyroxene and clinopyroxene are

magnesian, having Mg-numbers of 90.4-92.0 and 89.4-95.3, respectively. The pyroxenes show a wide range in contents of Cr₂O₃ (0.43-0.80 wt %, orthopyroxene; 0.74-1.80 wt %, clinopyroxene) and Al₂O₃ (2.13-5.44 wt %, orthopyroxene; 2.05-6.54 wt %, clinopyroxene), which correlate well with the Cr-numbers in coexisting spinel (Fig. 12). Such a wide range in R₂O₃ contents and Cr/Al ratios in pyroxene reflect variations in equilibration temperatures and degrees of depletion. Al₂O₃ contents are lowest and Cr/Al ratios are highest in pyroxene from upper equigranular xenoliths, whereas these quantities largely overlap in pyroxene from protogranular and lower equigranular xenoliths (Fig. 12). Na₂O contents in clinopyroxene range from 0.43 to 1.32 wt % (except for one anomalous sample) and correlate well with Cr-number. Clinopyroxene grains in upper equigranular samples have the lowest Na₂O contents and highest Cr-numbers, whereas those from the protogranular and lower equigranular layers have overlapping values for these quantities.

2.7.2. Trace elements

In the absence of other phases, the bulk of the REE in four-phase spinel lherzolites are sequestered in clinopyroxene (Table 5), and the REE patterns in clinopyroxene and whole-rocks should be similar. However, this is not the case for the two uppermost samples at 33 and 36 km. In the upper equigranular xenolith (33 km) the REE pattern in clinopyroxene is relatively flat (Fig. 13), whereas that for the whole-rock is LREE enriched (see Fig. 7). Such a difference suggests that the LREE in the whole-rock are either located in a grain-boundary component or reside in an unidentified, LREE-enriched phase. A similar situation occurs in the layered equigranular dunite (36 km), in which the REE pattern is LREE depleted in clinopyroxene, but LREE enriched in the whole-rock (compare Figs 7 and 13). In the protogranular xenoliths the REE patterns in clinopyroxene and whole-rocks are similar (compare Figs 7 and 13), both showing a concave-upward configuration, although the minimum point in clinopyroxene is located between Sm and Gd, and the minimum point in whole-rocks lies between Gd and Ho. Another difference is seen in the HREE, which are relatively flat in clinopyroxene, but have a slight to moderate positive slope in the whole-rocks. In the lower equigranular xenoliths the REE patterns in clinopyroxene and whole-rocks are also similar, both showing a LREE enrichment, except that the HREE have a slight to moderate negative slope in clinopyroxene, but a slight positive slope in the whole-rocks.

2.7.3. Compositional variation with depth

The depth variations in the major element compositions of minerals are more clearly defined than those for whole-rocks, probably because of a greater number of analyses. Except for the compositionally distinct equigranular dunite (36 km) and one lower equigranular sample (70 km), the Mg-number in olivine, Cr-number in spinel, Cr-number in orthopyroxene, and Cr-number in clinopyroxene (not shown) decrease with increasing depth, whereas the Na₂O content of clinopyroxene increases (Fig. 14). Samples from the upper equigranular layer are the most depleted,

Table 5. Trace element analyses of clinopyroxene and results of partial melting calculations

Sample	94KZS4	95KZS4	94KZSM1	ORKZC 3	ORKZS6	94KZSM4	94KZSM3	94KZSM5	94KZSM7
Texture	E	LE	P	P	P	E	E	E	E
Y	2.496	12.824	4.464	4.668	10.075	12.180	9.995	9.372	12.532
La	1.112	0.525	12.766	7.410	4.380	15.608	8.388	5.883	4.847
Ce	2.049	1.304	17.132	4.556	6.568	25.186	19.168	12.243	8.215
Pr	0.383	0.318	2.000	0.286	0.980	3.174	2.987	2.318	1.060
Nd	1.761	1.899	5.373	0.694	2.943	10.351	10.909	10.142	3.471
Sm	0.540	0.914	0.529	0.145	0.564	1.745	1.908	2.260	0.913
Eu	0.197	0.387	0.153	0.063	0.247	0.595	0.639	0.758	0.394
Gd	0.502	1.393	0.492	0.290	0.737	1.622	1.536	1.875	1.340
Tb	0.095	0.347	0.095	0.088	0.209	0.305	0.335	0.339	0.317
Dy	0.579	2.583	0.702	0.771	1.593	1.965	2.188	1.983	2.299
Ho	0.117	0.608	0.161	0.201	0.379	0.400	0.471	0.365	0.526
Er	0.362	1.867	0.524	0.672	1.168	1.135	1.377	0.943	1.593
Tm	0.059	0.277	0.077	0.102	0.173	0.149	0.196	0.115	0.223
Yb	0.403	1.945	0.547	0.720	1.120	0.956	1.247	0.710	1.504
Lu	0.066	0.299	0.081	0.109	0.169	0.133	0.182	0.095	0.217
F (%) ¹⁾	16.9	3.1	13.2	11.9	6.7	7.3	5.2	9.0	4.2
F (%) ²⁾	15.2	9.8	9.9	8.8	5.0	10.3	7.3	14.8	4.0

F, degree of melting

¹⁾ partial melting model after Norman (1998)

²⁾ partial melting model after Hellebrand et al. (2001)

protogranular samples exhibit a decreasing depletion with increasing depth, and samples from the lower equigranular layer (with one exception) have the least depleted compositions. Such variations suggest that the degree of depletion in the Kozákov mantle decreases with depth, as was previously inferred from the variations in whole-rock compositions.

Despite the relatively small number of trace element analyses for clinopyroxene separates, the variation trends in trace element compositions with depth (Fig. 14) are consistent with those for major elements. The contents of Y and Yb in clinopyroxene are lowest in a single sample from the upper equigranular layer, increase with depth in the protogranular layer, and are highest in the lower equigranular layer. Apart from the two samples in the upper equigranular layer, the degree of LREE enrichment, as measured by $(Ce/Sm)_N$, appears to decrease with increasing depth across the protogranular layer into the lower equigranular layer.

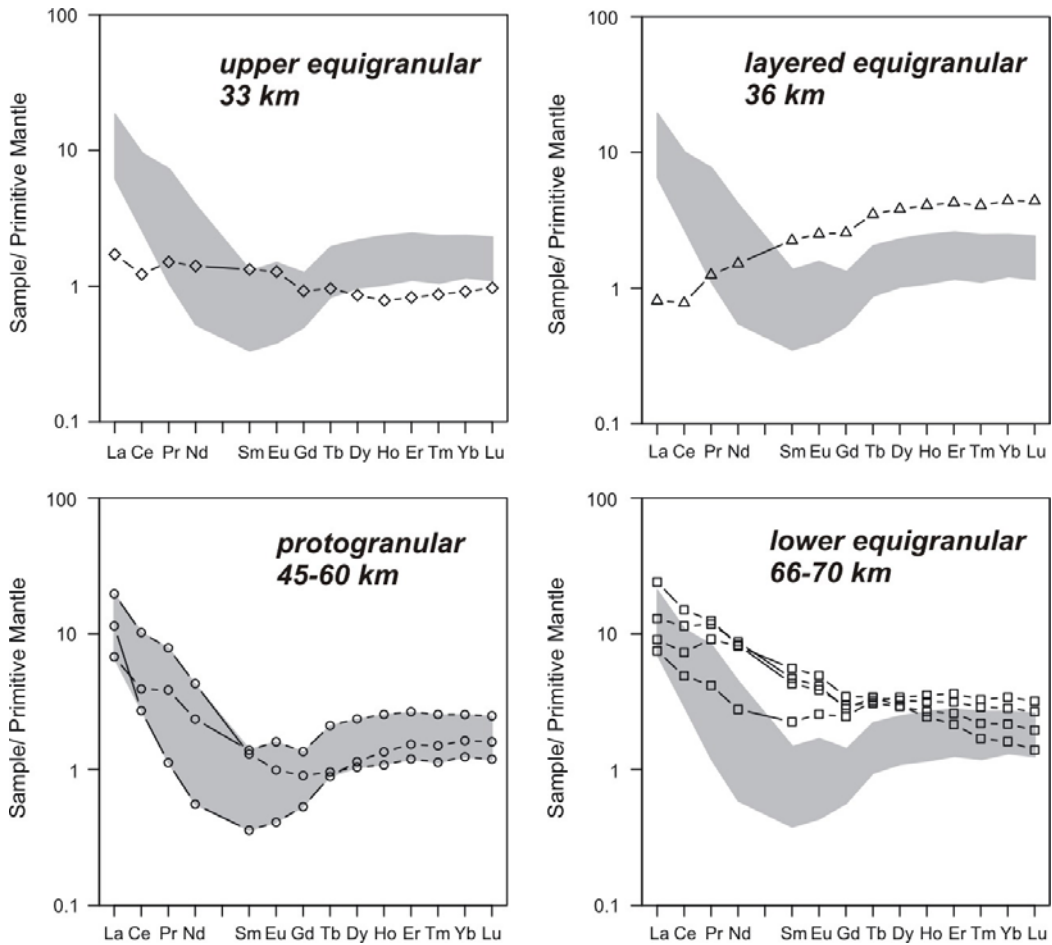


Fig. 13 REE abundance patterns for clinopyroxene separates, normalized to primitive mantle (McDonough and Sun, 1995). The field for protogranular samples is shown in grey for comparison. Symbols as in Fig. 3.

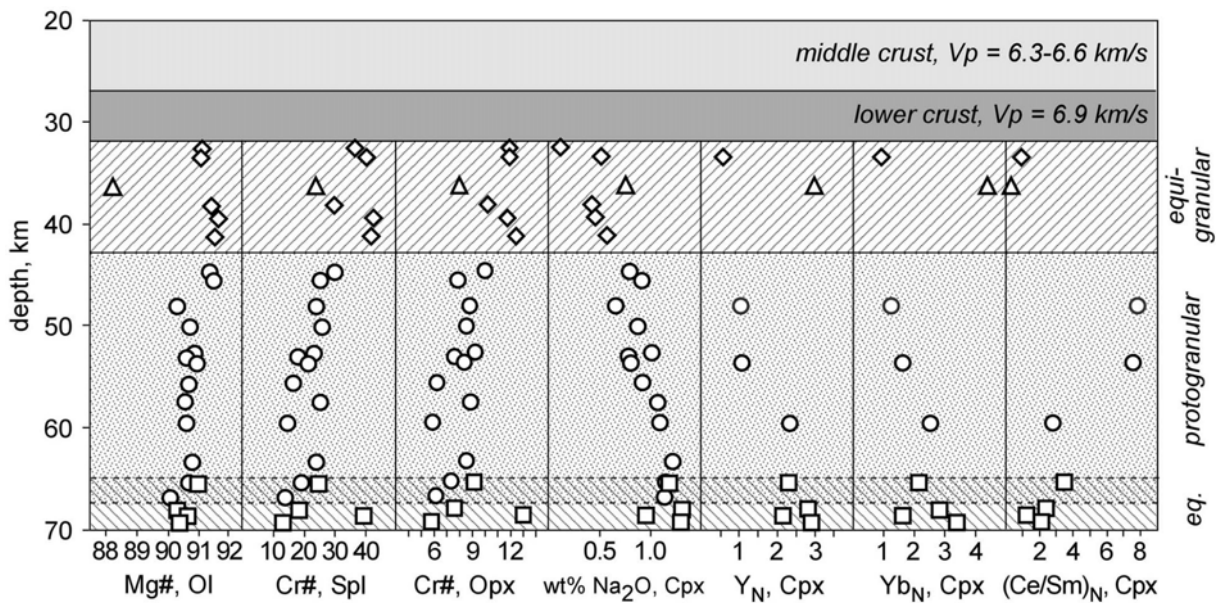


Fig. 14 Variation in selected major and trace element parameters in minerals with depth. Symbols as in Fig. 3.

2.8. SR AND ND ISOTOPES IN CLINOPYROXENE

Clinopyroxene separates from four protogranular and two lower equigranular xenoliths display a limited range of isotopic variation (Table 6; Fig. 15), with measured values of $^{87}\text{Sr}/^{86}\text{Sr}$ lying between 0.70328 and 0.70339, and $^{143}\text{Nd}/^{144}\text{Nd}$ ranging from 0.51287 to 0.51307 ($\epsilon_{\text{Nd}} = +4.6$ to $+8.4$). These values plot within the Nd-Sr isotopic array defined by anhydrous spinel peridotite xenoliths from other central European localities and overlap the field for clinopyroxene in enriched peridotite xenoliths from Ray Pic, Massif Central (Zangana et al., 1997; Fig. 15).

An interesting feature of this isotopic array is the restricted range of $^{87}\text{Sr}/^{86}\text{Sr}$ between 0.7031 and 0.7037 for many xenoliths, including those from Kozákov and Ray Pic. These values are similar to those proposed for upwelling mantle beneath Europe (low-velocity component in Fig. 15), which has been identified by seismic tomography and is thought to be responsible for much of the alkaline magmatism associated with the CERS (Hoernle et al., 1995).

Despite the limited amount of Kozákov isotopic data, it appears that values of $^{87}\text{Sr}/^{86}\text{Sr}$ and $^{143}\text{Nd}/^{144}\text{Nd}$ may be correlated with depth, as is the case for the major and trace elements. Two protogranular xenoliths at intermediate depths of 48 and 54 km have lower values of $^{87}\text{Sr}/^{86}\text{Sr}$ (0.703284-0.703285) and ϵ_{Nd} (both at $+4.6$) compared with four other samples at depths below 64 km, which have higher values of $^{87}\text{Sr}/^{86}\text{Sr}$ (0.703338-0.703394) and ϵ_{Nd} ($+5.1$ to $+8.5$). This isotopic variation may also be correlated with degree of LREE enrichment in clinopyroxene, the two samples at intermediate depths being more enriched, with $(\text{Ce}/\text{Sm})_{\text{N}} = 7.6$ - 7.9 , compared with the deeper samples, in which $(\text{Ce}/\text{Sm})_{\text{N}} = 2.2$ - 2.8 .

Table 6. Sm-Nd and Rb-Sr isotopic data of clinopyroxenes

Sample	Sm (ppm)	Nd (ppm)	$^{147}\text{Sm}/^{144}\text{Nd}$	$^{143}\text{Nd}/^{144}\text{Nd}$	ϵ_{Nd}	Rb (ppm)	Sr (ppm)	$^{87}\text{Rb}/^{86}\text{Sr}$	$^{87}\text{Sr}/^{86}\text{Sr}$	model depth (km)
<i>Protogranular</i>										
94KZSM1	0.66	6.89	0.05844	0.512872±14	4.6	0.10	132.91	0.00218	0.703285±11	48
ORKZC-3	0.43	3.00	0.08778	0.512872±13	4.6	0.12	65.66	0.00533	0.703284±11	54
94KZSM6 †	0.90	3.83	0.14261	0.513021±8	7.5	0.35	115.65	0.00870	0.703362±11	64
ORKZC6 †	1.21	6.11	0.11994	0.512950±12	6.1	0.50	69.17	0.02102	0.703338±10	68
<i>Lower Equigranular</i>										
94KZSM-3	1.76	10.46	0.10213	0.512901±10	5.1	0.88	108.36	0.02354	0.703376±10	69
94KZSM7	1.02	3.88	0.15952	0.513071±13	8.5	0.36	62.58	0.01641	0.703394±9	70

Note: † denotes average analyses for Rb-Sr data. Present-day CHUR $^{143}\text{Nd}/^{144}\text{Nd} = 0.512638$.

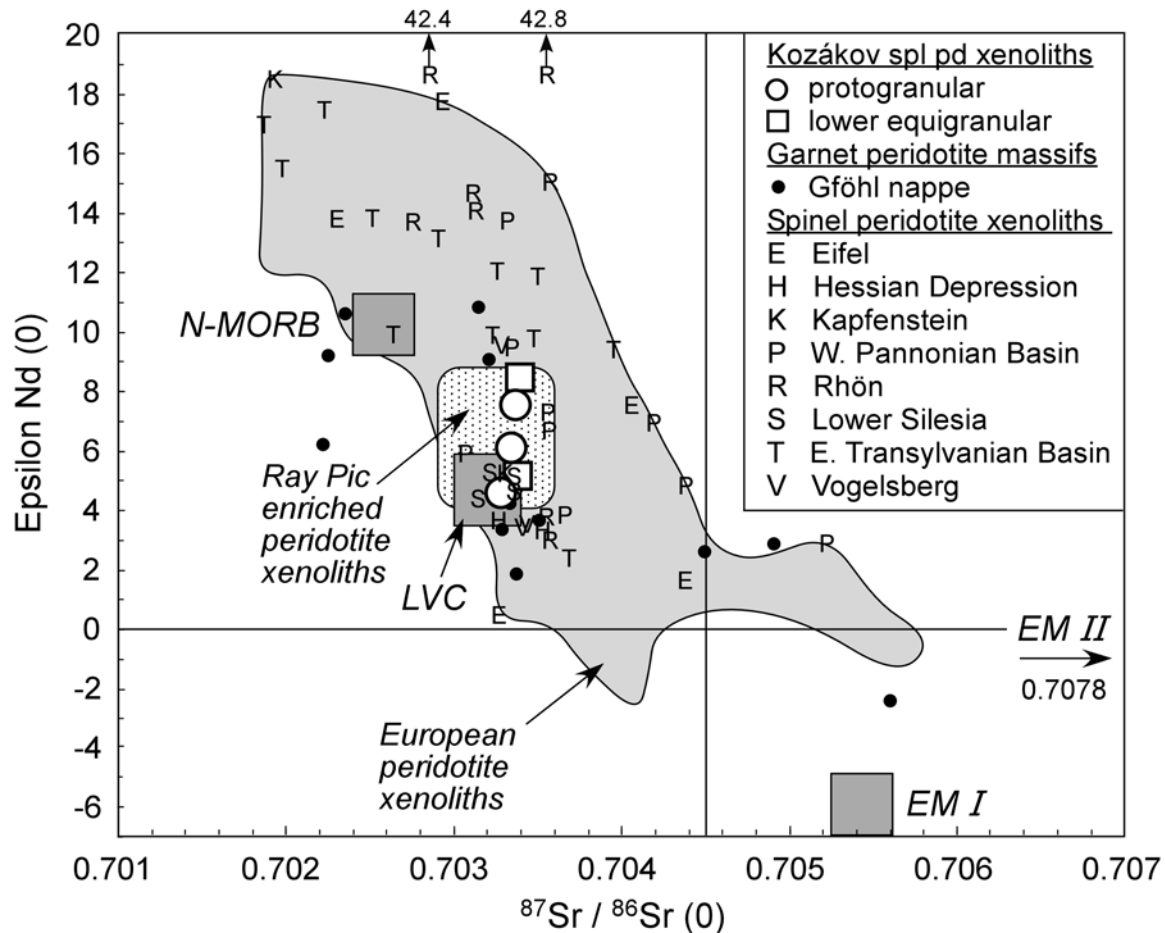


Fig. 15 Variation in Epsilon Nd (0) and $^{87}\text{Sr}/^{86}\text{Sr}$ (i) of clinopyroxene in Kozákov spinel peridotite xenoliths. Note that two protogranular samples overlap at Epsilon Nd = 4.6. The isotopic compositions of clinopyroxene in anhydrous spinel peridotites from other central European Cenozoic volcanic centers, identified by letters, are shown for comparison. The grey field includes all European Cenozoic peridotite xenoliths (Downes, 2001). LVC (low-velocity component) is the isotopic composition inferred for upwelling mantle beneath Europe (Hoernle et al., 1995). The field for enriched peridotite xenoliths from Ray Pic, Massif Central, is from Zangana et al. (1997).

2.9. DISCUSSION

2.9.1. Partial melting and depletion of the mantle sources of the xenoliths

Variations in the whole-rock and mineral compositions of the Kozákov mantle xenoliths are indicative of the progressive extraction of partial melts. Typical for the whole-rocks are a decrease in Al_2O_3 , CaO, and TiO_2 with increasing MgO, low HREE contents relative to primitive mantle, and a negative correlation between modal clinopyroxene and Cr-number. Complementary variations in mineral compositions include positive correlations between Mg-number and Cr-number between olivine, spinel, and pyroxenes, and decreases in TiO_2 , Na_2O , and HREE with increase in Cr-number in clinopyroxene. Low values of whole-rock Yb_N , which are 0.10-0.54 relative to primitive mantle, indicate that partial melting probably occurred in the absence of garnet, otherwise values of Yb_N would remain close to 1.0 in residual garnet peridotite for any low to moderate degree of batch or fractional melting.

Because clinopyroxene was probably the principal host for HREE in spinel peridotite when partial melting occurred, the degree of partial melting can be estimated by assuming that clinopyroxene is the only phase effectively contributing to the bulk distribution coefficient for the Y and Yb in the residual assemblage (Norman, 1998). Ti and Na in Kozákov clinopyroxenes show a positive correlation with Y and Yb, and the Cr-number in clinopyroxene is negatively correlated with Y and Yb, suggesting that distribution of these elements in clinopyroxene was controlled by partial melting, rather than metasomatism, and that application of the Norman melting model is appropriate in this case. The modelling results (Table 5; Fig. 16) indicate that batch melting requires an unreasonably high degree of partial melting for the more refractory samples, as found for xenolith suites elsewhere (Norman, 1998; Beccaluva et al., 2001). Fractional melting thus seems the best choice for the melting mode in the Kozákov xenoliths, yielding degrees of melting, F , of 4.2-9.0 % for lower equigranular samples, 6.7-13.2 % for protogranular samples, and 16.9% for the single upper equigranular sample. Although the absolute values of F are sensitive to the choice of model parameters, especially the initial composition of the protolith and the initial clinopyroxene mode, the relative values are consistent with the results from the major element chemistry of whole-rocks and minerals, demonstrating that the lower equigranular samples are the least depleted, the upper equigranular samples are most depleted, and the protogranular samples exhibit intermediate in level of depletion. Similar conclusions were reached based on a partial melting model utilizing all the REE, following the method of Johnson et al. (1990), the results of which are shown in Fig. 17, where the calculated REE patterns of clinopyroxene in residual spinel peridotite at different degrees of partial melting are compared with those measured in Kozákov clinopyroxenes.

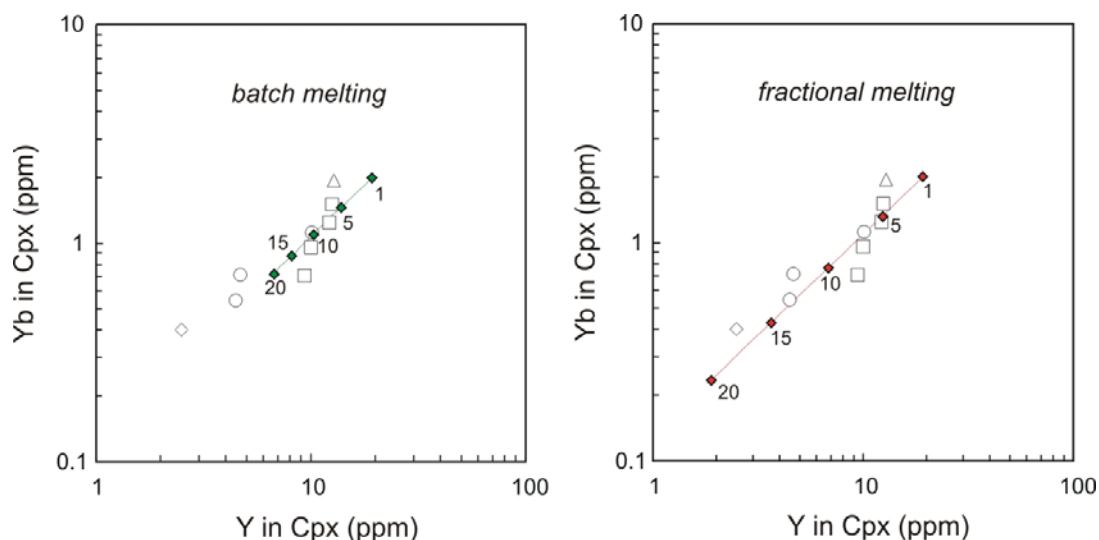


Fig. 16 Results of batch and fractional melting calculations for Y and Yb in clinopyroxene, following the model of Norman (1998). Batch melting requires unrealistically high degrees of melting for the three most refractory samples, whereas fractional melting yields reasonable results for all the analyzed xenoliths. Symbols as in Fig. 3.

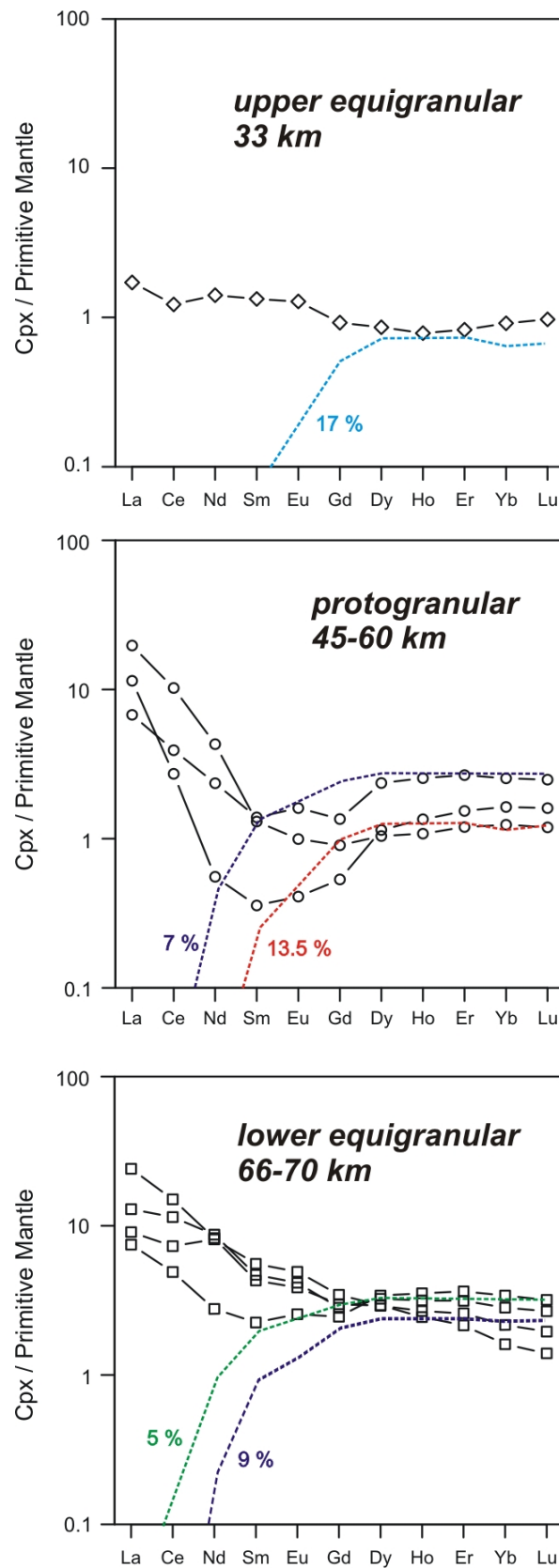


Fig. 17 Comparison of measured (solid lines and symbols) and calculated (dotted curves) REE contents of clinopyroxene in Kozákov mantle xenoliths. Compositions of clinopyroxene in peridotite residua were calculated following the melting model and parameters of Johnson et al. (1990). Numbers adjacent to dotted curves signify degrees of partial melting.

An alternative method for estimating the degree of partial melting in spinel peridotite is based on the spinel composition, the Cr-number of which is highly correlated with HREE contents of coexisting clinopyroxene in mid-ocean ridge peridotites (Hellebrand et al., 2001). Application of this method to spinel compositions in the Kozákov xenoliths yields results that are roughly comparable (with one exception) with those based on the Y and Yb contents of clinopyroxene (Table 4). The differences in the results from the two methods arise from differences in model parameters; for example, the fraction of clinopyroxene in the source, which was taken to be 0.20 by Norman (1998) and 0.14 by Hellebrand et al. (2001), among other factors. Regardless, results from the spinel calibration indicate that shallow mantle beneath Kozákov volcano is more refractory than the deeper mantle, with estimates of the degree of partial melting being 14.3 ± 1.4 % in five upper equigranular xenoliths, 8.0 ± 2.4 % in 11 protogranular samples, and 6.7 ± 3.1 % in three lower equigranular xenoliths (with one outlier at 14.8%).

Considering the results from the three methods described above, it appears that partial melting of the protolith of the four-phase spinel peridotite xenoliths varied between ~ 5 % and ~ 15 %. Such values and the paucity of harzburgite and dunite in the xenolith suite (Fediuk, 1971) suggest that the Kozákov lithospheric mantle experienced relatively low to moderate degrees of melt extraction.

2.9.2. Metasomatism of the xenoliths

The high concentrations of LREE, LILE, and HFSE, the occurrence of anhydrous mineral assemblages, and the absence of any recognized modal metasomatism in the Kozákov mantle xenoliths are consistent with cryptic metasomatism by a silicate melt, rather than a carbonatitic melt, H₂O fluid, or CO₂ fluid. Similar metasomatic effects occur in numerous other European lithospheric mantle xenoliths, which have been attributed to the influence of transient silicate melts (Downes, 2001). In addition, the Kozákov xenoliths exhibit positive Zr and Hf anomalies and, in some cases, positive Ti anomalies, in mantle-normalized trace element patterns, which have not been described so far from European peridotite xenoliths (e.g. Lenoir et al., 2000; Downes, 2001).

The concave-upward REE_N patterns for the Kozákov peridotites (Fig. 7) and clinopyroxene separates (Fig. 13) probably reflect the effects of chromatographic fractionation as a result of percolation of LREE-rich melts through porous, previously depleted peridotite. Calculated REE_N patterns for such a chromatographic process (see Navon and Stolper, 1987; Fig. 4) resemble those of the Kozákov peridotites, and similar concave-upward REE_N patterns were described for clinopyroxene from the Horoman peridotite, Japan, and for peridotite xenoliths from the Vogelsberg, Germany, where such patterns were also ascribed to chromatographic processes (Takazawa et al., 1992; Witt-Eickschen, 1993).

The REE patterns for xenoliths from the different mantle layers at Kozákov are compared with each other and with those in xenoliths from other localities by plotting (Ce/Tb)_N vs (Tb/Yb)_N for whole-rocks and (Ce/Sm)_N vs (Sm/Yb)_N for clinopyroxene (Figs 18 and 19). These plotting parameters are selected because the minimum points in the concave-upward REE patterns for Kozákov wholerock peridotites and clinopyroxenes occur at Tb and Sm, respectively. In such plots, REE patterns with positive,

concave-upward, negative, and convex-upward shapes plot in the lower left, upper left, upper right, and lower right quadrants of the figures, respectively. For whole-rocks, Fig. 18 illustrates that concave-upward REE patterns are more pronounced in Kozákov upper equigranular and protogranular peridotites than in lower equigranular peridotites, most samples of which have $(\text{Tb}/\text{Yb})_{\text{N}} \sim 1$. Similar differences are found in Kozákov clinopyroxenes, with two of three protogranular samples having pronounced concave-upper patterns and three of four equigranular samples having negative slopes (Fig. 19).

Peridotite xenoliths in central Europe are mostly LREE enriched, and those from the Vogelsberg and Hessian Depression have REE patterns varying from negative slopes to concave-upward shapes that overlap with those for most of the Kozákov peridotites (Fig. 18). Clinopyroxenes from central European peridotite xenoliths show a wide variety of REE patterns, but those from the Vogelsberg (Witt-Eickschen, 1993) are concave-upward and closely similar in shape and magnitude to those of the Kozákov protogranular samples (Fig. 19). Similarities include a predominance of anhydrous spinel ilherzolite, protogranular textures with spinel-pyroxene symplectites after garnet, whole-rock major element depletion trends, comparable REE patterns in whole-rocks and clinopyroxenes (Figs 18 and 19), and $^{143}\text{Nd}/^{144}\text{Nd}$ and $^{87}\text{Sr}/^{86}\text{Sr}$ values in clinopyroxene that closely bracket those for Kozákov (Fig. 15).

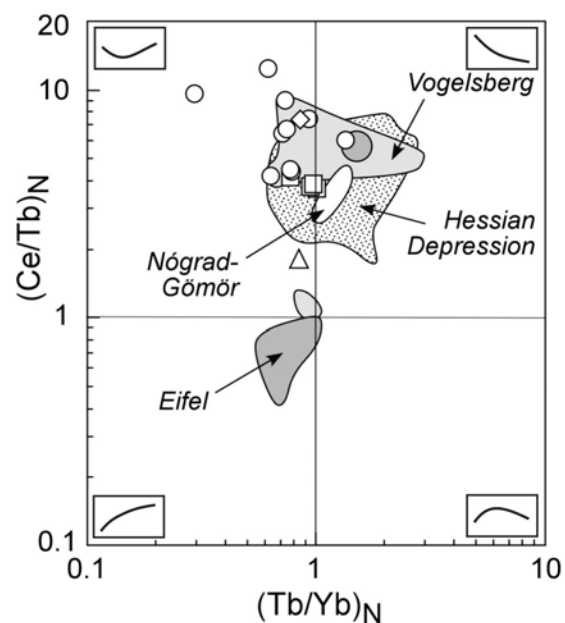


Fig. 18 $(\text{Ce}/\text{Tb})_{\text{N}}$ vs. $(\text{Tb}/\text{Yb})_{\text{N}}$ for Kozákov xenolith whole-rocks, compared to other anhydrous spinel peridotites from the Eifel (Stosch and Seck, 1980, Stosch and Lungmair 1986), Hessian Depression (Hartmann and Wedepohl, 1990), Nógrad-Gömör (Szabó and Taylor, 1994), and Vogelsberg (Witt-Eickschen, 1993). Normalized to primitive mantle (McDonough and Sun, 1995).

In addition to the LREE, the Kozákov peridotite xenoliths are enriched in the LILE, P, Nb, Zr, and Hf (Fig. 8). Although the LILE enrichment at Kozákov is similar to that in many other European mantle xenoliths, the HFSE enrichment coupled with positive anomalies in mantle-normalized trace element patterns appears to be unusual; where Zr and Hf anomalies occur in other European mantle xenoliths, they tend to be negative (Downes, 2001). The fractionation of HFSE from elements of similar compatibility cannot be accounted for by cryptic metasomatism, but more probably reflects modal metasomatism, the evidence for which remains unrecognized in the Kozákov xenoliths. Despite the lack of HFSE data for Kozákov clinopyroxenes, mass-balance calculations based on the REE demonstrate that clinopyroxene does not host all of the REE and that this REE ‘deficit’ is depth dependent, decreasing with depth. Lower equigranular and protogranular clinopyroxenes host generally more than 50 % of the HREE and 30 % of the LREE, but upper equigranular clinopyroxene accounts for only 40% of the HREE and only ~10 % of the LREE. This pattern of REE ‘deficit’ is accompanied by a decrease in $(\text{Hf}/\text{Sm})_N$ and $(\text{Nb}/\text{La})_N$ ratios with depth (Fig. 10). Such results may arise from the precipitation of LREE- and HFSE-enriched microphases during the fractionation of ascending metasomatic melts. Such enrichment in HFSE and LILE, in the absence of any visible metasomatic phase, is similar to that observed by Bodinier et al. (1996), who demonstrated the presence of microphases concentrated along spinel grain boundaries enriched in highly incompatible trace elements. The enrichment in the HFSE at Kozákov indicates that the metasomatic agent was probably a silicate melt, rather than a fluid, which would have low HFSE solubility.

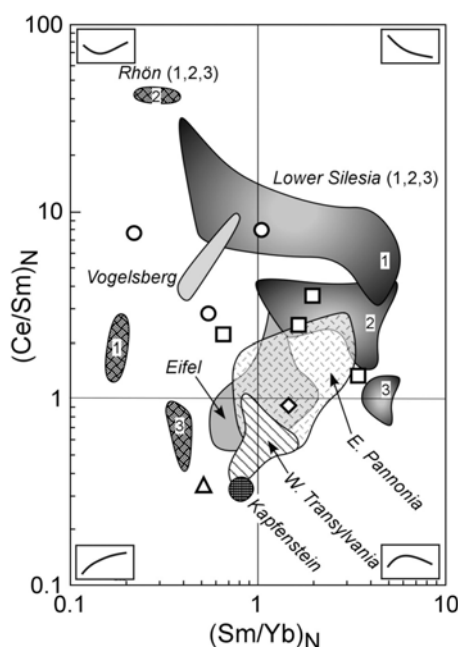


Fig. 19 $(\text{Ce}/\text{Sm})_N$ vs. $(\text{Sm}/\text{Yb})_N$ for Kozákov clinopyroxene, compared to clinopyroxene in other anhydrous spinel peridotites from the Eifel (Stosch and Seck, 1980, Stosch and Lungmair 1986), Kapfenstein (Vaselli et al., 1996), Rhön (Witt-Eickschen and Kramm, 1997), Vogelsberg (Witt-Eickschen, 1993), Lower Silesia (Blustajn and Shimizu, 1994), W. Transylvania (Downes et al., 1992), and E. Pannonia (Vaselli et al., 1995). Normalized to primitive mantle (McDonough and Sun, 1995).

2.9.3. Timing of depletion and metasomatism

The geochemical data presented here indicate that the Kozákov lithospheric mantle was depleted in incompatible elements through partial melt extraction and subsequently refertilized by cryptic metasomatism. Previously, Christensen et al. (2001) suggested that the tripartite layering of sub-Kozákov mantle originated during Variscan orogenesis, when deeper level, protogranular garnet peridotite was tectonically emplaced into shallower-level, equigranular spinel peridotite, where it resided metastably until Neogene heating promoted recrystallization. If so, in this geological context it is likely that partial melting and depletion of the three peridotite lithospheric layers occurred prior to, or during, Variscan juxtaposition. In addition, the low Yb contents of the protogranular peridotites (Fig. 7) require that partial melting occurred in the spinel stability field, which could have occurred prior to stabilization of garnet in this unit (i.e. in a pre-Variscan spinel peridotite protolith).

The regular variation of trace elements with depth across the three mantle layers, as monitored by $(\text{Ce/Tb})_N$, $(\text{Nb/La})_N$, and $(\text{Hf/Sm})_N$ in whole-rocks (Fig. 10) and $(\text{Ce/Sm})_N$ in clinopyroxene (Fig. 14), except for the single upper equigranular sample), implies that cryptic metasomatism occurred after assembly of the layers (i.e. in post-Variscan times). Values of these elemental ratios generally decrease with increasing depth, which may reflect the proportionately smaller metasomatic signature in the less depleted, deeper samples, compared with the more depleted, shallower samples.

In a plot of $^{143}\text{Nd}/^{144}\text{Nd}$ vs $^{147}\text{Sm}/^{144}\text{Nd}$, clinopyroxene from three protogranular and two equigranular samples yields an apparent age of 432 ± 26 Ma, if the single protogranular outlier is neglected. Inclusion of all six samples yields an apparent age of 329 ± 150 Ma. T_{DM} model ages of range from 105 to 275 Ma. However, in view of the complex history of the Kozákov mantle, the intermediate position of Kozákov clinopyroxene within the Nd-Sr isotopic array for European peridotite xenoliths (Fig. 15), and the positive correlation of $^{143}\text{Nd}/^{144}\text{Nd}$ with $1/\text{Nd}$ (not shown), such results are unlikely to represent true ages, but rather are probably due to mixing. It has been suggested that the Nd and Sr isotopic compositions of clinopyroxene in enriched peridotite xenoliths from Ray Pic, Massif Central, are the result of mixing between the Cenozoic low-velocity component and lithospheric mantle with variable ratios of Sm/Nd, $1/\text{Nd}$, and $^{143}\text{Nd}/^{144}\text{Nd}$, as a result of previous melting events (Zangana et al., 1997). Such a mixing process could equally well be invoked for the isotopically similar Kozákov clinopyroxene.

2.10. CONCLUSIONS

The Kozákov lithospheric mantle has a layered structure, consisting of an equigranular upper layer at depths from 32 to 43 km, a protogranular symplectite-bearing intermediate layer from 43 to 67 km, and an equigranular lower layer from 67 to 70 km. This layered configuration is thought to have originated during Variscan convergence, when deeper-level garnet peridotite was tectonically emplaced into shallower-level spinel peridotite, where it resided metastably, until Neogene heating promoted reaction of garnet and olivine to form spinel-pyroxene symplectite.

Variation patterns for major elements in spinel lherzolite whole-rocks and constituent minerals in the three layers are typical for peridotite that has undergone partial fusion and melt extraction, the degree of which is estimated to have varied from ~5 % to ~15 %. Subsequent to this depletion event, spinel lherzolite in all three layers was refertilized by metasomatism, most probably by a transient silicate melt, which resulted in enrichment in the LILE, LREE, and HFSE and development of positive P, Zr, and Hf anomalies, as a result of a combination of chromatographic fractionation and precipitation of HFSE-enriched microphases at grain boundaries.

The timing of depletion and cryptic metasomatism in the Kozákov lithospheric mantle remains uncertain. If the layered structure is the product of Variscan tectonics, then depletion of the juxtaposed lithospheric layers probably occurred prior to their assembly. The regular variation of trace elements with depth across the three mantle layers suggests that metasomatism occurred after assembly of the layers, and the likely influence of the low-velocity component on the isotopic evolution of the Kozákov lithospheric mantle implies that metasomatism may have been associated with Neogene rifting and magmatism.

Acknowledgments

We thank Orlando Vaselli and two anonymous reviewers for their constructive reviews on this manuscript. We are grateful to Anna Langrová for microprobe analysis of two samples in the Academy of Sciences of the Czech Republic, John Fournelle for direction in the electron microprobe analytical laboratory at the University of Wisconsin, and Shah Wali Faryad and František V. Holub for constructive comments on the manuscript. This research was supported by the Grant Agency of the Academy of Sciences, project IAA3013403 and the Scientific Programme CEZ: Z3-013-912 of the Institute of Geology, Academy of Sciences of the Czech Republic, and MSM 0021620855 of the Charles University, Faculty of Science.

CHAPTER 3. Effects of melt percolation on highly siderophile elements and Os isotopes in subcontinental lithospheric mantle: a study of the upper mantle profile beneath Central Europe

Lukáš Ackerman^{1,2}, Richard J. Walker³, Igor S. Puchtel³, Lynnette Pitcher³, Emil Jelínek², Ladislav Strnad⁴

¹*Institute of Geology v.v.i., Academy of Sciences of the Czech Republic, Rozvojová 269, 165 00, Praha 6, Czech Republic*

²*Institute of Geochemistry, Mineralogy and Mineral Resources, Faculty of Science, Charles University, Albertov 6, 128 43, Praha 2, Czech Republic*

³*Department of Geology, University of Maryland, College Park, MD 20742, USA*

⁴*Laboratories of the Geological Institutes, Faculty of Science, Charles University, Albertov 6, 128 43, Praha 2, Czech Republic*

Status: Under review in *Geochimica et Cosmochimica Acta*

Abstract

The effects of melt percolation on highly siderophile element (HSE) concentrations and Re-Os isotopic systematics of subcontinental lithospheric mantle are examined for a suite of spinel peridotite xenoliths from the Kozákovo volcano, Bohemian Massif, Czech Republic. The xenoliths have previously been estimated to originate from depths ranging from ~ 32 to 70 km and represent a layered upper mantle profile. Prior petrographic and lithophile trace element data for the xenoliths indicate that they were modified via metasomatism resulting from the percolation of basaltic melt derived from the asthenosphere. Chemical and isotopic data suggest that lower sections of the upper mantle profile interacted with melt characterized by a primitive, S-undersaturated composition at high melt/rock ratios. The middle and upper layers of the profile were modified by more evolved melt at moderate to low melt/rock ratios. This profile permits an unusual opportunity to examine the effects of variable melt percolation on HSE abundances and Os isotopes. Except for Pt (and in several cases, Os), all HSE concentrations in all studied rocks are significantly depleted compared to estimates for the primitive upper mantle (PUM). This depletion, which is most pronounced for Os, Ir, Ru (I-PGE) in the lower sections of the mantle profile, is coupled with strong HSE fractionation (e.g., Os_N/Ir_N ratios ranging from 0.4 to 2.3). Osmium isotopic compositions range considerably from subchondritic to approximately chondritic (γ_{Os} at 5 Ma from -6.9 to +2.1). The absence of correlations between $^{187}Os/^{188}Os$ and indicators of fertility suggests either a perturbation in the Os isotopic compositions of some of these rocks, or more likely, modifications to the indices of fertility. Osmium isotopic compositions yield model melt depletion ages consistent with late Proterozoic melt depletion. Our data provide evidence for large-scale incompatible behavior of HSE during melt percolation as a result of sulfide breakdown, consistent with observations of prior studies. The degree of incompatibility evidently depended on melt/rock ratios and the degree of S-undersaturation of the percolating melt. The high Pt contents of many of these rocks suggest that the Pt present in this pervasively metasomatized mantle was controlled by a phase other than sulfides. Further, high Os concentrations in several samples suggest deposition of Os in a minority of the samples during melt percolation. In these rocks, the mobilized Os was characterized by subchondritic $^{187}Os/^{188}Os$, compared to the suprachondritic compositions more commonly observed under such circumstances.

Keywords: mantle xenoliths; platinum-group elements; Re-Os; percolation; Bohemian Massif

3.1. INTRODUCTION

The absolute and relative abundances of highly siderophile elements (HSE; including Re, Os, Ir, Ru, Rh, Pt, Pd) and $^{187}\text{Os}/^{188}\text{Os}$ in the bulk mantle can potentially provide important information about global processes related to planetary differentiation and possibly late accretion of Earth (e.g. Brandon et al., 1996; Morgan et al., 2001). The HSE systematics of individual mantle rocks, however, commonly record complex histories of smaller-scale processes including melt depletion, melt percolation, and crustal recycling (e.g. Pearson et al., 1995; Widom et al., 2003). Such processes tend to obscure the primary HSE characteristics of the bulk mantle, but can provide a wealth of information about regional and local processes. For instance, Re typically behaves incompatibly during partial melting, whereas Os behaves compatibly. This leads to the creation of mantle residues with Re/Os that is lower than that of the estimated primitive upper mantle (PUM), which in turn leads to retardation in the growth of $^{187}\text{Os}/^{188}\text{Os}$. The magnitude of the retardation can be used to constrain the age of the melt depletion event for that portion of the mantle (e.g. Walker et al., 1989).

Metasomatic processes including silicate melt and aqueous fluid infiltration and percolation can also significantly alter absolute and relative HSE concentrations in mantle peridotites (Reisberg et al. 2005; Becker et al., 2006). For example, Brandon et al. (1996) and Widom et al. (2003) reported aqueous fluid transport of radiogenic Os from subducting slabs to overlying mantle wedges. Büchl et al. (2002) documented major changes in the relative abundances of HSE in mantle peridotites affected by melt percolation in the Troodos ophiolite.

Despite considerable study of the behavior of HSE and $^{187}\text{Os}/^{188}\text{Os}$ resulting from different types and extents of metasomatic processing, many contradictions and questions remain. For example, Chesley et al. (1999) reported that peridotites modified by interaction with basaltic melts were enriched in Re, ultimately resulting in the evolution of the affected rocks to suprachondritic $^{187}\text{Os}/^{188}\text{Os}$ ratios. Other studies have conversely reported Re loss during percolation of basaltic melts with similar composition (e.g. Reisberg et al., 2005). The causes of these types of opposing behaviors need to be better understood in order to take advantage of such data.

Here, we present Re, Os, Ir, Ru, Rh, Pd and Pt data, as well as $^{187}\text{Os}/^{188}\text{Os}$ isotopic compositions, of a compositionally well-characterized peridotite xenolith suite that samples a vertical profile of subcontinental lithospheric mantle (SCLM) beneath the Bohemian Massif, Czech Republic. These rocks are characterized by variable melt depletion and large-scale metasomatism via melt percolation that has been documented by the study of lithophile major and trace element compositions of the rocks (Ackerman et al., 2007). Thus, the suite provides a rare opportunity to examine HSE behavior during these processes at different temperatures and degrees of depletion/metasomatism.

3.2. MANTLE XENOLITHS

The xenoliths studied here were collected from three quarries in the Kozákov volcano in the northern part of the Bohemian Massif, Czech Republic (Fig. 1). The Kozákov basanite volcanic flows are Tertiary

(~ 4 Ma) and host abundant spinel lherzolite and subordinate harzburgite, dunite, websterite, olivine clinopyroxenite, clinopyroxenite, and orthopyroxenite mantle xenoliths (Fediuk, 1994). Two principal textural varieties of lherzolite occur at Kozákov (following the classification scheme of Mercier and Nicolas, 1975): (1) medium-grained *equigranular* lherzolite, which contains discrete, intergranular spinel, and (2) coarse- to very coarse-grained *protogranular* lherzolite, in which spinel occurs only in symplectic intergrowth with orthopyroxene and clinopyroxene. In both textural types, small amounts of very fine-grained silicates occur locally at spinel-pyroxene boundaries, due to incipient partial melting and subsequent quenching during eruption. The samples provide a generally continuous profile of the upper two-thirds of central European SCLM. Results of two-pyroxene geothermometry indicate temperatures for spinel lherzolites ranging from 680 °C to 1070 °C. From this, coupled with a tectonothermal model for basaltic underplating associated with Neogene rifting (Christensen et al. 2001), the xenoliths are estimated to originate from depths of approximately 30 to 70 km (see Christensen et al., 2001; Ackerman et al., 2007 for details on depth estimation). Although this method does not provide very precise absolute depth estimates, the overall relative depth relations among the xenolith suite are likely robust.

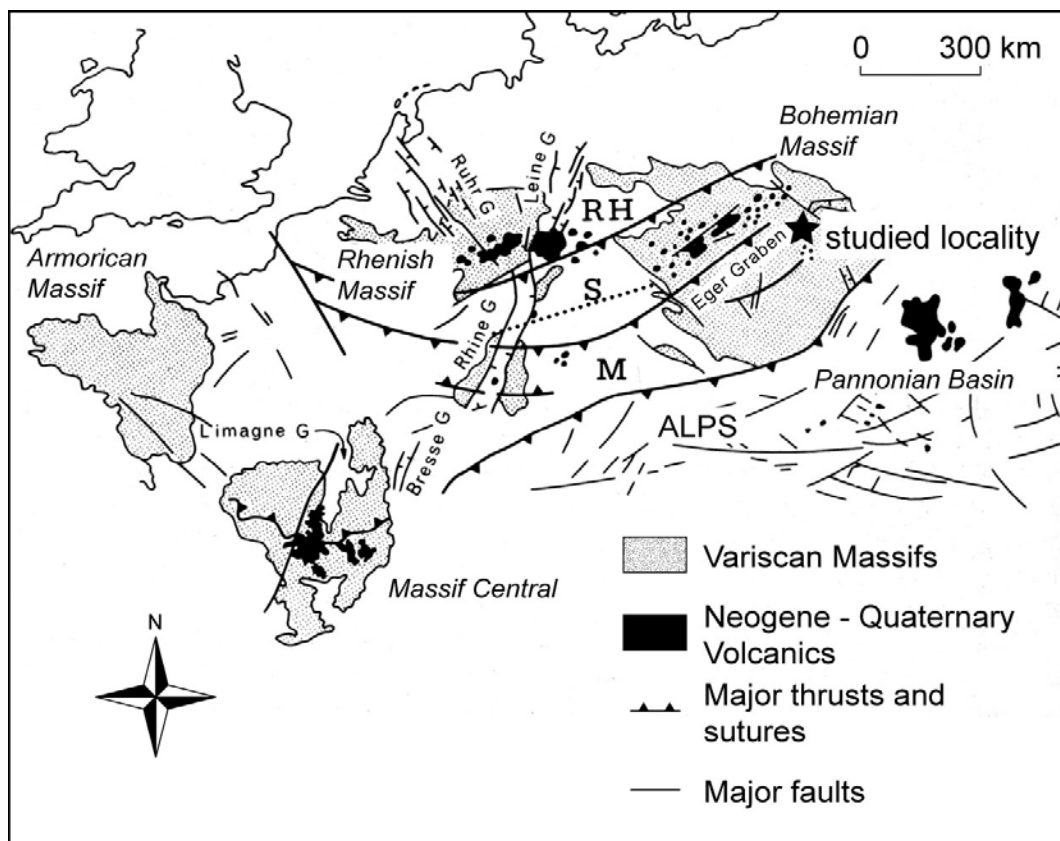


Fig. 1 Geological map of western-central Europe showing the distribution of Neogene-Quaternary volcanic fields and Variscan massifs (modified from Franke, 1989; Wilson and Downes, 1991). The location of the Kozákov volcano in Bohemian Massif is indicated by the star.

Previous study (Christensen et al., 2001) has concluded that the mantle beneath the Kozákov volcano is stratified (Fig. 2), consisting of an equigranular upper layer (~ 30 to 43 km), a protogranular intermediate layer which contains spinel-pyroxene symplectite after garnet (~ 43 to 65 km), and an equigranular lower layer (~ 65 to 70 km). Multiple samples from each of these layers are analyzed here.

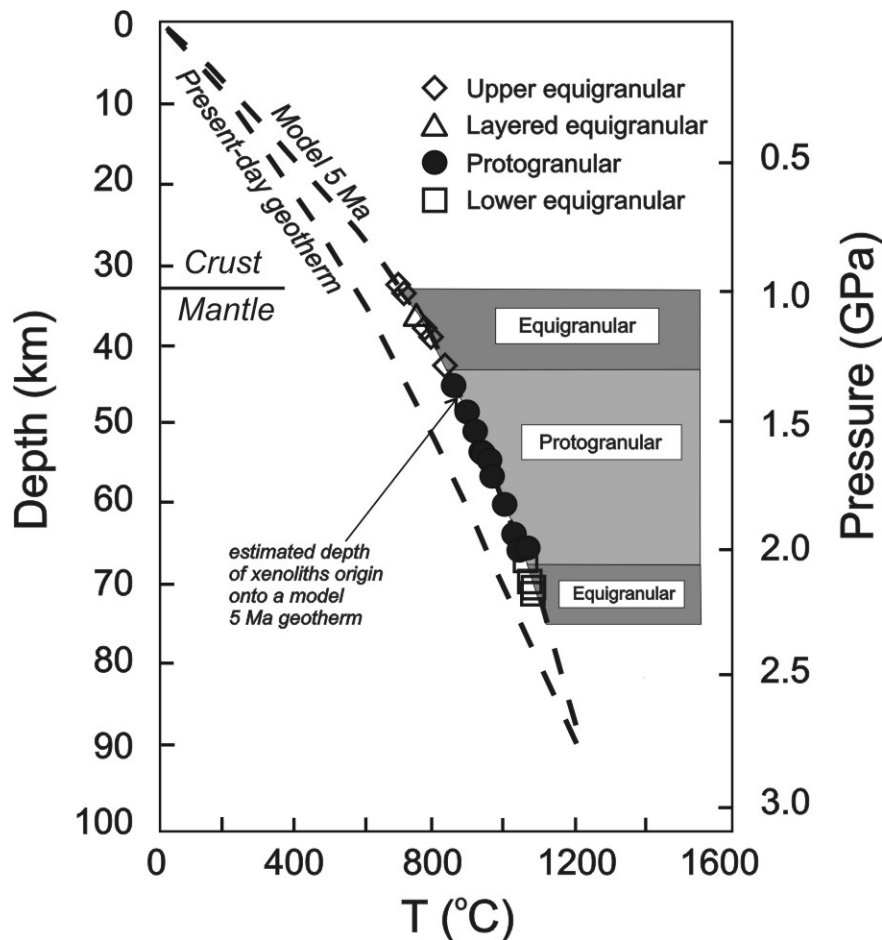


Fig. 2 Depth estimates for the Kozákov xenoliths and model geotherms, based on an underplating scenario (after Christensen et al., 2001).

All but one xenolith studied here have anhydrous lherzolitic compositions with variable olivine (58% to 82%), orthopyroxene (10% to 34%), clinopyroxene (5 % to 13%) and spinel (1% to 4%) contents. Sample 95KZS4 is characterized by a strong spinel-layering and its modal composition approaches dunite. More details on petrography can be found in Ackerman et al. (2007). For this xenolith suite, negative correlations of TiO_2 , Al_2O_3 , and CaO with MgO contents and between modal clinopyroxene and Cr-numbers implicate partial fusion and decreasing melt extraction with increasing depth from ~17 to ~5% (Ackerman et al., 2007).

Subsequent metasomatism of depleted lherzolite, most likely by percolation of silicate melt, produced enrichments in the large ion lithophile elements (LILE), light rare earth elements (LREE) and high field strength elements (HFSE). Although there are slight geochemical discontinuities at the boundaries between the three textural layers of mantle, there tends to be an overall decrease in the

apparent degree of melt depletion with depth, accompanied by a decrease in magnitude of metasomatism (Ackerman et al., 2007). Additionally, increasing Ce/Sm, Nb/La and Hf/Sm ratios of the xenoliths with decreasing depth suggest fractionation of the metasomatic melt with its ascent.

3.3. ANALYTICAL METHODS

Xenoliths were crushed to small pieces and whole-rock powders were prepared manually using an agate mortar and pestle. Major and trace element concentrations as well as Sr-Nd isotopic geochemistry have been previously reported (Ackerman et al., 2007).

Osmium isotopic and some HSE concentration data were obtained at the *Isotope Geochemistry Laboratory*, University of Maryland (UMd). Whole-rock powders (~ 2 g) were mixed with ^{185}Re - ^{190}Os and ^{191}Ir - ^{98}Ru - ^{105}Pd - ^{194}Pt spikes and dissolved in Carius tubes with using ~ 4g concentrated HCl and 6g concentrated HNO₃, and heated at 240 °C for 2-3 days (Shirey and Walker, 1995). Osmium was separated using solvent extraction to CCl₄ and back reduction to HBr (Cohen and Waters, 1996). The final fraction was purified by microdistillation (Birck et al., 1997). Rhenium was separated by anion exchange columns using AG 1x8 resin (BioRad) and purified on small columns using the same resin. The total procedural blanks were 3 to 6 pg and 7 pg for Os and Re, respectively.

Most of the samples were analyzed for Os concentrations and isotopic compositions as OsO₃⁻ using a *Sector 54* thermal ionization spectrometer with Faraday cups in static mode, or using an electron multiplier in a peak hopping mode. Blanks and some samples were analyzed using an NBS 12" mass spectrometer with an electron multiplier in a dynamic peak hoping mode. The samples were loaded with concentrated hydrobromic acid onto Pt filaments and dried. Ba(OH)₂ was subsequently added for electron production. In-run precision for both instruments was always better than ±0.3% (2σ). The external precision was monitored using UMCP standard solutions (Johnson-Matthey). External precision for $^{187}\text{Os}/^{188}\text{Os}$ via Faraday cup measurements of standards using comparable quantities of Os was ±0.2%. Precision for measurements using electron multipliers was ±0.3%. Osmium concentration measurements are estimated to be accurate and precise in these samples to better than ±0.2%. Rhenium was analyzed using a *Nu Plasma* multi-collector ICP-MS with two electron multipliers in a static mode. The isotopic fractionation was corrected using Re solutions prepared from zone refined Re ribbon. Ruthenium, Ir, Pd and Pt were separated together with Re on anion exchange columns also analyzed using multicollector ICP-MS. The isotopic fractionation of corresponding elements was corrected using standard UMCP Ir, Ru, Pd and Pt solutions and accuracy was monitored by occasionally analyzing well-characterized spiked samples that had be previously run. The total procedural blanks were 0.5 pg for Ir, 9 pg for Ru, <133 pg for Pd and <530 pg for Pt. Measurements of the UB-N reference material are periodically made in the UMD laboratory using the same techniques and are in good agreement with published values (Becker et al., 2006). With the exception of Re, based on measurement statistics and sample to blank ratios, HSE measurements (except where noted by *italics* in Table 1) are estimated to be accurate and precise to ±5%. Rhenium uncertainties are largely controlled by the sample to blank ratio

and are as high as $\pm 50\%$ in some highly Re-depleted samples, such as ORKZS5. Uncertainties for each sample are provided in Table 1.

Iridium, Ru, Rh, Pt and Pd were also analyzed by a NiS fire assay technique (Paukert and Rubeška, 1993) at Czech Geological Survey (Prague). For these measurements, 10 g of sample were mixed with a flux, heated up to 1000 °C, and the elements were extracted into a NiS beads. The bead was then dissolved in concentrated HCl, filtered and the HSE-bearing residue was separated from the frit by a mixture of concentrated HCl-H₂O₂. Finally, this solution was dried down, then re-dissolved in 1M HCl. Concentrations were measured by standard addition using a *VG PlasmaQuad 3* ICP-MS at the Faculty of Science, Charles University (Prague). The total procedural blanks were 3 pg for Ir, 230 pg for Ru, 2 pg for Rh, 9 pg for Pd and 50 pg for Pt. In-run precision was always better than $\pm 5\%$ (2σ). Accuracy was tested by multiple analyses of the UB-N reference material. The Ru, Pt and Pd values agree within 7% with Meisel and Moser (2004) values, whereas Rh and Ir values are 13% and 20% lower, respectively. This probably reflects incomplete fusion and digestion and/or higher heterogeneity of these two elements in UB-N, as reported in Meisel and Moser (2004).

Where data were obtained by both the Carius tube isotope dilution technique (CT ID) and NiS fire assay technique (NiS), agreement is generally good ($\sim \pm 30\%$) with no systematic offsets. Two samples (95KZS4 and ORKZC3), however, were found to have much higher Pd contents of 68.1 and 13.1 ppb by CT ID, respectively, compared to NiS analyses of the same splits, which gave significantly lower concentrations of 1.82 and 0.77 ppb, respectively. Because of the very high signals measured using the ID technique, we speculate that the samples were somehow contaminated during preparation of powder or chemical processing. Nevertheless, because of the very coarse-grained character of Kozákov xenoliths, combined with the relatively small weight of sample used for CT ID (2 g) the high Pd (and in some cases also Pt) values could be also caused by a nugget effect. Because of the larger sample size processed, which is presumably more representative of the rock, we will use the NiS fire assay data for Ir, Ru, Pd and Pt except for those samples where the NiS data are not available. All reported Re and Os data, however, are by CT ID.

Sulfur was determined using a *LECO SC230* analyzer at University of Leicester. Approximately 0.2 g was processed for each sample and 3 to 5 duplicates were run to get the best reproducibility. However, because of low sulfur contents, the precision (1σ) varied from ± 5 to $\pm 32\%$.

Copper was analyzed using the *VG PlasmaQuad 3* ICP-MS at the Faculty of Science, Charles University (Prague).

The GCDkit geochemical software program (Janoušek et al., 2006) was used for whole-rock data handling and plotting.

3.4. RESULTS

3.4.1. Sulfur and copper

Kozákov xenoliths define a narrow range of S and Cu contents (23 to 30 ppm and 6 to 21 ppm, respectively) that are similar to basalt-hosted peridotite xenoliths worldwide (e.g. Lorand and Alard, 2001; Lorand et al., 2003; Reisberg et al., 2005). There are no correlations between S and Cu versus indices of fertility, such as Al_2O_3 and Yb. Concentrations of S and Cu are much lower than are typical of massif peridotites (Lorand et al., 1999) and current estimates for the PUM (McDonough and Sun, 1995). Such depletions are commonly interpreted to be the result of surface or near surface loss of sulfides, such as by weathering or volcanic eruption (Lorand, 1990; O'Neill et al., 1995). The absence of sulfides and their alteration products in the studied rocks suggests that S was not lost due to sulfide alteration and/or breakdown during volcanic eruption. We will argue below that this characteristic of the xenoliths was likely generated in the mantle.

3.4.2. HSE concentrations

Concentrations of the HSE for all samples (Table 1) are broadly within the worldwide range of upper mantle peridotite xenoliths (e.g. Handler and Bennett, 1999; Lorand and Alard, 2001), but are characterized by some significant enrichments and depletions of HSE that are not common in the global database. For example, some samples are characterized by Os and Ir concentrations that are below 1 ppb, whereas two samples have very high Os concentrations of 5.37 and 11.8 ppb (Table 1, Fig. 3). Platinum and Pd concentrations vary considerably within the suite. Some samples have concentrations that are substantially lower than estimates for PUM. More atypical of samples of the upper mantle, however, is the fact that several samples have considerably higher Pt concentrations compared to the PUM. Rhenium concentrations are similar to, or substantially lower than the estimate for PUM, however, this characteristic is quite common in peridotites with a melt depletion history. Ruthenium and Rh concentrations are generally typical of mantle peridotites and are surprisingly uniform, varying only by maximum factors of ~ 7 and 4, respectively, in a suite where most other HSE concentrations vary by more than an order of magnitude. For the entire suite, all but three samples (ORKZS5, 94KZMS5 and 95KZS4) show good negative correlations between Os concentration and indexes of fertility, such as Al_2O_3 (Fig. 3) whereas other HSE do not show such a correlation (Fig. 3).

$(\text{Os}/\text{Ir})_{\text{N}}$, $(\text{Ru}/\text{Ir})_{\text{N}}$, $(\text{Pd}/\text{Ir})_{\text{N}}$ and $(\text{Pt}/\text{Pd})_{\text{N}}$ ratios vary considerably within the suite, with the greatest variability observed for Pt/Pd ratios (Fig. 6). No resolvable correlations are noted between HSE, Cu and S concentrations (Fig. 4). Chondrite normalized plots of the HSE exhibit strongly fractionated patterns, most of them with distinct positive Pt anomalies (Fig. 5). Two samples (95KZS4, ORKZS5) have patterns enriched in Os-Ir-Ru that are distinct relative to the other samples of this suite.

Some of the HSE heterogeneities within the suite appear to be related to the layer of mantle sampled. For example, concentrations of Os and Ir in the lower equigranular samples are substantially

Table 1. Re-Os isotopic ratios and Re, PGE, Al₂O₃, Cu, S concentrations of Kozákov xenoliths

Sample	Texture	Depth (km)	Method	Re (ppb)	Os (ppb)	Ir (ppb)	Ru (ppb)	Rh (ppb)	Pt (ppb)	Pd (ppb)	¹⁸⁷ Re/ ¹⁸⁸ Os	¹⁸⁷ Os/ ¹⁸⁸ Os	γ _{Os}	T _{RD} (Ga)	Al ₂ O ₃ (wt%)	Cu (ppm)	S (ppm)
<i>Upper equigranular</i>																	
94KZC13	E	32	CT ID	0.017	0.13	0.10	1.33		0.41	0.28	0.649	0.1297	2.1				
94KZS4	E	33	CT ID	0.022	1.56	0.90	2.65		16.1	0.22	0.069	0.1242	-2.2	0.7	1.81	10	30
95KZS4	LE	36	CT ID	0.022	5.37	2.04	4.21		1.74	68.1	0.020	0.1290	1.6	0.1	3.11	6	27
			CT ID*	0.013	5.87							0.011	0.1270		0.4		
			NiS			2.50	3.50	0.28	2.08	1.82							
<i>Protogranular</i>																	
ORKZC7A	P	45	CT ID	0.024	1.31	2.36	6.62		25.5	1.27	0.088	0.1245	-1.9	0.7	1.75	12	28
			NiS			1.26	6.40	0.76	9.21	1.27							
KS2	P	46	CT ID	0.261	1.69	2.51	3.66		1.90	0.61	0.743	0.1182	-6.9	1.6	1.12	12	22
			NiS			1.80	2.00	0.35	2.57	0.68							
94KZSM1	P	48	CT ID	0.014	0.86						0.080	0.1242	-2.2	0.7	2.41	20	
ORKZS5	P	50	CT ID	0.009	11.8						0.004	0.1238	-2.5	0.8	2.96	18	30
			NiS			5.05	9.36	0.75	16.2	0.70							
ORKZC2	P	53	CT ID	0.027	1.10	2.81	3.87		13.3	2.08	0.120	0.1291	1.7	0.1	2.45	21	32
			NiS			2.28	4.61	0.30	8.99	2.14							
ORKZC3	P	54	CT ID	0.026	2.13	1.20	3.28		24.9	13.1	0.060	0.1238	-2.5	0.8	0.95	6	34
			NiS			1.23	4.5	0.38	9.47	0.77							
KS4	P	58	CT ID	0.028	1.34	0.96	7.22		3.48	6.87	0.100	0.1243	-2.1	0.7	1.94	12	23
			NiS			0.90	5.60	0.74	3.90	5.45							
<i>Lower equigranular</i>																	
94KZSM4	E	66	CT ID	0.047	0.564						0.400	0.1212	-4.6	1.2	2.09	26	
94KZSM3	E	69	CT ID	0.006	0.190	0.30	1.14		0.33	0.47	0.163	0.1219	-4.0	1.1	2.85	11	23
94KZSM5	E	70	CT ID	0.014	0.349	1.07	3.11		1.07	0.59	0.200	0.1276	0.5	0.3	0.95	19	27
			NiS			0.70	1.10	0.19	2.82	1.17							
94KZSM7	E	70	CT ID	0.022	0.473	0.27	1.42		10.7	0.48	0.221	0.1239	-2.4	0.8	2.46	18	25

* duplicate analyses; texture: E - equigranular, LE - layered equigranular, P - protogranular

lower than samples from the upper equigranular and protogranular layers (except sample 94KZC13). Rhenium and Os concentrations are positively correlated in samples from the lower equigranular layer (not shown), suggesting similar behavior in this layer. This element pair is not correlated in the other two layers sampled.

Concentrations of the HSE among the protogranular samples vary considerably for similar Al_2O_3 (Fig. 3). For example, KS4 is the protogranular sample that is richest in Pd (5.45 ppb) whereas sample ORKZC7A has relatively low Pd (1.27 ppb), yet very similar Al_2O_3 and Yb contents. In general, there is no significant difference in extent of HSE fractionation with depth except for $(\text{Pd}/\text{Ir})_{\text{N}}$ ratios, which tend to decrease with decreasing depth (Fig. 6).

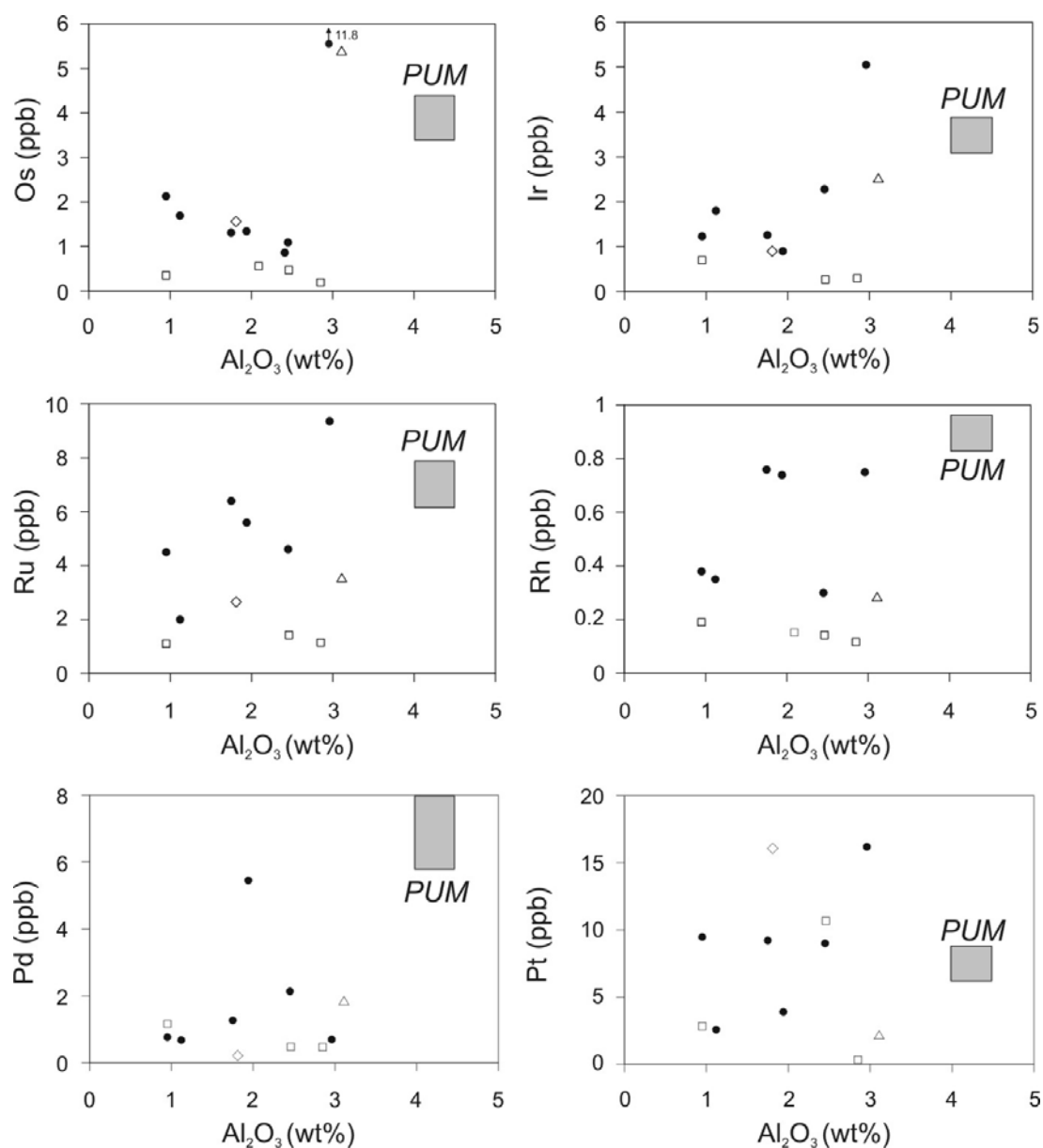


Fig. 3 HSE concentrations vs. Al_2O_3 diagrams. Primitive upper mantle (PUM) estimates after Becker et al. (2006) and McDonough and Sun (1995). Symbols as in Fig. 2.

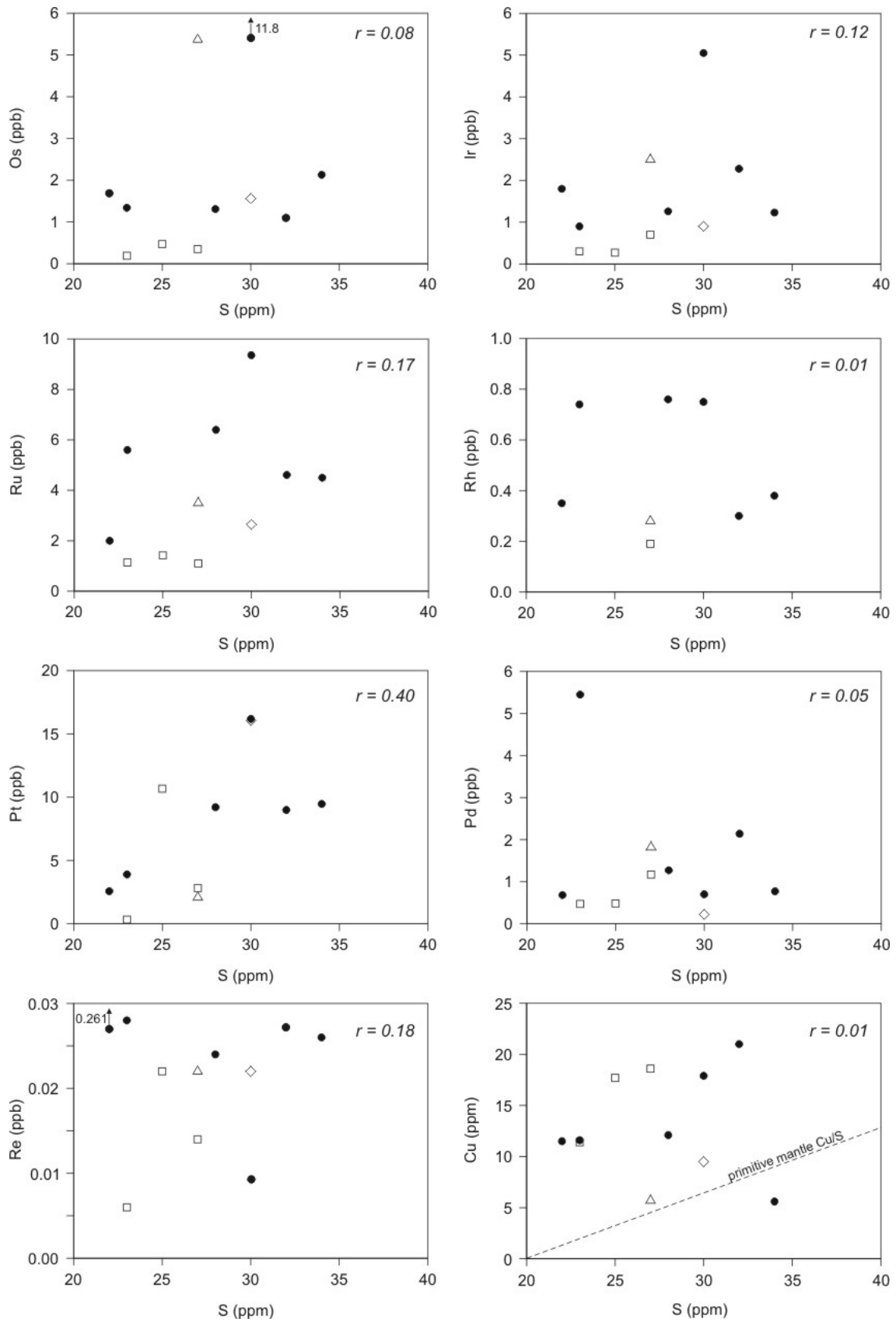


Fig. 4 PGE, Re and Cu variations with S contents. There is no obvious correlation between HSE and S suggesting a strong perturbation of the system. Note large variations in Cu/S ratios. Symbols as in Fig 2.

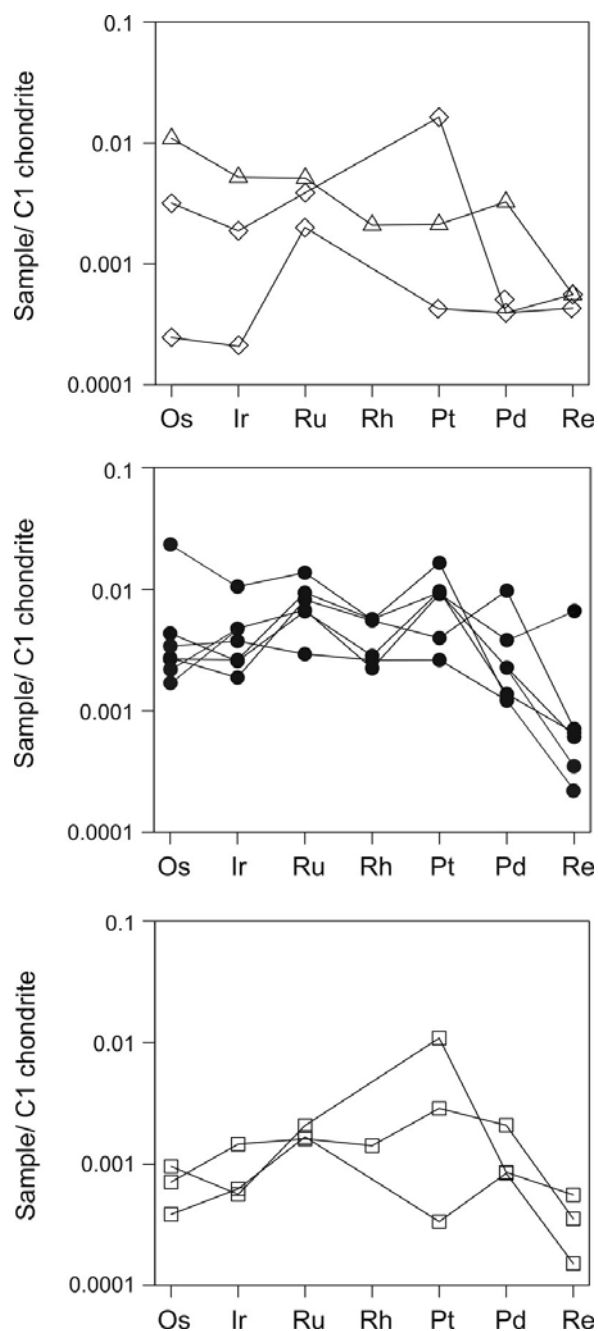


Fig. 5 Chondrite normalized HSE patterns of three studied mantle layers (upper equigranular-layered equigranular, protogranular and lower equigranular). Normalizing values after Anders and Grevesse (1989). Symbols as in Fig. 2.

3.4.3. Osmium Isotopes

The $^{187}\text{Os}/^{188}\text{Os}$ ratios for the suite range from 0.1182 to 0.1297 (Table 1), well within the range of isotopic compositions reported for SCLM, and even for materials within the convecting oceanic mantle (Meibom et al., 2002; Walker et al., 2002; Gannoun et al., 2007; Liu et al., 2008). Samples with the lowest (KS2) and highest (94KZC13) ratios are characterized by modestly suprachondritic

Re/Os ratios. When considering the entire suite, there is no correlation between $^{187}\text{Os}/^{188}\text{Os}$ versus either $^{187}\text{Re}/^{188}\text{Os}$ or melt depletion indicators (Al_2O_3 , Lu) (Fig. 7a,b), in contrast to many rocks from the SCLM worldwide (e.g. Walker et al., 1989; Meisel et al., 2001; Gao et al., 2002; Pearson et al., 2004). Further, no correlations are present between $^{187}\text{Os}/^{188}\text{Os}$ and Os or Re concentrations. Palladium concentrations, however, are weakly positively correlated with $^{187}\text{Os}/^{188}\text{Os}$ (Fig. 7c).

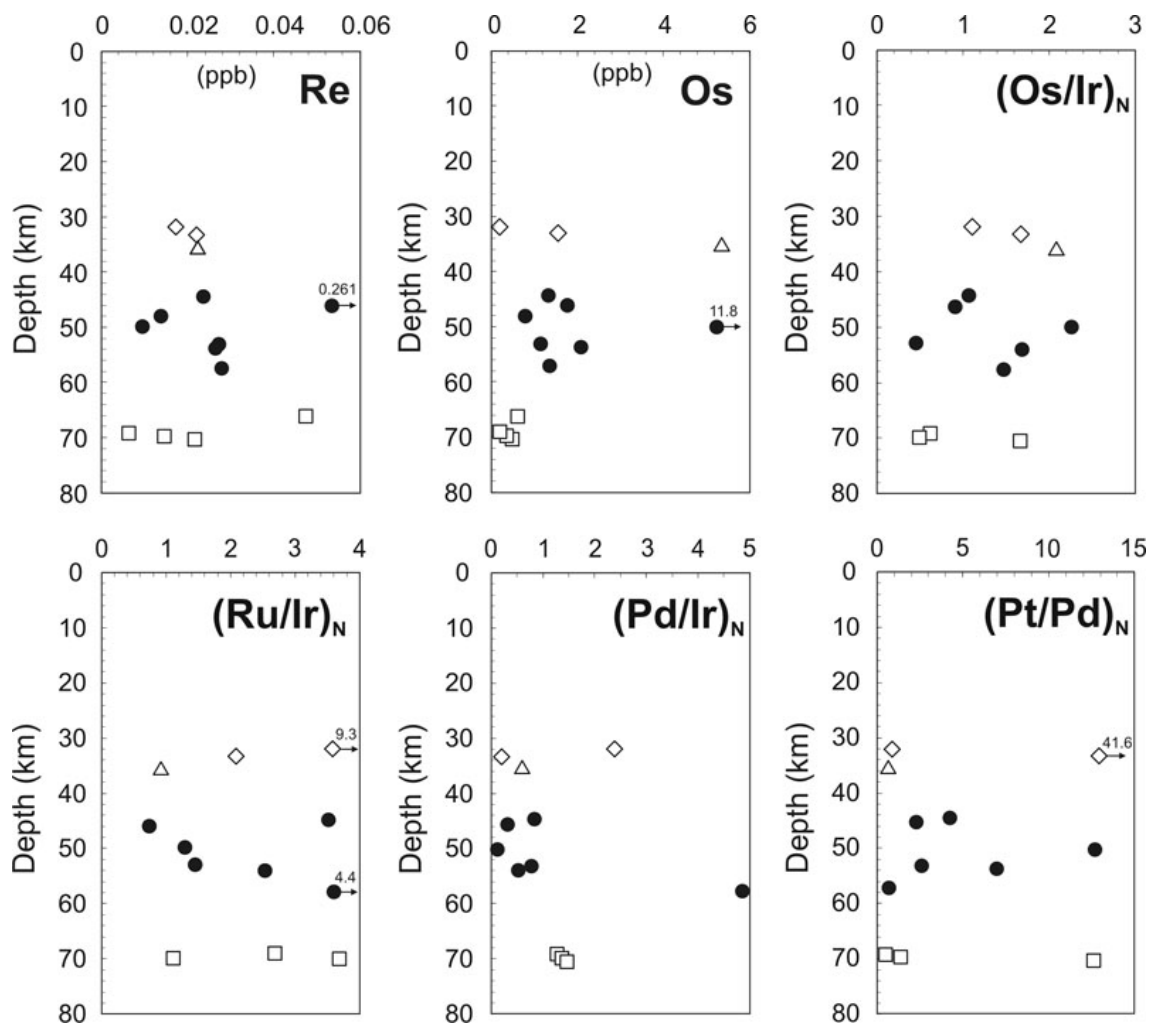


Fig. 6 Re, Os, $(\text{Os}/\text{Ir})_N$, $(\text{Ru}/\text{Ir})_N$, $(\text{Pd}/\text{Ir})_N$ and $(\text{Pt}/\text{Pd})_N$ variations with depth (N – chondrite normalized). Note differences in Re and Os concentrations among the mantle layers, as well as large Ru/Ir and Pt/Pd fractionations. Symbols as in Fig. 2.

3.5. DISCUSSION

The HSE abundances of the Kozákov suite are highly variable. There are a variety of processes that could lead to changes in relative and absolute abundances of HSE, as well as changes in the Os isotopic composition of mantle peridotites. It is important to emphasize here that the HSE are also typically very chalcophile, and that their abundances within the silicate Earth are largely controlled by

the behavior of sulfides. Thus, any process that affects the presence and type of sulfide in a system can also affect the HSE (Luguet et al., 2007). These processes include surface or near surface alteration, partial melting, and metasomatism. We consider these processes individually in order to assess the causes of HSE variations in the Kozákov xenolith suite.

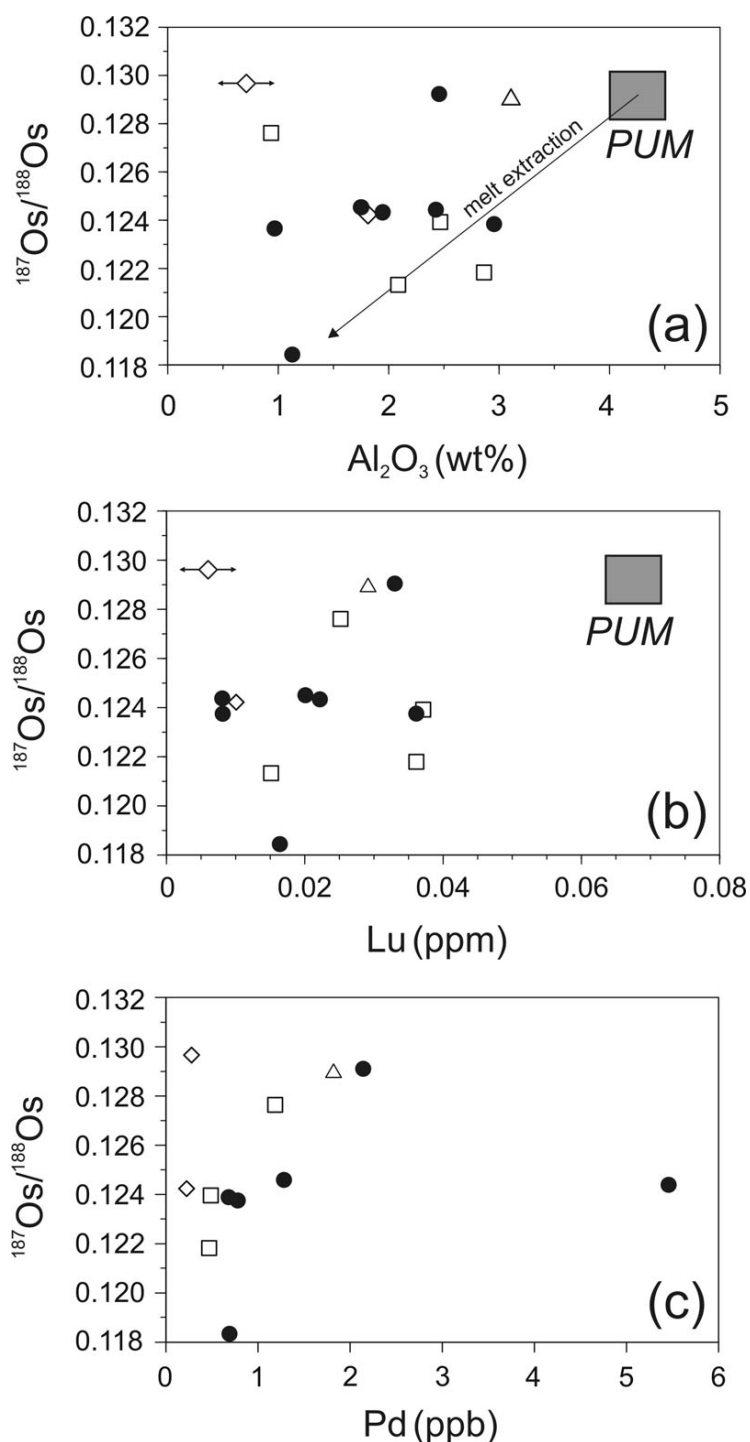


Fig. 7 $^{187}\text{Os}/^{188}\text{Os}$ vs. Al_2O_3 (a), Lu (b) and Pd (c) contents. PUM values after Meisel et al. (1996) and McDonough and Sun (1995). Arrows on one diamond symbol represent uncertainty in Al_2O_3 content (estimated). Symbols as in Fig. 2.

3.5.1. HSE mobility during eruption and emplacement of the xenoliths

The causes of low concentrations of HSE and S in many alkali-basalt hosted (off-craton) xenoliths, compared to massif peridotites and kimberlite-borne xenoliths, remain a matter of debate (e.g. Handler et al., 1999; Pearson et al., 2004). In general, two plausible explanations have been presented that are associated with secondary surface or near-surface processes that may lead to sulfide breakdown and HSE removal: (1) weathering and (2) syn-eruption processes. Alteration resulting from weathering of sulphides may lead to formation of Fe-hydroxides and higher Cu/S ratios compared to unaltered peridotites ($\text{Cu/S} < 0.15$; see Lorand et al. 2003 and references therein), due to the more limited mobility of Cu relative to S in ground water (Reisberg et al., 2005). Although Kozákov xenoliths have relatively high Cu/S ratios (0.2-0.7), reflecting their low S contents (~ 30 ppm) neither sulfides nor their alteration products were observed in these rocks. Additionally, there is no correlation between S, Cu and indicators of alteration (e.g. H_2O - content or $\text{Fe}_2\text{O}_3/\text{FeO}$ ratio). Therefore, we conclude that the effects of weathering were probably not a major control on HSE in these rocks. Nevertheless, the lack of correlation between Cu and S (Fig. 4), coupled with large variations in Cu/S ratios, suggests that the abundances of these elements were strongly perturbed by some process.

Handler et al. (1999) discussed the role of high oxygen fugacity and subsequent breakdown of sulfide accompanied by loss of HSE during volcanic eruptions. They suggested that Os is more volatile than Ir, and as a result, sulfide decomposition may lead to subchondritic Os/Ir ratios that are positively correlated with Cu/S ratio. However, the lack of a correlation between Os/Ir and Cu/S (Fig. 8), coupled with broad correlations between Os and Ir concentrations in almost all Kozákov xenoliths argue for similar behavior of these elements and, therefore, against selective removal through volatile loss.

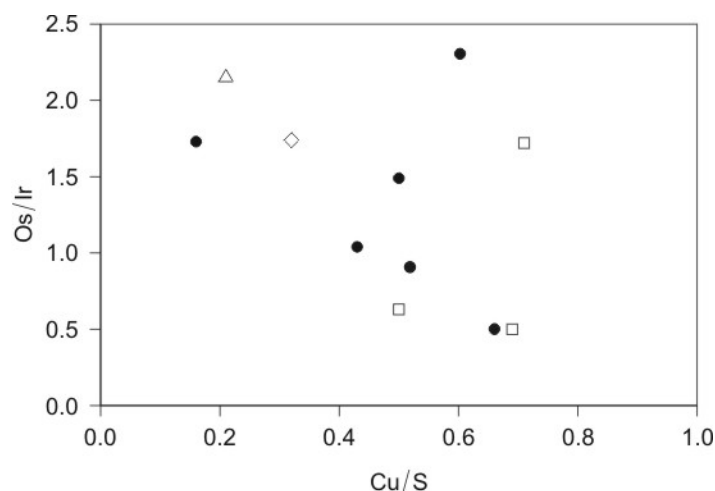


Fig. 8 Os/Ir vs. Cu/S diagram showing lack of positive correlation between Os/Ir and Cu/S ratios. Such correlations are usually ascribed to sulfide breakdown during volcanic eruption (e.g. Handler et al., 1999). Symbols as in Fig. 2.

3.5.2. Effects of partial melting on HSE

The HSE can also be fractionated via partial melting processes. Distribution of HSE in upper mantle is controlled by base metal sulphides (BMS; Mss, pyrrhotite, pentlandite, chalcopyrite) due to very high ($>10^3$) sulfide/silicate melt partition coefficients (e.g. Fleet et al., 1999; Sattari et al., 2002; Ballhaus et al., 2006) and also by HSE-bearing alloys (Luguet et al., 2007). Experiments and *in situ* data for sulfides present in mantle rocks indicate that monosulfide solid solution (Mss) preferentially concentrates I-PGE (Os, Ir, Ru), whereas Pd, Pt and Re tend to reside in Cu-rich sulfides (Lorand et al., 1999; Alard, 2000; Lorand and Alard, 2001; Luguet et al., 2007). Low degrees of mantle melting tend to lead to partial removal of the Cu-rich sulfides prior to dissolution of the Mss (Bockrath et al., 2004). This selective removal of sulfide commonly results in the formation of melting residues that are modestly depleted in Pt, Pd and Re, and enriched in Os, Ir and Ru. Higher degrees of melting, such as may occur during the production of some komatiitic lavas, can lead to the consumption of all sulfides, including Mss, whereupon all HSE can become incompatible. There are, however, exceptions to this. For example, Puchtel et al. (2004) have shown that Os, Ir and Ru can behave compatibly, even at very high degrees ($\sim 50\%$) of partial melting. This is probably due to stabilization of high melting point Os-Ir-Ru sulfides or alloys (e.g. Brenan and Andrews, 2001) during incongruent melting of BMS. Variable melt depletion can, therefore, lead to strongly, variably fractionated HSE in residues. Fractionation of HSE resulting from variable extents of melting is often indicated by correlations between HSE ratios and absolute abundances versus indices of fertility (e.g. Becker et al., 2006).

The upper mantle beneath the Kozákov volcano experienced low to moderate (5-17%) degrees of partial melting (Ackerman et al., 2007), so some of the variability in HSE concentrations is likely attributable to variable extents of partial melting. Indeed, most of upper equigranular and protogranular samples are significantly depleted in Re and Pd (low Re/Os and Pd/Ir ratios), which may reflect some Pd and Re depletion during partial melting. Moreover, $(\text{Pd/Ir})_N$ ratios tend to decrease with decreasing depth, which is also correlated with increasing degree of partial melting in this suite. However, most xenoliths show consistently low concentrations of all HSE, and highly fractionated HSE patterns that do not correlate with indices of fertility (Figs. 3, 6). Further, Pd-Ir- Al_2O_3 melting models (e.g. Lorand et al., 2004) suggest that very high degrees of partial melting ($> \sim 25\%$) would be necessary to generate the low Ir-Pd contents found in Kozákov xenoliths. Such high degrees of partial melting are not supported by other data. We conclude that, although variable extents of partial melting may have had an effect on the HSE contained in the Kozákov xenolith suite, it was not the dominant process controlling absolute or relative abundances.

3.5.3. Melt percolation

3.5.3.1. Evidence for metasomatism in the Kozákov xenoliths

Bedini et al. (1997) proposed a model for the chemical evolution of a basaltic melt infiltrating the SCLM underlying the East African rift during ascent. They concluded that the lithospheric mantle close to the asthenosphere has higher porosity than mantle just below the Moho. If correct, this could permit infiltration of large volumes of asthenospheric melts into the lower portions of the SCLM. High melt/rock ratios at this level would lead to a partial to complete re-equilibration of host peridotite with the ascending basaltic melts. Because of the conductive thermal gradient, reaction between peridotites and infiltrated melts must eventually occur at decreasing melt mass, producing small fractions of residual melts, which will migrate upward because of their low viscosity (e.g. Kelemen et al., 1995).

Trace element concentrations (REE, LILE, HFSE) of Kozákov xenoliths reveal significant differences among the sampled mantle layers. Ackerman et al. (2007) concluded that the $(\text{Ce}/\text{Sm})_N$, $(\text{Hf}/\text{Sm})_N$ and $(\text{Nb}/\text{La})_N$ ratios of the xenoliths reflect chemical modifications induced by a metasomatic agent. These ratios tend to increase with decreasing depth, suggesting progressive evolution of the metasomatic agent with its ascent. For example, REE patterns in the lower equigranular layer (~ 66 to 70 km) exhibit flat, unfractionated middle-REE and heavy-REE patterns, whereas upper equigranular and protogranular samples (33 to 66 km) have U-shaped REE patterns usually ascribed to melt percolation of small melt fractions at low melt/rock ratios (e.g. Navon and Stolper, 1987).

These observations suggest reaction of unfractionated silicate melt with peridotite at large melt/rock ratios in the lower equigranular layer (66 to 70 km), and as a result of melt-peridotite interaction, formation of small melt fractions. As these melts migrated upward, they became more fractionated due to chromatographic processes and mineral precipitation, causing large scale metasomatism of protogranular and upper equigranular mantle (33-65 km) at low to moderate melt/rock ratios.

The layered dunitic sample (95KZS4 – ~36 km) from the upper equigranular layer is compositionally distinct from other xenoliths of this suite. The sample is characterized by a low Mg#, a REE pattern shape that is similar to whole-rock samples of the lower equigranular layer, and LREE-depletion in clinopyroxene (Ackerman et al., 2007). Such features rule out the possibility that the dunite represents a cumulate. More likely, it is a product of open-system intensive melt/rock reaction (e.g. Kelemen et al., 1992; Batanova and Sobolev, 2000). The LREE-enriched pattern of the whole-rock is likely a result of melt/rock reaction where LREE-enriched phases precipitated from the melt, leading to a LREE-depleted signature in the resulting melt that equilibrated with clinopyroxene, or more likely precipitation of LREE-depleted clinopyroxene from the melt.

3.5.3.2. HSE fractionation during melt percolation

It was shown above that selective addition/removal of individual different sulfide phases could lead to strongly fractionated HSE in the host peridotite, due to differential HSE partitioning among sulfide phases. Several recent studies (e.g. Reisberg et al., 2004; Reisberg et al., 2005) have shown that melt percolation of S-undersaturated melt can cause the breakdown of selective sulfides and consequent removal of some HSE from the affected rock. For example, a study of the Troodos ophiolite (Büchl et al., 2002; Büchl et al., 2004) showed that during melt percolation, the I-PGE (Os, Ir, Ru) behaved incompatibly (in contrast to partial melting) leading to a strong fractionation among the I-PGE and HSE in general. These authors also showed that melt percolation led to significant changes in the Os isotopic compositions of the affected peridotites due to the removal of primary (with low $^{187}\text{Os}/^{188}\text{Os}$) sulfides, and subsequent precipitation of sulfides bearing radiogenic Os from the percolating melt.

As discussed above, HSE and S concentrations in Kozákov xenoliths, together with strong HSE fractionations were likely caused by neither high-level processes (weathering or sulfide breakdown during eruption), nor by partial melting. Here we consider the possibility that absolute and relative abundances of the HSE in these rocks are primarily a result of the percolation of S-undersaturated melts and attempt to relate the HSE characteristics to the lithophile element evidence for percolation as reported by Ackerman et al. (2007) for these rocks.

The lower I-PGE concentrations and strongly fractionated I-PGE ratios (e.g., $\text{Os}_\text{N}/\text{Ir}_\text{N}$ variation between 0.4 and 2.2; Fig. 6) that are characteristic for the Kozákov xenoliths are generally consistent with the melt percolation scenario. The absence of correlations between S, HSE contents and degrees of metasomatism/melt fractionation (Nb/La, Hf/Sm, Ce/Sm) suggest that HSE fractionation was not directly connected with the degree of melt metasomatism and/or composition. This is in agreement with previous studies (e.g. Handler and Bennett, 1999). On the contrary, such fractionations can reflect different HSE partition coefficients in the absence/presence of fluids (Bezmen et al., 1994; Fleet et al., 1999), or more probably, variable melt/rock ratios (see below). Although it is possible that some fractionations could partly reflect heterogeneities in HSE distributions within the upper mantle resulting from ancient, variable degrees of partial melting that affected sulfides (and thus HSE budget), it is clear that such I-PGE depletion must dominantly reflect removal of I-PGE-bearing sulfides (Mss) during melt percolation (e.g. Lorand et al., 2004). The most interesting feature of this suite is that Pt concentrations are highly variable (0.33-16.2 ppb), but in general are significantly higher than in comparable mantle rocks. Compositional variability is even a hallmark of duplicate analyses of the same powder (Table 1). This implies that Pt distribution is controlled by a different phase than the other HSE. This phase must be much more resistant to melt percolation, and is therefore probably not a sulfide. The existence of Pt-rich phases in nature is supported by the presence of negative Pt-anomalies in some sulfides (e.g. Luguet et al., 2001). Detailed study of strongly depleted harzburgites (Luguet et al., 2007) has revealed the existence of Pt-rich alloys that remain in

mantle residues after high degrees of partial melting. This type of phase is a good candidate to be the major host of Pt in our residues after extensive melt percolation. Platinum may also be partly hosted in so-called nanonuggets (Ertel and Dingwell, 2007), but these are mostly observed at much lower oxygen fugacities than appears likely for the Kozákov suite (see below).

3.5.3.3. Evolution of HSE and $^{187}\text{Os}/^{188}\text{Os}$ of the upper mantle profile beneath the Kozákov volcano

It was shown above, that peridotites from the lower equigranular layer (66-70 km) reacted with basaltic melts at high melt/rock ratios. This could be the result of melt accumulation near the lithosphere-asthenosphere boundary due to asthenospheric upwelling beneath Central Europe (Hoernle et al., 1995). The absence of volatile-bearing phases (e.g. phlogopite, amphibole) in the Kozákov suite points to the primitive nature of the percolating melt (volatile- and sulfur-undersaturated), consistent with the very low S contents of the rocks. High melt/rock ratios caused sulfide breakdown and consequently, HSE removal (Fig. 9). The very low HSE concentrations in most rocks from the lower layer suggest that melt flux was sufficiently high to dissolve and remove most of the sulfides from this layer. For example, because Os is much more chalcophile than Re, lower Re/Os should be expected if some sulfides remained (Reisberg et al., 2005). Surprisingly, the lower equigranular layer has the highest Re/Os ratios among all samples due to the very low Os contents (0.19-0.564 ppb). High equilibration temperatures of lower equigranular samples ($> 1000\text{ }^{\circ}\text{C}$; Christensen et al., 2001) are in excess of the melting point of sulfides (Lorand and Alard, 2001) and therefore, could enhance their complete extraction. Alternatively, Mungall et al. (2006) noted that a high oxidation state ($f\text{O}_2 = \Delta \text{FMQ} = +2$) can also lead to sulfide breakdown and, thus, to perturbation of HSE, but this is unlikely for the Kozákov suite because of calculated low oxygen fugacity in the xenoliths ($\Delta \text{FMQ} = -0.04$ to $+0.65$; Ackerman et al., 2007).

We speculate that small melt fractions migrated upward and caused large-scale metasomatism at low to moderate melt/rock ratios and variable fluid and S saturation. This in turn caused spatially restricted sulfide breakdown and, therefore, variable HSE removal (Fig. 9). The strong HSE fractionations, therefore, most likely reflect the different rock-melt partition coefficients for these elements during melt percolation. Further, the fact that the low Pd-Re-S contents of protogranular/upper equigranular samples (except KS4) are similar to those in the lower equigranular samples suggests that the melt fractions that interacted with the peridotites were not S-saturated.

For the standpoint of Re-Os isotopic systematics, the low Re contents of these rocks indicate that Re was likely not transported into the rocks via the metasomatic process. Melt percolation is often reflected by *increases* in Re content (e.g. van Acken et al., 2008), which evidently did not occur in these rocks. Thus, the isotopic evolution of these rocks subsequent to the percolation event was likely little affected by this process. Similarly, extensive melt percolation tends to result in the production of rocks with suprachondritic $^{187}\text{Os}/^{188}\text{Os}$ (e.g. Büchl et al., 2004; van Acken et al., 2008). All rocks

examined here have essentially chondritic or subchondritic Os isotopic compositions, so transport of radiogenic Os was also evidently not a major factor in the generation of these rocks.

In order to account for the Os isotopic heterogeneities present in the suite we consider two additional possibilities: (1) the present range in $^{187}\text{Os}/^{188}\text{Os}$ resulted from melt percolation either via removal of variable proportions of relatively Re-rich, Os-bearing minerals (sulfides?) that were more radiogenic than the bulk rock at the time of metasomatism, or transport of Os with low $^{187}\text{Os}/^{188}\text{Os}$ from the lower portion of the stratigraphy to the upper portions via the percolating melts, and/or (2) $^{187}\text{Os}/^{188}\text{Os}$ ratio heterogeneities reflect ancient, variable melt depletion events.

The high Os contents of two samples (95KZS4, ORKZS5) suggest that at least some of the Os present in these rocks may have been imported from the percolating melt. Unlike previous studies that have documented transport of radiogenic Os, if these isotopic compositions were established by percolation, the low $^{187}\text{Os}/^{188}\text{Os}$ of these samples would require the scavenging of Os from peridotites with low $^{187}\text{Os}/^{188}\text{Os}$ that are from lower in the stratigraphy (lower equigranular samples) and consequent precipitation of this Os, along with other I-PGE (Ir, Ru), during the ascent of the percolating melt (i.e. samples 95KZS4, ORKZS5). Because of the low Pd, Re and S contents found in these two xenoliths, we conclude that I-PGE precipitation could not have been generated from a S-saturated melt. Instead we suggest precipitation of I-PGE-bearing alloys (Brenan and Andrews, 2001).

Another mechanism that could lead to the generation of low $^{187}\text{Os}/^{188}\text{Os}$ ratios in highly metasomatized peridotites would be if the melt selectively scavenged sulfides that were characterized by enrichment in Re and $^{187}\text{Os}/^{188}\text{Os}$ relative to the original bulk rock.

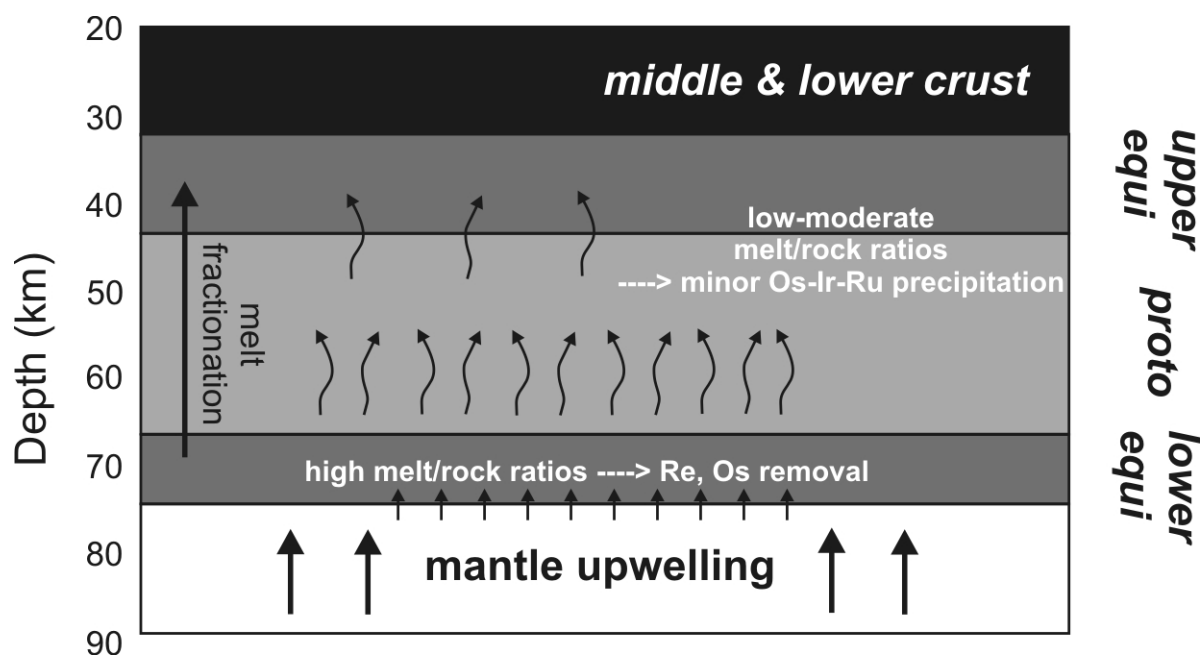


Fig. 9 Model of mantle evolution beneath the Kozákov volcano. For details see the text.

Selective removal of radiogenic $^{187}\text{Os}/^{188}\text{Os}$ by aqueous fluids has been proposed as a means of explaining negative correlations between the degree of aqueous metasomatism and $^{187}\text{Os}/^{188}\text{Os}$ in some peridotites (e.g. Walker et al., 2007), but we know of no evidence that this can occur by melt percolation.

We note instead that the range of $^{187}\text{Os}/^{188}\text{Os}$ ratios in the Kozákov suite is comparable to that present in the modern convecting upper mantle and some SCLM (e.g. Liu et al., 2008). The Os isotopic variations may simply reflect the variable, ancient melt depletion history of sub-oceanic and sub-continental lithospheric mantle. If this is true, it means that Os isotopes of even pervasively metasomatized mantle could provide useful geochronological insights into the SCLM depletion.

3.5.4. Consideration of model melt depletion ages

It is clear that the whole-rock chemical compositions of the xenoliths were intensively modified during melt percolation. We conclude that is probably the main reason, why Kozákov xenoliths do not display positive correlations between $^{187}\text{Os}/^{188}\text{Os}$ and melt extraction indices (e.g. Al_2O_3 , Lu; Fig. 7a). Such correlations have been described from many mantle suites and interpreted as the result of retarded ingrowth of ^{187}Os since the time of melt extraction (e.g. Walker et al., 1989; Handler et al., 2005; Wu et al., 2006).

It is useful to consider model Re-depletion ages (T_{RD} , Walker et al., 1989) within the context of other chronologic constraints on these rocks and the associated overlying crust. The regular trace element variations with depth and Sr-Nd isotopes (Ackerman et al., 2007) imply that metasomatism occurred after Variscan orogenesis (280-360 Ma) because the layered structure appears to have been assembled during the Variscan convergence and imbrication (Christensen et al., 2001). Thus, apparent perturbation of HSE systematics linked with metasomatism was probably associated with Tertiary rifting and magmatism (5-25 Ma). For this suite, model T_{RD} ages show large variations from ~ 0.1 to 1.6 Ga. However, most of the samples have model ages of about 0.8 Ga (Fig. 10). Therefore, because of the putative lower melt/rock ratios in the upper equigranular and protogranular layer samples, the very low Re/Os ratios, and presumed negligible effects of the metasomatism on Re-Os isotopic systematics, it is possible that the dominant T_{RD} age (~ 0.8 Ga) of these samples could reflect an actual melt depletion event. If so, the event is much later than melt depletion events recorded in xenoliths from the Massif Central and Eifel (1.5-1.6 Ga), but is similar to model ages reported for xenoliths from Kapfenstein (Austria), which have ca. 0.7 Ga model ages (Meisel et al., 2001; Schmidt and Snow, 2002). The one Kozákov sample (KS2) with a particularly depleted $^{187}\text{Os}/^{188}\text{Os}$ has a T_{RD} age of 1.6 Ga, which is identical to depletion ages of xenoliths from Massif Central. Crustal rocks throughout the Bohemian Massif are generally younger (Variscan – 280-360 Ma and Cadomian – 500-550 Ma; Vrána and Štědrá, 1997) although the Světlík orthogneiss from southern part of the Bohemian Massif has been dated to 2.1 Ga (Wendt et al., 1993). However, the Nd T_{DM} model ages of the majority Variscan crustal rocks lie in interval between 1.25 and 1.85 Ga (e.g. Gebauer et al., 1989; Janoušek et

al., 1995), which were interpreted to be a mixtures of Archean (> 2.5 Ga) and Late Proterozoic (~ 0.6 Ga) sources (e.g. Gebauer et al., 1989; Wendt et al., 1993). Therefore, our new T_{RD} ages for the SCLM underlying the Bohemian Massif do not match most crust formation events. In greatest note is that the dominant model age does not correspond with the Variscan orogenesis during which is thought the Bohemian Massif was consolidated. The different apparent ages may mean that the SCLM underlying the Bohemian Massif does not represent the orogenic root of the overlying crust. Instead, the crustal terranes may have been thrust onto mantle lithosphere during Cadomian and Variscan orogenesis. This is in contrast to Archean and Early Proterozoic terranes which usually have similar SCLM depletion age as the age of overlying crust, but in agreement with results of Peslier et al. (2000) from similar “young” terrane. Therefore, it is possible that this is a general feature of terranes consolidated during Paleozoic-Mesozoic.

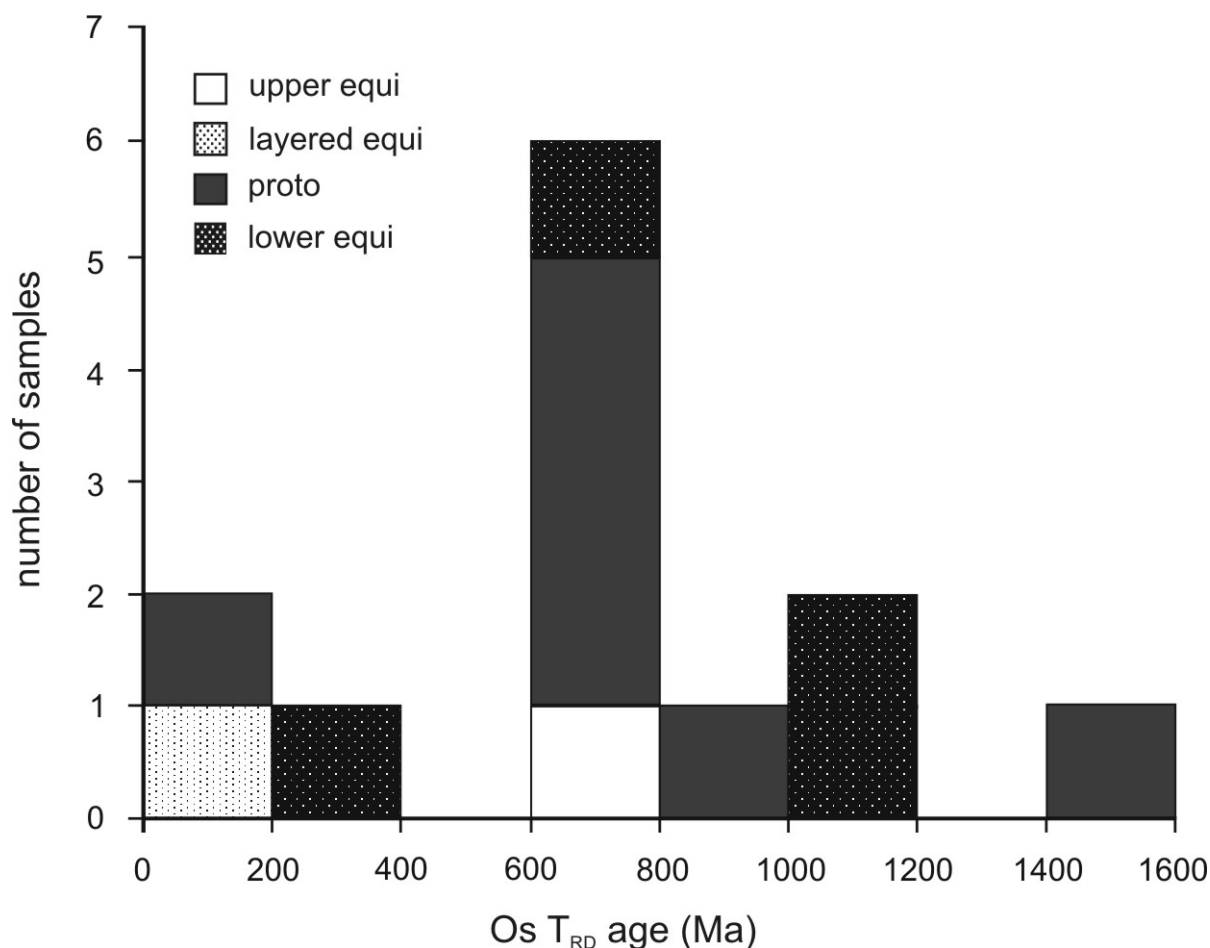


Fig. 10 Model Os depletion ages (T_{RD}) of Kozákov xenoliths. Ages range from 0.1 to 1.6 Ga, but most protogranular and upper equigranular samples define a relatively narrow age interval.

3.6. CONCLUSIONS

Mantle xenoliths from the Kozákov volcano of the Bohemian Massif sample a lithospheric mantle profile extending from depths of ~ 32 to 70 km. Previous studies have concluded that pervasive melt percolation affected all rocks sampled. The HSE concentrations in a suite of these xenoliths indicate that most of these elements behaved incompatibly during melt percolation, most probably due to removal of sulfides. The depletion is the most extensive in the lowest section of the profile, which experienced the highest melt/rock ratios. In contrast, middle and upper sections of the mantle were affected by low to moderate melt/rock ratios. Rocks from the shallower depths show smaller and more variable HSE depletions. A few xenoliths have much higher I-PGE contents than estimates for the primitive upper mantle, suggesting that in some cases, the I-PGE were transported into the mantle rocks via the percolating melt. Strong depletions in Pd point to the S-undersaturated character of the percolating melt. The I-PGE enrichments are not, therefore, associated with sulfide addition as has been suggested for other locales (e.g. Büchl et al., 2002; Luguet et al., 2004). Moreover, in contrast to other studies of mantle peridotites (e.g. Chesley et al., 1999; van Acken et al. 2008), the transport and deposition of some HSE was evidently not accompanied by transport and deposition of Re and radiogenic Os. Chondritic to subchondritic Os isotopic compositions likely reflect variable, ancient melt depletion. Model Os depletion ages (T_{RD}) cluster around 0.8 Ga. We interpret this age to indicate that the subcontinental lithospheric mantle underlying the Bohemian Massif does not represent the orogenic root of the overlying Variscan (280-360 Ma) crust, but that the crustal terranes may have been thrust onto the mantle lithosphere during Cadomian and Variscan orogenesis.

Acknowledgments

We thank Sarah Lee (University of Leicester) for sulfur analyses. This research was supported by the Grant Agency of the Academy of Sciences (projects IAA3013403 to E. J. and KJB300130612 to L. A.), the Scientific Programs CEZ: Z3-013-912 of the Institute of Geology, Acad. Sci. CR, MSM 0021620855 of the Charles University, Faculty of Science and Student Mobility Fund of Charles University, and EAR-CSEDI grant number EAR-0330528 from the U.S. National Science Foundation (to R. J. W).

CHAPTER 4. Geochemistry of Fe-rich peridotites and associated pyroxenites from Horní Bory, Bohemian Massif: insights into subduction-related melt-rock reactions

Lukáš Ackerman^{1,2}, Emil Jelínek², Gordon Medaris Jr.³, Josef Ježek⁴, Wolfgang Siebel⁵,
Ladislav Strnad⁶

¹ *Institute of Geology v.v.i., Academy of Sciences of the Czech Republic, Rozvojová 269, 165 00, Praha 6, Czech Republic*

² *Institute of Geochemistry, Mineralogy and Mineral Resources, Faculty of Science, Charles University, Albertov 6, 128 43, Praha 2, Czech Republic*

³ *Department of Geology and Geophysics, University of Wisconsin-Madison, WI 53706, USA*

⁴ *Faculty of Science, Charles University, Albertov 6, 128 43, Praha 2, Czech Republic*

⁵ *Institute of Geosciences, Eberhard-Karls-Universität Tübingen, Wilhelmstraße 56, 72074 Tübingen, Germany*

⁶ *Laboratories of the Geological Institutes, Faculty of Science, Charles University, Albertov 6, 128 43, Praha 2, Czech Republic*

Status: Submitted to Chemical Geology

Abstract

Variscan, mantle-derived peridotites and associated pyroxenites occur as boudins in Moldanubian granulite near the town of Horní Bory in western Moravia. The peridotites consist of two compositionally distinct suites, one of magnesian lherzolite (Mg # = 89.1-90.9, $^{87}\text{Sr}/^{86}\text{Sr} = 0.7046\text{-}0.7068$, $\epsilon_{\text{Nd}} = +4.1$ to $+5.3$), and another of more Fe-rich dunite and wehrlite (Mg # = 83.2-88.2, $^{87}\text{Sr}/^{86}\text{Sr} = 0.7079\text{-}0.7087$, $\epsilon_{\text{Nd}} = -2.8$ to -1.3). Modelling of Mg-Fe exchange between peridotite and Fe-rich melts reveals that the modal and chemical composition of the dunite-wehrlite suite can be produced by melt-rock reactions between magnesian lherzolite and SiO₂-undersaturated melts of basaltic composition at melt/rock ratios ranging from 0.3 to 2. In such a model, pyroxenites represent the crystalline product (\pm trapped liquid) of melts migrating along conduits in peridotite. The trace element compositions of melts, calculated from the compositions of clinopyroxene in pyroxenite, are enriched in the LILE and LREE and depleted in the HFSE. The trace element and Sr-Nd isotopic compositions of Horní Bory peridotites and pyroxenites point to a significant component of crustal material in the invasive melts. The melt-rock reactions recorded in the Horní Bory ultramafic boudins are attributed to melt percolation in a mantle wedge above a Variscan subduction zone.

Keywords: peridotite; dunite-wehrlite; melt-rock reaction; subduction zone; Sm-Nd geochronology; Bohemian Massif

4.1. INTRODUCTION

Peridotites occurring in orogenic massifs, ophiolite complexes and xenoliths in volcanic rocks provide direct evidence for mantle evolution throughout Earth history. The lithology of mantle peridotite ranges from fertile lherzolite to refractory harzburgite and dunite, and such variation has commonly been ascribed to depletion of fertile mantle by partial melting and extraction of fusible components (e.g. Downes, 2001; Pearson et al., 2003 and references therein). In contrast to the partial melting model, there is evidence that some harzburgite, wehrlite, and dunite form by the reaction of transient melts with fertile mantle wall rocks (e.g. Kelemen et al., 1990; Takazawa et al., 1992). Harzburgite is thought to develop by reaction of host peridotite with SiO₂-saturated, subduction-related melts (e.g. Kelemen et al., 1992; Kelemen et al., 1998), and the formation of wehrlite and associated dunite has been attributed to reaction with carbonate-rich liquids (Yaxley et al., 1991) or alkaline SiO₂-undersaturated basaltic melts (Batanova et al., 1998; Peslier et al., 2002; Ionov et al., 2005).

Mantle-derived peridotites and pyroxenites are widespread in several tectonostratigraphic units of the Bohemian Massif, where they occur as Carboniferous orogenic massifs and Neogene-Quaternary mantle xenoliths. The uppermost tectonic unit in the Moldanubian zone of the Bohemian Massif, the Gföhl Unit, contains numerous disrupted bodies of spinel and garnet peridotites (Machart, 1984). Based on their mineralogies, P-T conditions, and chemical compositions, the Gföhl peridotites have been divided into three groups, including a Mg-Cr type of suboceanic origin, another Mg-Cr type of subcontinental derivation, and an Fe-rich type associated with abundant pyroxenite (Medaris et al., 1990, 2005).

The Horní Bory granulite in the Gföhl Nappe contains conspicuous peridotite, pyroxenite, and eclogite boudins, which are well exposed in a quarry near the town of Horní Bory (Mísař and Jelínek, 1981; Mísař et al., 1984). Although some peridotite boudins in the Bory quarry are of the Mg-Cr type, most of the peridotite boudins have relatively low Mg-numbers, are interlayered with pyroxenite, and belong to the Fe-rich type of peridotite defined by Medaris et al. (2005).

Here, we present petrographic, geochemical and isotopic data for the Horní Bory ultramafic suite, including Mg-lherzolite, Fe-rich dunite to wehrlite, and associated pyroxenite, aiming to interpret their origin and evolution. We show that melt-rock reactions played a key role in the formation of Fe-rich dunite, wehrlite, and pyroxenite and suggest that such a process may have occurred in a mantle wedge above a subduction zone.

4.2. GEOLOGICAL SETTINGS

The Gföhl Nappe represents the uppermost lithostratigraphic unit in the Moldanubian Zone of the Bohemian Massif. It comprises a lower unit of orthogneiss with subordinate amphibolite and paragneiss and an upper unit with high-pressure felsic granulite. Spinel peridotites, garnet peridotites, eclogites and skarns occur as boudins or large bodies (Mohelno, Nové Dvory) in all of the above

mentioned rocks. The Gföhl granulites mostly yield consistent U-Pb zircon and monazite ages clustering around ~ 340 Ma (Becker, 1997; O'Brien and Rötzler, 2003; Janoušek and Holub, 2007) and many authors suggest that this age represents the peak of HT-HP metamorphism. However, numerous data (especially Sm-Nd data on garnets) show older ages up to ~ 370 Ma, clustering between 345 and 355 Ma (e.g. Košler et al., 1999; Prince et al., 2000). Three P-T-t evolution stages are suggested for Gföhl granulites: (1) HP-HT metamorphism at 1100 °C and 15-18 kbar at 354 Ma, followed by (2) near-isothermal decompression down to 5-7 kbar at ~ 700 °C in less than 10 Ma, and finally (3) near-isobaric cooling to 300 °C at ca. 330-310 Ma (Carswell and O'Brien, 1993; Svojtka et al., 2002). The Bory granulite massif forms a lens-shaped ENE-WSW trending body consisting of felsic garnet-kyanite granulite, which is extensively retrograded to garnet-sillimanite granulite, garnet-biotite±cordierite granulite, and biotite granulitic gneisses (Kotková et al., 2003). The felsic rocks commonly contain retrograde reaction textures, such as replacement of kyanite by sillimanite, development of hercynitic spinel coronas around aluminosilicates, and growth of biotite after garnet.

The investigated peridotite and pyroxenite boudins from the Horní Bory granulite were collected from a quarry near the village of Horní Bory (Fig. 1).

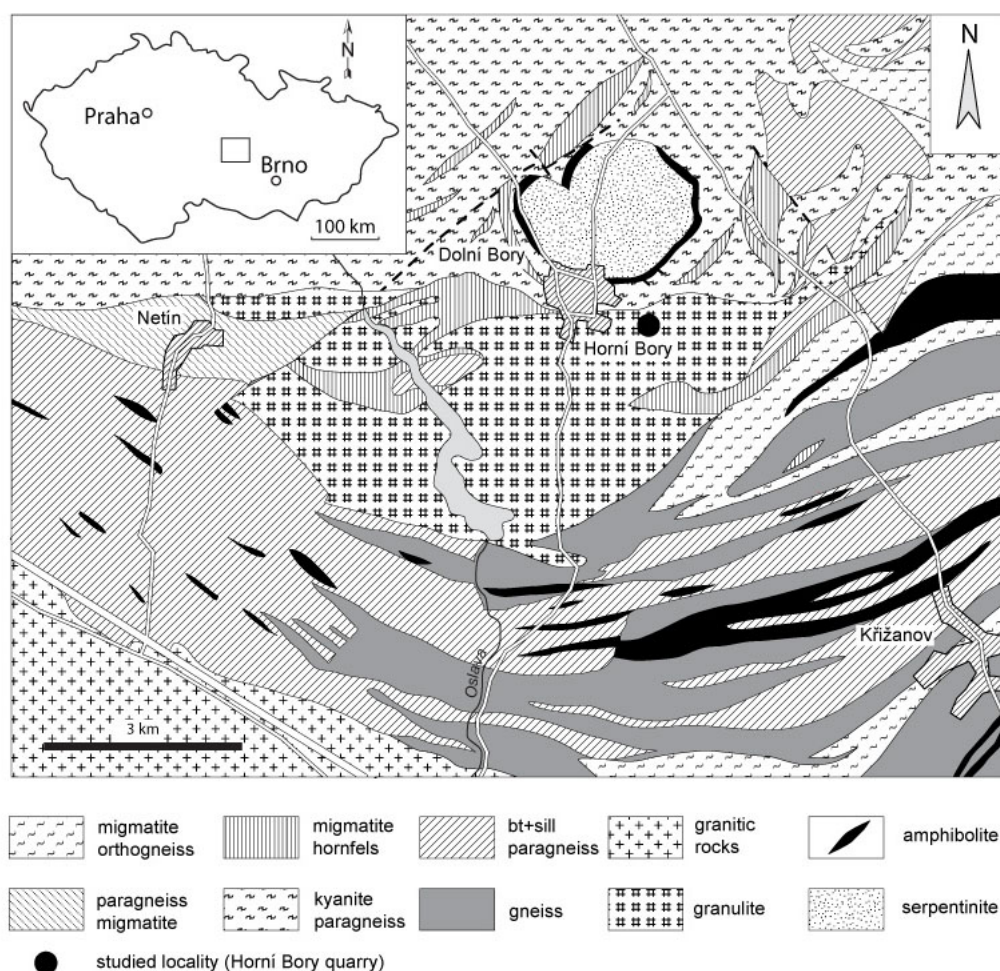


Fig. 1 Geological map of the Horní Bory area

4.3. ANALYTICAL METHODS

Whole-rock major element XRF analyses were performed at XRAL Laboratories (Ontario) and the Institute of Chemical Technology (Prague). Analyses of international reference whole-rock materials (UB-N, DTS-2B) yield a total error (1-sigma) for whole-rock analyses less than $\pm 5\%$. Trace element ICP-MS analyses followed the methods of Strnad et al. (2005), in which external reproducibility was controlled using the UB-N reference material (CRPG).

Analyses of minerals in five samples of peridotite and pyroxenite were carried out at the Institute of Geology, Academy of Sciences of the Czech Republic, Prague, on a CAMECA SX 100 electron microprobe equipped with a WDS analyzer. Analytical conditions were 15 kV accelerating voltage, 10 nA beam current and 2 μm beam diameter. Synthetic and natural minerals were used as internal standards for corresponding elements. Data reduction was performed by the Merlet data reduction program (Merlet, 1994). Mineral analyses of the remaining samples were determined at the University of Wisconsin on a CAMECA SX 50 electron microprobe with a WDS analyzer, using a 15 kV accelerating voltage, 20 nA beam current, and 1 μm beam diameter. Synthetic and natural minerals were used as standards, and data reduction was performed by the Phi-rho-z program of Armstrong (1988). For both mineral data sets, trivalent iron in spinel was calculated assuming stoichiometry.

Clinopyroxene and garnet separates were obtained using a combination of heavy liquid separation and magnetic separation, resulting in $> 95\%$ pure separates. All separates were then acid leached, using the following leaching steps: garnet – 6N HCl for 1 day, 7N HNO₃ for 1 day and 11N HF for 10 min; clinopyroxene – 6N HCl for 1 hour and 6N HNO₃ for 1 hour. Leaching was performed in hot acids ($\sim 60\text{ }^\circ\text{C}$). Trace-elements were analyzed by ICP-MS at the Faculty of Science, Charles University, Prague using the same procedures as mentioned above (Strnad et al., 2005).

Sr-Nd isotopic analyses were performed at the Institute of Geosciences (Eberhard-Karls-University Tübingen). For isotope analyses, whole-rocks, clinopyroxenes and garnets were spiked with a mixed ⁸⁴Sr-⁸⁷Rb and ¹⁴⁹Sm-¹⁵⁰Nd tracer solutions. All samples were digested in 52% HF for seven days at 180°C in a Teflon bomb surrounded by a steel jacket. Before digestion, clinopyroxenes and garnets were leached using the procedure described above. The whole-rock powders were not leached prior to digestion. Digested samples were dried and re-dissolved in 6N HCl, dried again, and re-dissolved in 2.5N HCl. Rb, Sr and light rare-earth element separation was accomplished on quartz columns by conventional ion exchange chromatography with a 5 ml resin bed of Bio Rad AG 50W-X12, 200-400 mesh. Nd was separated from Sm and other rare-earth elements on quartz columns using 1.7 ml Teflon powder coated with HDEHP, di(2-ethylhexyl)orthophosphoric acid, as cation exchange medium. All isotopic measurements were made by Thermal Ionization Mass Spectrometry on a Finnigan MAT 262 mass spectrometer. Sr was loaded with a Ta-HF activator on pre-conditioned W filaments and was measured in single-filament mode. Rb was loaded with ultra-pure H₂O on pre-conditioned Re-filaments and measurements were performed in a Re double filament configuration. Sm and Nd were loaded as phosphates and measured in a double Re-filament configuration mode. The ⁸⁷Sr/⁸⁶Sr ratios

were normalized to $^{86}\text{Sr}/^{88}\text{Sr} = 0.1194$, the $^{143}\text{Nd}/^{144}\text{Nd}$ ratios to $^{146}\text{Nd}/^{144}\text{Nd} = 0.7219$, and Sm isotopic ratios to $^{147}\text{Sm}/^{152}\text{Sm} = 0.56081$. Analyses of two different loads of La Jolla standard gave $^{143}\text{Nd}/^{144}\text{Nd}$ ratios of 0.511842 ± 0.000008 and 0.511833 ± 0.000008 (errors are $2\sigma_m$) while two analyses of the NBS 987 Sr standard yielded $^{87}\text{Sr}/^{86}\text{Sr}$ ratios of 0.710259 ± 0.000010 and 0.710246 ± 0.000009 ($2\sigma_m$). Total procedural blanks (chemistry and loading) were 125 pg for Sr, 35 pg for Nd and 4 pg for Sm. Single stage depleted mantle model-ages (T_{DM}) were calculated with depleted present-day parameters $^{143}\text{Nd}/^{144}\text{Nd} = 0.513151$ and $^{147}\text{Sm}/^{144}\text{Nd} = 0.219$ (Liew and Hofmann, 1988). $^{143}\text{Nd}/^{144}\text{Nd}$ ratios are quoted in the ϵNd notation of DePaolo and Wasserburg (1976) as deviations from a chondritic reference (CHUR) with present-day $^{143}\text{Nd}/^{144}\text{Nd} = 0.512638$ (Jacobsen and Wasserburg, 1980). Least-square regression of the Sm-Nd isotopic data with assessment of fit using the mean square of the weighted deviates (MSWD), were calculated after Ludwig (2003).

Modal compositions of peridotite and pyroxenite samples were calculated from whole-rock and mineral compositions, using an inversion method of constrained least-squares as outlined by Albarède (1995). The GCDkit geochemical software program (Janoušek et al., 2006) was used for whole-rock and trace element data handling and plotting.

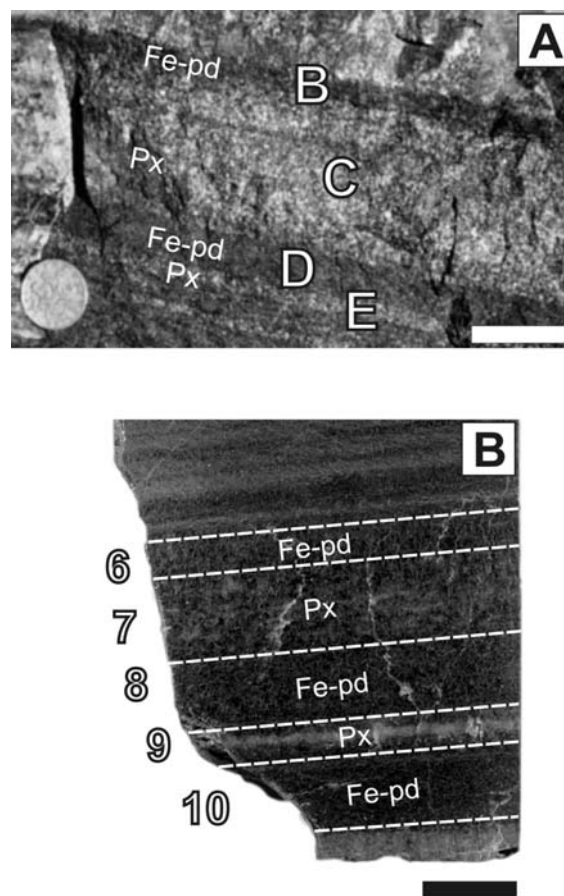


Fig. 2 Examples of layered Fe-peridotite and pyroxenite boudins from the Horní Bory quarry. A: sample 06HB2; B: sample HB70. Scale bar is 3 cm in both panels.

4.4. PETROGRAPHY

In total, 19 peridotite and 10 pyroxenite boudins with sizes ranging from decimetres to metres were examined. From this sample suite, twelve peridotites and seven pyroxenites were selected for detailed investigation. In addition, two layered peridotite-pyroxenite samples (06HB2, HB70; Fig. 2) were included to provide more information on the relations between peridotite and pyroxenite, where these two rock types are in direct contact. The peridotites were divided into two groups, Mg-peridotite (Mg-pd) and Fe-peridotite (Fe-pd), based on their modes and whole-rock Mg-numbers, as summarized in Table 1.

Table 1. Summary of main petrographic features and modal compositions of Horní Bory peridotites and pyroxenites

Sample	Type	Texture	Lithology	Modal composition				Bulk #Mg
				ol	opx	cpx	sp/grt	
06HB4	Mg-pd	discrete	lherz	78	13	6	2	90.9
HB2	Mg-pd	discrete	lherz	66	23	9	3	89.1
HB8	Mg-pd	discrete	lherz					89.7
97CZ3C	Mg-pd	discrete	lherz	67	21	5	7	90.6
99BY1B	Mg-pd	discrete	lherz	61	22	15	3	90.0
HB7	Fe-pd	discrete	lherz	88	5	5	3	85.5
HB9	Fe-pd	discrete	wehr	86	3	8	3	87.8
HB13	Fe-pd	discrete	wehr	88	<1	9	3	86.3
HB14	Fe-pd	discrete	wehr	83	4	11	2	88.2
99BY3A	Fe-pd	discrete	dun	87	2	4	7	86.2
HB3	Px	discrete	cpx	0	4	75	21	82.3
HB4	Px	discrete	webs	0	10	68	22	77.2
BY3BB	Px	layered	webs	0	14	56	30	82.2
85GM8B	Fe-pd-px	layered	wehr-px	68	<1	15	22	80.3
06HB2B	Fe-pd	layered	wehr	77	<1	18	5	83.2
06HB2C	Px	layered	cpx	9	<1	69	22	84.3
06HB2D	Fe-pd	layered	wehr	74	<1	23	3	87.3
06HB2E	Px	layered	ol cpx	31	<1	43	26	85.3
HB70-6	Fe-pd	layered	wehr	87	<1	7	6	85.7
HB70-7	Px	layered	ol cpx	24	<1	52	24	82.1
HB70-8	Fe-pd-px	layered	wehr-px	45	<1	36	19	83.4
HB70-9	Px	layered	webs	0	7	67	26	84.7
HB70-10	Fe-pd	layered	wehr	77	2	10	11	86.9

lherz - lherzolite, wehr - wehrlite, dun - dunite, wehr-px - wehrlite with pyroxenite layers, webs - websterite, cpx - clinopyroxenite, ol cpx - olivine clinopyroxenite

4.4.1. Mg-peridotite

The Mg-peridotite from Horní Bory is a five-phase lherzolite (Fig. 3), consisting of variable proportions of olivine (61–78 %), orthopyroxene (13–23 %), clinopyroxene (5–13 %), spinel (3 %), and garnet (5–7 %). Spinel occurs as discrete, intergranular grains (Fig. 4A) and as inclusions in garnet, indicating the stable coexistence of spinel and garnet. Minor phlogopite is present in several

samples. A slightly foliated, granoblastic texture is locally preserved in Mg-pd, but extensive recrystallization has led to common development of an equigranular (foam) texture, nearly complete replacement of garnet by kelyphite (Fig. 4A), growth of amphibole, and late-stage serpentinization.

4.4.2. Fe-peridotite

Fe-peridotite is the predominant type of boudin in the Horní Bory quarry. In contrast to Mg-pd lherzolite, Fe-pd consists of ilmenite-bearing dunite and wehrlite (Table 1, Fig. 3). Further distinction between Fe-pd and Mg-pd is illustrated by a plot of clinopyroxene mode and olivine composition *vs.* olivine mode (Fig. 5), which illustrates the relative abundance of clinopyroxene and low Mg-number of olivine in Fe-pd compared to Mg-pd. Spinel occurs as discrete, intergranular grains (Fig. 4B) and as inclusions in garnet, indicating the stable coexistence of these two aluminous phases, as in the case for Mg-pd. Most olivine in Fe-pd has been recrystallized to a fine-grained foam texture, with well-developed triple junction grain boundaries (Fig. 4C). Fe-pd has a slightly foliated, equigranular texture, in which the foliation is defined by the alignment of small spinel, ilmenite, and garnet grains. This foliation is accentuated by a layered structure formed by thin seams of clinopyroxene, which locally are accompanied by small amounts of phlogopite.

Some boudins show an interlayering of Fe-pd and pyroxenite on a scale of 1 to 6 cm (e.g. samples 06HB2 and HB70, Fig. 2). In these two samples (and other similar composite samples, for example 85GM8B) the modal compositions of the peridotite and pyroxenite layers tend to be intermediate between those of solitary peridotite and pyroxenite boudins (Fig. 3).

As is the case for Mg-pd, recrystallization in Fe-pd has been extensive. Garnet is almost completely replaced by kelyphite, and in addition to late-stage serpentinization, thin veins of clinopyroxene (Cr_2O_3 - and Na_2O -poor), tremolite, carbonate, and chlorite (after phlogopite) occur parallel to foliation and layering.

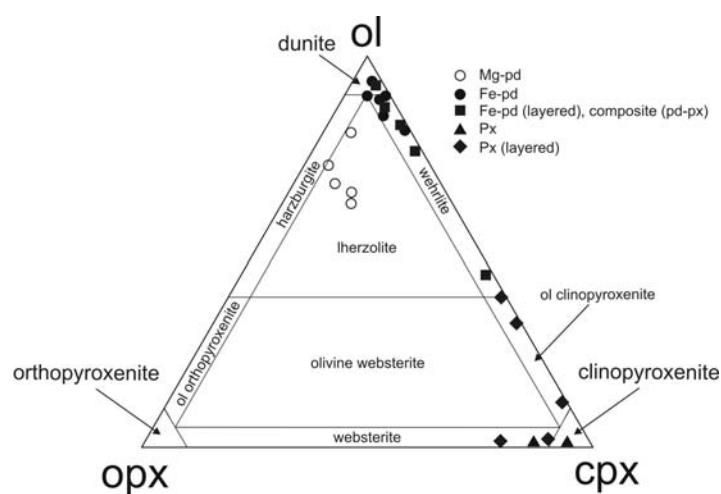


Fig. 3 Modal compositions of peridotites and pyroxenites from the Horní Bory quarry. Abbreviations: Mg-pd, Mg-peridotite; Fe-pd, Fe-peridotite; px, pyroxenite.

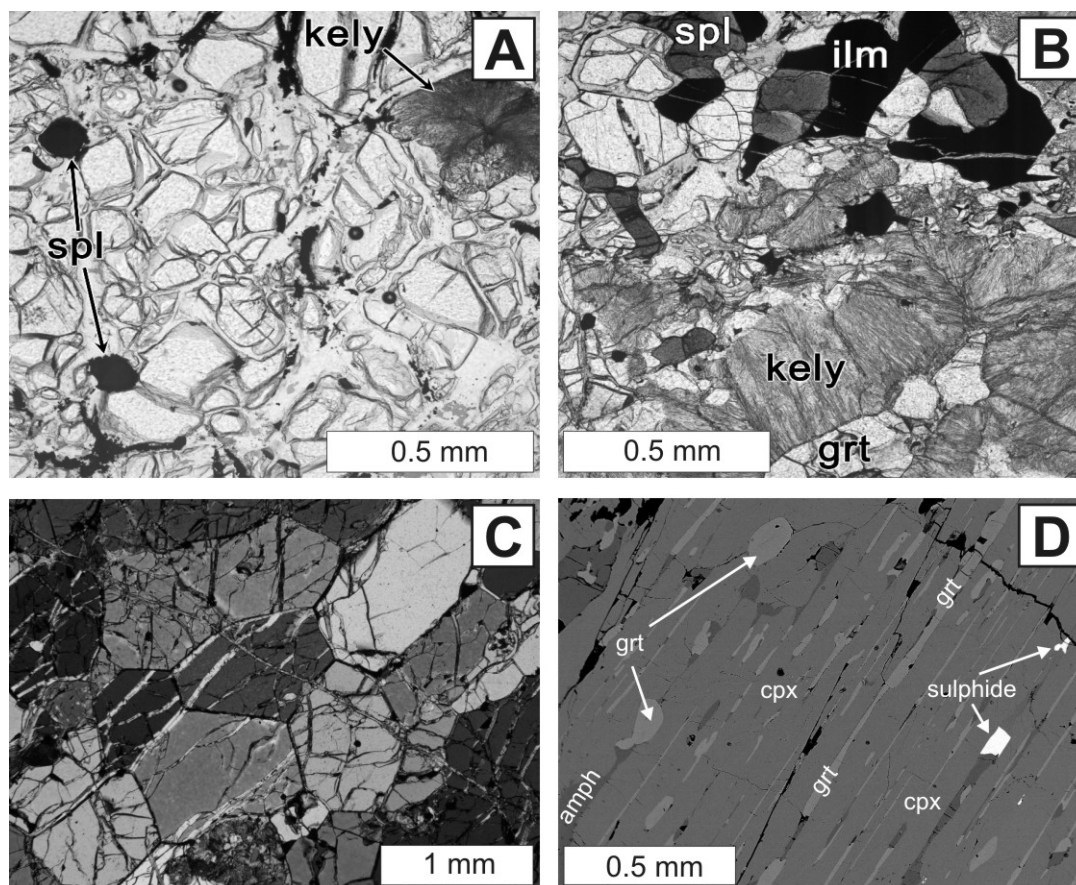


Fig. 4 Representative textures of Horní Bory peridotites and pyroxenites. (A) Mg-peridotite, (B) Fe-peridotite (note coexistence of spinel and garnet in both rock types), (C) foam texture of olivine in Fe-peridotite (dunite), (D) garnet lamellae in clinopyroxene porphyroclast in pyroxenite. Abbreviations: amph, amphibole; cpx, clinopyroxene; grt, garnet; ilm, ilmenite; kely, kelyphite; spl, spinel.

4.4.3. Pyroxenites

Two solitary pyroxenite boudins consist of clinopyroxenite and websterite, and pyroxenite layers from the two layered boudins include olivine clinopyroxenite and websterite (Table 1, Fig. 3). All pyroxenite samples contain garnet and ilmenite, and rutile is commonly associated with ilmenite. Minor amounts of amphibole (pargasite to Mg-hornblende) are commonly located at garnet boundaries and associated with ilmenite. Small amounts of phlogopite occur locally along several peridotite-pyroxenite boundaries in the two layered samples.

Pyroxenite has a porphyroclastic texture, in which medium-grained clinopyroxene porphyroclasts are set in a fine-grained equigranular matrix. Clinopyroxene porphyroclasts in the two pyroxenite boudins (samples HB3 and HB4) contain garnet lamellae (Fig. 4D), which likely formed by exsolution during recrystallization. In contrast to the peridotites, garnet has escaped kelyphitization during recrystallization, due to the absence or paucity of olivine in the pyroxenites.

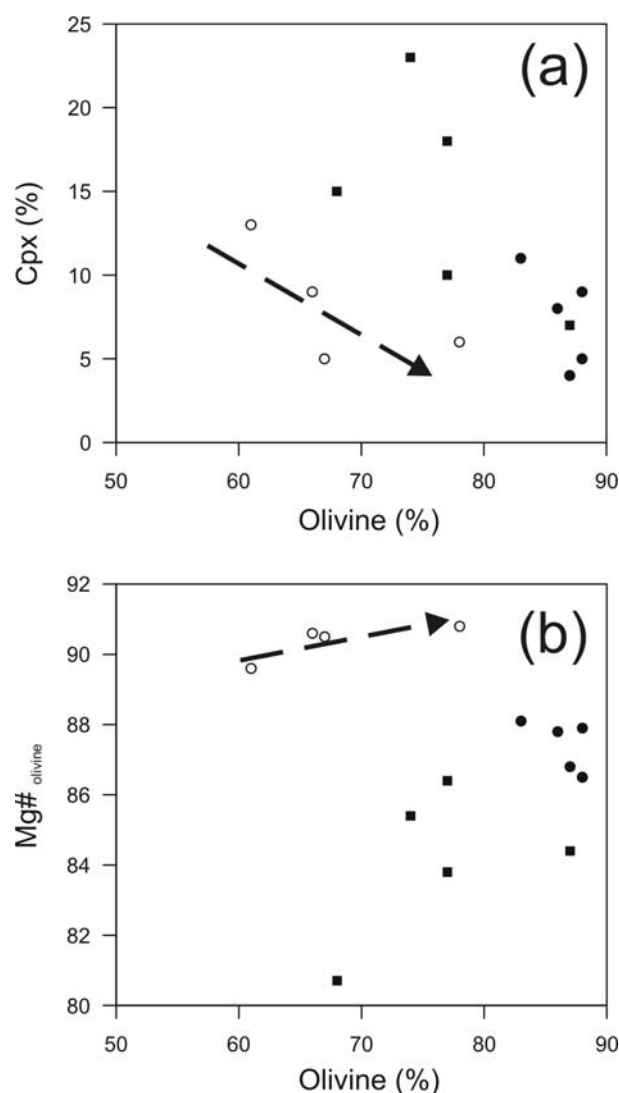


Fig. 5 Co-variation plots of (a) olivine and clinopyroxene contents and (b) olivine content and Mg# in olivine. The arrow represents a typical depletion trend for Mg-peridotite, resulting from partial melt extraction. Symbols as in Fig. 3.

4.5. WHOLE-ROCK CHEMISTRY

4.5.1. Major and minor elements

Mg-peridotite and Fe-peridotite are compositionally distinct (Medaris et al., 2005 and Table 1 in Electronic Supplementary Material), as seen in plots of various oxides vs. MgO (Fig. 6). Analyses of Mg-pd are similar to those of Mg-Cr peridotites elsewhere and generally cluster around the mantle depletion trend defined by the well-characterized Ronda peridotite suite (Suen and Frey, 1987). Compared to Mg-pd, Fe-pd is notably higher in FeO and TiO₂ and lower in SiO₂ and NiO. Horní Bory Fe-pd is similar in composition to Fe-rich lherzolite and wehrlite xenoliths from Tok, Siberia (Ionov et al., 2005), with the exception of lower NiO and Na₂O contents (Fig. 6).

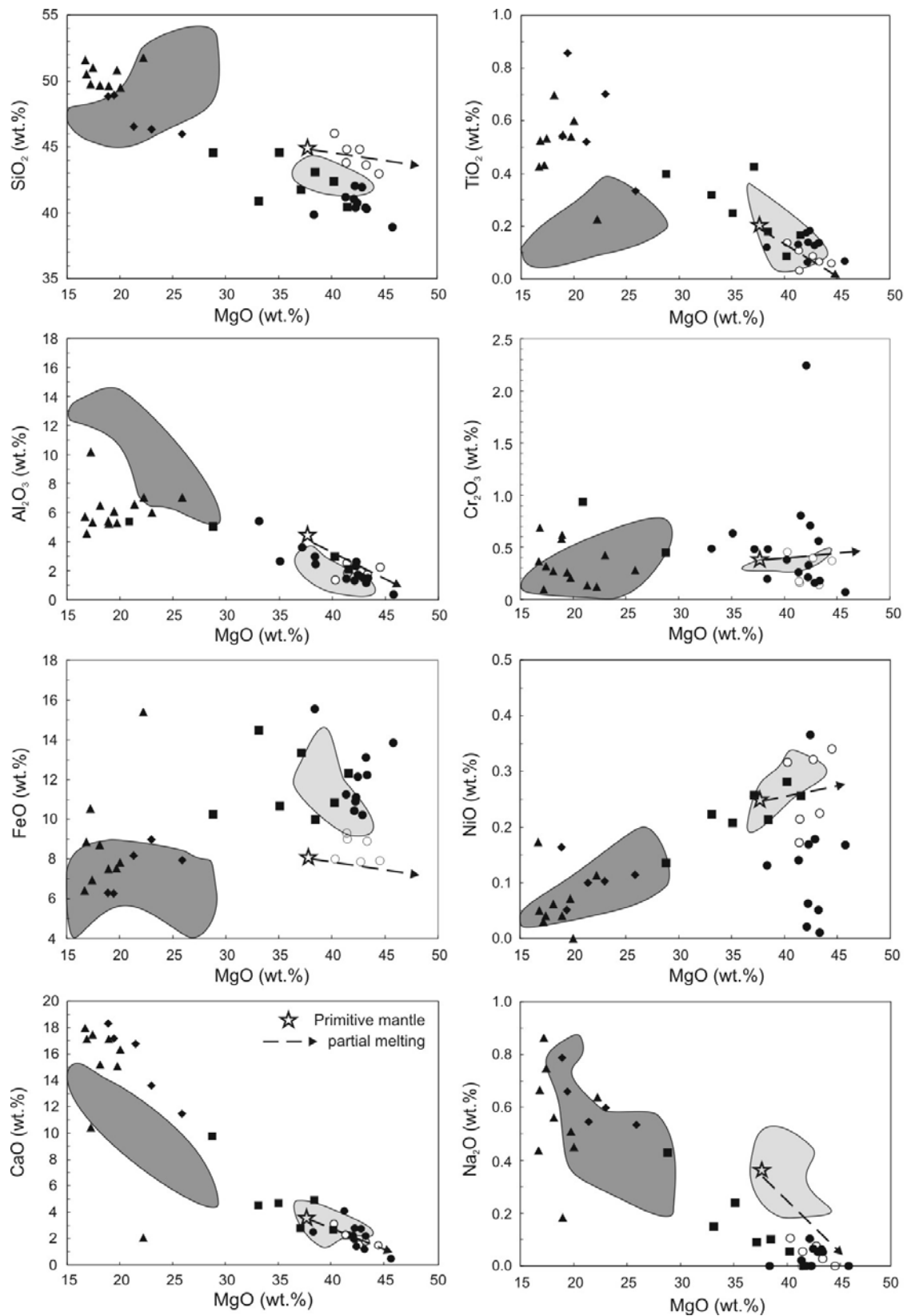


Fig. 6 Variation of whole-rock major oxides, relative to wt. % MgO, for Horni Bory peridotites and pyroxenites. Light grey field encompasses the Fe-rich lherzolite-wehrlite xenoliths from Tok (Ionov et al., 2005); the dark grey field includes garnet pyroxenites from peridotite bodies in the Gföhl Unit (Medaris et al., 2006). Symbols as in Fig. 3.

Horní Bory pyroxenites show a wide range in composition (Fig. 6), with Mg-numbers ranging from 72 to 82. Compared to pyroxenite lenses in Mg-Cr peridotites in other localities in the Gföhl Nappe, the Horní Bory pyroxenites are higher in SiO₂, TiO₂, and CaO and lower in Al₂O₃ (Fig. 6). The large scatter in the compositions of Gföhl pyroxenites has been ascribed to crystallization and accumulation of variable proportions of clinopyroxene and garnet ± trapped melt (Medaris et al., 1995), and such a process may have contributed to the scatter in the Horní Bory pyroxenite data, as well.

The compositions of layered Fe-pd and pyroxenite are intermediate between those of solitary Fe-pd and pyroxenite boudins, most likely reflecting the influence of melt-rock interactions (see Discussion). Despite the wide scatter in the Horní Bory data for both Fe-pd and pyroxenite, there is a rough negative correlation between SiO₂, TiO₂, CaO, and Na₂O with MgO and a positive correlation between FeO and MgO, pointing to the chemical coherence of the Fe-pd and pyroxenite suite. Note, however, that there may be a discontinuity in Al₂O₃ and NiO variations. No trend is apparent in Cr₂O₃ variation, and the extreme scatter for this oxide might be due to the difficulty in obtaining representative splits for analysis in samples where small grains of spinel are commonly concentrated along thin layers.

4.5.2. Rare earth and other trace elements

With respect to primitive mantle (McDonough and Sun, 1995), five samples of Mg-peridotite have relatively flat rare earth element (REE) patterns ($Ce_N/Yb_N = 0.4-1.6$), with a wide range in total REE contents and degree of depletion (Table 2, Fig. 7). One sample has a negative Eu anomaly, and another, a positive anomaly. Five samples of Fe-peridotite also have relatively flat REE patterns with a wide range of depletion (Fig. 7), but in contrast to Mg-peridotite, there is a slight overall LREE enrichment ($Ce_N/Yb_N = 1.1-2.5$).

Pyroxenites have significantly different REE and trace element patterns. Two samples of pyroxenite have convex-upward REE patterns, one of which has a small negative/positive Eu anomaly (Table 2, Fig. 7). Such patterns reflect the influence of clinopyroxene, which strongly concentrates the LREE in a convex-upward configuration. Although most anhydrous pyroxenites from ultramafic massifs generally show LREE-depleted patterns (Bodinier and Godard, 2003 and references therein), Horní Bory pyroxenites have LREE enriched patterns ($Ce_N/Yb_N = 1.6-1.9$) similar to some pyroxenites from Lower Austria (Becker, 1996b). As is the case for major elements, the REE contents and patterns for pyroxenite and Fe-pd in the layered samples tend to be intermediate between those for the solitary pyroxenite and Fe-pd boudins (Table 3, Fig. 7). The patterns for layered pyroxenites lie slightly below those for solitary pyroxenites, with the convex apex displaced to a more intermediate REE position. Although the REE contents of the two groups of Fe-peridotite overlap to a large degree, the layered Fe-peridotites display convex-upward REE patterns. The shapes and configurations of REE patterns

in the various Horní Bory ultramafic lithologies are best compared in a plot of $(\text{Ce}/\text{Sm})_N$ vs. $(\text{Sm}/\text{Yb})_N$ (Fig. 8), in which samples of pyroxenite and layered Fe-pd and pyroxenite are located farther from the center of the plot compared to Fe-pd and Mg-pd, due to their pronounced convex-upward configurations.

Table 2. Trace element contents (ppm) of discrete peridotite and pyroxenite boudins from Horní Bory

Sample	06HB4	HB2	HB8	HB7	HB9	HB13	HB14	97CZ3C	99BY1B	99BY3A	HB3	HB4
Lithology	lherz	lherz	lherz	wehr	wehr	wehr	wehr	lherz	lherz	dun	cpx	webs
Type	Mg-pd	Mg-pd	Mg-pd	Fe-pd	Fe-pd	Fe-pd	Fe-pd	Mg-pd	Mg-pd	Fe-pd	Px	Px
Rb	0.32	0.56	1.55	0.15	10.09	0.36	1.25	0.56	0.83	0.84	3.08	0.58
Sr	10.47	13.31	11.39	12.73	12.28	20.51	30.28	10.37	26.23	12.51	118.60	202.10
Y	0.94	6.56	0.85	0.90	1.59	1.13	1.56	1.09	1.97	1.13	11.08	11.47
Zr	2.70	1.50	8.31	1.24	8.29	1.81	5.58	3.45	4.12	3.45	13.85	17.21
Nb	0.16	0.16	0.22	0.20	0.23	0.21	0.65	0.88	0.20	0.24	0.42	1.78
Cs	0.10	0.04	0.20	0.02	0.62	0.03	0.17	0.08	0.12	0.07	0.29	0.16
La	0.13	0.65	0.30	0.17	0.31	0.16	0.59	0.33	0.34	0.40	1.75	2.36
Ce	0.41	0.63	0.66	0.47	0.98	0.49	1.54	0.91	0.95	1.06	5.64	7.29
Pr	0.07	0.17	0.08	0.07	0.18	0.07	0.25	0.14	0.19	0.18	1.02	1.30
Nd	0.29	0.81	0.31	0.32	0.88	0.33	1.10	0.60	0.77	0.85	5.75	7.03
Sm	0.13	0.25	0.09	0.13	0.32	0.11	0.30	0.17	0.25	0.30	2.05	2.30
Eu	0.04	0.12	0.02	0.05	0.17	0.04	0.11	0.06	0.09	0.08	0.57	0.69
Gd	0.12	0.31	0.11	0.15	0.28	0.14	0.30	0.19	0.34	0.29	1.91	2.03
Tb	0.02	0.07	0.03	0.02	0.05	0.03	0.06	0.04	0.06	0.04	0.34	0.33
Dy	0.14	0.53	0.15	0.14	0.31	0.16	0.30	0.20	0.36	0.22	2.07	2.01
Ho	0.03	0.16	0.04	0.03	0.08	0.04	0.06	0.05	0.08	0.05	0.43	0.43
Er	0.09	0.48	0.12	0.10	0.23	0.11	0.18	0.14	0.24	0.13	1.17	1.22
Tm	0.02	0.06	0.02	0.01	0.04	0.02	0.03	0.03	0.04	0.02	0.16	0.18
Yb	0.13	0.40	0.20	0.09	0.19	0.13	0.20	0.16	0.24	0.12	0.96	1.02
Lu	0.02	0.08	0.03	0.02	0.04	0.02	0.03	0.03	0.04	0.02	0.14	0.16
Hf	0.10	0.05	0.25	0.04	0.27	0.06	0.22	0.10	0.14	0.26	0.10	0.87
Th	0.13	0.13	0.15	0.06	0.14	0.07	0.12	0.07	0.07	0.05	0.16	0.47
U	0.02	0.06	2.67	0.05	1.59	0.06	0.13	0.03	0.08	0.12	0.09	0.77

Although the concentrations of CaO and Al₂O₃ in the Bory ultramafic suite show considerable scatter when plotted vs. wt% MgO (Fig. 6), they show much less scatter when plotted vs. ppm Ce and ppm Yb, respectively (Fig. 9). Because Ce is concentrated by clinopyroxene (a Ca-rich phase), and Yb is concentrated by garnet (an Al₂O₃-rich phase), such a plot suggests that the concentrations of CaO and Al₂O₃ in the Bory ultramafic boudins reflect the relative abundance of these two phases.

Samples of Mg-pd and Fe-pd have similar extended trace element patterns (Fig. 7). Peridotites in both groups tend to be slightly enriched in large ion lithophile elements (LILE) and have prominent positive U and Sr anomalies in most, but not all, samples (U_N/Th_N up to 51 and $Sr_N/Nd_N = 0.9-3.9$). In contrast, the high field strength elements (HFSE) tend to be depleted, with many samples showing weak negative anomalies for Nb, Zr, and Hf ($Nb_N/La_N = 0.2-2.6$, $Hf_N/Sm_N = 0.3-1.2$). An exception to

this pattern is sample HB8 (Mg-pd), which has positive Zr and Hf anomalies, coupled with the most pronounced U anomaly among the peridotites.

The extended trace element pattern for pyroxenite is similar to that for peridotite, i.e. positive anomalies for U and Sr and negative anomalies for Nb, Zr, and Hf, only at higher concentrations throughout (Fig. 7). The trace element patterns for layered pyroxenite and Fe-pd are comparable to those for their solitary counterparts, but the negative Nb anomaly in layered Fe-pd is more pronounced than that in solitary Fe-pd (Fig. 7).

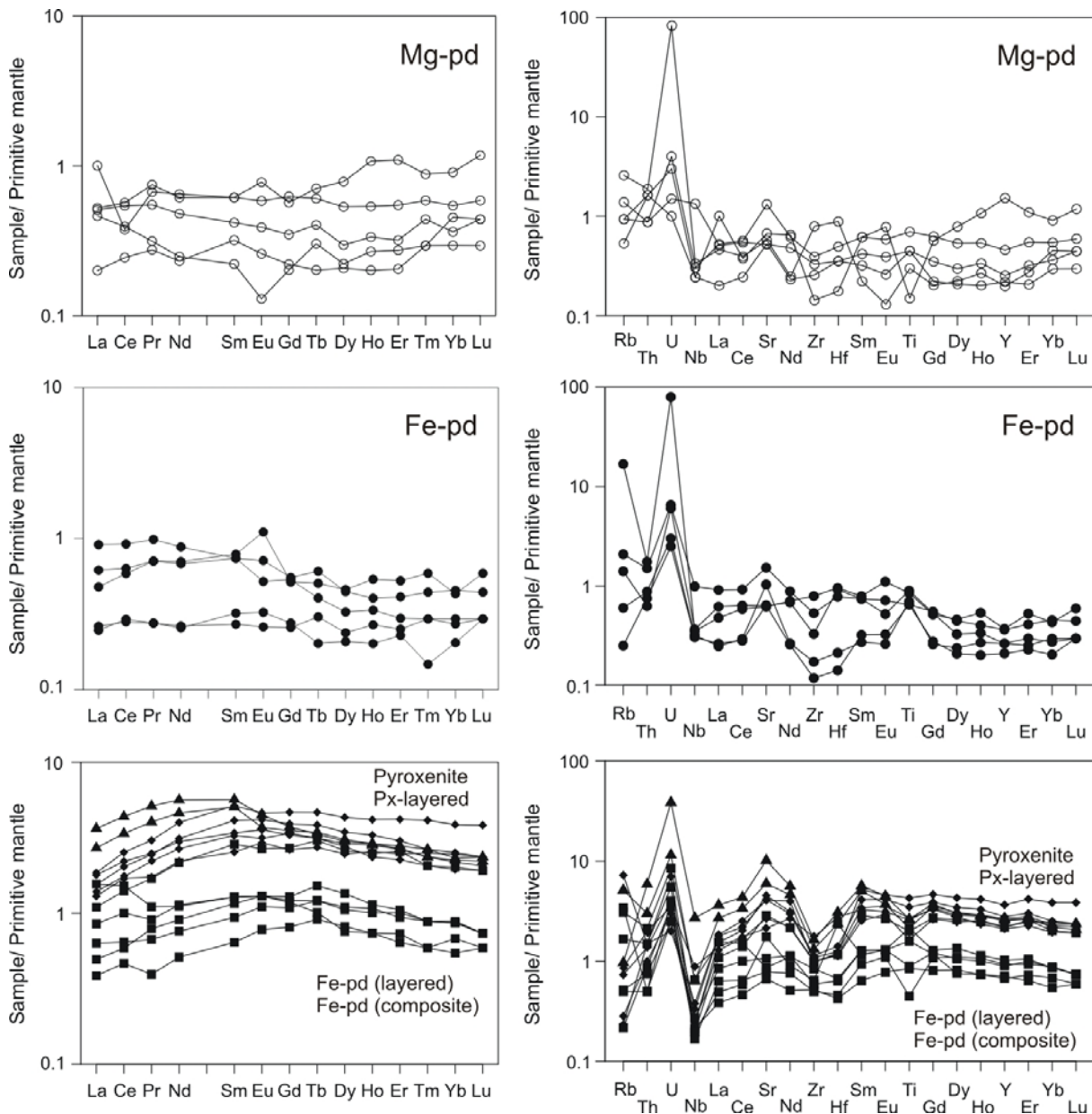


Fig. 7 Whole-rock REE and extended trace element compositions of Horní Bory peridotites and pyroxenites, normalized to primitive mantle (McDonough and Sun, 1995). Symbols as in Fig. 3.

Table 3. Trace element contents (ppm) of layered peridotites and pyroxenites from Horní Bory

Sample	85GM8B	BY3BB	06HB2B	06HB2C	06HB2D	06HB2E	HB70 (6)	HB70 (7)	HB70 (8)	HB70 (9)	HB70 (10)
Lithology	wehr-px	webs	wehr	ol cpx	wehr	ol cpx	wehr	ol cpx	wehr-px	webs	wehr
Type	Fe-pd-px	Px	Fe-pd	Px	Fe-pd	Px	Fe-pd	Px	Fe-pd-px	Px	Fe-pd
Rb	0.99	0.52	1.86	0.44	0.31	4.34	0.30	0.17	0.13	0.14	2.06
Sr	32.52	42.46	17.19	82.00	21.33	53.05	13.25	90.44	57.04	80.90	15.67
Y	2.94	10.91	4.41	9.06	3.86	9.48	2.90	11.97	9.41	15.73	4.02
Zr	21.45	18.34	8.84	11.48	6.21	10.62	5.46	11.94	10.41	10.25	5.24
Nb	0.42	0.58	0.43	0.22	0.18	0.16	0.14	0.16	0.13	0.25	0.11
Cs	0.08	0.23	0.58	0.20	0.15	0.94	0.11	0.15	0.13	0.21	0.67
La	0.32	0.90	1.01	1.16	0.55	0.84	0.25	1.00	0.71	1.20	0.41
Ce	0.98	2.93	2.54	3.69	1.68	2.84	0.78	3.40	2.35	4.23	1.08
Pr	0.20	0.56	0.28	0.63	0.23	0.44	0.10	0.62	0.43	0.77	0.17
Nd	1.13	3.34	1.39	3.72	1.42	2.76	0.64	3.90	2.70	4.98	0.95
Sm	0.47	1.33	0.52	1.38	0.52	1.03	0.26	1.67	1.16	2.09	0.38
Eu	0.20	0.48	0.20	0.55	0.20	0.45	0.12	0.64	0.41	0.71	0.17
Gd	0.64	1.84	0.70	1.79	0.66	1.43	0.44	2.12	1.47	2.53	0.59
Tb	0.10	0.31	0.15	0.31	0.12	0.27	0.09	0.38	0.30	0.46	0.12
Dy	0.51	1.95	0.91	1.86	0.71	1.66	0.55	2.32	1.75	2.90	0.74
Ho	0.11	0.42	0.17	0.35	0.15	0.38	0.11	0.49	0.37	0.62	0.16
Er	0.28	1.16	0.46	0.99	0.44	1.08	0.32	1.32	1.12	1.83	0.41
Tm	0.04	0.16	0.06	0.14	0.06	0.17	0.04	0.18	0.14	0.28	0.06
Yb	0.24	0.99	0.38	0.86	0.38	1.08	0.30	1.11	0.89	1.70	0.39
Lu	0.04	0.15	0.05	0.13	0.05	0.16	0.04	0.16	0.13	0.26	0.05
Hf	0.67	0.78	0.19	0.35	0.18	0.32	0.12	0.40	0.33	0.34	0.13
Th	0.12	0.16	0.17	0.11	0.06	0.12	0.04	0.08	0.07	0.12	0.04
U	0.11	0.07	0.17	0.08	0.05	0.14	0.05	0.06	0.07	0.04	0.08

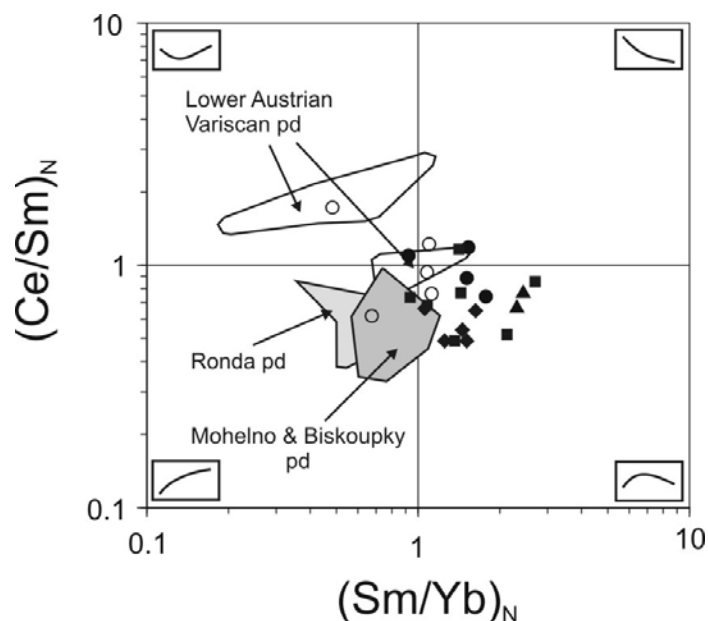


Fig. 8 Ratios of $(\text{Ce}/\text{Sm})_N$ vs $(\text{Sm}/\text{Yb})_N$ for Horní Bory peridotites and pyroxenites (N: normalized to primitive mantle; McDonough and Sun, 1995). Other fields: lower Austrian peridotites (Becker, 1996a); Ronda peridotite, (Frey et al., 1985); Mohelno and Biskoupky peridotites (Medaris et al., 2005). Symbols as in Fig. 3.

4.6. MINERAL COMPOSITIONS AND T-P ESTIMATES

4.6.1. Major and minor elements

The ultramafic boudins in the Horní Bory quarry consist predominantly of various proportions of olivine, orthopyroxene, clinopyroxene, garnet, spinel, and ilmenite (Table 1, Fig. 3), whose Fe/Mg ratios are controlled largely by whole-rock Fe/Mg ratios. Representative mineral analyses can be found in Table 2 included in Electronic Supplementary Material. Representative compositions of the silicate minerals are illustrated in Fig. 10, which illustrates the progressive decrease in Mg-number for minerals from Mg-peridotite through Fe-peridotite to pyroxenite. Minerals in pyroxenite exhibit the widest range in Fe/Mg ratio, and the compositions of minerals in Fe-peridotite overlap slightly with those in pyroxenite in terms of Ca, Mg, and Fe (Fig. 10).

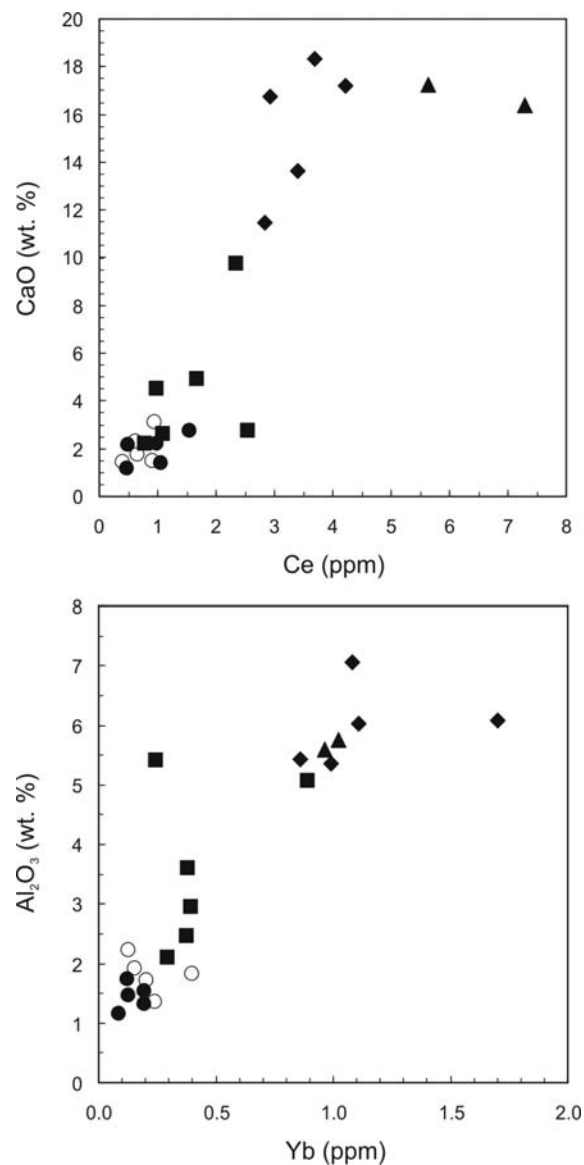


Fig. 9 Co-variation plots of CaO vs. Ce and Al₂O₃ vs. Yb for Horní Bory peridotites and pyroxenites. Positive correlations suggest the influence of garnet and clinopyroxene accumulation on whole-rock major element compositions. Symbols as in Fig. 3.

Olivine varies in composition from Fo_{90.5-90.6} in Mg-peridotite to Fo_{80.7-87.3} in Fe-peridotite; olivine in a single clinopyroxenite sample is Fo_{82.4}. NiO contents for olivine in Mg-pd are higher than those in Fe-pd, 0.37-0.38 wt% vs. 0.15-0.22 wt%, respectively.

Orthopyroxene is slightly more magnesian than coexisting olivine, varying in Mg-number from 91.1-91.4 in Mg-pd, to 82.4-87.3 in Fe-pd, and 73.7-85.0 in pyroxenite. Al₂O₃ contents, which range from 0.5 to 2.7 wt% for the entire boudin suite, are variable within individual samples on the inter- and intragrain scales, due to arrested re-equilibration and cation exchange during retrogression. For example, orthopyroxene is commonly zoned, with Al₂O₃ increasing from cores to rims. Such variability tends to obscure any differences in Al₂O₃ on the mineral scale that might have existed between the different groups of boudins.

The highest Mg-numbers among the silicate minerals are found in clinopyroxene, where they vary from 94.3-94.5 in Mg-peridotite, to 89.1-93.8 in Fe-peridotite, and 90.0-91.8 in pyroxenite. Al₂O₃ contents of clinopyroxene range from 0.9 to 2.6 wt%, and as in orthopyroxene, are variable on the inter- and intragrain scales, e.g. clinopyroxene commonly exhibits a core to rim increase in Al₂O₃ and decrease in Na₂O. Cr₂O₃ and TiO₂, like Al₂O₃, also show grain scale variations within samples, reflecting the partial re-equilibration during retrogression of these slowly diffusing constituents.

Garnet, which has the lowest Mg-numbers among the silicate minerals, varies in composition from Prp₇₀Alm₁₈Sps₁Grs₁₁ in Mg-peridotite, to Prp₅₅₋₆₁Alm₂₃₋₂₈Sps₁₋₂Grs₁₅₋₁₆ in Fe-peridotite, and Prp₄₇₋₅₉Alm₂₄₋₃₈Sps₁₋₂Grs₁₃₋₁₇ in pyroxenite. Cr₂O₃ contents of garnet in these three rock types are 0.4 wt%, 0.5-2.3 wt%, and 0.3-2.6 wt%, and like the whole-rock Cr₂O₃ contents, show no distinction among the rock types.

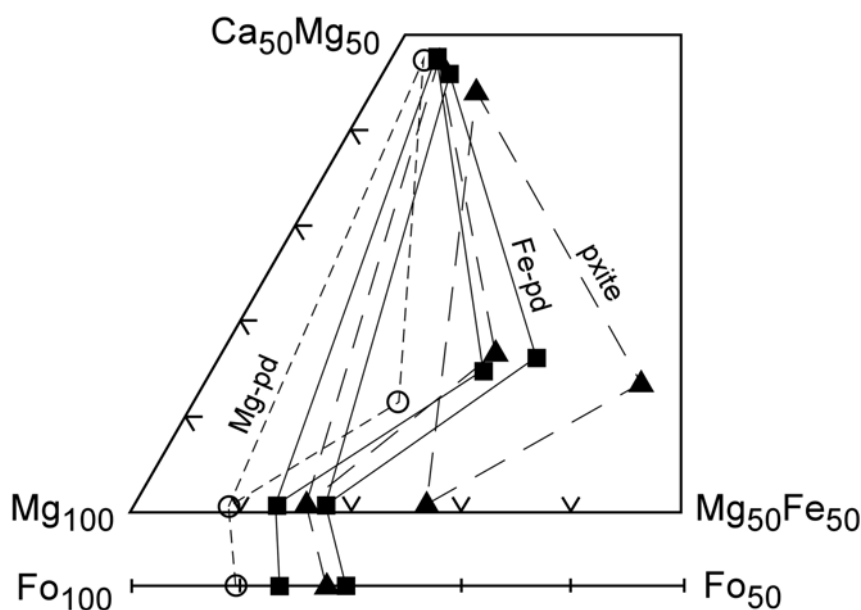


Fig. 10 The compositions of co-existing minerals in Horní Bory peridotites and pyroxenites, in terms of CaO, MgO, and FeO. The filled squares indicate the compositional ranges for minerals in Fe-peridotite and layered Fe-peridotite, and the filled triangles, the ranges for pyroxenite and layered pyroxenite.

Although the Mg-numbers of each silicate mineral species differ significantly among discrete Mg-pd, Fe-Pd, and pyroxenite boudins, such differences are less pronounced in the peridotite and pyroxenite layers in the layered samples, 06HB2 and HB70 (Fig. 2), in which the compositions of minerals adjacent to layer boundaries tend to converge. Appraisal of mineral compositional variation among the layers is problematic, due to the kelyphitization of garnet in peridotite, sparse presence of orthopyroxene, which occurs only in layers 8-11 in sample HB70, and paucity of olivine in pyroxenite. While acknowledging these limitations, the Mg-number in olivine tends to be slightly higher in peridotite layers compared to pyroxenite layers, *i.e.* 84-85.4 *vs.* 82-85 in 06HB2 and 84-86 *vs.* 81-83 in HB70. Clinopyroxene is the only mineral common to all layers, and its Mg-number varies little from layer to layer, lying between 89.5 and 91.5 for all layers in 06HB2 and between 89 and 91 in HB70. The most prominent compositional variation recognized is a difference in Cr-number in clinopyroxene, which ranges from 22 to 27 in peridotite compared to 6 to 20 in pyroxenite in sample 06HB2, and 31 to 33 *vs.* 8 to 22 in sample HB70.

Intergranular spinel grains and spinel inclusions in garnet have Mg-numbers and Cr-numbers [$100 \cdot \text{Cr}/(\text{Cr}+\text{Al})$] that range from 48-51 and 38-69 in Mg-peridotite, to 36-57 and 31-61 in Fe-peridotite, and 51-56 and 24-42 in pyroxenite. The large variations in Cr-numbers of spinel in each rock type are due to compositional zoning of spinel grains, in which the ratio of Cr/Al decreases from cores to rims, with Cr-numbers typically decreasing by 15 to 30 units. Spinel in kelyphite has Mg- and Cr-numbers of 60-70 and 7-9, respectively, and this Cr-poor composition is due to the inheritance of the Cr/Al ratio from garnet during the formation of kelyphite spinel by the reaction, $\text{grt}+\text{ol} = \text{spl}+\text{opx}+\text{cpx}$.

Ilmenite in Fe-peridotite contains 5.0 to 6.9 wt% MgO, and in pyroxenite, 4.1 to 8.0 wt%. Such MgO contents represent a geikielite component in ilmenite of 19 to 26 % in Fe-pd and 15 to 29 % in pyroxenite.

Small amounts of phlogopite are distributed parallel to layering in the boudins and are commonly localized at boundaries between different lithologies. The phlogopite has an Mg-number of 88 to 94, a proportion of Si:Al in the tetrahedral site of ~5:3 (eastonite), TiO₂ contents from 0.7 to 2.9 wt%, and Cr₂O₃ contents from 0.3 to 0.7 wt%.

4.6.2. Trace elements

Clinopyroxenes from eleven Horní Bory ultramafic samples have pronounced convex-upward REE patterns, with an ~5-fold range in normalized element concentrations and considerable compositional overlap among the various rock types (Fig. 11). Concentrations of the LREE generally decrease in the order, Fe-peridotite, pyroxenite, composite Fe-peridotite (*i.e.* Fe-pd with vein-lets of Px), and Mg-pd, but in contrast, the concentration of Yb decreases in the order, composite Fe-pd-px, Mg-pd, Fe-pd, and pyroxenite. Consequently, (Ce/Yb)_N ratios are higher in Fe-pd and pyroxenite,

11.6-14.4, than those in Mg-pd and composite Fe-pd-px (5.0-6.5). The high ratios of $(\text{Sm}/\text{Yb})_N$ from 3 to 18 for clinopyroxene in the Horní Bory ultramafic suite reflect equilibration with garnet and are comparable to those in high-temperature peridotites in cratonic suites elsewhere (Pearson et al., 2003). Extended trace element patterns for clinopyroxene (Fig. 11) are similar to those in the whole rocks, showing HFSE depletion and LILE enrichment.

Due to the almost complete kelyphitization of garnet in Mg-pd and Fe-pd, only garnet from pyroxenite and some composite Fe-pd-px samples could be analyzed. REE patterns for garnet from two pyroxenite samples and one composite Fe-pd-px show significant LREE depletion and MREE to HREE enrichment, with concentrations in pyroxenite being higher than those in composite Fe-pd-px (Fig. 11). Such patterns are typical for garnet from melt-depleted mantle residues or garnet equilibrated with silicate melts (Pearson et al., 2003 and references therein). Garnet in both rock types exhibits positive Rb, Th, U, and Pb anomalies, and in addition, garnet in composite Fe-pd-px has a negative Sr anomaly.

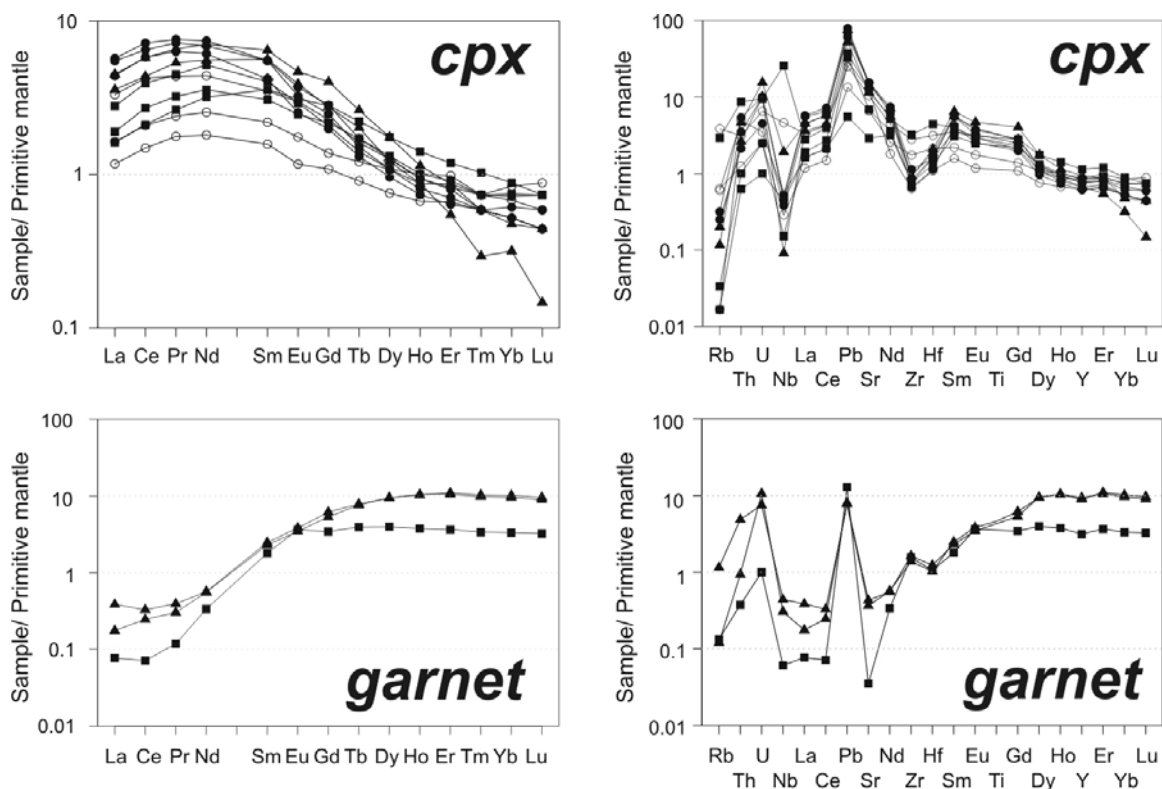


Fig. 11 REE and extended trace element compositions of separated clinopyroxenes and garnets, normalized to primitive mantle (McDonough and Sun, 1995). Symbols as in Fig. 3.

Table 4. Trace element composition (ppm) of separated minerals (clinopyroxene and garnet)

Sample	06HB4	99BY1B	97CZ3C	HB9	HB13	HB14	HB11	85GM8B	BY3BB	HB3	HB4	85GM8B	HB3	HB4
Mineral	cpx	cpx	cpx	cpx	cpx	cpx	cpx	cpx	cpx	cpx	cpx	grt	grt	grt
Type	Mg-pd	Mg-pd	Mg-pd	Fe-pd	Fe-pd	Fe-pd	Fe-pd-px	Fe-pd-px	Fe-pd-px	Px	Px	Fe-pd-px	Px	Px
Rb	0.36	2.30	0.38	0.15	0.19	0.01	0.02	1.75	0.01	0.12	0.07	0.08	0.69	0.07
Sr	131	207	246	308	307	306	136	252	58	229	280	1	7	9
Y	3.73	3.33	2.63	2.64	2.84	3.22	3.59	3.61	4.89	2.88	4.02	13.51	40.27	38.51
Zr	18.30	29.31	6.63	6.91	8.70	11.90	8.04	33.73	8.06	9.75	9.67	16.35	14.53	17.13
Nb	0.35	3.03	0.19	0.25	0.30	0.34	0.10	16.79	0.29	0.06	1.26	0.04	0.29	0.20
Cs	0.02	0.11	0.01	0.01	0.02	0.01	0.01	0.02	0.00	0.02	0.01	0.03	0.06	0.01
Ba	5.05	12.37	6.08	3.11	0.40	0.10	1.43	2.77	0.25	1.06	1.78	1.18	1.42	1.13
La	1.06	2.15	0.76	2.85	3.57	3.70	1.23	1.81	1.05	2.32	2.92	0.05	0.25	0.11
Ce	3.50	7.11	2.49	9.76	10.86	12.05	4.55	6.58	3.54	7.30	9.67	0.12	0.55	0.41
Pr	0.61	1.11	0.45	1.61	1.83	1.93	0.82	1.14	0.67	1.36	1.67	0.03	0.10	0.08
Nd	3.18	5.51	2.26	7.66	8.60	9.30	4.46	6.46	4.00	6.97	8.81	0.42	0.71	0.70
Sm	0.89	1.42	0.64	1.70	2.24	2.25	1.25	1.64	1.45	2.29	2.62	0.73	1.01	0.94
Eu	0.27	0.46	0.18	0.39	0.50	0.57	0.38	0.45	0.48	0.60	0.72	0.56	0.59	0.53
Gd	0.75	1.24	0.59	1.08	1.35	1.54	1.18	1.13	1.53	1.50	2.19	1.87	3.36	2.91
Tb	0.12	0.16	0.09	0.13	0.15	0.17	0.17	0.14	0.22	0.20	0.26	0.39	0.78	0.76
Dy	0.73	0.85	0.51	0.65	0.73	0.86	0.89	0.73	1.18	0.82	1.18	2.68	6.37	6.42
Ho	0.15	0.14	0.10	0.11	0.12	0.14	0.15	0.13	0.21	0.13	0.17	0.56	1.56	1.55
Er	0.43	0.36	0.29	0.28	0.31	0.35	0.40	0.38	0.52	0.24	0.38	1.60	4.62	4.82
Tm	0.05	0.05	0.04	0.04	0.04	0.04	0.05	0.05	0.07	0.02	0.04	0.23	0.67	0.70
Yb	0.37	0.30	0.23	0.23	0.23	0.27	0.32	0.33	0.39	0.14	0.21	1.47	4.25	4.49
Lu	0.06	0.04	0.03	0.03	0.03	0.04	0.05	0.05	0.05	0.01	0.03	0.22	0.61	0.65
Hf	0.60	0.89	0.31	0.32	0.46	0.44	0.37	1.25	0.45	0.53	0.59	0.30	0.29	0.35
Pb	2.01	3.75	4.34	10.24	9.06	11.83	4.93	5.58	0.83	7.83	11.30	1.94	1.16	1.21
Th	0.39	0.25	0.10	0.17	0.43	0.28	0.08	0.69	0.05	0.21	0.37	0.03	0.39	0.08
U	0.07	0.13	0.05	0.09	0.20	0.20	0.05	0.19	0.02	0.20	0.31	0.02	0.15	0.21

4.6.3. Temperature-Pressure estimates

Accurate temperature and pressure estimates are difficult to obtain in the ultramafic xenoliths because of the compositional variability in minerals arising from recrystallization and partial re-equilibration during cooling and decompression. Estimates of equilibration conditions for the highest temperature and pressure stage of the boudins are based on the core compositions of minerals that are judged on the basis of textures to represent the earliest assemblages. Further difficulty arises from the extensive kelyphitization of garnet in peridotites and the absence of orthopyroxene in many wehrlites and clinopyroxenites, which prohibits pressure estimates for these rock types.

Following the approach of Brenker and Brey (1997), T-P estimates for peridotite are obtained by application of the olivine-garnet Mg-Fe exchange geothermometer (O'Neill and Wood, 1979; O'Neill, 1980) and the Al-in-orthopyroxene geobarometer (Brey and Köhler, 1990). The results for one sample of Mg-peridotite are 910 °C, 38.3 kbar, and for two samples of Fe-pd are 960 °C, 24.6 kbar, and 870 °C, 25.6 kbar. Two peridotite layers in HB70 yield 955 ± 11 °C, 35.6 ± 4.5 kbar, and five domains in two wehrlite layers in 06HB2 yield a temperature of 945 ± 80 °C, calculated at 30 kbar.

T-P estimates for orthopyroxene-bearing pyroxenite are obtained from the orthopyroxene-garnet Mg-Fe exchange geothermometer (Harley, 1984) and the Al-in-orthopyroxene geobarometer (Brey and Köhler, 1990). One sample of pyroxenite yields 980 °C, 21.3 kbar, and four pyroxenite layers in HB70 give 895 ± 12 °C, 31.9 ± 2.8 kbar.

This range of T-P estimates, 870-980 °C and 21.3-38.3 kbar, is consistent with the stable coexistence of garnet and Cr-spinel in the Horní Bory boudins, in which spinel cores have Cr-numbers from 42 to 69, depending on rock type. Of regional geologic interest, this T-P range is intermediate to, and fills the gap between, the T-P fields previously established for the two groups of Mg-Cr peridotites in the Gföhl Nappe, a higher-pressure group of subcontinental origin and a lower pressure group of suboceanic origin (Medaris et al., 2005).

4.7. SR-ND GEOCHEMISTRY

4.7.1. Sm-Nd geochronology

A garnet pyroxenite, sample HB3, yields a poorly defined Sm-Nd isochron age of 331 ± 150 Ma for clinopyroxene, garnet and whole-rock (Table 5, Fig. 12). As indicated by the large MSWD value (72), isotopic equilibrium between whole rock and minerals was either not achieved or disturbed by later processes. The clinopyroxene-garnet pair yields an age of 337 ± 3.3 Ma, which is the same as those for peridotite-hosted pyroxenite and eclogite elsewhere in the Gföhl Unit (mean age = 336 ± 7 Ma, $n = 9$; Medaris et al., 2006). Such ages record the closure age (blocking temperature) of the Sm-Nd system in these samples, following their earliest, high-temperature and high-pressure stage of equilibration.

Table 5. Rb-Sr and Sm-Nd isotopic data for Horní Bory rocks and mineral separates

Sample	Type	Rb	Sr	$^{87}\text{Rb}/^{86}\text{Sr}$	$^{87}\text{Sr}/^{86}\text{Sr}$	$^{87}\text{Sr}/^{86}\text{Sr}$ (i)	Sm	Nd	$^{147}\text{Sm}/^{144}\text{Nd}$	$^{143}\text{Nd}/^{144}\text{Nd}$	ϵ Nd (i)	Age (Ma)	T_{DM} (Ga)
06HB4 cpx	Mg-pd	0.259	133.2	0.006	0.7046	0.7045	0.829	3.159	0.1586	0.512829 ± 8	+ 5.3	–	0.64
99BY1B cpx	Mg-pd	2.574	334.8	0.022	0.7056	0.7055	1.376	5.255	0.1583	0.512799 ± 9	+ 4.8	–	0.68
97CZ3C cpx	Mg-pd	0.365	260	0.004	0.7068	0.7068	1.413	6.38	0.1339	0.512729 ± 10	+ 4.4	–	0.71
97CZ3C wr	Mg-pd	n.a.	n.a.	n.a.	n.a.	n.a.	0.139	0.512	0.1646	0.512779 ± 10	+ 4.1	–	0.74
HB9 cpx	Fe-pd	5.635	406.6	0.040	0.7079	0.7077	1.44	6.632	0.1313	0.512432 ± 9	– 1.3	–	1.18
HB13 cpx	Fe-pd	0.081	319	0.001	0.7085	0.7085	2.033	8.42	0.146	0.512386 ± 7	– 2.8	–	1.30
HB14 cpx	Fe-pd	0.896	477.6	0.005	0.7087	0.7087	2.149	9.192	0.1413	0.512417 ± 9	– 2.0	–	1.23
HB11 cpx	Fe-pd-px	0.147	215	0.002	0.7059	0.7059	1.236	4.374	0.1708	0.512846 ± 7	+ 5.2	–	0.65
85GM8B cpx	Fe-pd-px	1.419	397.2	0.010	0.7046	0.7046	1.488	6.19	0.1454	0.512831 ± 7	+ 5.9	–	0.59
BY3BB cpx	Fe-pd-px	0.035	89.7	0.001	0.7041	0.7041	1.377	3.901	0.2135	0.513014 ± 8	+ 6.6	–	0.53
HB3 cpx	Px	0.051	238.4	0.001	0.7078	0.7078	2.123	7.059	0.1818	0.512696 ± 9	+ 1.8	337 ± 3	0.93
HB3 grt	Px	n.a.	n.a.	n.a.	n.a.	n.a.	0.958	0.637	0.9092	0.514301 ± 13	+ 2.4	324 ± 3	0.88
HB3 wr	Px	n.a.	n.a.	n.a.	n.a.	n.a.	1.729	5.137	0.2035	0.512805 ± 9	+ 3.0	–	0.83
HB4 cpx	Px	0.108	420.9	0.001	0.7082	0.7082	2.552	8.552	0.1804	0.512617 ± 10	+ 0.3	–	1.05

4.7.2. Sr and Nd isotopes

Sr and Nd data for leached clinopyroxene and garnet and un-leached whole-rock analyses are given in Table 5, and initial Sr and Nd isotopic ratios for clinopyroxene, calculated at to 330 Ma, are plotted in Fig. 13. ϵ_{Nd} values and $^{87}\text{Sr}/^{86}\text{Sr}$ ratios for clinopyroxene are negatively correlated (Fig. 13), but displaced from the field for Gföhl garnet pyroxenite and eclogite (Medaris et al., 2006) and the typical array for depleted oceanic mantle (Faure, 2001). With respect to their Sr-Nd isotopic compositions, the Horní Bory clinopyroxenes fall into two groups: those from the Mg-pd and Fe-pd-px have $\epsilon_{\text{Nd } 330\text{Ma}}$ values between +4.4 and +6.6 and $^{87}\text{Sr}/^{86}\text{Sr}_{(330\text{ Ma})}$ ratios between 0.7041 and 0.7068, and those from Fe-pd and pyroxenite have $\epsilon_{\text{Nd}(330\text{ Ma})}$ values between +1.8 and -2.8 and $^{87}\text{Sr}/^{86}\text{Sr}_{(330\text{ Ma})}$ ratios between 0.7077 and 0.7087. Clinopyroxenes from the Fe-pd samples have less radiogenic Nd, but similar Sr ratios, than those from pyroxenites. Surprisingly, clinopyroxenes from the Fe-pd-px composite samples (HB11, 85GM8B, BY3BB) are isotopically similar to those from Mg-pd, rather than being intermediate in the isotopic array. All these features can be also illustrated on Sr-Nd isotopic composition vs. Sr-Nd concentrations plots for all samples comprising also garnets and whole-rocks (Fig. 14).

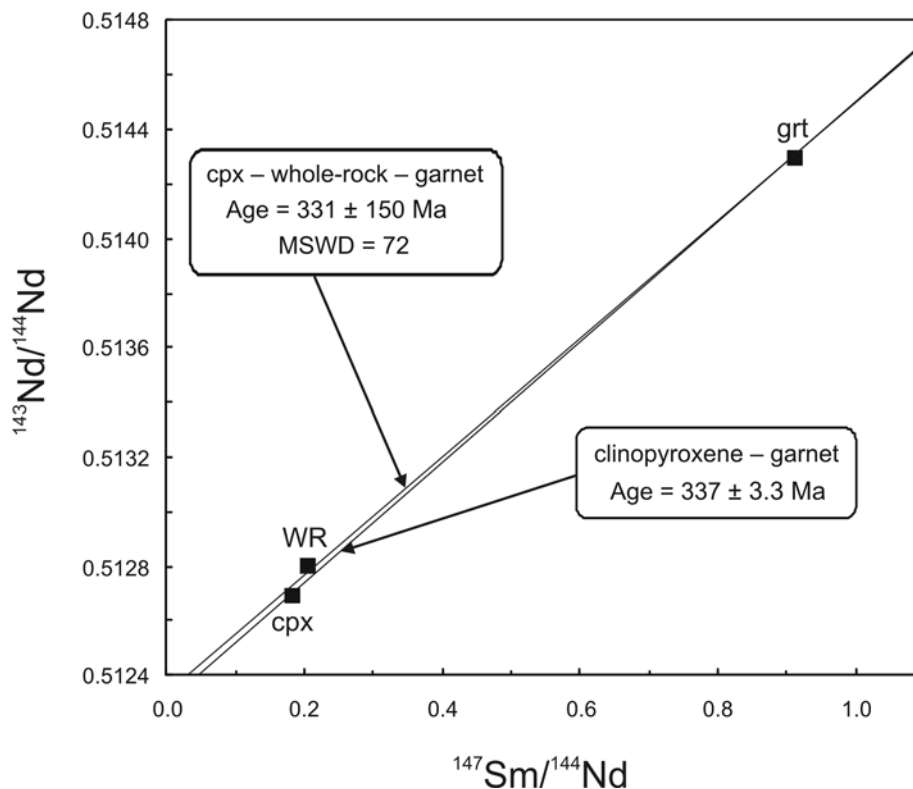


Fig. 12 Sm-Nd isochrons for garnet pyroxenite (websterite, sample HB3). The three-point point isochron yields an age of 331 Ma, but with a large MSWD and error, suggesting isotopic disequilibrium among garnet, clinopyroxene, and whole rock. The garnet-clinopyroxene isochron yields an age of 337 Ma, with a much smaller uncertainty.

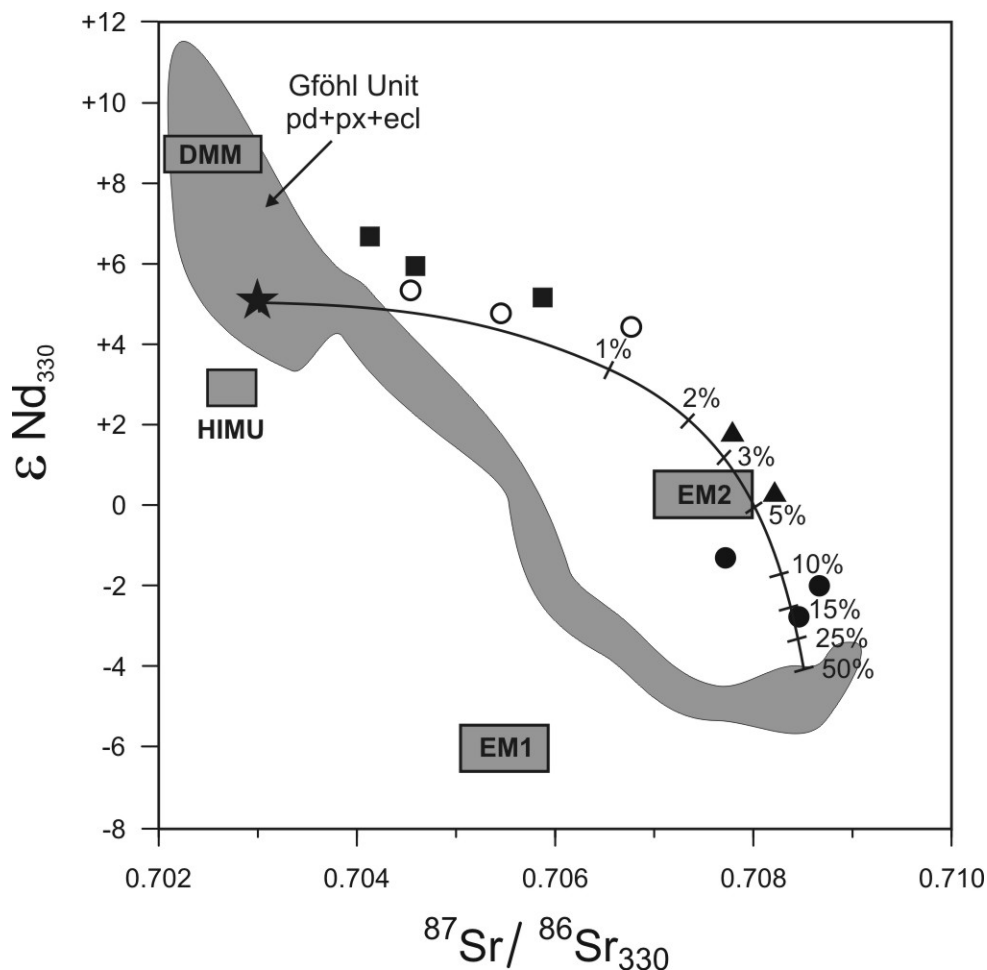


Fig. 13 ϵ_{Nd} versus $^{87}\text{Sr}/^{86}\text{Sr}_i$ of clinopyroxenes from Horní Bory peridotites and pyroxenites. Mantle components (DMM, EM1, EM2, HIMU) are from Faure (2001), calculated at 330 Ma. The field for peridotites, pyroxenites, and eclogites in the Gföhl Unit is based on data of Becker (1996a,b), Medaris et al. (1995) and Medaris et al. (2006). End member compositions used in mixing calculations: mantle ($\epsilon_{\text{Nd}} = +4.8$, $^{87}\text{Sr}/^{86}\text{Sr} = 0.703$, Sr = 8 ppm, Nd = 0.6 ppm), subducted oceanic crust ($\epsilon_{\text{Nd}} = -4.7$, $^{87}\text{Sr}/^{86}\text{Sr} = 0.709$, Sr = 1500 ppm, Nd = 13 ppm). Symbols as in Fig. 3.

4.8. DISCUSSION

4.8.1. Petrogenetic model

It was previously suggested that peridotite boudins at Horní Bory might represent fragments of a disrupted mafic-ultramafic cumulate complex, based on the relatively Fe-rich composition of some peridotite, the scatter in major element variation diagrams, association with abundant pyroxenite and layered texture of many samples (Medaris et al., 2005). However, the results of our more extensive investigation indicate that the Horní Bory ultramafic suite formed more likely by the reaction of peridotite with transient melt. In this model, Fe-peridotite is the result of reaction between Mg-peridotite and percolating melt, and pyroxenite is the crystalline product (\pm trapped liquid) of melt

migrating along conduits in the peridotite. Such a model is consistent with the layered aspect of certain samples, the presence of thin, discontinuous lenses of pyroxenite in peridotite, the major and trace element compositions of layered peridotite and pyroxenite samples, which are generally intermediate between those of Fe-peridotite and pyroxenite, and Sr-Nd isotopic data for the boudin suite.

A similar model has been used successfully to explain the characteristics and origin of Fe-rich lherzolite-wehrlite xenoliths from Tok, Siberia (Ionov et al., 2005), with which the Horní Bory Fe-rich dunite-wehrlite boudins share many similar mineralogical and chemical features. In the Tok xenolith suite, Mg-lherzolite-harzburgerite was transformed to Fe-lherzolite-wehrlite by reaction with percolating, silica-undersaturated melt, during which orthopyroxene was replaced by clinopyroxene and whole-rock Mg-numbers decreased, as demonstrated by textural features and compositional trends (Ionov et al., 2005). In the Bory Fe-dunite-wehrlite suite, orthopyroxene was also likely replaced by clinopyroxene, as indicated by modal and compositional data, but replacement textures in peridotite (and presumed, original igneous textures in pyroxenite) have been obliterated by extensive recrystallization at high temperatures and pressures, followed by further recrystallization during cooling and decompression.

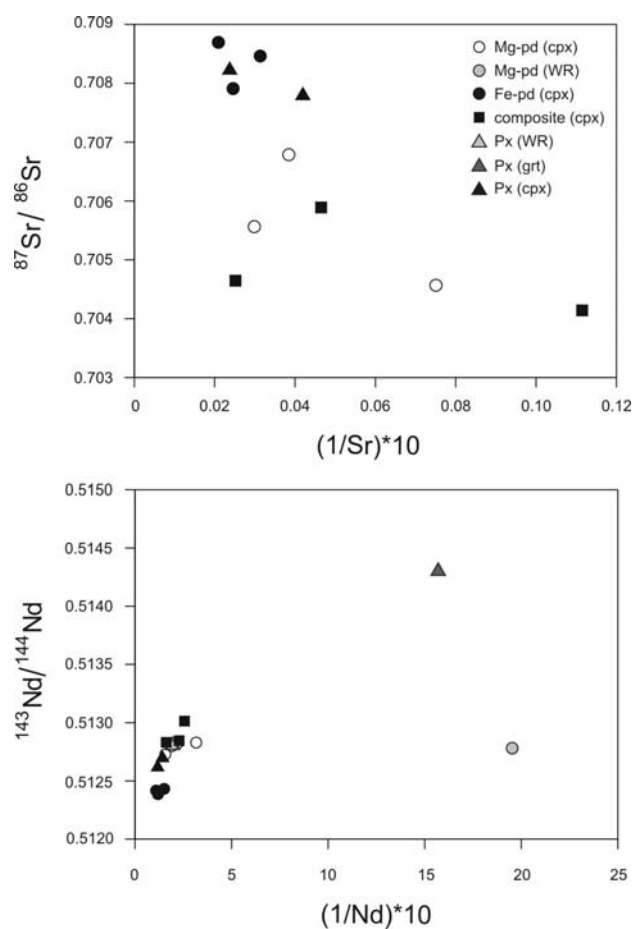


Fig. 14 Variation of $^{87}\text{Sr}/^{86}\text{Sr}$ vs $1/\text{Sr}$ and $^{143}\text{Nd}/^{144}\text{Nd}$ vs $1/\text{Nd}$ for Horní Bory peridotites and pyroxenites. Note negative correlation between $^{87}\text{Sr}/^{86}\text{Sr}$ and $1/\text{Sr}$ and positive correlation between $^{143}\text{Nd}/^{144}\text{Nd}$ and $1/\text{Nd}$, suggesting the effects of metasomatism.

4.8.2. Constraints on the origin and evolution of Mg-pd and Fe-pd-px

Although Horní Bory Mg-peridotite is similar to depleted mantle peridotite in certain respects, e.g. high Mg- and Cr-numbers and negative correlations of Al_2O_3 , TiO_2 , CaO , and Na_2O with MgO , some Mg-peridotite samples have relatively high FeO and trace element contents, contain phlogopite, and host clinopyroxene with $^{87}\text{Sr}/^{86}\text{Sr}_{330\text{ Ma}}$ ratios ranging from 0.7045 to 0.7068. Thus, it is likely that Mg-peridotite also reacted with percolating melt, as did Fe-peridotite, but to a lesser degree (i.e. at lower melt/rock ratios).

In contrast to Mg-peridotite, the major and trace element composition of Fe-peridotite can not be explained by partial melting. Rather, the modal composition (dunite to wehrlite), major and trace element variations, and Sr-Nd isotopic composition of Fe-peridotite indicate that metasomatism plays a dominant role in its origin. Moreover, the mineralogical and chemical characteristics of Fe-peridotite can not be explained by simple cryptic or modal metasomatism by melts, but instead, by intensive melt-rock reactions between peridotite and migrating melts.

Experimental studies (Kelemen et al., 1990) have shown that orthopyroxene-poor peridotites could result from melt-rock reaction between peridotite and basaltic melt, which is undersaturated with respect to orthopyroxene at shallow mantle depths. In this type of reaction, dissolution of orthopyroxene in peridotite is accompanied by crystallization of olivine and clinopyroxene, leading to formation of a dunite-wehrlite series. Such a reaction scheme was successfully used by Peslier et al. (2002) and Ionov et al. (2005) to explain wehrlite-series xenoliths in the Canadian Cordillera and Siberia. Alternatively, wehrlites have been interpreted as the product of reaction between peridotite and carbonatite melt (Yaxley et al., 1991), but this process fails to account for the marked Fe-enrichment in Horní Bory Fe-peridotite.

4.8.3. Mg-Fe modelling

To evaluate the possibility of melt-rock reaction in the Horní Bory suite, we have utilized the numerical model of Ionov et al. (2005), which is based on the “Plate Model” for trace element exchange of Vernieres et al. (1997) and modified for major element exchange of Mg and Fe (see Ionov et al. 2005 for more details). The model incorporates the total inversion method of Tarantola and Vallette (1982) to constrain Mg-Fe distribution between solid and liquid phases during reaction and to maintain stoichiometry of the solid phases. Mineral-melt partition coefficients for Mg and Fe at 1250 °C and 1.5 GPa were adopted from the experimental calibrations of Ulmer (1989) and Brey and Köhler (1990). During melt-rock reaction, dissolution of orthopyroxene in peridotite is accompanied by crystallization of clinopyroxene and olivine, and an olivine/cpx ratio of 9 was chosen for this reaction.

The average composition of Bory Mg-peridotite (Mg # = 0.9; olivine/opx = 2.96) was selected for the composition of starting peridotite.

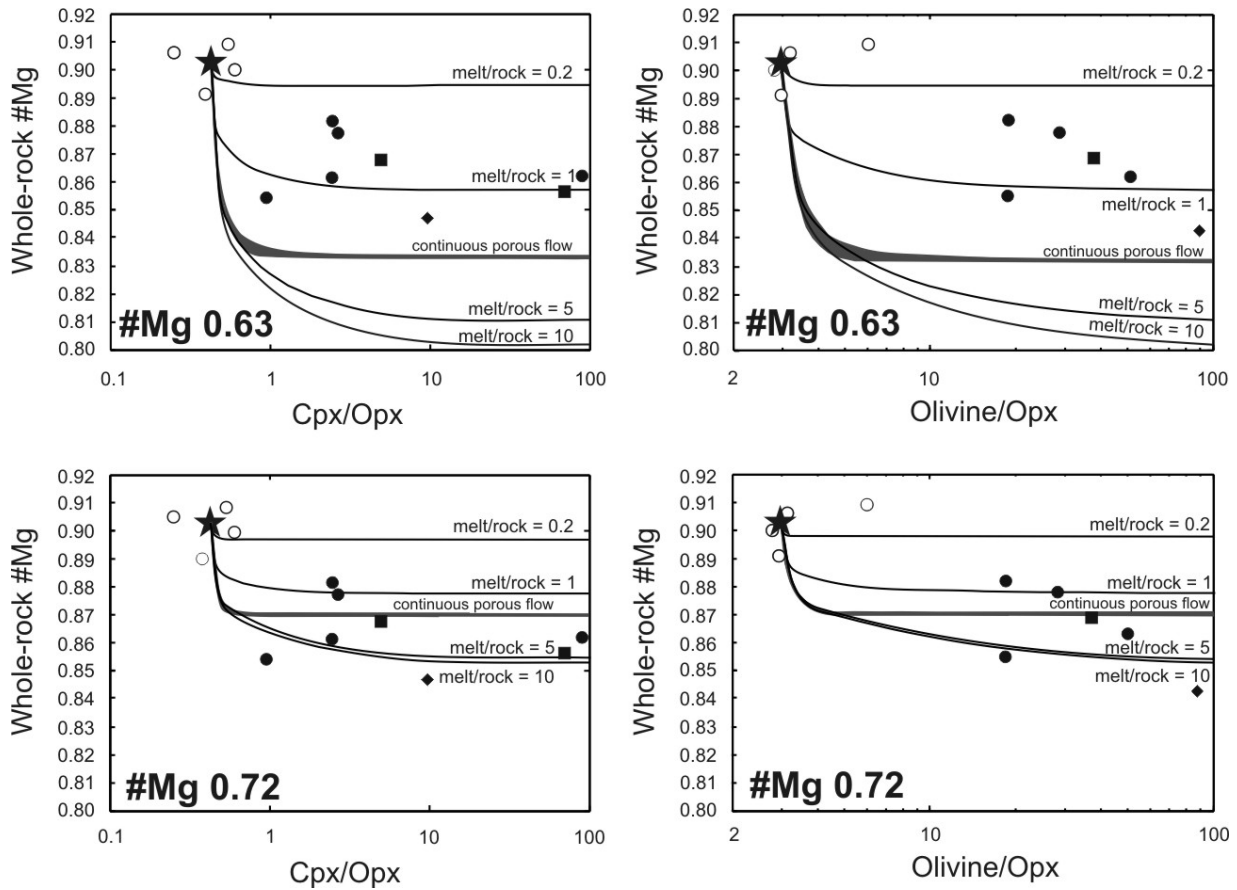


Fig. 15 Results of Mg-Fe modelling, following the adapted model of Ionov et al. (2005). Two hypothetical infiltrated melts with Mg #'s of 0.63 and 0.72 were tested. The curves were calculated for single batch infiltration (lines) and continuous melt infiltration (grey fields). For details on the model and discussion see the text. The star indicates the average composition of Mg-pd used as a starting material. Symbols as in Fig. 3.

With respect to observed Mg # values in Fe-pd, three different values for the initial Mg # of infiltrating melt were tested, including a value of 0.80, which is that for pyroxenite, and values of 0.72 and 0.63, which lie within the range for those in Horní Bory eclogite boudins. Two different reaction models were evaluated, one for single batch melt infiltration, and another for continuous porous melt flow.

Model results for the two initial melt compositions at Mg # = 0.63 and 0.72 are shown in Fig. 15. For continuous melt infiltration, the resulting Mg # of peridotite remains nearly constant at melt/rock ratios between 0.2 and 10, achieving values of ~0.83 and ~0.87 for the two melt starting compositions at 0.63 and 0.72, respectively. In contrast, for single batch melt infiltration the resulting Mg #'s in peridotite are strongly dependent on melt/rock ratios. For melt with Mg# = 0.63, the compositions of peridotite calculated at melt/rock ratios of 0.3 and 2 encompass those of Bory Fe-peridotites and layered Fe-peridotites, whereas for melt with Mg# = 0.72, melt/rock ratios of 1 to 20 are required to match the compositions of Bory Fe-peridotites. For melt with pyroxenite starting composition at Mg # = 80, calculated Mg #'s for peridotite are no lower than 0.90, regardless of melt/rock ratio. Thus,

within the parameters of the Mg-Fe modelling, the compositions of Bory Fe-peridotites (discrete and layered) can best be explained by reaction of Mg-peridotite with an evolved melt (Mg # = ~0.6), at different melt/rock ratios between ~0.2 and ~1. Reaction with less evolved melt would require much higher melt/rock ratios to match the compositions of the Bory samples. Note that for the Tok Fe-lherzolite-wehrlite xenolith suite, an evolved melt composition (Mg# = 0.63) was also necessary to reproduce the xenolith compositions (Ionov et al., 2005).

4.8.4. Sr-Nd isotopic constraints

The Nd and Sr isotopic compositions of clinopyroxene in Horní Bory ultramafic boudins define a convex-upward array, with values for ϵ_{Nd} extending from +6.6 to -2.8 and $^{87}\text{Sr}/^{86}\text{Sr}$ (330 Ma), from 0.7041 to 0.7087 (Fig. 13). Such an isotopic array can be generated by mixing of depleted mantle (ϵ_{Nd} , +4.8; Nd, 0.6 ppm; $^{87}\text{Sr}/^{86}\text{Sr}$, 0.703; Sr, 8 ppm) with an end-member that is enriched in Sr with respect to Nd (ϵ_{Nd} , -4.7; Nd, 13 ppm; $^{87}\text{Sr}/^{86}\text{Sr}$, 0.709; Sr, 1500 ppm), e.g. melt derived from subducted oceanic crust (Fig. 16). Note that the Nd-Sr isotopic array for pyroxenites and eclogites in other Mg-peridotite bodies in the Gföhl Unit is convex downward, which has been attributed to mixing between depleted mantle and oceanic clay (Nd, 30 ppm; Sr, 50 ppm; Medaris et al., 1995). These two markedly distinct Nd-Sr isotopic arrays emphasize the unusual chemical composition of the Horní Bory ultramafic suite and its contrast with the more common Mg-peridotite bodies elsewhere in the Gföhl Unit.

Isotopically, Fe-peridotite could be formed by mixing of depleted mantle with ~5-15% of the Sr-rich end-member, pyroxenite, by ~3-5%, and Mg-peridotite, by $\leq 1\%$. Surprisingly, the isotopic compositions of composite Fe-pd-px samples are similar to those for Mg-peridotite, although Mg-Fe modelling indicates that the composite Fe-pd-px samples have experienced the same degree of melt/rock interaction as have the Fe-peridotites, which are isotopically more enriched (*cf.* Figs. 13 and 15). This apparent decoupling of Nd-Sr isotopes and major elements may be due to incomplete trace element and isotopic equilibration in those samples, where host peridotite is cut by pyroxenite veinlets (intrusive melt).

4.8.5. Composition and source of infiltrating melt

The Horní Bory pyroxenites are thought to represent the crystalline products of melts that were responsible for metasomatism of the peridotites. Although the pyroxenites are probably mineral cumulates (\pm trapped melt) and do not represent melt compositions themselves, the trace element compositions of melts from which they crystallized can be calculated from the compositions of mineral separates. Accordingly, the trace element compositions of melts have been calculated from the compositions of clinopyroxene and garnet in pyroxenite, using the partition coefficients of Miller et al. (1992) and Hauri et al. (1994), which were slightly modified for some elements (Table 4) to bring the

results from clinopyroxene and garnet into concordance. Melt compositions were also calculated from the clinopyroxene compositions in three samples of Fe-peridotite, which are closely similar to those in pyroxenite.

The trace element compositions of melt, calculated from clinopyroxene in pyroxenite and Fe-peridotite, are plotted in Fig. 16. The resulting REE patterns, normalized to primitive mantle, show a marked enrichment in the LREE, with Ce_N/Yb_N ratios ranging from 41.5 to 51.3 and averaging 45.9. Such a steep REE pattern suggests the likely presence of garnet in the source from which the melt was derived. The calculated extended trace element patterns show enrichment in the LILE (except for Rb), negative anomalies for the HFSE, a large, positive anomaly for Pb, and a smaller positive anomaly for Sr. Although the calculated trace element composition of the melt reflects the geochemical character of its source region, it may not represent the trace element concentrations in the initial melt exactly, because Mg-Fe modelling indicates that the melt was relatively evolved at the time of infiltration and reaction, having an Mg # of ~ 0.6 .

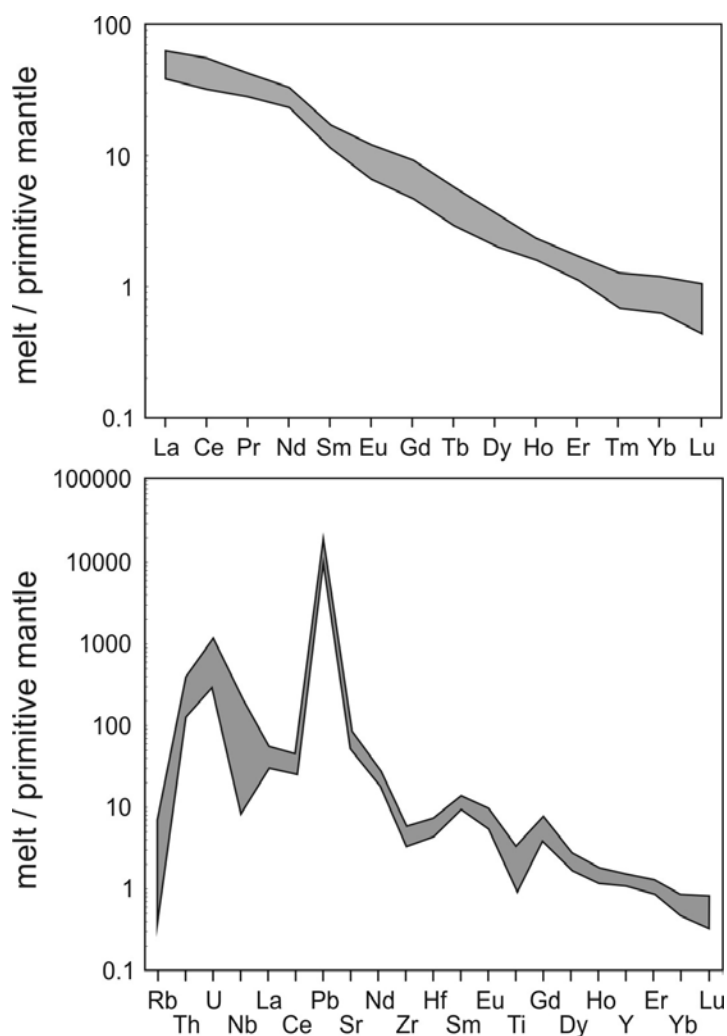


Fig. 16 REE and extended trace element composition of transient melt, calculated from the composition of clinopyroxene in pyroxenite and Fe-peridotite. See text for discussion.

The infiltrating melt was probably basaltic in composition and undersaturated with respect to SiO_2 , based on the paucity of orthopyroxene in the Fe-dunite to wehrlite suite. This melt was not a direct partial melting product of subducted oceanic crust in the eclogite or amphibolite facies, because fusion of such material produces SiO_2 -saturated melts (Rapp et al., 2003; Prouteau et al., 2001). Rather, the infiltrated melt was most probably derived by partial melting of the peridotite wedge above a subduction zone, due to infiltration of subduction-related melts/fluids, which imparted the trace element fingerprints of subducted crust to the mantle wedge. One such fingerprint is the positive Pb anomaly observed in Horní Bory clinopyroxenes (Fig. 11) and the modelled melt composition (Fig. 16). This enrichment could be explained by selective concentration and transport of Pb by fluids from the subducting slab into the mantle wedge, where melting then occurred (e.g. Miller et al. 1994). Melt fractionation and mineral precipitation during melt percolation, following extraction from a garnet-bearing source, led to an evolved melt ($\text{Mg} \# = 0.6$) that was strongly enriched in the LILE and LREE, and depleted in the HFSE and HREE. The Fe-dunite-wehrlite suite was produced by reaction of such melt with Mg-peridotite, and pyroxenite formed by crystallization of clinopyroxene and garnet (\pm trapped melt) in melt conduits. Crystallization of anhydrous minerals in pyroxenite and precipitation of olivine and clinopyroxene during reaction with peridotite led to an increase in H_2O activity in the infiltrating melts and eventual stabilization of phlogopite and amphibole.

4.9. CONCLUSIONS

In many orogenic peridotite massifs and mantle xenolith suites, lherzolite has been converted to harzburgite by reaction with silica-rich (subduction-related) transient melt. On the other hand, a lherzolite-dunite-wehrlite series can be produced by reaction of mantle peridotite with fractionated, SiO_2 -undersaturated basaltic melts (e.g. Kelemen et al., 1990; Kelemen et al., 1998). Both processes lead to the partial/complete dissolution of clinopyroxene or orthopyroxene, depending on the level of SiO_2 -saturation of the infiltrating melt.

Mg-lherzolite from Horní Bory has been transformed to Fe-dunite-wehrlite, which is similar in many respects to the modification of lherzolite to Fe-lherzolite-wehrlite in several xenolith suites of subcontinental lithospheric mantle (Lee and Rudnick, 1999; Peslier et al., 2002; Ionov et al., 2005). The melts responsible for the production of Fe-peridotites at Horní Bory have isotopic and trace element characteristics of subduction-related melts, and were undersaturated with respect to SiO_2 , leading to the dissolution of orthopyroxene, precipitation of clinopyroxene and olivine, and production of wehrlite. The predominance of Fe-rich peridotites over Mg-lherzolites at Horní Bory points to the local importance of pervasive melt-rock reactions in the mantle wedge, driven by the infiltration of subduction-related melts/fluids.

Acknowledgments

This research was supported by the Grant Agency of the Academy of Sciences, project No. IAA3013403 and the Scientific Programme CEZ: Z3-013-912 of the Institute of Geology, Acad. Sci. CR and MSM 0021620855 of the Charles University, Faculty of Science. The authors thank Elmar Reitter (Tübingen) for Rb-Sr and Sm-Nd isotope analyses, Anna Langrová and Vlasta Böhmová (Acad. Sci. CR) for microprobe analyses, Václav Sedláček (Acad. Sci. CR) for mineral separation and Jaromír Ulrych for consultations during preparation of the manuscript.

Table 1 (Electronic Supplementary Material). Whole-rock analyses (wt. %, recalculated to anhydrous base) of Horní Bory ultramafic suite. For the rest of the analyses of the studied rock, see Medaris et al. (2005) - Lithos

Sample	Rock	Type	Texture	SiO ₂	TiO ₂	Al ₂ O ₃	Cr ₂ O ₃	NiO	FeO _{TOT}	MnO	MgO	CaO	Na ₂ O	K ₂ O	P ₂ O ₅	#Mg	#Cr
06HB4	lherzolite	Mg-pd	discrete	44.84	0.09	1.91	0.40	0.32	7.87	0.11	42.70	1.50	0.08	0.15	0.04	90.9	10.1
97CZ3C	lherzolite	Mg-pd	discrete	44.86	0.09	1.91	0.37	0.30	7.88	0.11	42.72	1.50	0.08	0.15	0.04	90.6	12.2
99BY1B	lherzolite	Mg-pd	discrete	46.03	0.14	1.35	0.43	0.30	8.00	0.13	40.31	3.13	0.11	0.04	0.03	90.0	18.4
99BY3A	dunite	Fe-pd	discrete	40.78	0.18	1.74	0.66	0.34	12.16	0.14	42.47	1.39	0.06	0.01	0.05	86.2	21.5
HB3	pyroxenite	Px	discrete	51.57	0.43	5.73	0.37	0.17	6.42	0.09	16.72	18.00	0.44	0.07	0.00	82.3	4.1
HB4	pyroxenite	Px	discrete	50.50	0.53	4.58	0.69	0.05	8.87	0.08	16.84	17.15	0.67	0.06	0.00	77.2	9.1
BY3BB	pyroxenite	Px	discrete	46.53	0.52	5.36	0.94	0.10	8.09	0.24	20.89	16.77	0.54	0.00	0.01	82.0	10.5
06HB2B	dunite	Fe-pd	layered	41.74	0.43	3.59	0.48	0.26	13.33	0.15	37.15	2.75	0.09	0.00	0.02	83.2	8.20
06HB2C	pyroxenite	Px	layered	48.82	0.54	5.43	0.58	0.16	6.29	0.13	18.90	18.34	0.79	0.00	0.01	84.3	6.70
06HB2D	dunite	Fe-pd	layered	43.07	0.18	2.46	0.48	0.21	9.98	0.13	38.44	4.93	0.10	0.00	0.01	87.3	11.60
06HB2E	pyroxenite	Px	layered	45.98	0.33	7.05	0.28	0.11	7.95	0.19	25.89	11.49	0.53	0.18	0.01	85.3	2.61
HB70-6	dunite	Fe-pd	layered	40.44	0.17	2.09	0.80	0.26	12.32	0.16	41.54	2.23	0.00	0.00	0.00	85.7	20.44
HB70-7	pyroxenite	Px	layered	46.34	0.70	6.03	0.42	0.10	8.97	0.20	23.01	13.63	0.60	0.00	0.01	82.1	4.49
HB70-8	dunite-px	Fe-pd/px	layered	44.57	0.40	5.06	0.45	0.14	10.25	0.18	28.79	9.74	0.43	0.00	0.00	83.4	5.61
HB70-9	pyroxenite	Px	layered	48.93	0.86	6.09	0.26	0.05	6.27	0.25	19.44	17.19	0.66	0.00	0.01	84.7	2.76
HB70-10	dunite	Fe-pd	layered	42.40	0.09	2.95	0.38	0.28	10.83	0.13	40.24	2.64	0.05	0.00	0.00	86.9	7.92

Table 2 (Electronic Supplementary Material). Microprobe analyses (wt. %) of minerals from Horní Bory ultramafic suite

Sample	DISCRETE SAMPLES												
	06HB4	HB2	97CZ3C	99BY1B	HB7	HB9	HB13	HB14	99BY3A	85GM8B	BY3BB	HB3	HB4
Rock	lherzolite	lherzolite	lherzolite	lherzolite	lherzolite	wehrlite	wehrlite	wehrlite	dunite	wehrlite-px	wehrlite-px	Px	Px
Type	Mg-pd	Mg-pd	Mg-pd	Mg-pd	Fe-pd	Fe-pd	Fe-pd	Fe-pd	Fe-pd	Fe-pd-px	Fe-pd-px	Px	Px
SiO ₂	41.36	41.39	40.52	40.62	40.07	40.86	40.22	40.67	39.86	39.15	40.08	-	-
FeO	8.94	9.06	9.26	10.06	12.91	11.62	11.68	11.40	12.55	17.89	15.47	-	-
MnO	0.10	0.17	0.16	0.15	0.23	0.22	0.16	0.16	0.29	0.22	0.24	-	-
MgO	49.48	48.91	49.49	48.71	46.31	47.02	47.53	47.48	46.33	41.95	43.06	-	-
NiO	0.38	0.01	0.37	0.36	0.14	0.34	0.12	0.20	0.29	0.22	0.04	-	-
Sum	100.28	99.91	99.81	99.96	99.72	100.07	99.73	100.04	99.32	99.43	98.88	-	-
Mg #	90.8	90.6	90.5	89.6	86.5	87.8	87.9	88.1	86.8	80.7	83.2	-	-

Sample	ORTHOPYROXENE												
	06HB4	HB2	97CZ3C	99BY1B	HB7	HB9	HB13	HB14	99BY3A	85GM8B	BY3BB	HB3	HB4
Rock	lherzolite	lherzolite	lherzolite	lherzolite	lherzolite	wehrlite	wehrlite	wehrlite	dunite	wehrlite-px	wehrlite-px	Px	Px
Type	Mg-pd	Mg-pd	Mg-pd	Mg-pd	Fe-pd	Fe-pd	Fe-pd	Fe-pd	Fe-pd	Fe-pd-px	Fe-pd-px	Px	Px
SiO ₂	57.10	57.88	57.29	57.32	56.36	57.22	57.01	56.29	56.80	55.46	56.19	57.49	55.66
TiO ₂	0.08	0.02	0.06	0.07	0.08	0.06	0.10	0.11	0.11	0.05	0.11	0.04	0.06
Al ₂ O ₃	1.45	1.33	0.85	0.76	1.70	1.36	1.39	2.45	1.19	1.78	2.02	0.47	2.26
Cr ₂ O ₃	0.17	0.15	0.17	6.46	0.26	0.21	0.28	0.31	0.16	0.04	0.22	0.10	0.26
FeO	5.95	5.98	5.90	0.10	8.52	7.26	7.11	7.26	8.89	11.59	9.99	8.98	12.21
MnO	0.16	0.07	0.13	0.11	0.26	0.21	0.17	0.19	0.34	0.29	0.26	0.10	0.18
MgO	34.86	34.24	35.37	34.74	32.59	33.00	33.76	33.09	33.02	30.53	30.74	32.97	29.56
CaO	0.27	0.24	0.27	0.26	0.31	0.27	0.31	0.31	0.29	0.31	0.33	0.23	0.38
Na ₂ O	0.00	0.01	0.01	0.01	0.01	0.03	0.02	0.00	0.00	0.01	0.00	0.02	0.02
Sum	100.14	99.92	100.05	99.88	100.13	99.71	100.21	100.03	100.80	100.06	99.86	100.41	100.59
Mg #	91.3	91.1	91.5	90.5	87.2	89.0	89.5	89.1	86.9	82.4	84.6	86.7	81.2

Table 2 (Electronic Supplementary Material). Continued

CLINOPYROXENE													
DISCRETE SAMPLES													
Sample	06HB4	HB2	97CZ3C	99BY1B	HB7	HB9	HB13	HB14	99BY3A	85GM8B	BY3BB	HB3	HB4
Rock	lherzolite	lherzolite	lherzolite	lherzolite	lherzolite	wehrlite	wehrlite	wehrlite	dunite	wehrlite-px	wehrlite-px	Px	Px
Type	Mg-pd	Mg-pd	Mg-pd	Mg-pd	Fe-pd	Fe-pd	Fe-pd	Fe-pd	Fe-pd	Fe-pd-px	Fe-pd-px	Px	Px
SiO ₂	53.61	54.32	54.80	54.44	54.44	54.78	54.23	54.35	-	54.51	54.65	54.46	54.58
TiO ₂	0.19	0.03	0.10	0.09	0.10	0.09	0.12	0.07	-	0.09	0.16	0.10	0.11
Al ₂ O ₃	1.69	1.06	1.38	1.07	1.13	0.95	1.12	0.73	-	1.53	1.42	1.72	1.59
Cr ₂ O ₃	1.80	1.71	1.86	0.47	2.39	2.23	2.39	2.04	-	3.68	3.15	2.97	3.34
FeO	0.55	0.41	0.69	1.99	0.63	0.47	0.62	0.45	-	0.32	0.42	0.70	0.63
MnO	0.04	0.05	0.06	0.03	0.06	0.07	0.03	0.06	-	0.06	0.14	0.06	0.06
MgO	17.37	17.62	17.30	17.46	17.11	17.05	17.35	17.65	-	16.80	16.49	16.54	15.98
CaO	24.09	24.34	22.92	23.25	23.17	24.18	23.53	23.95	-	22.31	23.20	22.45	22.48
Na ₂ O	0.28	0.24	0.73	0.65	0.44	0.38	0.47	0.38	-	0.46	0.36	0.93	0.80
Sum	99.70	99.78	99.84	99.53	99.47	100.27	99.89	99.73	-	99.76	99.99	99.93	99.57
Mg #	94.5	94.8	94.3	94.0	92.7	93.2	92.8	93.9	-	89.1	90.2	90.9	89.5

SPINEL													
Sample	06HB4	HB2	97CZ3C	99BY1B	HB7	HB9	HB13	HB14	99BY3A	85GM8B	BY3BB	HB3	HB4
Rock	lherzolite	lherzolite	lherzolite	lherzolite	lherzolite	wehrlite	wehrlite	wehrlite	dunite	wehrlite-px	wehrlite-px	Px	Px
Type	Mg-pd	Mg-pd	Mg-pd	Mg-pd	Fe-pd	Fe-pd	Fe-pd	Fe-pd	Fe-pd	Fe-pd-px	Fe-pd-px	Px	Px
TiO ₂	-	0.12	-	0.11	0.35	-	0.37	0.40	0.34	0.14	0.09	0.59	0.76
Al ₂ O ₃	-	22.87	-	37.84	34.52	-	27.24	24.16	28.67	38.86	41.96	35.41	36.61
Cr ₂ O ₃	-	44.87	-	29.66	32.33	-	38.82	40.68	36.60	26.31	23.30	31.73	29.72
FeO	-	18.87	-	16.18	19.59	-	22.55	24.42	22.50	22.88	19.41	18.99	20.01
MnO	-	0.00	-	0.00	0.00	-	0.00	0.00	0.36	0.18	0.00	0	0
MgO	-	10.50	-	14.54	11.79	-	9.99	8.87	9.88	10.38	12.84	11.61	11.2
NiO	-	0.13	-	0.01	0.17	-	0.06	0.10	0.08	0.05	0.21	0.07	0.08
Sum	-	97.34	-	97.99	98.80	-	99.06	98.96	98.72	99.28	97.95	98.43	98.47

Table 2 (Electronic Supplementary Material). Continued

GARNET													
	DISCRETE SAMPLES												
Sample	06HB4	HB2	97CZ3C	99BY1B	HB7	HB9	HB13	HB14	99BY3A	85GM8B	BY3BB	HB3	HB4
Rock	lherzolite	lherzolite	lherzolite	lherzolite	lherzolite	wehrlite	wehrlite	wehrlite	dunite	wehrlite-px	wehrlite-px	Px	Px
Type	Mg-pd	Mg-pd	Mg-pd	Mg-pd	Fe-pd	Fe-pd	Fe-pd	Fe-pd	Fe-pd	Fe-pd-px	Fe-pd-px	Px	Px
SiO ₂	-	-	42.14	42.09	-	-	-	-	41.06	41.24	40.91	40.94	41.04
TiO ₂	-	-	0.05	0.08	-	-	-	-	0.04	0.04	0.07	0.06	0.09
Al ₂ O ₃	-	-	23.37	23.11	-	-	-	-	21.37	22.72	20.36	22.12	21.58
Cr ₂ O ₃	-	-	0.38	0.45	-	-	-	-	2.28	0.53	2.55	1.38	1.56
FeO	-	-	8.96	9.62	-	-	-	-	11.44	13.77	13.22	14.58	14.81
MnO	-	-	0.47	0.41	-	-	-	-	0.75	0.49	0.63	0.45	0.50
MgO	-	-	19.92	19.33	-	-	-	-	16.81	15.31	15.17	15.61	14.21
CaO	-	-	4.55	4.79	-	-	-	-	5.69	6.27	6.43	5.23	5.65
Sum	-	-	99.83	99.91	-	-	-	-	99.46	100.38	99.34	100.39	99.44

PHLOGOPITE													
Sample	06HB4	HB2	97CZ3C	99BY1B	HB7	HB9	HB13	HB14	99BY3A	85GM8B	BY3BB	HB3	HB4
Rock	lherzolite	lherzolite	lherzolite	lherzolite	lherzolite	wehrlite	wehrlite	wehrlite	dunite	wehrlite-px	wehrlite-px	Px	Px
Type	Mg-pd	Mg-pd	Mg-pd	Mg-pd	Fe-pd	Fe-pd	Fe-pd	Fe-pd	Fe-pd	Fe-pd-px	Fe-pd-px	Px	Px
SiO ₂	-	-	38.23	38.17	-	-	-	39.77	-	-	-	-	-
TiO ₂	-	-	0.74	2.24	-	-	-	0.47	-	-	-	-	-
Al ₂ O ₃	-	-	16.53	16.62	-	-	-	13.46	-	-	-	-	-
Cr ₂ O ₃	-	-	0.26	0.47	-	-	-	0.73	-	-	-	-	-
FeO	-	-	4.12	3.47	-	-	-	3.06	-	-	-	-	-
MnO	-	-	0.14	0.04	-	-	-	0.01	-	-	-	-	-
MgO	-	-	23.65	22.45	-	-	-	27.02	-	-	-	-	-
CaO	-	-	0.15	0.01	-	-	-	0.02	-	-	-	-	-
Na ₂ O	-	-	0.31	0.29	-	-	-	0.04	-	-	-	-	-
K ₂ O	-	-	7.77	9.27	-	-	-	8.06	-	-	-	-	-
Sum	-	-	91.91	93.19	-	-	-	92.76	-	-	-	-	-

Table 2 (Electronic Supplementary Material). Microprobe analyses (wt. %) of minerals from Horní Bory ultramafic suite

OLIVINE		LAYERED SAMPLES							
Sample	06HB2B	06HB2C	06HB2D	06HB2E	HB70-6	HB70-7	HB70-8	HB70-9	HB70-10
Rock	dunite	Px	dunite	Px	dunite	Px	dunite-px	Px	dunite
Type	Fe-pd	Px	Fe-pd	Px	Fe-pd	Px	Fe-pd-px	Px	Fe-pd
SiO ₂	39.66	39.61	40.10	39.87	39.88	39.64	39.98	-	40.61
FeO	15.26	15.89	13.87	14.69	14.68	17.03	16.39	-	13.04
MnO	0.15	0.23	0.20	0.27	0.25	0.24	0.23	-	0.19
MgO	44.35	43.58	45.37	44.52	44.43	42.65	43.10	-	46.52
NiO	0.18	0.21	0.23	0.24	0.26	0.18	0.19	-	0.34
Sum	99.60	99.52	99.78	99.58	99.50	99.75	99.88	-	100.70
Mg #	83.8	83.0	85.4	84.4	84.4	81.7	82.4	-	86.4
ORTHOPIYROXENE									
Sample	06HB2B	06HB2C	06HB2D	06HB2E	HB70-6	HB70-7	HB70-8	HB70-9	HB70-10
Rock	dunite	Px	dunite	Px	dunite	Px	dunite-px	Px	dunite
Type	Fe-pd	Px	Fe-pd	Px	Fe-pd	Px	Fe-pd-px	Px	Fe-pd
SiO ₂	-	-	-	-	-	56.17	56.25	56.74	57.15
TiO ₂	-	-	-	-	-	0.05	0.07	0.09	0.06
Al ₂ O ₃	-	-	-	-	-	0.76	1.18	1.00	0.69
Cr ₂ O ₃	-	-	-	-	-	0.08	0.15	0.04	0.06
FeO	-	-	-	-	-	10.12	10.24	9.35	8.25
MnO	-	-	-	-	-	0.19	0.21	0.15	0.15
MgO	-	-	-	-	-	32.25	31.64	32.81	33.48
CaO	-	-	-	-	-	0.30	0.32	0.32	0.24
Na ₂ O	-	-	-	-	-	0.00	0.00	0.00	0.00
Sum	-	-	-	-	-	99.92	100.06	100.49	100.08
Mg #	-	-	-	-	-	85.0	84.6	86.2	87.8

Table 2 (Electronic Supplementary Material). Continued

CLINOPYROXENE			LAYERED SAMPLES						
Sample	06HB2B	06HB2C	06HB2D	06HB2E	HB70-6	HB70-7	HB70-8	HB70-9	HB70-10
Rock	dunite	Px	dunite	Px	dunite	Px	dunite-px	Px	dunite
Type	Fe-pd	Px	Fe-pd	Px	Fe-pd	Px	Fe-pd-px	Px	Fe-pd
SiO ₂	54.83	54.99	54.99	54.99	54.63	54.42	54.40	55.04	55.15
TiO ₂	0.06	0.07	0.08	0.08	0.05	0.09	0.11	0.10	0.06
Al ₂ O ₃	1.20	1.31	1.13	1.30	1.12	1.35	1.31	1.29	1.23
Cr ₂ O ₃	0.53	0.37	0.64	0.21	0.67	0.39	0.46	0.25	0.36
FeO	3.23	2.92	2.77	2.87	3.18	3.56	3.37	3.26	3.04
MnO	0.03	0.05	0.02	0.07	0.05	0.06	0.09	0.05	0.03
MgO	16.37	16.84	16.85	17.05	16.79	16.67	16.81	16.93	16.69
CaO	22.66	22.93	22.92	22.81	22.64	22.41	22.53	22.63	22.57
Na ₂ O	0.86	0.71	0.78	0.72	0.77	0.70	0.72	0.73	0.96
Sum	99.76	100.19	100.19	100.09	99.90	99.66	99.81	100.27	100.07
Mg #	90.0	91.1	91.6	91.4	90.4	89.3	89.9	90.3	90.7

SPINEL									
Sample	06HB2B	06HB2C	06HB2D	06HB2E	HB70-6	HB70-7	HB70-8	HB70-9	HB70-10
Rock	dunite	Px	dunite	Px	dunite	Px	dunite-px	Px	dunite
Type	Fe-pd	Px	Fe-pd	Px	Fe-pd	Px	Fe-pd-px	Px	Fe-pd
TiO ₂	-	0.02	0.05	-	0.04	-	-	-	-
Al ₂ O ₃	-	59.75	41.72	-	50.73	-	-	-	-
Cr ₂ O ₃	-	4.72	24.82	-	14.77	-	-	-	-
FeO	-	0.05	0.16	-	0.10	-	-	-	-
MnO	-	18.85	18.79	-	18.82	-	-	-	-
MgO	-	0.21	0.19	-	0.20	-	-	-	-
ZnO	-	15.66	13.48	-	14.57	-	-	-	-
NiO	-	0.12	0.28	-	0.20	-	-	-	-
Sum	-	0.18	0.12	-	0.15	-	-	-	-

Table 2 (Electronic Supplementary Material). Continued

GARNET		LAYERED SAMPLES							
Sample	06HB2B	06HB2C	06HB2D	06HB2E	HB70-6	HB70-7	HB70-8	HB70-9	HB70-10
Rock	dunite	Px	dunite	Px	dunite	Px	dunite-px	Px	dunite
Type	Fe-pd	Px	Fe-pd	Px	Fe-pd	Px	Fe-pd-px	Px	Fe-pd
SiO ₂	-	41.43	-	41.61	41.45	41.39	41.54	41.62	42.07
TiO ₂	-	0.06	-	0.04	0.05	0.05	0.10	0.06	0.05
Al ₂ O ₃	-	22.48	-	23.04	22.21	22.60	22.34	22.90	23.12
Cr ₂ O ₃	-	1.06	-	0.66	1.32	0.77	1.21	0.63	0.41
FeO	-	12.47	-	12.41	13.73	13.84	13.72	13.43	12.90
MnO	-	0.45	-	0.58	0.50	0.47	0.57	0.57	0.51
MgO	-	16.00	-	17.01	16.00	16.27	16.04	16.85	17.23
CaO	-	6.35	-	4.93	5.52	5.16	5.33	4.74	4.52
Sum	-	100.31	-	100.27	100.77	100.55	100.86	100.80	100.81

PHLOGOPITE									
Sample	06HB2B	06HB2C	06HB2D	06HB2E	HB70-6	HB70-7	HB70-8	HB70-9	HB70-10
Rock	dunite	Px	dunite	Px	dunite	Px	dunite-px	Px	dunite
Type	Fe-pd	Px	Fe-pd	Px	Fe-pd	Px	Fe-pd-px	Px	Fe-pd
SiO ₂	-	-	-	38.91	-	-	-	-	-
TiO ₂	-	-	-	0.83	-	-	-	-	-
Al ₂ O ₃	-	-	-	15.89	-	-	-	-	-
Cr ₂ O ₃	-	-	-	0.28	-	-	-	-	-
FeO	-	-	-	4.12	-	-	-	-	-
MnO	-	-	-	0.03	-	-	-	-	-
MgO	-	-	-	23.78	-	-	-	-	-
CaO	-	-	-	0.04	-	-	-	-	-
Na ₂ O	-	-	-	0.60	-	-	-	-	-
K ₂ O	-	-	-	8.95	-	-	-	-	-
Sum	-	-	-	93.42	-	-	-	-	-

CHAPTER 5. General conclusions

This dissertation presents an extensive geochemical dataset including major and trace elements, mineral chemistry and radiogenic isotopes for two upper mantle suites located in the Bohemian Massif: (1) mantle xenoliths from the Kozákov volcano and (2) peridotite-pyroxenite boudins from the Horní Bory granulite massif.

The Kozákov xenolith suite represents mostly lherzolites which sample a layered mantle profile, consisting of an equigranular upper layer at depths from 32 to 43 km, a protogranular symplectite-bearing intermediate layer from 43 to 67 km, and an equigranular lower layer from 67 to 70 km.

Whole-rock and mineral major elements variations point to different partial melting degrees from ~5 % for the lower equigranular to ~15 % for the upper equigranular layers, suggesting a progressive increase in partial melting degrees with decreasing depth. Subsequent metasomatism, most probably by a transient silicate melt, affecting the whole mantle profile beneath the Kozákov volcano resulted in an enrichment in the large ion lithophile elements (LILE), light rare earth elements (LREE), and high field strength elements (HFSE). Trace element patterns and ratios (e.g. Nb/La, Hf/Sm) show that the lower equigranular layer interacted with percolating melt at high melt/rock ratios. As a result of melt-peridotite interaction, small melt fractions were formed and migrated upward, causing large-scale metasomatism at low to moderate melt/rock ratios.

Such mantle evolution makes Kozákov xenoliths ideal targets for the study of behaviour of highly siderophile elements (HSE) and osmium isotopes during mantle depletion and metasomatism. The HSE concentrations in a suite of these xenoliths indicate that most of these elements behaved incompatibly during melt percolation, most probably due to removal of sulphides. The depletion is the most extensive in the lowermost part of the profile, which experienced the highest melt/rock ratios. In contrast, rocks from shallower depths show smaller and more variable HSE depletions. A few xenoliths have much higher I-PGE (Os, Ir, Ru) contents than estimated for the primitive upper mantle, suggesting that in some cases, the I-PGE were transported into the mantle rocks via the percolating melt, but strong depletions in Pd point to the S-undersaturated character of the percolating melt. Therefore, the I-PGE enrichments are not associated with sulphide addition as has been suggested in other studies (e.g. Büchl et al., 2002; Luguet et al., 2004). Moreover, in contrast to other studies on mantle peridotites (e.g. Chesley et al., 1999; van Acken et al. 2008), the transport and deposition of some HSE was evidently not accompanied by transport and deposition of Re and radiogenic Os.

The timing of the depletion can be estimated by the Re-Os system. Model Os depletion ages (T_{RD}) cluster around 0.8 Ga and even this age probably represent a rather minimal age estimation; this indicates that the subcontinental lithospheric mantle underlying the Bohemian Massif does not represent the orogenic root of the overlying Variscan (280-360 Ma) crust. Rather, crustal terranes may have been thrust onto the mantle lithosphere during the Cadomian and Variscan orogenies. The age of

cryptic metasomatism in the Kozákov lithospheric mantle remains uncertain. However, the regular variation in trace elements with depth across the three mantle layers suggests that metasomatism occurred after the assembly of the layered mantle structure beneath Kozákov (i.e. post-Variscan). Moreover, likely influence of the low-velocity component on the Sr-Nd isotopic evolution of the Kozákov lithospheric mantle implies that the metasomatism may have been associated with Neogene rifting and magmatism.

The ultramafic suite found at Horní Bory show a completely different story than Kozákov xenoliths. The Horní Bory mantle-derived rocks form boudins in Gföhl Unit granulites consisting of lherzolites and dunite-wehrlites associated with pyroxenites. Whereas lherzolites (Mg-Cr-peridotite) show a composition similar to other mantle-derived rocks elsewhere ($Mg \# = 89.1-90.9$, $^{87}Sr/^{86}Sr < 0.7068$, $^{143}Nd/^{144}Nd > 0.512729$), the dunite-wehrlite series (Fe-rich peridotite) is characterized by much lower Mg # (83.2-88.2) and different Sr-Nd isotopic compositions ($^{87}Sr/^{86}Sr > 0.7079$, $^{143}Nd/^{144}Nd < 0.512432$).

Numerous studies have shown that lherzolite has been converted to harzburgite by reaction with silica-rich (subduction-related) transient melt (e.g. Zanetti et al., 1999). On the other hand, lherzolite-dunite-wehrlite series can be produced during an infiltration into, and reaction with mantle peridotite, by fractionated SiO₂-undersaturated melt of basaltic composition (e.g. Kelemen et al., 1990; Kelemen et al., 1998; Ionov et al., 2005). Nevertheless, both reactions lead to partial/complete dissolution of mantle minerals (opx, cpx) with respect to SiO₂-saturation of infiltrated melt.

Modelling of Mg-Fe exchange between Mg-pd and Fe-rich melts coupled with Sr-Nd isotopic modelling revealed that modal and chemical compositions of dunite-wehrlites from Horní Bory can be produced by melt-rock reactions between lherzolites and SiO₂-undersaturated melts of basaltic composition at variable melt/rock ratios. In such model, pyroxenites represent crystalline product (\pm trapped liquid) of melt migrating along conduits in the peridotite. Thus, Mg-lherzolite from Horní Bory has been transformed to Fe-dunite-wehrlite, similar in many respects to the modification of lherzolite to Fe-rich lherzolite-wehrlite series found in several mantle xenolith localities sampled subcontinental lithospheric mantle (Lee and Rudnick, 1999; Peslier et al., 2002; Ionov et al., 2005). However, in contrast to these studies, the calculated trace element compositions of melts equilibrated with pyroxenites and Sr-Nd composition of Horní Bory peridotites point to a significant contribution of crustal material in interacted melts. Therefore, melt-rock reactions were probably associated with melt percolation in a mantle wedge above the subduction zone, which could be driven by the infiltration of subduction-related melts/fluids, if the melt/fluid flux was high enough to enhance partial melting in the mantle wedge.

The differences between the Kozákov and Horní Bory upper mantle suites revealed complex heterogeneity of upper mantle beneath the Bohemian Massif. Different types of metasomatism (melt-rock reactions) which reflect sources of metasomatic agents (subcontinental vs. subduction-related) at these two localities suggest different evolutions of mantle beneath the Bohemian Massif. In turn, this

means that upper mantle beneath the Bohemian Massif should comprise mantle domains with different evolution histories (i.e. ancient partial melting) which survived even the Cadomian/Variscan orogeny. This is supported by Re-Os data from Kozákov (see above) as well as by the different orientation of anisotropy (Babuška and Plomerová, 2006). On the other hand, the geochemical study on Kozákov and Horní Bory suggests that secondary processes (metasomatism, melt-rock reactions) are probably associated with Variscan orogeny and Neogene magmatism.

The highly siderophile element (HSE) and Re-Os isotopic study on pervasively metasomatized mantle xenoliths from Kozákov provide insights into the behaviour of these elements and Os isotopes during melt percolation. In agreement with other studies, it has been shown that HSE systematics is highly dependent on removal/addition of sulphides (represents their principal hosts) and S-saturation of percolating melt. On the other hand, we reported addition of I-PGE from a S-undersaturated percolating melt, suggesting a possibility of precipitation of I-PGE-bearing alloys during melt percolation. In the case of Kozákov, this was not coupled with an import of radiogenic Os, but is of high importance due to the possible I-PGE enrichment in the upper mantle and its possible effect on Re-Os isotopic geochemistry.

Although this thesis answers some principal questions, some still remain open, some were introduced by this study and should be answered in a future research. These can be summarized as follows:

- the extent of mantle depletion beneath the Bohemian Massif – although this thesis provided some data on mantle depletion, there is still a lack of data from many important localities, especially in the Ohře/Eger Rift and northern Silesia. Respective studies are necessary to obtain a complex picture on mantle depletion
- what are the different styles of metasomatism briefly mentioned by other authors (e.g. Frýda and Vokurka, 1995; Geissler et al., 2007) and how are they connected with tectonomagmatic processes in the Bohemian Massif?
- how does mantle refertilization by subduction-related melts at Horní Bory affects HSE and Re-Os isotopes and what does this tell us about crustal recycling into the Earth's mantle?

REFERENCES

- Ackerman L., Mahlen N., Jelínek E., Medaris L.G., Ulrych J., Strnad L. and Mihaljevič M. (2007) Geochemistry and Evolution of Subcontinental Lithospheric Mantle in Central Europe: Evidence from Peridotite Xenoliths of the Kozákov Volcano, Czech Republic. *J. Petrol.* **48**, 2235-2260.
- Alard O., Griffin W. L., Lorand J. -P., Jackson S. E. and O'Reilly S. Y. (2000) Non-chondritic distribution of the highly siderophile elements in mantle sulfides. *Nature* **407**, 891-894.
- Albarède F. (1995) Introduction to Geochemical Modelling. Cambridge: Cambridge University Press.
- Anders E. and Grevesse N. (1989) Abundances of the elements: meteoritic and solar. *Geochim. Cosmochim. Acta* **53**, 197-214.
- Armstrong J. T. (1988) Quantitative analysis of silicate and oxide materials: Comparison of Monte Carlo, ZAF, an $\phi(\rho z)$ procedures. In: Newbury D. E. (ed.) Microbeam Analysis, Proceedings of the 23rd Annual Conference of the Microbeam Analysis Society. San Francisco: San Francisco Press, 239-246.
- Babuška V. and Plomerová J. (1992) The lithosphere in central Europe - Seismological and petrological aspects. *Tectonophysics* **207**, 141-163.
- Babuška V. and Plomerová J. (2001) Subcrustal lithosphere around the Saxothuringian-Moldanubian Suture Zone - a model derived from anisotropy of seismic wave velocities. *Tectonophysics* **332**, 185-199.
- Babuška V. and Plomerová J. (2006) European mantle lithosphere assembled from rigid microplates with inherited seismic anisotropy. *Phys. Earth Planet. Int.* **158**, 264-280.
- Ballhaus C., Berry R. F. and Green D. H. (1991) High pressure experimental calibration of olivine-orthopyroxene-spinel oxygen geobarometer: implications for the oxidation state of the upper mantle. *Contrib. Mineral. Petrol.* **107**, 27-40.
- Ballhaus C., Bockrath C., Wohlgemuth-Ueberwasser C., Laurenz V. and Berndt J. (2006) Fractionation of the noble metals by physical processes. *Contrib. Mineral. Petrol.* **152**, 667-684.
- Barnes S. J. and Roeder P. L. (2001) The range of spinel composition in terrestrial mafic and ultramafic rocks. *J. Petrol.* **42**, 2279-2302.
- Batanova V. G. and Sobolev A. V. (2000) Compositional heterogeneity in subduction-related mantle peridotites, Troodos massif, Cyprus. *Geology* **28**, 55-58.
- Batanova V.G., Suhr G. and Sobolev A. V. (1998) Origin of geochemical heterogeneity in the mantle peridotites from the Bay of Islands ophiolite, Newfoundland, Canada: ion probe study of clinopyroxenes. *Geochim. Cosmochim. Acta* **62**, 853-866.
- Beard B. L., Medaris L. G., Johnson C. M., Brueckner H. K. and Mísař, Z. (1992) Petrogenesis of Variscan high-temperature Group A eclogites from the Moldanubian Zone of the Bohemian Massif, Czechoslovakia. *Contrib. Mineral. Petrol.* **111**, 468-483.

- Beard B. L., Medaris L. G., Johnson C. M., Jelinek E., Tonika J. and Riciputi L. R. (1995) Geochronology and geochemistry of eclogites from Mariánské lázně complex, Czech Republic – Implications for Variscan orogenesis. *Geol. Rund.* **84**, 552-567.
- Beccaluva L., Bonadiman C., Coltorti M., Salvini L. and Siena F. (2001) Depletion events, nature of metasomatizing agent and timing of enrichment processes in lithospheric mantle xenoliths from the Veneto Volcanic Province. *J. Petrol.* **42**, 173-187.
- Becker H. (1996a) Geochemistry of garnet peridotite massifs from lower Austria and the composition of deep lithosphere beneath a Paleozoic convergent plate margin. *Chem. Geol.* **134**, 49-65.
- Becker H. (1996b) Crustal trace element and isotopic signatures in garnet pyroxenites from garnet peridotite massifs from Lower Austria. *J. Petrol.* **37**, 785-810.
- Becker H. (1997) Sm–Nd garnet ages and cooling history of high-temperature garnet peridotite massifs and high-pressure granulites from lower Austria. *Contrib. Mineral. Petrol.* **127**, 224-236.
- Becker H., Horan M. F., Walker R. J., Gao S., Lorand J. -P. and Rudnick R. L. (2006) Highly siderophile element compositions of the Earth's primitive mantle. *Geochim. Cosmochim. Acta* **70**, 4528-4550.
- Bedini R. M., Bodinier J. L., Dautria J. M. and Morten L. (1997) Evolution of LILE-enriched small melt fractions in the lithospheric mantle: A case from the East African Rift. *Earth Planet. Sci. Lett.* **153**, 67-83.
- Bertrand P. and Mercier J.-C. C. (1985) The mutual solubility of coexisting ortho- and clinopyroxene: toward an absolute geothermometer for the natural system? *Earth Planet. Sci. Lett.* **76**, 109-122.
- Bezmen N. I., Asif M., Brüggemann G. E., Romanenko I. M. and Naldrett A. J. (1994) Distribution of Pd, Rh, Ru, Ir, Os and Au between sulfide and silicate metals, *Geochim. Cosmochim. Acta* **58**, 1251-1260.
- Birck J. L., Barman M. R. and Campas F. (1997) Re-Os isotopic measurements at the femtomole level in natural samples. *J. Geostand. Geoanal.* **21**, 19-27.
- Blusztajn J. and Shimizu N. (1994) The trace-element variations in clinopyroxenes from spinel peridotite xenoliths from southwest Poland. *Chem. Geol.* **111**, 227-243.
- Bockrath C., Ballhaus C. and Holzheid A. (2004) Fractionation of the platinum-group elements during mantle melting. *Science* **305**, 1951-1953.
- Bodinier J. -L., Merlet C., Bedini R. M., Simien F., Remaidi M. and Garrido C. J. (1996) Distribution of niobium, tantalum, and other highly incompatible trace elements in the lithospheric mantle: The spinel paradox. *Geochim. Cosmochim. Acta* **60**, 545-550.
- Bodinier J. -L. and Godard M. (2003) Orogenic, ophiolitic and abyssal peridotites. In: Carlson R.W. (Ed.), *Treatise in Geochemistry, Volume 2 - The Mantle and Core*, Elsevier Pergamon, 103-157.
- Bodinier J. -L., Menzies M., Shimizu N., Frey F.A. and McPherson E. (2004) Silicate, hydrous and carbonate metasomatism at Lherz, France: Contemporaneous derivatives of silicate melt harzburgite reaction. *J. Petrol.* **45**, 299-320.

- Brandon A. D., Creaser R. A., Shirey S. B. and Carlson R. W. (1996) Osmium recycling in subduction zones. *Science* **272**, 861-864.
- Brenan J. M. and Andrews D. (2001) High-temperature stability of laurite and Ru-Os-Ir alloy and their role in PGE fractionation in mafic magmas. *Can. Mineral.* **39**, 1747-1748.
- Brenker F. E. and Brey G. P. (1997) Reconstruction of the exhumation path of the Alpe Arami garnet-peridotite body from depths exceeding 160 km. *J. Metamorph. Geol.* **15**, 581-592.
- Brey G. P. and Köhler T. (1990) Geothermobarometry in four-phase lherzolites: II. New thermobarometers and practical assessment of existing thermobarometry. *J. Petrol.* **31**, 1352-1378.
- Brueckner H. K., Medaris L. G. and Bakunczubarow N. (1991) Nd and Sr age and isotope patterns from Variscan eclogites of the eastern Bohemian Massif. *Neues Jahrb. Mineral. Abh.* **163**, 169-196.
- Büchl A., Brüggmann G., Batanova V. G., Münker C. and Hofmann A. W. (2002) Melt percolation monitored by Os isotopes and PGE abundances: a case study from the mantle section of the Troodos Ophiolite. *Earth Planet. Sci. Lett.* **204**, 385-402.
- Büchl A., Brüggmann G., Batanova V. G. and Hofmann A. W. (2004) Os mobilization during melt percolation: The evolution of Os isotope heterogeneities in the mantle sequence of the Troodos ophiolite, Cyprus. *Geochim. Cosmochim. Acta* **68**, 3397-3408.
- Carlson R. W. (2005) Application of the Pt-Re-Os isotopic systems to mantle geochemistry and geochronology. *Lithos* **82**, 249-272.
- Carswell D. A. and Jamtveit B. (1990) Variscan Sm-Nd ages for the high-pressure metamorphism in the Moldanubian Zone of the Bohemian Massif, Lower Austria. *Neues Jahrb. Mineral. Abh.* **162**, 69-78.
- Carswell D. A. and O'Brien P. J. (1993) Thermobarometry and geotectonic significance of high pressure granulites: examples from the Moldanubian Zone of the Bohemian Massif in Lower Austria. *J. Petrol.* **34**, 427-459.
- Čermák V. (1989) Crustal heat production and mantle heat flow in central and eastern Europe. *Tectonophysics* **159**, 195-215.
- Čermák V., Král M., Krešl M., Kubík J. and Šafanda J. (1991) Heat flow, regional geophysics, and lithosphere structure in Czechoslovakia and adjacent parts of central Europe. In: Čermák V and Rybach L. (eds.) *Terrestrial Heat Flow and Lithosphere Structure*. New York: Springer-Verlag, 33-165.
- Cháb J. (1973) An ancient oceanic crust and upper mantle on the recent land surface. *Věst. Ústř. Úst. Geol.* **48**, 303-310. (In Czech).
- Chesley J. T., Rudnick R. L. and Lee C. T. (1999) Re-Os systematics of mantle xenoliths from the East African Rift; age, structure and history of the Tanzanian Craton. *Geochim. Cosmochim. Acta* **63**, 1203-1217.

- Christensen N. I., Medaris Jr. L. G., Wang H. F. and Jelínek E. (2001) Depth variation of seismic anisotropy and petrology in central European lithosphere: A tectonothermal synthesis from spinel lherzolite. *J. Geophys. Res.* **106**, 645-664.
- Cohen A. S. and Waters F. G. (1996) Separation of osmium from geologic materials by solvent extraction for analysis by TIMS. *Anal. Chim. Acta* **332**, 269-275.
- DePaolo D. J. and Wasserburg G. J. (1976) Nd isotope variations and petrogenetic models. *Geophys. Res. Lett.* **4**, 465-468.
- Downes H. (2001) Formation and modification of the shallow sub-continental lithospheric mantle: a review of geochemical evidence from ultramafic xenolith suites and tectonically emplaced ultramafic massifs of Western and Central Europe. *J. Petrol.* **42**, 233-250.
- Downes H. (2007) Origin and significance of spinel and garnet pyroxenites in the shallow lithospheric mantle: Ultramafic massifs in orogenic belts in Western Europe and NW Africa. *Lithos* **99**, 1-24.
- Downes H., Embey-Isztin A. and Thirlwall M. F. (1992) Petrology and geochemistry of spinel peridotite xenoliths from the western Pannonian Basin (Hungary): evidence for an association between enrichment and texture in the upper mantle. *Contrib. Mineral. Petrol.* **107**, 340-354.
- Ertel W. and Dingwell D. B. (2007) Nanonuggets and their implication for core formation. *Geochim. Cosmochim. Acta* **71**, A261.
- Farský F. (1876) Mineralogische Notizen I. Mineralien aus der Kosakover Basaltkugeln. Verhandlungen der Kaiserlichen und Königlichen Geologischen Reichsanstalt (Wien), 205-208.
- Faure G. (2001) Origin of Igneous rocks, The isotopic evidence. Springer-Verlag Berlin Heidelberg New York, 496 pp.
- Fediuk F. (1971) Ultramafics of Krkonoše-Jizerské hory region. *Acta Univ. Carol. Geol.* **4**, 310-343.
- Fediuk F. (1994) Deep-origin xenoliths in volcanics of Czechoslovakia. In: Bucha V. and Blížkovský M. (eds.) Crustal Structure of the Bohemian Massif and the West Carpathians. New York: Springer-Verlag, 277-281.
- Fleet M. E., Crocket J. H., Liu M. and Stone W. E. (1999) Laboratory partitioning of platinum-group elements (PGE) and gold with application to magmatic sulfide-PGE deposits. *Lithos* **47**, 127-142.
- Franke W. (1989) Variscan plate tectonics in Central Europe - current ideas and open questions. *Tectonophysics* **169**, 221-228.
- Franke W. (2000) The mid-European segment of the Variscides: tectonostratigraphic units, terrane boundaries and plate tectonic evolution. In: Franke W., Haak V., Oncken O. and Tanner D. (eds.). Orogenic Processes: Quantification and Modelling in the Variscan Belt. *Geol. Soc. London, Spec. Publ.* **179**, 35-61.
- Frey F. A., Suen C. J. and Stockman H. W. (1985) The Ronda high temperature peridotite: geochemistry and petrogenesis. *Geochim. Cosmochim. Acta* **49**, 2469-2491.
- Fryda J. and Vokurka K. (1995) Evidence for carbonatite metasomatism in the upper mantle beneath the Bohemian Massif. *J. Czech Geol. Soc.* **40**, 9-10.

- Gannoun A., Burton K. W., Parkinson I. J., Alard O., Schiano P. and Thomas L. E. (2007) The scale and origin of the osmium isotope variations in mid-ocean ridge basalts. *Earth Planet. Sci. Lett.* **259**, 541-556.
- Gao S., Rudnick R. L., Carlson R. W., McDonough W. F. and Liu Y. S. (2002) Re-Os evidence for replacement of ancient mantle lithosphere beneath the North China Craton. *Earth Planet. Sci. Lett.* **198**, 307-322.
- Gaul O. F., O'Reilly S. Y. and Griffin W. L. (2003) Lithosphere structure and evolution in southeastern Australia. *Geol. Soc. Am. Spec. Paper* **372**, 185-202.
- Gebauer D., Williams I. S., Compston W. and Grünenfelder M. (1989) The development of the Central European continental crust since the Early Archean based on conventional and ion-microprobe dating of up to 3.84 b.y. old detrital zircons. *Tectonophysics* **157**, 91-96.
- Geissler W. H., Kämpf H., Seifert W. and Dulski P. (2007) Petrological and seismic studies of the lithosphere in the earthquake swarm region Vogtland/NW Bohemia, central Europe. *J. Volcanol. Geoth. Res.* **159**, 33-69.
- Govindaraju K. (1989) 1989 compilation of working values and sample description for 273 geostandards. *Geostand. Newslett.* **13** (special issue), 113 pp.
- Griffin W. L., Zhang A., O'Reilly S. Y. and Ryan C. G. (1998) Phanerozoic evolution of the lithosphere beneath the Sino-Korean Craton. In: Flower M., Chung S. L., Lo C. H. and Lee T. Y. (eds.) *Mantle Dynamics and Plate Interactions in East Asia*. Geodynamics Series 27, Washington DC: American Geophysical Union, 107-126.
- Handler M. R. and Bennett V. C. (1999) Behaviour of Platinum-group elements in the subcontinental mantle of eastern Australia during variable metasomatism and melt depletion. *Geochim. Cosmochim. Acta* **63**, 3597-3618.
- Handler M. R., Bennett V. C. and Dreibus G. (1999) Evidence from correlated Ir/Os and Cu/S for late-stage Os mobility in peridotite xenoliths: Implications for Re-Os systematics. *Geology* **27**, 75-78.
- Handler M. R., Bennett V. C. and Carlson R. W. (2005) Nd, Sr and Os isotope systematics in young, fertile spinel peridotite xenoliths from northern Queensland, Australia: A unique view of depleted MORB mantle? *Geochim. Cosmochim. Acta* **69**, 5747-5763.
- Harley S. L. (1984) An experimental study of the partitioning of Fe and Mg between garnet and orthopyroxene. *Contrib. Mineral. Petrol.* **86**, 359-373.
- Hartmann G. and Wedepohl K. H. (1990) Metasomatically altered peridotite xenoliths from Hessian depression (Northwest Germany). *Geochim. Cosmochim. Acta* **54**, 71-86.
- Hauri E. H., Wagner T. P. and Grove T. L. (1994) Experimental and natural partitioning of Th, U, Pb and other trace-elements between garnet, clinopyroxene and basaltic melts. *Chem. Geol.* **117**, 149-166.

- Hellebrand E., Snow J. E., Dick H. J. B. and Hofmann A. W. (2001) Coupled major and trace elements as indicators of the extent of melting in mid-ocean-ridge peridotites. *Nature* **410**, 677-681.
- Hoernle K., Zhang Y.-S. and Graham D. (1995) Seismic and geochemical evidence for large-scale mantle upwelling beneath the eastern Atlantic and western and central Europe. *Nature* **374**, 34-39.
- Ionov D. A., Mukasa S. B. and Bodinier J. -L. (2002) Sr-Nd-Pb isotopic compositions of peridotite xenoliths from Spitzbergen: numerical modelling indicates Sr-Nd decoupling in the mantle by melt percolation metasomatism. *J. Petrol.* **43**, 2261-2278.
- Ionov D. A., Chanefo I. and Bodinier J. -L. (2005) Origin of Fe-rich lherzolites and wehrlites from Tok, SE Siberia by reactive melt percolation in refractory mantle peridotites. *Contrib. Mineral. Petrol.* **150**, 335-353.
- Irvine T. N. (1965) Chromian spinel as a petrogenetic indicator. Part I. Theory. *Can. J. Earth Sci.* **2**, 648-672.
- Jacobsen S. B. and Wasserburg G. J. (1980) Sm-Nd isotopic evolution of chondrites. *Earth Planet. Sci. Lett.* **50**, 139-155.
- Janoušek V. and Holub F. V. (2007) The causal link between HP–HT metamorphism and ultrapotassic magmatism in collisional orogens: case study from the Moldanubian Zone of the Bohemian Massif. *Proc. Geol. Assoc.* **118**, 1-12.
- Janoušek V., Rogers G. and Bowes D. R. (1995) Sr-Nd isotopic constrains on the petrogenesis of the Central Bohemian Pluton, Czech Republic. *Geol. Rundsch.* **84**, 520-534.
- Janoušek V., Farrow C. M. and Erban V. (2003) GCDkit: New PC software for interpretation of whole-rock geochemical data from igneous rocks. *Geochim. Cosmochim. Acta* **67**, A186
- Jelínek E., Pačesová M., Mísař Z., Martinec P. and Weiss Z. (1984) Geochemistry of a dismembered metaophiolite complex, Letovice, Czechoslovakia. *Trans. Roy. Soc. Edin-Earth* **75**, 37-48.
- Jelínek E., Štědrá V. and Cháb J. (1997) The Mariánské lázně complex. In: Vrána S. and Štědrá V. (eds.) Geological model of Western Bohemia related to the KTB borehole in Germany. Czech Geological Survey, Prague, 61-70.
- Johnson C. M. and Thompson R. A. (1991) Isotopic composition of oligocene mafic volcanic rocks in the northern Rio Grande rift – evidence for contributions of ancient intraplate and subduction magmatism to evolution of the lithosphere. *J. Geophys. Res.* **96**, 13593-13608.
- Johnson K. T. M., Dick H. J. B. and Shimizu, N. (1990) Melting in the oceanic upper mantle: an ion microprobe study of diopsides in abyssal peridotites. *J. Geophys. Res.* **95**, 2661-2678.
- Kastl E. and Tonika J. (1984) The Mariánské lázně metaophiolitic complex (west Bohemia). *Krystalinikum* **17**, 59–76.
- Kelemen P. B. (1990) Reaction between ultramafic rock and fractionating basaltic magma I. Phase relations, the origin of calc-alkaline magma Series, and the formation of discordant dunite. *J. Petrol.* **31**, 51-98.

- Kelemen P. B., Joyce D. B., Webster J. D. and Holloway J. R. (1990) Reaction between ultramafic rock and fractionating basaltic magma: II. Experimental investigation of reaction between olivine tholeiite and harzburgite at 1150-1050°C and 5kb. *J. Petrol.* **31**, 99-134.
- Kelemen P. B., Dick H. J. B. and Quick J. E. (1992) Formation of harzburgite by pervasive melt/rock reaction in the upper mantle. *Nature* **358**, 635-641.
- Kelemen P. B., Shimizu N. and Salters V. J. M. (1995) Extraction of mid-ocean-ridge basalt from the upwelling mantle by focused flow of melt in dunite channels. *Nature* **375**, 747-753.
- Kelemen P. B., Hart S. R. and Bernstein S. (1998) Silica enrichment in the continental upper mantle via melt-rock reaction. *Earth Planet. Sci. Lett.* **164**, 387-406.
- Konečný P., Ulrych J., Schovánek P., Huraiová M. and Řanda Z. (2006) Upper mantle xenoliths from the Pliocene Kozákov volcano, NE Bohemia: P-T-fO₂ and geochemical constrains. *Geol. Carpath.* **57**, 379-396.
- Kopecký L. (1986) Geological development and block structure of the Cenozoic Ohre Rift (Czechoslovakia). In: Aldrich M. J. and Laughlin A. W. (eds.) Proceedings of the 6th International Conference on Basement Tectonics, Salt Lake City, 114-124.
- Košler J., Kelley S. P., Vance D. and Svojtka M. (1999) Independent dating of cooling and decompression of high grade rocks in the southern Bohemian Massif with Ar-Ar, Sm-Nd and U-Pb techniques. *J. Conf. Abstr.* **4**, 39.
- Kossmat F. (1927) Gliederung des Variskischen Gebirgshauer. *Abh. Säch. Geol. Land.* **1**, 1-39.
- Kotková J., Melichar R. and Pokorná J. (2003) Story of Bory Granulites - Early Thoughts. Proceedings of the 8th Meeting of the Czech Tectonic Studies Group/1st Meeting of the Central European Tectonics Group, Hrubá Skála Chateau, Czech Republic, April 24-27, 57.
- Lee C. -T. and Rudnick R. L. (1999) Compositionally stratified cratonic lithosphere: petrology and geochemistry of peridotite xenoliths the Labait volcano, Tanzania. In: Gurney J. J., Gurney J. L., Pascoe M. D. and Richardson S. H. (eds.), Proc. 7th Int. Kimberlite Conf., vol 1. RedRoof Design, Cape Town, 503-521.
- Lenoir X., Garrido C. J., Bodinier J. L. and Dautria J. M. (2000) Contrasting lithospheric mantle domains beneath the Massif Central (France) revealed by geochemistry of peridotite xenoliths. *Earth Planet. Sci. Lett.* **181**, 359-375.
- Liew T. C. and Hofmann A. W. (1988) Precambrian crustal components, plutonic associations, plate environment of the Hercynian Fold Belt of central Europe: Indications from a Nd and Sr isotopic study. *Contrib. Mineral. Petrol.* **98**, 129-138.
- Liu C. -Z., Snow J. E., Hellebrand E., Brüggemann G., von der Handt A., Büchl A. and Hofmann A. W. (2008) Ancient, highly heterogeneous mantle beneath Gakkel ridge, Arctic Ocean. *Nature* **452**, 311-316.
- Lorand J. -P. (1990) Are spinel lherzolites xenoliths representative of the abundance of sulfur in the upper mantle? *Geochim. Cosmochim. Acta* **54**, 1487-1492.

- Lorand J. -P. and Alard O. (2001) Platinum-group element abundances in the upper mantle: New constraints from in-situ and whole rock analyses of massif central xenoliths (France). *Geochim. Cosmochim. Acta* **65**, 2789-2806.
- Lorand J. -P., Gros M. and Pattou L. (1999) Fractionation of platinum-group element in the upper mantle: A detailed study in Pyrenean orogenic peridotites. *J. Petrol.* **40**, 951-987.
- Lorand J. -P., Reisberg L. and Bedini R. M. (2003) Platinum-group elements and melt percolation processes in Sidamo spinel peridotite xenoliths, Ethiopia, East African rift. *Chem. Geol.* **196**, 57-75.
- Lorand J. -P., Delpech G., Gregoire M., Moine B., O'Reilly S. Y. and Cottin J. Y. (2004) Platinum-group elements and the multistage metasomatic history of Kerguelen lithospheric mantle (South Indian Ocean). *Chem. Geol.* **208**, 195-215.
- Ludwig K. R. (2003) Isoplot 3.00 - a geochronological toolkit for Microsoft Excel: Berkeley Geochronology Center, Spec. Publ. 4.
- Luguet A., Alard O., Lorand J. -P., Pearson N. J., Ryan C. and O'Reilly S. Y. (2001) Laser-ablation microprobe (LAM)-ICPMS unravels the highly siderophile element geochemistry of the oceanic mantle. *Earth Planet. Sci. Lett.* **189**, 285-294.
- Luguet A., Lorand J. -P., Alard O. and Cottin J. Y. (2004) A multi-technique study of platinum group element systematic in some Ligurian ophiolitic peridotites, Italy. *Chem. Geol.* **208**, 175-194.
- Luguet A., Shirey S. B., Lorand J. -P., Horan M. F. and Carlson R. W. (2007) Residual platinum group minerals from highly depleted harzburgites of the Lherz massif (France) and their role in HSE fractionation of the mantle. *Geochim. Cosmochim. Acta* **71**, 3082-3097.
- Machart J. (1984) Ultramafic rocks in the Bohemian part of the Moldanubicum and central Bohemian islet zone (Bohemian Massif). *Krystalinikum* **17**, 13-32.
- Matte P. (2001) The Variscan collage and orogeny (480-290 Ma) and the tectonic definition of the Armorica microplate: a review. *Terra Nova* **13**, 122-128.
- McDonough W. F. and Sun S. (1995) The composition of the Earth. *Chem. Geol.* **120**, 223-253.
- McInnes B. I. A., Gregoire M., Binns R. A., Herzig P. M. and Hannington M. D. (2001) Hydrous metasomatism of oceanic sub-arc mantle, Lihir, Papua New Guinea: petrology and geochemistry of fluid-metasomatised mantle wedge xenoliths. *Earth Planet. Sci. Lett.* **188**, 169-183.
- Medaris L. G. Jr., Wang H. F., Mísař Z. and Jelínek E. (1990) Thermobarometry, diffusion modelling and cooling rates of crustal garnet peridotites: two examples from the Moldanubian zone of the Bohemian Massif. *Lithos* **25**, 189-202.
- Medaris L. G. Jr., Beard B. L., Johnson C. M., Valley J. W., Spicuzza M. J., Jelínek E. and Mísař Z. (1995) Garnet pyroxenite and eclogite in the Bohemian Massif: geochemical evidence for Variscan recycling of subducted lithosphere. *Geol. Rundsch.* **84**, 489-505.

- Medaris L. G. Jr., Fournelle J. H., Wang H. F. and Jelínek E. (1997) Thermobarometry and reconstructed chemical compositions of spinel-pyroxene symplectites: evidence for pre-existing garnet in lherzolite xenoliths from Czech Neogene lavas. *Rus. Geol. Geophys.* **38**, 277-286.
- Medaris L. G. Jr., Wang H. F., Fournelle J. H., Zimmer J. H. and Jelínek E. (1999) A cautionary tale of spinel peridotite thermobarometry: an example from xenoliths of Kozákov volcano, Czech Republic. *Geolines* **9**, 92-95.
- Medaris L. G. Jr., Wang H. F., Jelínek E., Mihaljevič M. and Jakeš P. (2005) Characteristics and origins of diverse Variscan peridotites in the Gföhl Nappe, Bohemian Massif, Czech Republic. *Lithos* **82**, 1-23.
- Medaris L. G. Jr., Beard B. L. and Jelínek E. (2006) Mantle-derived, UHP garnet pyroxentite and eclogite in the Moldanubian Gföhl nappe, Bohemian Massif: A geochemical review, new P-T determinations, and tectonic interpretation. *Int. Geol. Rev.* **48**, 765-777.
- Meibom A., Sleep N. H., Chamberlain C. P., Coleman R. G., Frei R., Hren M. T. and Wooden J. L. (2002) Re-Os isotopic evidence for long-lived heterogeneity and equilibration processes in the Earth's upper mantle. *Nature* **419**, 705-708.
- Meisel T. and Moser J. (2004) Reference materials for geochemical PGE analysis: new analytical data for Ru, Rh, Pd, Os, Ir, Pt and Re by isotope dilution ICP-MS in 11 geological reference materials. *Chem. Geol.* **208**, 319-338.
- Meisel T., Walker R. J. and Morgan J. W. (1996) The osmium isotopic composition of the Earth's primitive upper mantle. *Nature* **383**, 517-520.
- Meisel T., Walker R. J. and Irving A. J. (2001) Osmium isotopic compositions of mantle xenoliths: A global perspective. *Geochim. Cosmochim. Acta* **65**, 1311-1323.
- Menzies M. A. and Bodinier J. -L. (1993) Growth of the European lithospheric mantle - dependence of upper-mantle peridotite facies and chemical heterogeneity on tectonics and age. *Phys. Earth Planet. Int.* **79**, 219-240.
- Mercier J. C. and Nicolas A. (1975) Textures and fabrics of upper-mantle peridotites as illustrated by xenoliths from basalts. *J. Petrol.* **16**, 454-487.
- Merlet C. (1994) An accurate computer correction program for quantitative electron-probe microanalyses. *Microchim. Acta* **114**, 363-376.
- Miller D. M., Langmuir C. H., Goldstein S. L. and Franks A. L. (1992) The importance of parental magma composition to calc-alkaline and tholeiitic evolution. Evidence from Umnak Island in the Aleutians. *J. Geophys. Res.* **97**, 321-343.
- Miller D. M., Goldstein S. L. and Langmuir C. H. (1994) Cerium, lead and lead-isotope ratios in arc magmas and the enrichment of lead in the continents. *Nature* **368**, 514-520.
- Mísař Z. and Jelínek E. (1981) Inclusions of peridotites, pyroxenites, eclogites and opals in the leptynites of the Moldanubicum at the locality Bory (SW Moravia) (in Czech). *Věst. Ústř. Úst. Geol.* **56**, 13-20.

- Misař Z., Jelínek E. and Jakeš P. (1984) Inclusions of peridotite, pyroxenite and eclogite in granulite rocks of pre-Hercynian upper mantle and lower crust in the eastern Bohemian Massif (Czechoslovakia). *Ann. Sci. Univ. Clermont-Ferrand II* **74**, 85-95.
- Morgan J. W., Walker R. J., Brandon A. D. and Horan M. (2001) Siderophile elements in Earth's upper mantle and lunar breccias: Data synthesis suggest manifestations of the same late influx. *Meteorit. Planet. Sci.* **36**, 1257-1275.
- Mungall J. E., Hanley J. J., Arndt N. T. and Debecdelievre A. (2006) Evidence from meimechites and other low-degree mantle melts for redox controls on mantle-crust fractionation of platinum-group elements. *Proc. Natl. Acad. Sci. USA* **103**, 12695-12700.
- Navon O. and Stolper E. (1987) Geochemical consequences of melt percolation: the upper mantle as chromatographic column. *J. Geol.* **95**, 285-307.
- Neumann E. R., Griffin W. L., Pearson N. J. and O'Really S. Y. (2004) The evolution of the upper mantle beneath the Canary Islands: Information from trace elements and Sr isotope ratios in minerals in mantle xenoliths. *J. Petrol.* **45**, 2573-2612.
- Norman M. D. (1998) Melting and metasomatism in the continental lithosphere: laser ablation ICPMS analysis of minerals in spinel lherzolites from eastern Australia. *Contrib. Mineral. Petrol.* **130**, 240-255.
- O'Brien P. J. and Rötzler J. (2003) High-pressure granulites: formation, recovery of peak conditions and implications for tectonics. *J. Metamorph. Geol.* **21**, 3-20.
- O'Neill H.St.C. (1980) An experimental study of Fe–Mg partitioning between garnet and olivine and its calibration as a geothermometer: corrections. *Contrib. Mineral. Petrol.* **72**, 337.
- O'Neill H. St. C. (1981) The transition between spinel lherzolite and garnet lherzolite, and its use as a geobarometer. *Contrib. Mineral. Petrol.* **77**, 185-194.
- O'Neill H.St.C. and Wood B. J. (1979) An experimental study of Fe–Mg partitioning between garnet and olivine and its calibration as a geothermometer. *Contrib. Mineral. Petrol.* **70**, 59-70.
- O'Neill H. St. C., Dingwell D. B., Borisov A., Spettel B. and Palme H. (1995) Experimental petrochemistry of some highly siderophile elements at high temperatures, and some implications for core formation at the mantle's early history. *Chem. Geol.* **120**, 255-273.
- Paukert T. and Rubeška I. (1993) Effects of fusion charge composition on the determination of platinum group elements using collection into a minimized nickel sulphide button. *Anal. Chim. Acta* **278**, 125-136.
- Pearson D. G., Carlson R. W., Shirey S. B., Boyd F. R. and Nixon P. H. (1995) Stabilisation of Archaean lithospheric mantle: A Re-Os isotope study of peridotite xenoliths from the Kaapvaal craton. *Earth Planet. Sci. Lett.* **134**, 341-357.
- Pearson D. G., Canil D. and Shirey S. B. (2003) Mantle samples included in volcanic rocks: xenoliths and diamonds. In: Carlson R.W. (ed.) *Treatise in Geochemistry, Volume 2 - The Mantle and Core*, Elsevier Pergamon, 171-275.

- Pearson D. G., Irvine G. J., Ionov D. A., Boyd F. R. and Dreibus G. E. (2004) Re-Os isotope systematics and platinum group element fractionation during mantle melt extraction: A study of massif and xenolith peridotite suites. *Chem. Geol.* **208**, 29-59.
- Peslier A. H., Reisberg L., Ludden J. and Francis D. (2000) Os isotopic systematics in mantle xenoliths; age constrains on the Canadian Cordillera lithosphere. *Chem. Geol.* **166**, 85-101.
- Peslier A. H., Francis D. and Ludden J. (2002) The lithospheric mantle beneath continental margins: melting and melt-rock reactions in Canadian Cordillera xenoliths. *J. Petrol.* **43**, 2013-2047.
- Plomerová J., Vecsey L., Babuška V., Granet M. and Achauer U. (2005) Passive seismic experiment MOSAIC - a pilot study of mantle lithosphere anisotropy of the Bohemian Massif. *Stud. Geophys. Geod.* **49**, 541-560.
- Prince C. I., Košler J., Vance D. and Günther D. (2000) Comparison of laser ablation ICP-MS and isotope dilution REE analyses – implications for Sm-Nd garnet geochronology. *Chem. Geol.* **168**, 255-274.
- Prouteau G., Scaillet B., Pichavant M. and Maury R. (2001) Evidence for mantle metasomatism by hydrous silicic melts derived from subducted oceanic crust. *Nature* **410**, 197-200.
- Puchtel I. S., Humayun M., Campbell A. J., Sproule R. A. and Lesher C. M. (2004) Platinum group element geochemistry of komatiites from the Alexo and Pyke Hill areas, Ontario, Canada. *Geochim. Cosmochim. Acta* **68**, 1361-1383.
- Rapp R. P., Shimizu N. and Norman M. D. (2003) Growth of early continental crust by partial melting of eclogite. *Nature* **425**, 605-608.
- Reisberg L., Lorand J. -P. and Bedini R. M. (2004) Reliability of Os model ages in pervasively metasomatized continental mantle lithosphere: a case study of Sidamo spinel peridotite xenoliths (East African Rift, Ethiopia). *Chem. Geol.* **208**, 119-140.
- Reisberg L., Zhi X., Lorand J. -P., Wagner C., Peng Z. and Zimmermann C. (2005) Re-Os and S systematics of spinel peridotite xenoliths from east central China: Evidence for contrasting effects of melt percolation. *Earth Planet. Sci. Lett.* **239**, 286-308.
- Sattari P., Brenan J. M., Horn I. and McDonough W. F. (2002) Experimental constraints on the sulfide- and chromite-silicate melt partitioning behavior of rhenium and platinum-group elements. *Econ. Geol.* **97**, 385-398.
- Schmidt G. and Snow J. E. (2002) Os isotopes in mantle xenoliths from the Eifel volcanic field and the Vogelsberg (Germany): age constraints on the lithospheric mantle. *Contrib. Mineral. Petrol.* **143**, 694-705.
- Shirey S. B. and Walker R. J. (1995) Carius tube digestions for low-blank rhenium-osmium analysis. *Anal. Chem.* **67**, 2136-2141.
- Stosch H. G. and Seck H. A. (1980) Geochemistry and mineralogy of two spinel peridotite suites from Dreiser Weiher, West Germany. *Geochim. Cosmochim. Acta* **44**, 457-470.

- Stosch H. G. and Lugmair G. W. (1986) Trace element and Sr and Nd isotope geochemistry of peridotite xenoliths from the Eifel (West Germany) and their bearing on the evolution of the subcontinental lithosphere. *Earth Planet. Sci. Lett.* **80**, 281-298.
- Strnad L., Mihaljevič M. and Šebek O. (2005) Laser ablation and solution ICP-MS determination of rare earth elements in USGS BIR-1G, BHVO-2G and BCR-2G glass reference material. *Geostand. Geoanal. Res.* **29**, 303-314.
- Suen C. J. and Frey F. A. (1987) Origins of the mafic and ultramafic rocks in the Ronda peridotite. *Earth Planet. Sci. Lett.* **85**, 183-202.
- Svojtka M., Košler J. and Venera Z. (2002) Dating granulite-facies structures and the exhumation of lower crust in the Moldanubian Zone of the Bohemian Massif. *Int. J. Earth Sci.* **91**, 373-385.
- Szabó C. and Taylor L. (1994) Mantle petrology and geochemistry beneath the Nógrád-Gömör Volcanic Field, Carpathian-Pannonian Region. *Int. Geol. Rev.* **36**, 328-358.
- Šibrava V. and Havlíček P. (1980) Radiometric age of Plio-Pleistocene volcanic rocks of the Bohemian Massif. *Věst. Ústř. Úst. Geol.* **55**, 129-139.
- Takazawa E., Frey F. A., Shimizu N., Obata M. and Bodinier J. -L. (1992) Geochemical evidence for melt migration and reaction in the upper mantle. *Nature* **359**, 55-58.
- Tarantola A. and Valette B. (1982) Generalized non-linear inverse problems solved using least-squares criterion. *Rev. Geophys. Space Phys.* **20**, 219-232.
- Taylor W. R. (1998) An experimental test of some geothermometer and geobarometer formulations for upper mantle peridotites with application to the thermobarometry of fertile lherzolite and garnet websterite. *Neues Jahrb. Mineral. Abh.* **172**, 381-408.
- Ulmer P. (1989) The dependence of the Fe²⁺-Mg cation-partitioning between olivine and basaltic liquid on pressure, temperature and composition: an experimental study to 30 kbar. *Contrib. Mineral. Petrol.* **101**, 261-273.
- Ulrych J. and Adamovič J. (2004) (Ultra)mafic mantle xenoliths in Cenozoic alkaline volcanics of the Bohemian Massif (Czech Republic). *Mineral. Slov.* **36**, 205-215. (in Czech)
- Ulrych J., Pivec E., Lang M., Balogh K. and Kropáček V. (1999) Cenozoic intraplate volcanic rock series of the Bohemian Massif: A review. *Geolines* **9**, 123-129.
- van Acken D., Becker H. and Walker R. J. (2008) Refertilization of Jurassic oceanic peridotites from the Tethys Ocean-implications for the Re-Os systematics of the upper mantle. *Earth Planet. Sci. Lett.* **268**, 171-181.
- Vaselli O., Downes H., Thirwall M. F., Dobosi G., Coradossi N., Seghedi I., Szakacs A. and Vannucci R. (1995) Ultramafic xenoliths in Plio-pleistocene alkali basalts from the eastern Transylvanian Basin: depleted mantle enriched by vein metasomatism. *J. Petrol.* **36**, 23-53.
- Vaselli O., Downes H., Thirwall M. F., Vannucci R. and Coradossi N. (1996) Spinel-peridotite xenoliths from Kapfenstein (Graz Basin, Eastern Austria): A geochemical and petrological study. *Mineral. Petrol.* **57**, 23-50.

- Vernieres J., Godard M. and Bodinier, J. -L. (1997) A plate model for the simulation of trace element fractionation during partial melting and magma transport in the Earth's upper mantle. *J. Geophys. Res.* **102**, 24771-24784.
- Vokurka K. and Povondra P (1983) Geothermometry and geobarometry of lherzolite nodules from Kozákov, NE Bohemia, Czechoslovakia, *Acta Univ. Carol. Geol.* **4**, 261-272.
- Vrána S. and Štědrá V. (1997) Geological model of Western Bohemia related to the KTB borehole in Germany. *J. Geol. Sci.* **47**, 1-240.
- Walker R. J., Carlson R. W. and Shirey S. B. (1989) Os, Sr, Nd, and Pb isotope systematics of southern African peridotite xenoliths - implications for the chemical evolution of the subcontinental mantle. *Geochim. Cosmochim. Acta* **53**, 1583-1595.
- Walker R. J., Prichard H. M., Ishiwatari A. and Pimentel M. (2002) The osmium isotopic composition of convecting upper mantle deduced from ophiolite chromites. *Geochim. Cosmochim. Acta* **66**, 329-345.
- Walker R. J., Böhlke J. -K., McDonough W. F. and Li J. (2007) Combined Re-Os isotope, gold and platinum-group element study of epigenetic gold ores, Alleghany District, California. *Econ. Geol.* **102**, 1079-1089.
- Wendt J. I., Kröner A., Fiala J. and Todt W. (1993) Evidence from zircon dating for existence of approximately 2.1 Ga old crystalline basement in southern Bohemia, Czech Republic. *Geol. Rundsch.* **82**, 42-50.
- Widom E., Kepezhinskas P. and Defant M. (2003) The nature of metasomatism in the sub-arc mantle wedge: Evidence from Re-Os isotopes in Kamchatka peridotite xenoliths. *Chem. Geol.* **196**, 283-306.
- Wilson M. and Downes H. (1991) Tertiary–Quaternary extension-related alkaline magmatism in western and central Europe. *J. Petrol.* **32**, 811-850.
- Witt-Eickschen G. (1993) Upper mantle xenoliths from alkali basalts of the Vogelsberg, Germany: implications for mantle upwelling and metasomatism. *Eur. J. Mineral.* **5**, 361-376.
- Witt-Eickschen G. and Seck H. A. (1991) Solubility of Ca and Al in orthopyroxene from spinel peridotite: An improved version of an empirical geothermometer. *Contrib. Mineral. Petrol.* **106**, 431-439.
- Witt-Eickschen G. and Kramm U. (1997) Mantle upwelling and metasomatism beneath central Europe: geochemical and isotopic constrains from mantle xenoliths from the Rhön (Germany). *J. Petrol.* **38**, 479-493.
- Wu F. Y., Walker R. J., Yang Y. H., Yuan H. L. and Yang J. H. (2006) The chemical-temporal evolution of lithospheric mantle underlying the North China Craton. *Geochim. Cosmochim. Acta* **70**, 5013-5034.
- Yaxley G. M., Crawford A. J. and Green D. H. (1991) Evidence for carbonatite metasomatism in spinel peridotites from western Victoria, Australia. *Earth Planet. Sci. Lett.* **107**, 305-317.

- Zangana N. A., Downes H., Thirlwall M. F. and Hegner E. (1997) Relationship between deformation, equilibration temperatures, REE and radiogenic isotopes in mantle xenoliths (Ray Pic, Massif Central, France): an example of plume-lithosphere interaction? *Contrib. Mineral. Petrol.* **127**, 187-203.
- Zangana N. A., Downes H., Thirlwall M. F., Marriner G. F. and Bea F. (1999) Geochemical variation in peridotite xenoliths and their constituent clinopyroxenes from Ray Pic (French Massif Central): implications for the composition of the shallow lithospheric mantle. *Chem. Geol.* **153**, 11-35.
- Zanetti A., Mazzucchelli M., Rivalenti G. and Vannucci R. (1999) The Finero phlogopite-peridotite massif: an example of subduction-related metasomatism. *Contrib. Mineral. Petrol.* **134**, 107-122.
- Ziegler P. A. (1992) European Cenozoic rift system. *Tectonophysics* **208**, 91-111.

CURRICULUM VITAE of Lukáš Ackerman

Date and place of birth: 28. 1. 1979, Prague

Education

- 1999-2002 Bc. (BSc. degree) - Management of Natural Resources, Faculty of Science, Charles University; BSc. Thesis - Experimental weathering of arsenopyrites from the Mokrsko and Kasperske Hory gold deposits
- 2002-2004 Mgr. (MSc. degree) - Economic Geology, Faculty of Science, Charles University; MSc. Thesis - Pegmatites near Vlastejovice
- since 2004 PhD. study - Geochemistry, Faculty of Science, Charles University; PhD. Thesis – Geochemistry of upper mantle beneath Bohemian Massif, Central Europe

Current & past jobs

- since 2004 Pre-doctoral research fellow, Institute of Geology v.v.i., Academy of Sciences of the Czech Republic

Professional experience

- 10/2006-11/2006 visiting scientist, Isotope Geochemistry Laboratory, Department of Geology, University of Maryland, USA

Research Interest

- petrology and trace element geochemistry of upper mantle and magmatic rocks
- platinum-group element geochemistry
- isotope geochemistry
- laser ablation ICP-MS technique
- fluid inclusions
- geochemistry of pegmatites

Shortcourses & Workshops

- 3rd Workshop on Highly Siderophile Element Geochemistry. Durham 4-7.7.2006
- Short Course on Geochemistry, Mineralogy and Metallogeny of platinum-group element deposits. Prague 12-14.10.2004 (organizer)
- Short Course on Mantle petrology and petrogenesis. Munchen 28-30.4.2003

Research projects

- 2004-2008 Character of upper mantle/lower crust beneath the Bohemian Massif on the basis of geochemical signs of (ultra)mafic xenoliths in Cenozoic volcanics (J. Ulrych & E. Jelinek) - Grant Agency of the Academy of Sciences of the Czech Republic
- 2006-2008 Platinum group element geochemistry of strongly differentiated magmatic complexes: examples from the Bohemian Massif (L. Ackerman, L. Strnad & F. Laufek) - Grant Agency of the Academy of Sciences of the Czech Republic
- 2006-2007 Distribution and fractionation of highly siderophile elements between mineral phases of upper mantle xenoliths (L. Ackerman, E. Jelinek & L. Strnad) - Grant Agency of the Charles University
- 2006-2008 Determination of platinum group elements in natural material by ICP-MS after collection into nickel sulphide button (L. Strnad, L. Barsova & L. Ackerman) - Grant Agency of the Charles University

Professional Membership

- The Geochemical Society
- Czech Geological Society

Selected publications

- Ulrych, J., Dostal, J., Hegner, E., Balogh, K. & **Ackerman, L.** (2008) Melilitic volcanic rocks of the Cenozoic Ohre/Eger Rift in northern Bohemia, Czech Republic, *Lithos* **101**, 141-161. (IF = 2.6)
- Ackerman, L.**, Mahlen, N., Jelínek, E., Medaris, L. G., Ulrych, J., Strnad, L. & Mihaljevič, M. (2007) Geochemistry and evolution of Subcontinental Lithospheric mantle in Central Europe: evidence from peridotite xenoliths of the Kozákov volcano, Czech Republic, *Journal of Petrology* **48**, 2235-2260. (IF = 3.8)
- Ackerman, L.**, Zachariáš, J. & Pudilová, M. (2007) P-T conditions and fluid composition of barren and lithium pegmatites from Vlastějovice, Bohemian Massif, Czech Republic, *International Journal of Earth Sciences* **96**, 623-638 (IF = 1.9)
- Ackerman, L.**, Puchtel, I. S., Walker, R. J. & Jelinek, E. (2007) Re-Os depth profile of the upper mantle beneath Kozakov volcano. *Geochimica et Cosmochimica Acta*, 71, A4
- Pašava, J., Vymazalová, A., Knésl, I. & **Ackerman, L.** (2007) PGE in ultramafic rocks of the hidden ophiolite complex near Svitavy, Bohemian Massif. In: Andrew, C.J. et al. (eds) *Digging Deeper" Proceedings of the 9th Biennial Meeting of the Society for Geology Applied to Mineral Deposits, vol. 2*, Dublin, Ireland, 1591-1594
- Ackerman, L. (2005) Magmatic vs. hydrothermal origin of fluorites from Vlastějovice, Bohemian Massif. *Journal of the Czech Geological Society* **50**, 35-41.